Development of the G3 Designed ankyrin repeat protein (DARPin) for HER2 imaging

Robert Michael Goldstein

A thesis submitted to the University College London for the degree Doctor of Philosophy (PhD) in the Faculty of Medical Sciences, Department of Oncology,
UCL Cancer Institute,
University College London

2015

Abstract

Background: Human epidermal growth factor receptor-2 (HER2) expression predicts response to anti-HER2 therapy in breast and gastric cancer. HER2 status is assessed by tumour biopsy but this may not be representative of the larger tumour mass or other metastatic sites; risking misclassification and selection of suboptimal therapy. The G3 designed ankyrin repeat protein (DARPin) binds HER2 with high affinity at an epitope that does not overlap with trastuzumab and is biologically inert. This research aims to assess the pre-clinical efficacy and safety of G3 DARPin HER2 PET and SPECT imaging.

Methods: Hexahistidine (His_6), histidine-glutamate $(HE)_3$ and untagged-G3 DARPins were manufactured using a GMP-compatible *Pichia pastoris* protocol and radiolabelled with ^{125}I or site-specifically with ^{111}In. BALB/c mice were injected with radiolabelled-G3 DARPins and biodistribution was evaluated. The lead construct, $(HE)_3$-G3 was radiolabelled with ^{111}In, ^{125}I or ^{68}Ga for assessment in mice bearing HER2-positive human breast tumour (BT474) xenografts. Mice received $(HE)_3$-G3 at 50-100 times the human equivalent dose to assess acute toxicity.

Results: $(HE)_3$-G3 had significantly lower liver uptake than His_6-G3 and untagged-G3 in non-tumour bearing mice when radiolabelled with ^{125}I or ^{111}In. In mice bearing HER2-positive tumour xenografts, ^{111}In-$(HE)_3$-G3 was better maintained in tumours and cleared faster from serum than ^{125}I-$(HE)_3$-G3, achieving superior tumour-to-blood ratios of 343.7±161.3 vs. 22.0±11.3 at 24 h, respectively. On microSPECT/CT ^{111}In and ^{125}I labelled $(HE)_3$-G3, imaged HER2-positive tumours at 4 h post-administration but ^{111}In-$(HE)_3$-G3 had less non-specific uptake. ^{68}Ga-$(HE)_3$-G3 can image HER2-positive tumours at up to 2 h post-administration by PET scanning. $(HE)_3$-G3 DARPin was well tolerated by mice treated at 50-100 times the human equivalent dose over 24 h.

Conclusion: Radiolabelled $(HE)_3$-G3 is a versatile radioligand with potential to acquire whole-body HER2 scans. $(HE)_3$-G3 will be assessed in a regulatory standard pre-clinical toxicity study, prior to embarking on a first in human trial.

Declaration of Originality

I, Robert Michael Goldstein, confirm that the work presented in this thesis is my own. I confirm that I have indicated where information has been obtained from other sources.

Robert Michael Goldstein

Table of contents

List of Figures

List of Tables

List of Abbreviations

% ID/g	percentage of injected dose per gram of tissue
^{18}F	Fluorine-18
[^{18}F]SFB	N-succinimidyl-4-[^{18}F]fluorobenzoate
^{64}Cu	Copper-64
^{68}Ga	Gallium-68
^{68}Ge	Germanium-68
$[^{99m}Tc(CO)_3]^+$	^{99m}Tc-tricarbonyl
^{111}In	Indium-111
^{177}Lu	Lutetium-177
^{123}I	Iodine-123
^{124}I	Iodine-124
^{125}I	Iodine-125
^{188}Re	Rhenium-188
ADCC	antibody-dependent cell-mediated cytotoxicity
AOX	Alcohol oxidase
ASCO	American Society of Clinical Oncology
B_{Max}	Maximum amount of radioligand which can bind specifically to the receptors in a membrane preparation (Maximum binding capacity)
BMGY	Buffered Glycerol-complex medium
BMMY	Buffered Methanol-complex medium
BSA	bovine serum albumin
bp	base pair
C6.5db	C6.5 diabody
C	cysteine
CAP	College of American Pathologists
CDER	Center for Drug Evaluation and Research
CEP17	centromere chromosome 17
CISH	Chromogenic in situ hybridisation
ClogP	calculated logP
cm	centimetre
CRUK	Cancer Research UK
Da	Dalton
DAB	3,3′-Diaminobenzidine tetrahydrochloride
DARPin	designed ankyrin repeat protein
db	Diabody
DC	detergent compatible
dH_2O	deionised water
DIG	Digoxigenin
DMEM	Dulbecco's Modified Eagle Medium
DNP	Dinitrophenyl
dNTP	deoxyribose nucleoside triphosphates
DOTA	1,4,7,10-tetraazacyclododecane-1,4,7,10-tetraacetic acid

DTPA	diethylenetriamine penta-acetic acid
DTT	Dithiothreitol
E. coli	*Escherichia coli*
ECD	Extracellular domain
EDC	*N*-(dimethylaminopropy)l-*N*-ethylcarbodiimide hydrochloride
EDTA	Ethylenediaminetetraacetic acid
EGFR	Epidermal growth factor receptor
ELISA	enzyme-linked immunosorbent assay
EU	Endotoxin Units
[^{18}F]FBEM	N-2-(4-[^{18}F]fluorobenzamido)ethyl]maleimide
Fab	fragment antigen binding
FACS	fluorescence-activated cell sorter
Fc	fragment crystallisable region
FDA	US Food and Drug Administration
^{18}F-FDG	^{18}F-fluorodeoxyglucose
FISH	fluorescent in situ hybridisation
FPLC	Fast protein liquid chromatography
g	gram
GLP	Good laboratory practice
GRAVY	grand average of hydropathy
h	hour
H&E	Haemotoxylin and Eosin
$(HA)_3$	histidine_alanine
$(HE)_3$	histidine_glutamate tag
HED	human equivalent dose
HER2	human epidermal growth factor receptor 2
$(HI)_3$	histidine_ isoleucine tag
HIF	hypoxia-inducible factor
His_6	hexahistidine tag
$(HK)_3$	histidine_lysine
HPLC	High performance liquid chromatography
HRP	horse radish peroxidase
HRV	human rhinovirus
Hsp90	heat shock protein 90
Ig	Immunoglobulin
IL-2	interleukin-2
IHC	Immunohistochemistry
IMAC	Immobilised-metal affinity chromatography
ISH	in situ hybridisation
iTLC-SG	Instant thin layer chromatography- silica gel
iTLC-SA	Instant thin layer chromatography -salicylic acid
K_a	on rate or association
K_d	off rate or dissociation
K_D	binding affinity
K_{OW}	Octanol-Water Partition Coefficient
keV	kiloelectronvolts

kVP	peak kilovoltage
L	Litre
LB	Luria Bertani
LC-MS	Liquid chromatography mass spectrometry
logP	logarithm of K_{OW} in a compounds non-ionised (neutral) form
M	molar
MALDI	Matrix-assisted laser desorption/ionization
MBq	megabecquerel
MCC	[*N*-maleimidomethyl]cyclohexane-1-carboxylate
MeV	megaelectronvolts
mg	milligram
µg	microgram
ml	millilitre
µl	microlitre
mM	millimolar
µM	micromolar
ms	millisecond
mV	millivolt
min	minute
MAPK	mitogen-activated protein kinase
MEK	mitogen extracellular signal kinase
MHRA	Medicines and Healthcare Products Regulatory Agency
MIP	Maximum intensity projection
MIRD	medical internal radiation dose
mTOR	mammalian target of rapamycin
MW	molecular weight
MWCO	molecular weight cut off
NaCl	sodium chloride
NAFLD	non-alcoholic fatty liver disease
NASH	non-alcoholic steatohepatitis
ng	nanogram
NHS	*N*-hydroxysulfosuccinimide
NOTA	1,4,7-triazacyclononane-1,4,7-triacetic acid
OD_{280}	optical density measured at 280 nm
OD_{600}	optical density measured at 600 nm
PBS	Phosphate Buffered Saline
PCR	polymerase chain reaction
PEG	polyethylene glycol
PES	Polyethersulfone
PET	positron emission tomography
PFS	progression-free survival
pI	pH of isoelectric point
PI3K	phosphatidylinositol 3-kinase
PIB	*p*-iodobenzoate
P. pastoris	*Pichia pastoris*
PVDF	polyvinylidene difluoride

RAF	receptor activation factor
RAS	rat sarcoma
RT	room temperature
Rpm	revolutions per minute
RUV_{mean}	mean relative uptake value
RU	response unit
SA	specific activity
scFv	single-chain variable fragment
SD	standard deviation
SDS-PAGE	sodium dodecyl sulfate polyacrylamide gel electrophoresis
SHPP	water soluble Bolton-Hunter reagent sulfosuccinimidyl-3-(4-hydroxyphenyl)propionate
Sm1	small protein 1
SPECT	single photon emission computed tomography
SPR	Surface Plasmon Resonance
SUV	Standardized uptake value
SUV_{max}	maximum standardized uptake value
TAE	Tris-acetate-EDTA
TCEP	Tris(2-carboxyethyl)phosphine hydrochloride
T-DM1	Trastuzumab emtansine
TFF	tangential flow filter
TLC	thin layer chromatography
TMA	tissue microarray
TTP	time to progression
U	Unit
UK	United Kingdom
US	United States
V	Voltage
V_L	variable light chain
V_H	variable heavy chain
VOI	volume of interest
v/v	percentage of volume per volume
W	Watt
WAP	whey acidic protein
w/v	percentage of weight to volume
YEPD	Yeast Extract Peptone Dextrose medium (primary culture)
YPD	Yeast Extract Peptone Dextrose
YPDS	Yeast Extract Peptone Dextrose Sorbitol

Dedication

I am eternally grateful to the love and support of my wife, Annabel and my parents, Bella and Barrie. In particular, to my mother Bella (لطيفة) who as a refugee from Syria was never afforded the opportunities in education and freedoms I have enjoyed but provided me with the foundations to learn.

Acknowledgements

The work presented in this thesis was only made possible with the help, advice and support from many people.

Firstly, I would like to thank my supervisors, Professor Tim Meyer and Professor Kerry Chester. I have been blessed to have two very enthusiastic, knowledgeable and supportive supervisors, who complement each other very well. With their support I have been able to attend conferences and a protocol development workshop, as well as being able to maintain clinical involvement during research.

Numerous people have helped me in the laboratory.

Dr Kim Vigor, Miss Maria Livanos and Miss Leah Ensell (UCL Cancer Institute) were a great help in producing the G3 DARPins.

Mr Gaurav Bhavsar and Dr Berend Tolner (UCL Cancer Institute), for their help with the fermentation, harvest and purification of the G3 DARPin proteins.

Dr Jane Sosabowski, Dr Julius Leyton, Dr Julie Foster and Professor Steve Mather (Barts Cancer Institute, Queen Mary University of London) for help and guidance with the G3 DARPin radiolabelling and *in vivo* assessment. Dr Maggie Cooper (King's College London) for help with Gallium-68 radiolabelling.

Dr Lisa Haigh (Imperial College London) for teaching me how to perform mass spectrometry.

Dr Gabriela Nagy-Davidescu (University of Zurich), for helping to assess G3 DARPin affinities and kinetics with surface plasmon resonance.

Professor Lars Baltzer (University of Uppsala) for allowing me to spend a week in his laboratory to learn about the principles of protein conjugation and radiolabelling.

Mr Mohammed Rashid (UCL Cancer Institute) for assistance with performing HER2 immunohistochemistry on tumour samples.

This work would not have been possible without support from the Seventh Framework Programme (FP7) for HER Imaging and Molecular Interaction Mapping

in Breast Cancer (Imagint EC GRANT: 259881) and the Breast Cancer Campaign, to develop the G3 DARPin for clinical application.

Chapter 1 Introduction

1.1 Background

In recent years, our knowledge and understanding of the molecular processes which cause cancer and result in cancer progression have increased greatly. This has led to the development of targeted therapies which disrupt these molecular processes. It is important to stratify patients on the basis of biomarkers which reflect these molecular processes to improve patient outcome in response to targeted agents. Although histological analysis is the main method used to determine molecular biomarker expression, it does not sufficiently address tumour heterogeneity and is limited by sampling a single site at a single time point. Molecular imaging could potentially assess whole body biomarker expression, which could serve as a means to predict and assess treatment responses to targeted agents.

1.2 Human epidermal growth factor receptor 2

Human epidermal growth factor receptor 2 (HER2) is one of four members of the HER family (HER 1-4), which are collectively involved in the regulation of cell survival, growth and differentiation (Ross, Slodkowska et al. 2009). The HER2 gene was discovered by Weinberg and colleagues in 1984 (Schechter, Stern et al. 1984). The gene is located on the long arm of chromosome 17 (17q12) and encodes for a 185,000 Da transmembrane receptor protein with tyrosine kinase activity (Akiyama, Sudo et al. 1986).

In 1985, HER2 gene amplification was reported in the human breast cancer cell line, MAC117 (King, Kraus et al. 1985). In 1987, Slamon *et al*. determined that HER2 gene amplification was an independent prognostic factor which predicted overall survival and time to relapse among 189 breast cancer patients (Slamon, Clark et al. 1987). HER2 is overexpressed in 20-25% of breast cancer patients (Slamon, Clark et al. 1987; Owens, Horten et al. 2004; Ross, Slodkowska et al. 2009). Assessment of HER2 status is now an important prognostic and predictive marker in the management of early and advanced breast cancer.

1.2.1 Biology of HER2

The HER pathway is a complex biological network composed of extracellular polypeptides, transmembrane receptors and protein kinases that transmit signals to

the nucleus which activate or inhibit transcription factors of genes that regulate cellular function (Figure 1.1) (Citri and Yarden 2006).

Ligand binding to a HER extracellular domain can activate HER dimerisation and trans-phosphorylation of the intracellular domains. HER2 is unique in not having a ligand, so HER2 activation depends on heterodimerisation with another HER family member, as HER2 homodimerisation only occurs when it is expressed at high levels (Citri and Yarden 2006). The phosphorylated tyrosine residues interact with multiple intracellular signalling molecules leading to activation of downstream pathways. Signalling through the phosphatidylinositol 3'-kinase (PI3K)-Akt-mammalian target of rapamycin (mTOR) pathway inhibits apoptosis, while the rat sarcoma (RAS)-receptor activation factor (RAF)-mitogen extracellular signal kinase (MEK)-mitogen-activated protein kinase (MAPK)-pathway activates cell proliferation (Hudis 2007).

HER2 is the preferred dimerisation partner for HER1 (epidermal growth factor receptor, EGFR), HER3 and HER4, since its dimerisation domains are continually exposed. HER3 is activated by the ligand neuregulin-1 but does not have any tyrosine kinase activity and thus it must form heterodimers to effect intracellular signalling. HER3 has multiple sites which can interact with PI3K, thus HER2-HER3 heterodimers are potent activators of the anti-apoptosis pathway PI3K-Akt-mTOR (Citri and Yarden 2006; Moasser 2007).

HER2 can also be activated by forming complexes with other transmembrane receptors. For example, HER2 interacts with insulin-like growth factor receptor-1, which contributes to resistance against the HER2 targeted monoclonal antibody, trastuzumab (Nahta, Yuan et al. 2005). The oestrogen receptor can activate HER2 signalling and HER2/oestrogen receptor cross-talk has been shown to cause tamoxifen-resistance *in vitro* (Shou, Massarweh et al. 2004). p95HER2 is an aberrant form of HER2 which is constitutively active as it has lost its extracellular domain which normally serves as an inhibitor prior to its activation by receptor dimerisation (Molina, Saez et al. 2002). Breast cancer cells expressing p95HER2 are resistant to trastuzumab as it cannot bind to the extracellular domain but remain sensitive to the receptor tyrosine kinase inhibitor, lapatinib (Scaltriti, Rojo et al. 2007).

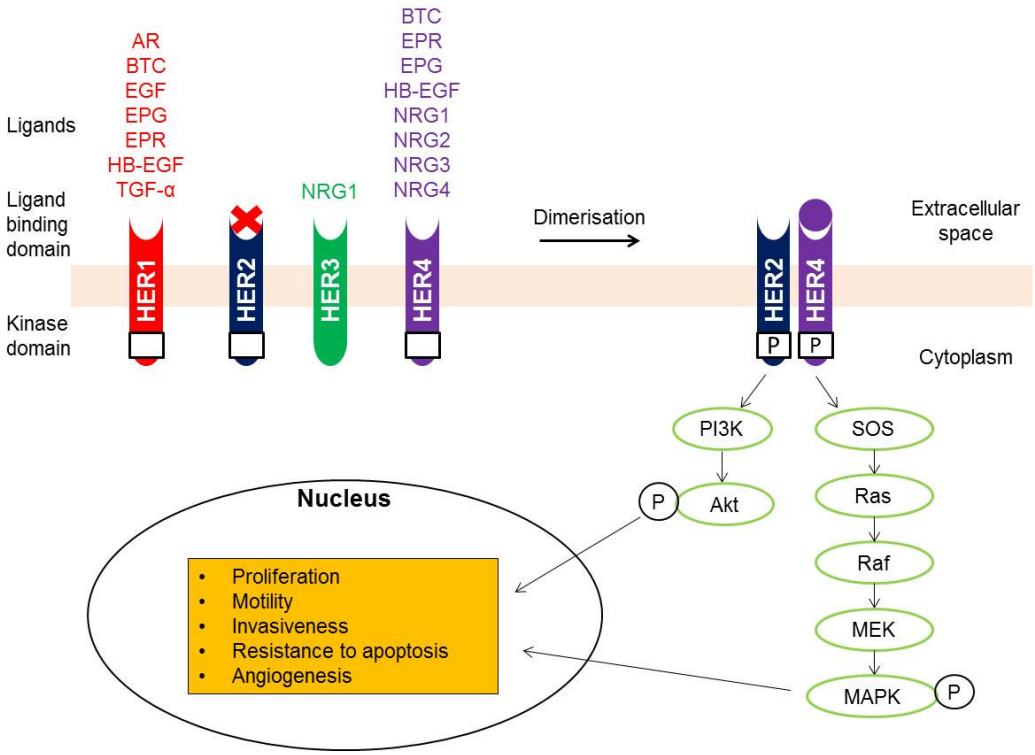

Figure 1.1 HER family heterodimer formation and downstream signalling, resulting in vascular endothelial growth factor transcription and other physiological responses required for carcinogenesis. Adapted from (Arteaga, Sliwkowski et al. 2012).
(AR, amphiregulin; BTC, betacellulin; EPG, epigen; EPR, epiregulin; HB-EFG, heparin-binding EGF-like ligand; NRG, neuregulin, TGF; transforming growth factor)

1.2.2 Prognostic significance of HER2 in breast cancer

Between 1987 and 2009, 107 studies involving 39,730 patients have assessed the role of HER2 status in breast cancer. The majority of these studies (88%) have confirmed that either HER2 gene amplification or HER2 protein expression levels predict breast cancer outcome by univariate or multivariate analysis (Ross, Slodkowska et al. 2009).

HER2 overexpression occurs less frequently with invasive lobular carcinoma than with invasive ductal carcinoma but when present in either, it confers a significantly worse prognosis (Rosenthal, Depowski et al. 2002). HER2 status is frequently associated with high grade invasive carcinoma (Ross, Slodkowska et al. 2009). HER2 overexpression is consistently associated with extra-mammary and intra-mammary Paget's disease (Fu, Lobocki et al. 2001). In node positive breast cancer, HER2 overexpression is associated with a poor outcome but in node negative

disease, the prognostic value of HER2 status is less certain (Quenel, Wafflart et al. 1995).

The introduction of anti-HER2 therapy has altered the prognosis as well as the pattern of distribution of metastatic HER2-positive breast cancer. Previously, HER2-positive breast cancer was more likely to spread to the major viscera. However, since the advent of anti-HER2 therapy, progressive metastatic extra-cranial disease has diminished and has been superseded by central nervous system involvement (Lin and Winer 2007).

1.2.3 Rate and clinical implications of HER2 discordance in breast cancer

Turner *et al.* identified 60 studies reporting HER2 discordance; interestingly both HER2 loss and HER2 gain were reported in many of these studies. The reviewed studies were assigned to three different categories (Turner and Di Leo 2013):

i. The primary tumour and distant metastases, HER2 discordance rates were 0-34% in 21 studies.

ii. The primary tumour and local regional recurrence and/or distant metastases, HER2 discordance rates ranged from 0-22% in 25 studies.

iii. The primary tumour and synchronous lymph node metastases, HER2 discordance rates were 0-9% in 14 studies.

In a large pooled analysis of two prospective studies involving 289 patients, the reported rate of HER2 discordance assessed by fluorescent in situ hybridisation (FISH) between primary and corresponding recurrent disease was only 5.5% (Amir, Clemons et al. 2012). Furthermore, there is evidence that HER2 status between metastatic disease relapses is not stable. Lindström *et al.* found that HER2 status changed in 15.7% (5/32) of patients between consecutive relapses with changes from negative to positive and vice versa (Gancberg, Di Leo et al. 2002; Lindstrom, Karlsson et al. 2012).

The available literature concerning the clinical impact of HER2 discordance is limited, inconclusive and conflicting. For example, Turner *et al.* used nine retrospective studies and one prospective study to determine the impact of HER2 discordance between primary disease and metastatic recurrence on survival. Based on their analysis, HER2 loss appears to result in worse post-relapse survival and overall survival but these data are confounded by lack of treatment in the receptor loss setting. Although re-biopsy of metastatic relapse can lead to changes in management, this does not occur in all patients with receptor discordance, as clinicians are concerned by false negative or false positive histology results (Turner and Di Leo 2013).

HER2 discordance occurs between primary and metastatic disease and between relapses of metastatic disease. Due to the limitations of biopsies and design of studies investigating discordance, the true rate of HER2 discordance and clinical impact of discordance are uncertain.

1.2.4 Current methods for detecting HER2-positive breast cancer

It is important to have a standardised and validated method for accurate assessment of HER2 status in breast cancer. HER2 status can be determined by either HER2 protein expression or gene amplification. Methods employed to test HER2 protein expression include immunohistochemistry (IHC), western blotting and enzyme-linked immunosorbent assay (ELISA) of tumour cytosol. Southern blotting, chromogenic in situ hybridisation (CISH), polymerase chain reaction (PCR) and fluorescent in situ hybridisation (FISH) have been used to assess HER2 gene amplification (Ross 2009).

Southern blotting, western blotting and PCR require large amounts of tissue, they are prone to false negatives due to combined analysis with surrounding benign tissue and false positives due to combined analysis with adjacent in situ HER2 expressing benign breast disease (Moreno, Lloveras et al. 1997; Pegram, Pauletti et al. 1998). By contrast, FISH and IHC correlate HER2 expression with tissue morphology so are able to identify both benign surrounding tissue and in situ disease, limiting the risks of both false positives and false negatives.

1.2.4.1 HER2 Immunohistochemistry

According to the American Society of Clinical Oncologists (ASCO) / College of American Pathologists (CAP) guideline update, a positive HER2 IHC test result (score 3+), is defined as circumferential membrane staining that is complete, intense, and within >10% of tumour cells (Wolff, Hammond et al. 2007; Wolff, Hammond et al. 2013). The advantages of HER2 IHC analysis are that it is easy to perform, inexpensive and widely available. However, test accuracy is affected by a series of factors, including antibody sensitivity, antibody specificity, assay dilution and antibody clonality (monoclonal or polyclonal). The method of tissue fixation is important; fresh frozen tissue is preferable as paraffin-embedded tissues limit antibody access to the HER2 epitope (Press, Hung et al. 1994; Vani, Sompuram et al. 2008). Furthermore, inaccuracies can occur as a result of interpretation errors (Vani, Sompuram et al. 2008).

The US Food and Drug Administration (FDA) have approved the HercepTest (Dako) which utilises a polyclonal antibody (Jacobs, Gown et al. 1999). The Pathway kit (Ventana) which utilises a monoclonal antibody for HER2 IHC testing is also FDA approved (Powell, Hicks et al. 2007).

1.2.4.2 HER2 fluorescent in situ hybridisation

FISH combines simultaneous evaluation of tissue morphology and gene amplification. In contrast to IHC, it is less affected by tissue fixation and analytical variables, while being reliable, sensitive, reproducible and accurate. However, FISH is more labour intensive and complex than IHC (Shah and Chen 2011).

According to the ASCO/CAP guideline update, a positive result for HER2 gene amplification by FISH is either ≥ 6 HER2 gene copies per cell or a FISH ratio of HER2 gene signals to centromere chromosome 17 (CEP17) signals ≥ 2.0 (Wolff, Hammond et al. 2013). The FDA has approved the PathVysion (Abbott Molecular), INFORM (Ventana) and HER2 FISH pharmDx (Dako) for HER2 FISH testing. PathVysion and HER2 FISH pharmDx use probes targeting CEP17 and HER2 gene, enabling calculation of a HER2/CEP17 ratio. While INFORM uses a single probe targeting the HER2 gene.

Conventionally, the number of CEP17 signals has been assumed to reflect the number of copies of chromosome 17 in the tumour cell. Thus, tumours with increased CEP17 signals have been thought to represent tumour chromosome 17 polysomy. On this basis, the incidence of polysomy 17 in invasive breast cancer has been reported in 20-30% of invasive breast carcinoma patients (Shah, Wang et al. 2009). However, the HER2 gene is located near the centromere, so both CEP17 and HER2 could be co-amplified in the absence of true chromosome 17 polysomy and this may result in under reporting of HER2 gene amplification by FISH (Yeh, Martin et al. 2009). Probes for other chromosome 17 genes can be used to distinguish between centromere amplification and true polysomy. Patients with increased mean CEP17 and HER2 copy numbers (or assumed polysomy) who had been classified as unequivocal or non-amplified were reclassified as HER2 amplified when other chromosome 17 genes were co-evaluated. Although this re-classification affects approximately 3% of breast cancer patients it would be worth assessing chromosome 17 reference genes among patients assessed as unequivocal and non-amplified by FISH (Tse, Hwang et al. 2011). However, the 2013 ASCO/CAP guideline update does not require the discrimination of true polysomy from centromere amplification (Wolff, Hammond et al. 2013).

1.2.4.3 Correlation between HER2 IHC and FISH

There is good concordance between tumours which score 0, 1+ & 3+ on IHC and FISH test results. The concordance rate is 96% using single probe FISH testing and 97% for dual probe FISH testing which co-utilises CEP17 signals (Lal, Salazar et al. 2004). Disagreement between IHC 3+ and FISH may be due to intra-tumour heterogeneity, variable processing, variable tissue fixation and difficulty distinguishing between chromosome 17 centromere amplification and genuine polysomy (Shah and Chen 2011). By contrast, one quarter of breast tumours which have an IHC score 2+ are HER2-positive on FISH testing (Lal, Salazar et al. 2004).

Parallel assessment of 2963 breast cancer specimens from 135 different hospitals demonstrated that FISH has a significantly higher failure rate (5% vs. 0.08%), longer testing time (36 h vs. 4 h), longer interpretation time (7 minutes vs. 45 seconds) and higher reagent cost ($140 vs. $10) than IHC. The authors recommended the broad use of IHC and only limited use of FISH for IHC 2+ cases, which is supported by the

ASCO/CAP guideline update (Yaziji, Goldstein et al. 2004; Wolff, Hammond et al. 2013).

1.2.5 Treatment for HER2-positive breast cancer

In modern clinical trials, HER2-positive breast cancer patients are defined as patients with tumours with an IHC score 3+ or a FISH amplification ratio ≥ 2.0, thus in keeping with the ASCO/CAP guideline update (Baselga, Cortes et al. 2012; Wolff, Hammond et al. 2013).

1.2.5.1 Trastuzumab

Trastuzumab was the first anti-HER2 therapy and further anti-HER2 therapies are now available which target both the HER2 extracellular and intracellular pathway. Anti-HER2 therapies have dramatically improved the prognosis of early and advanced HER2-positive breast cancer. HER2 status is the most important factor for predicting responses to anti-HER2 therapies.

Trastuzumab is a humanised monoclonal antibody, widely used for HER2-positive patients in the neo-adjuvant, adjuvant and metastatic setting. Although trastuzumab is approved as a single agent therapy it is frequently combined with chemotherapy. Trastuzumab is composed of two antigen-specific sites which bind to the juxtamembrane portion of the HER2 receptor extracellular domain (ECD: subdomain 4) and the remainder of the antibody is a human immunoglobulin (Ig) G_1 with a conserved fragment crystallisable region (Fc). Binding of trastuzumab to HER2 suppresses downstream signalling; resulting in cell cycle arrest and reduced angiogenesis (Figure 1.1). Trastuzumab recruits immune effector cells which are responsible for antibody-dependent cell-mediated cytotoxicity (ADCC), prevents HER2 ECD cleavage from forming p95HER2 and increases endocytotic HER2 receptor destruction but has a limited effect on HER2 heterodimerisation (Hudis 2007).

In the seminal phase III trial, Slamon *et al*. compared chemotherapy alone with combined chemotherapy and trastuzumab for patients receiving first line treatment for metastatic HER2-positive disease determined by IHC (Table 1.1). Patients received combination chemotherapy consisting of anthracycline (doxorubicin or

epirubicin) and cyclophosphamide or single-agent paclitaxel if they had previously received adjuvant anthracycline chemotherapy. Combining chemotherapy with trastuzumab significantly increased the median time to disease progression (7.4 months vs. 4.6 months, $p<0.001$), objective response rate (50% vs. 32%, $p<0.001$) and median survival (25.1 months vs. 20.3 months, $p=0.046$). Cardiac dysfunction assessed using the New York Heart Association criteria was higher among patients who received trastuzumab with chemotherapy compared to their counterparts who received anthracycline-cyclophosphamide alone (27% vs. 8%) and paclitaxel chemotherapy alone (13% vs. 1%) (Slamon, Leyland-Jones et al. 2001). In a subsequent study for patients receiving first line therapy for metastatic HER2-positive disease, combined docetaxel and trastuzumab increased the median time to disease progression (11.7 months vs. 6.1 months, $p=0.0001$) and median survival (31.2 months vs. 22.7 months, $p=0.325$) compared to docetaxel alone. Only 1% of patients who received docetaxel-trastuzumab experienced symptomatic heart failure (Marty, Cognetti et al. 2005).

Table 1.1 Seminal phase III anti-HER2 therapy trials in patients with advanced HER2-positive breast cancer.

Trial	Patients (n)	Treatment	Median progression-free survival (PSF) or time to progression (TTP) (p value)	Median overall survival (p value)
Trastuzumab and chemotherapy (Slamon, Leyland-Jones et al. 2001)	First line treatment for metastatic breast cancer (469)	Chemotherapy Chemotherapy + trastuzumab	4.6 months 7.4 months ($p<0.001$) TTP	20.3 months 25.1 months ($p=0.046$)
Lapatinib and capecitabine (Cameron, Casey et al. 2008)	Trastuzumab-refractory metastatic breast cancer (399)	Capecitabine Capecitabine + lapatinib	4.3 months 6.2 months ($p<0.001$) TTP	15.3 months 15.6 months ($p=0.177$)
CLEOPATRA (Baselga, Cortes et al. 2012)	First line treatment for metastatic breast cancer (808)	Pertuzumab, trastuzumab + docetaxel Placebo, trastuzumab + docetaxel	18.5 months 12.4 months ($p<0.001$) PFS	Not reported Not reported
EMILIA (Verma, Miles et al. 2012)	Trastuzumab-refractory metastatic breast cancer (991)	T-DM1 Lapatinib + capecitabine	9.6 months 6.4 months ($p<0.001$) PFS	30.9 months 25.1 months ($p<0.001$)

TTP: time from randomisation to time of progressive disease (deaths are censored).
PFS: time from randomisation to objective tumour progression or death.

In the adjuvant setting, four large randomised phase III studies have assessed combined trastuzumab with chemotherapy for HER2-positive disease; NSABP B-31, Herceptin Adjuvant (HERA), North Central Cancer Treatment Group N9831 and Breast Cancer International Research Group (BCIRG) 006 trials. The addition of one year of trastuzumab to adjuvant chemotherapy increases disease-free survival and overall survival (Piccart-Gebhart, Procter et al. 2005; Romond, Perez et al. 2005; Joensuu, Kellokumpu-Lehtinen et al. 2006; Slamon, Eiermann et al. 2011). For example, BCIRG 006 demonstrated that at a median follow up 65 months, the overall survival rate was 87% for patients who received adjuvant chemotherapy alone compared to 91-92% (p<0.05) for patients who received adjuvant trastuzumab combined with chemotherapy (Slamon, Eiermann et al. 2011). However, 2 years of adjuvant trastuzumab does not improve disease-free survival (p=0.86) and overall survival (p=0. 63) compared to 1 year of adjuvant trastuzumab (Table 1.2).

Table 1.2 Seminal phase III adjuvant trastuzumab trials in patients with HER2-positive early stage breast cancer.

Trial Name (follow up)	Patients (n)	Treatment	Disease-free survival (p value)	Overall survival (p value)
BCIRG 006 (65 months) (Slamon, Eiermann et al. 2011)	Node positive or high risk node negative (3,222)	Dox-Cyclo→ Docetaxel Dox-Cyclo→ Docetaxel-T Docetaxel-Carbo-T	75% 84% (p<0.001 vs. chemo alone) 81% (p<0.04 vs. chemo alone)	87% 92% (p< 0.001 vs. chemo alone) 91% (p=0.04 vs. chemo alone)
HERA (8 years) (Goldhirsch, Gelber et al. 2013)	Node positive or high risk node negative completed adjuvant chemotherapy (5,099)	Observation T for 1 year T for 2 years	64.8% 71.2% (p<0.0001 vs. observation) 71% (p<0.0001 vs. observation)	77.4% 82.7% (p=0.0001 vs. observation) 82.4% (p=0.0001 vs. observation)

(Carbo, carboplatin; Chemo, chemotherapy; Cyclo, cyclophosphamide; Dox, doxorubicin; T, trastuzumab)

1.2.5.2 Pertuzumab

Trastuzumab can prevent spontaneous formation of homodimers (HER2-HER2) and ligand-independent heterodimer (HER2-HER1, HER2-HER3 and HER2-HER4), by binding to subdomain 4 of the HER2 ECD but cannot prevent ligand-induced HER2 heterodimers. Pertuzumab is an IgG_1 class humanised monoclonal antibody which binds to the dimerisation domain (subdomain 2) of the HER2 ECD, blocking ligand-induced HER2 heterodimerisation, including the potent HER2-HER3 heterodimer.

Pertuzumab can also induce ADCC. (Agus, Gordon et al. 2005; Metzger-Filho, Winer et al. 2013).

In a phase III study patients with metastatic HER2-positive disease received trastuzumab and docetaxel with or without pertuzumab as first line therapy. The addition of pertuzumab increased median progression-free survival from 12.4 months to 18.5 months (p<0.001) and the interim analysis of overall survival showed a strong trend in favour of the pertuzumab treatment arm. Furthermore, the addition of pertuzumab does not adversely affect the side effect profile of chemotherapy and trastuzumab, including left ventricular dysfunction (Table 1.1) (Baselga, Cortes et al. 2012). In a phase II neo-adjuvant study, patients with early HER2-positive breast cancer who received combined pertuzumab with trastuzumab-docetaxel therapy had significantly improved pathological complete response (pCR) rates compared with patients who received trastuzumab-docetaxel therapy alone (49% vs. 31%, p=0.0141). Pertuzumab is currently being investigated in the adjuvant setting (Gianni, Pienkowski et al. 2012).

1.2.5.3 Lapatinib

Lapatinib is an oral receptor tyrosine kinase inhibitor of HER1 and HER2. It is approved for use in combination with capecitabine for trastuzumab-refractory HER2-positive metastatic breast cancer. In a phase III trial, the median time to progression was increased from 4.3 months for capecitabine alone to 6.3 months (p<0.001) with combined treatment (Table 1.1). The addition of lapatinib did not significantly improve overall survival (HR: 0.78, 95% CI: 0.55-1.12, p=0.177) but did significantly improve the overall response rate (24% vs. 14%, p=0.017) (Cameron, Casey et al. 2008).

1.2.5.4 Trastuzumab emtansine

Trastuzumab emtansine (T-DM1) is an antibody drug-conjugate which enables specific delivery to HER2 expressing cells. T-DM1 is composed of the cytotoxic anti-microtubule agent DM1, a maytansine 1 derivative conjugated with trastuzumab via the linker [*N*-maleimidomethyl]cyclohexane-1-carboxylate (MCC). On average there are 3.5 DM1 molecules conjugated to the Fc region of trastuzumab via MCC linkers (Lewis Phillips, Li et al. 2008; Krop, Beeram et al. 2010). In the EMILIA phase III

trial, T-DM1 significantly prolonged progression-free survival (9.6 vs. 6.4 months, p<0.001) and overall survival (30.9 vs. 25.1 months, p<0.001) for patients with advanced trastuzumab refractory HER2-positive metastatic disease compared to capecitabine and lapatinib combined (Table 1.1). In addition, T-DM1 had lower rates of grade 3 or 4 adverse events than combined capecitabine and lapatinib; 41% vs. 57% (Verma, Miles et al. 2012).

1.3 Molecular Imaging

Molecular imaging is defined as the visualisation, characterisation and measurement of biological processes at the molecular and cellular level (Mankoff 2007). There is a great need to develop molecular imaging in cancer medicine for HER2 and other important molecular biomarkers. Histological analysis remains vital but it is neither feasible nor safe to biopsy multiple metastatic sites in each patient. Furthermore, histology is limited by single site and single time point sampling, intra-tumour heterogeneity, tumour accessibility and tumour evolution resulting in discordance between disease relapses. Whilst conventional imaging lacks specificity and sensitivity, particularly for sub-centimetre lesions, in addition it does not inform clinical decisions regarding molecular targeted agents.

Molecular imaging potentially offers whole body, real-time information, which can evaluate expression of a molecular marker with implications for treatment and prognosis. It has the potential to enhance the sensitivity and specificity of cancer imaging.

HER2 imaging using single photon emission computed tomography (SPECT) and positron emission tomography (PET), could potentially be used to inform clinical decisions in the treatment of patients with advanced breast cancer. Firstly, HER2 imaging could be used to identify patients who were HER2-negative at the outset but become HER2-positive during follow-up and thus could benefit from anti-HER2 therapy. Secondly, it could be used to monitor patients receiving anti-HER2 therapy who develop HER2-negative disease, these patients would either require cessation of anti-HER2 therapy or additional combination therapy. The cost of anti-HER2 therapy is considerable and better methods are needed in order to inform clinical

decisions to start and stop these therapies. HER2 imaging may prove to be a cost effective way of achieving this (Goldstein, Sosabowski et al. 2013).

1.3.1 Nuclear medicine imaging modalities

SPECT and PET molecular imaging are based on the detection of radiolabelled ligands. Ideally, the physical half-life of the selected radioisotope should match the biological half-life of the ligand.

1.3.1.1 Single photon emission computed tomography

Radioisotopes used in SPECT imaging emit single gamma photons which are detected by a gamma camera. Detection of single photons provides no information about the direction of travel, so photons are filtered by a lead collimator containing small parallel holes which excludes photons that do not travel perpendicular to the detector surface. Counting events are acquired using detectors that rotate around the subject from which 3-dimensional images can be reconstructed using a computer algorithm.

1.3.1.2 Positron emission tomography imaging

The radioisotopes used in PET scanning emit positrons. Each positron combines with an electron, which then annihilate and convert into two 511 keV gamma photons which are emitted in opposite directions, 180 ± 0.5° apart. The PET camera contains a ring of oppositely paired detectors (coincidence coupled detectors) which identify the two gamma photons simultaneously (a coincidence event) and determines their direction of travel. There is therefore no need for a lead collimator and events without an equal and opposite event are excluded as scatter events.

Most cancers exhibit increased glucose metabolism, which may be partly driven by cancer growth in the presence of a strained blood supply, resulting in hypoxia. Hypoxic conditions upregulate the GLUT1 glucose transporter and stimulate anaerobic glycolysis. However, under normoxia and hypoxia, cancer cells demonstrate accelerated glucose metabolism compared to non-cancer cells, which may be partly related to hypoxia-inducible factor (HIF)-1α up-regulation and oncogenic mutations (Wahl, Herman et al. 2011).

Fluorine18-fluorodeoxyglucose (^{18}F-FDG) positron emission tomography (PET)/CT can identify tumour sites with high levels of glucose uptake and is used to image a range of solid malignancies and lymphoma. ^{18}F-FDG-PET has an established role in staging patients with potentially operable high risk breast cancer, since PET has equal sensitivity to conventional CT in detecting metastatic disease but leads to fewer false-positive results in this setting (Port, Yeung et al. 2006). Preliminary studies have not shown any convincing evidence that the maximum standardized uptake value (SUV_{max}) on ^{18}F-FDG-PET scans can distinguish between HER2-positive and HER2-negative disease in high risk operable breast cancer (Osborne, Port et al. 2010). Thus, an alternative approach is required to image HER2-positive disease.

1.3.1.3 Comparison of single photon emission computed tomography and positron emission tomography imaging

PET has a higher sensitivity than SPECT imaging by approximately two to three orders of magnitude, as PET is able to detect a higher proportion of emitted events. As discussed, SPECT rejects photons which do not approach the lead collimator at the correct angle to pass through its holes; consequently SPECT detects approximately 0.01% of emitted events. Physical collimators are not required for PET imaging, as each positron interaction with an electron, generates two photons which travel in opposite directions reaching the oppositely paired PET cameras simultaneously (coincidence detection). Consequently, approximately 1% of emitted events are detected by PET (Rahmim and Zaidi 2008).

The enhanced sensitivity of PET has important advantages compared to SPECT. PET has improved signal-to-noise ratios and higher spatial resolution (~5 mm vs. ~10 mm) (Zanzonico 2012). In addition, PET has a shorter scan acquisition time and more accurate data quantification compared to SPECT (Rahmim and Zaidi 2008).

An advantage of SPECT is that its radiotracers typically have longer half-lives than PET tracers. Thus, SPECT can be used to analyse slower biological processes, such as the localisation of monoclonal antibodies to tumours which can take several days (Wahl, Herman et al. 2011).

1.3.2 HER2 molecular imaging

A range of immunoglobulins, immunoglobulin-derivatives and non-immunoglobulin binding proteins have been investigated for HER2 molecular imaging (Table 1.3). Assessed immunoglobulin-derivatives include fragment antigen binding (Fab) regions of antibodies, diabodies which are composed of non-covalent single chain fragment variable (scFv) dimers and nanobodies consisting of a solitary heavy chain (Figure 1.2). Non-immunoglobulin binding proteins developed for HER2 imaging include affibody molecules (Figure 1.3) and designed ankyrin repeat proteins (Figure 1.5).

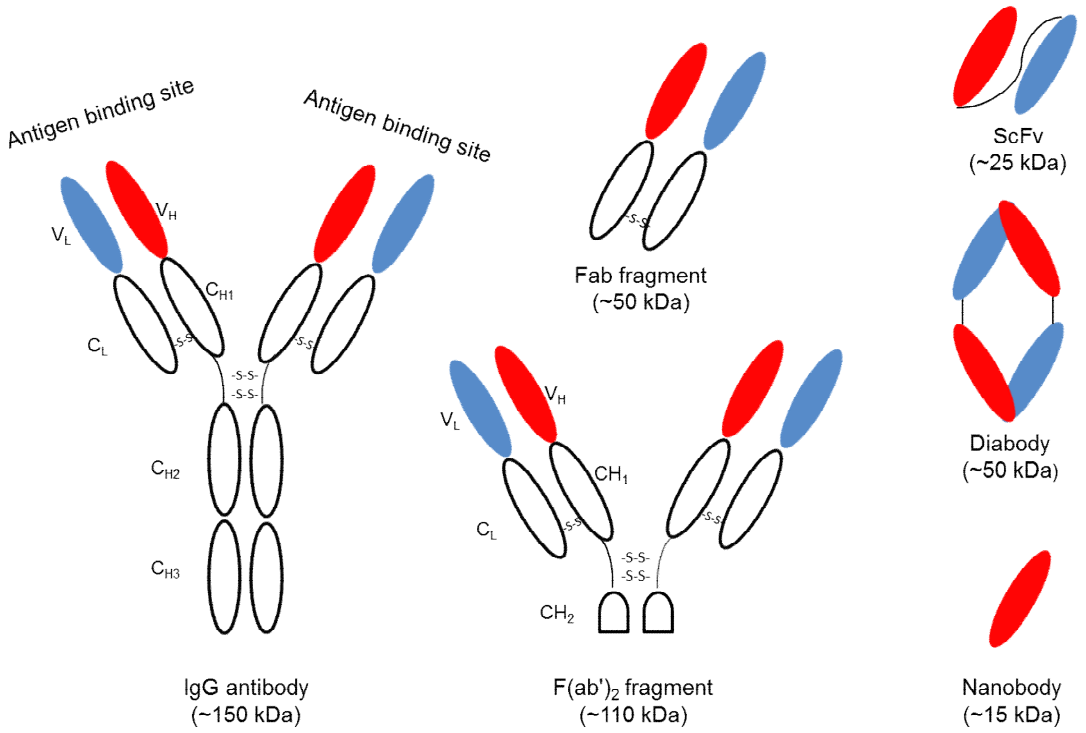

V: variable region, C: constant region, L: light chain , H: heavy chain, S-S: disulphide bond, scFv single-chain fragment variable

Figure 1.2 IgG antibody and its derivatives; fragment antigen binding (Fab) regions, F(ab')$_2$, diabody and nanobody with their approximate molecular weights.

The properties of the 'ideal' radioligand for molecular imaging; include the ability to reach the tumour site(s) rapidly, efficient extravasation, good tissue penetration, high affinity for the target and high specificity for the tumour. Meanwhile unbound ligand should be rapidly excreted from the bloodstream with limited hepatic uptake,

facilitating high contrast images and reducing the time between infusion and optimal image acquisition (Table 1.4).

Table 1.3 Human HER2 imaging trials in advanced breast cancer.

Imaging agent	Imaging modality	No. of patients & characteristics	No. patients all tumours identified by HER2 imaging	New lesions identified	Limitations
Copper-64 Trastuzumab (Mortimer, Bading et al. 2013)	PET	8 metastatic and HER2-positive patients	Unknown Overall 89% of all lesions identified at 2 days post Copper-64 Trastuzumab Comparator: ^{18}F-FDG PET and CT	None	-Lower sensitivity than ^{18}F-FDG-PET (93%) -Incomplete whole body imaging -Difficulty visualising lymph nodes
Zirconium-89 Trastuzumab (Dijkers, Oude Munnink et al. 2010)	PET	14 metastatic & HER2-positive patients	6 of 12 patients (50%) who received sufficient doses Comparator: CT, MRI & Bone scan	2 patients with brain lesions, confirmed by MRI	-Low Sensitivity -No biopsies to confirm specificity
Indium-111 Trastuzumab (Perik, Lub-De Hooge et al. 2006)	SPECT	17 recruited (15 assessed) metastatic & HER2-positive	Unknown Overall 45% of all known tumour lesions identified & only 1 patient no tumour lesions identified. Comparator: routine staging including CT	13 patients new lesions identified (but none biopsied)	-Low Sensitivity -No biopsies to confirm specificity
Gallium-68 F(ab')2-trastuzumab (Beylergil, Morris et al. 2013)	PET	15 metastatic patients, including HER2-positive (n=8) & HER2-negative (n=7)	0 of 8 HER2-positive patients, including 4 HER2+ patients no lesions identified Among the 7 HER2-negative patients no lesions identified. Comparator: ^{18}F-FDG-PET	None	-Low sensitivity and not confirmed by biopsies.
1st generation affibody molecule (ABY-002) with Indium-111 and Gallium-68 (Baum, Prasad et al. 2010)	SPECT (Indium-111) and PET (Gallium-68)	3 metastatic & HER2-positive patients	1 of 3 patients. -Patient 1: 4 of 5 known lesions -Patient 2: 0 of 2 known lesions -Patient 3: 5 of 5 known lesions Comparator :^{18}F-FDG PET/CT.	Chest wall lesion (not biopsied) Sartorius muscle lesion (biopsy, HER2 IHC score 2+)	-High background liver & kidney uptake
2nd generation affibody molecule (ABY-025) with Indium-111 (Sorensen, Sandberg et al. 2014)	SPECT	7 metastatic patients, including HER2-positive (n=5) & HER2-negative (n=2) primary disease	2 of 7 patients	None	-24/4h tumour uptake ratio to determine HER2 status requires scans over 2 days

Table 1.4 Pharmacokinetic and physical properties of an 'ideal' radioligand for molecular imaging.

Stages	'Ideal' pharmacokinetics and physical properties
Extravascular accumulation	Efficient extravasation
	Good tissue penetration
Tumour identification	High tumour affinity
	High tumour specificity
	High tumour retention
Biodistribution	Low normal tissue retention
Excretion	Rapid clearance from bloodstream & whole body

1.3.3 Antibody based imaging

IgG molecules have high affinity for target antigens and ideal pharmacokinetics for therapeutic applications. Their long half-life limits application for molecular imaging. As sufficient blood clearance is required to achieve optimal tumour-to-blood ratios prior to imaging but during this time interval tumour uptake can fall. Furthermore, their large molecular weight (150 kDa) results in low tumour penetration (Figure 1.2). Radiolabelled trastuzumab and pertuzumab have been investigated in pre-clinical imaging studies and radiolabelled trastuzumab has been tested in clinical imaging trials (Table 1.3).

Antibody based single photon emission computed tomography

Trastuzumab radiolabelled with indium-111 (^{111}In; half-life 2.8 days) via diethylenetriamine penta-acetic acid (DTPA) has been developed for clinical SPECT imaging. ^{111}In-DTPA-trastuzumab has high stability, high labelling yields, high immunoreactivity and maintains the internalisation properties of trastuzumab (Lub-de Hooge, Kosterink et al. 2004).

In mice xenografts, ^{111}In-DTPA-trastuzumab uptake was significantly higher in mice bearing HER2-positive tumours from the human ovarian cancer cell line, SKOV3, than in mice bearing HER2-negative tumours from the human small cell lung cancer cell line, GLC4. At 48 h, ^{111}In-DTPA-trastuzumab HER2-positive tumour uptake peaked at 16.30±0.64 percent of the injected radioactive dose per gram of tissue (% ID/g), while for HER2-negative tumours it was 4.40±0.70 % ID/g (p<0.001). ^{111}In-

DTPA-trastuzumab was cleared slowly from blood, so the tumour-to-blood ratio was <3 over 48 h and the tumour-to-blood ratio only reached 6 at 168 h. In addition, the liver, kidneys and spleen had high ^{111}In-DTPA-trastuzumab uptake. Interestingly, HER2-positive metastases had higher uptake than their corresponding HER2-positive primary tumours in mouse xenografts (Lub-de Hooge, Kosterink et al. 2004). In breast cancer xenografts, corrected ^{111}In-DTPA-trastuzumab tumour uptake can differentiate between HER2 IHC scores 0 to 3+, provided circulating radioactivity and non-specific antibody localisation are taken into consideration. The uncorrected ^{111}In-DTPA-trastuzumab tumour uptake was associated with a tumour response to trastuzumab in mouse xenografts (McLarty, Cornelissen et al. 2009).

A clinical trial, assessed 15 patients with metastatic HER2-positive breast cancer receiving paclitaxel and trastuzumab by ^{111}In-DTPA-trastuzumab SPECT scanning (5 mg, 100-150 MBq) during the first and twelfth week of their treatment (Table 1.3). Planar whole body imaging using a two headed gamma camera was performed at five time points over 7 days post-administration of ^{111}In-DTPA-trastuzumab. ^{111}In-DTPA-trastuzumab SPECT imaging identified 45% of tumour lesions seen by conventional imaging and one patient had no visible lesions on HER2 scanning. For most patients more tumour lesions were visualised on HER2 scans performed during the first week of treatment than after 12 weeks of paclitaxel and trastuzumab. For 13 patients, lesions not previously identified by conventional scanning were identified by HER2 SPECT scans performed during the first week of treatment but no biopsies were performed to assess the HER2 status of the new lesions (Perik, Lub-De Hooge et al. 2006).

In the absence of biopsies from lesions seen on conventional imaging but not detected on HER2 SPECT scans and vice versa, it is not possible to assess the accuracy of ^{111}In-DTPA-trastuzumab SPECT scanning. The assumed low detection rate (45%) could be due to limitations in identifying small tumours. It could also reflect the unsuitable pharmacokinetics of antibodies for imaging, including low tumour-to-blood ratios which limit the identification of tumour sites even at later imaging time points. (Perik, Lub-De Hooge et al. 2006).

In pre-clinical tests, ^{111}In-DTPA-pertuzumab SPECT scans detected HER2 down regulation following trastuzumab therapy. In mice bearing HER2-positive tumours (MDA-MB-361), ^{111}In-DTPA-pertuzumab tumour uptake decreased 2-fold after three days of trastuzumab and 4.5-fold after three weeks of trastuzumab compared to phosphate buffered saline (PBS) treated controls. Following three weeks of trastuzumab, the decreased ^{111}In-DTPA-pertuzumab uptake was associated with reduced HER2 expression and elimination of tumour cells assessed by IHC. If down regulation of HER2 detected by ^{111}In-DTPA-pertuzumab SPECT imaging correlates with clinical response then it could be used as an early predictor of trastuzumab response and non-responders could commence an alternative therapy sooner (McLarty, Cornelissen et al. 2009).

Antibody based positron emission tomography

Antibody based PET imaging requires positron emitters with a relatively long half-life to enable image acquisition several days post-infusions, when tumour-to-blood ratios reach sufficiently high levels for scanning. Zirconium-89 (^{89}Zr; half-life 3.3 days) radiolabelled trastuzumab has been developed for HER2 PET imaging, as its half-life enables imaging up to 7 days post-infusion. The radiolabelling efficiency after conjugation with the succinylated derivative of desferrioxamine B (*N*-SucDf) chelating group and ultrafiltration was 98.1±1.1 %, similar to that achieved with ^{111}In-DTPA-trastuzumab. ^{89}Zr-trastuzumab was stable *in vitro* for up to 7 days, had preserved high binding for HER2-positive cells (SKOV3) and low binding for HER2-negative cells (GLC4) (Dijkers, Kosterink et al. 2009).

The biodistribution of ^{89}Zr-trastuzumab and ^{111}In-trastuzumab were compared in HER2-positive (SKOV3) and HER2-negative (GLC4) tumour bearing mice. Both radioligands achieved significantly higher uptake in the HER2-positive tumours than HER2-negative tumours at day 1 and by day 6 the differences between HER2-positive and HER2-negative tumour radioligand uptake were even greater. For ^{89}Zr-trastuzumab and ^{111}In-trastuzumab blood levels (%ID/g) fell by over 3-fold from day 1 to day 6, resulting in optimal tumour-to-blood and tumour-to-normal tissue ratios 6 days post-administration. For both ^{89}Zr-trastuzumab and ^{111}In-trastuzumab, the liver and spleen had the highest normal tissue uptake (Dijkers, Kosterink et al. 2009).

^{89}Zr-trastuzumab HER2 PET imaging has been used to assess changes in HER2 expression of SKOV3 tumour bearing mice treated with NVP-AUY922, a heat shock protein 90 (Hsp90) inhibitor, since HER2 down regulation is a potential biomarker for early response. MicroPET imaging demonstrated a 41% reduction in ^{89}Zr-trastuzumab tumour uptake after NVP-AUY922 therapy. The PET scan results were confirmed by *ex vivo* ^{89}Zr-trastuzumab biodistribution and HER2 IHC staining (Oude Munnink, Korte et al. 2010).

The ^{89}Zr-trastuzumab PET trial recruited 14 patients with HER2-positive metastatic breast cancer to determine the optimal dosage and timing for imaging (Table 1.3). Patients received 37 MBq of ^{89}Zr-trastuzumab intravenously and were tested in three cohorts. Trastuzumab-naïve patients received 10 mg (cohort 1, n=2) or 50 mg (cohort 2, n=5), while patients receiving concomitant trastuzumab received 10 mg (cohort 3, n=7). Each dose consisted of ^{89}Zr-trastuzumab (~1.5 mg) and non-radioactive trastuzumab (~8.5 or 48.5 mg). Each patient had a PET scan at an early time point (1-3 days) and later time point (4-7 days) post ^{89}Zr-trastuzumab administration (Dijkers, Oude Munnink et al. 2010).

For trastuzumab-naïve patients, 10 mg trastuzumab produced sub-optimal tumour imaging with a low blood pool, high liver uptake and enhanced intestinal excretion, probably due to rapid hepatic clearance. However, 50 mg trastuzumab administered to naïve patients resulted in lower liver uptake, lower intestinal excretion, prolonged serum pooling and reasonable tumour-to-non-tumour ratios. Trastuzumab has dose-dependent pharmacokinetics, as its terminal half-life is extended by increased trastuzumab exposure, possibly due to saturable elimination of low doses from circulation, thus supporting this finding. Serum HER2 ECD levels can fall during trastuzumab therapy and the authours' hypothesised that HER2 ECD could have bound to the administered trastuzumab in treatment-naïve patients, resulting in enhanced hepatic clearance. However, serum HER2 ECD levels were not measured to confirm this (Leary, Hanna et al. 2009; Dijkers, Oude Munnink et al. 2010).

For patients receiving concomitant trastuzumab the 10 mg trastuzumab dose was adequate as it was associated with slow serum clearance. The optimal time to perform ^{89}Zr-trastuzumab PET scans was at 4-5 days post-administration, as there

was time for blood clearance and there was sufficient tumour uptake, resulting in good tumour-to-non-tumour ratios (Dijkers, Oude Munnink et al. 2010).

Although cohorts 2 and 3 had sufficient ^{89}Zr-trastuzumab in circulation, in six of these twelve patients ^{89}Zr-trastuzumab PET did not detect all known tumour lesions. Liver lesions were not visualised in three of the seven patients with known liver metastases, including two patients in cohort 2 and one patient in cohort 3. Bone lesions were not visualised in two of the nine patients with known bone metastases, both patients were in cohort 3. Three patients had known lung metastases (all in cohort 3) which were only detected in one patient by ^{89}Zr-trastuzumab PET scanning. Yet, brain metastases were identified in three patients; this was a new finding for two patients, subsequently confirmed by MRI brain scans. The mean relative uptake value (RUV_{mean}) was highest in liver metastases which was significantly higher than the normal liver, 12.8±5.8 vs. 5.9±2.4, p=0.007. In addition, RUV_{mean} for brain metastases and bone metastases were significantly higher than their normal surrounding tissue (Dijkers, Oude Munnink et al. 2010).

No biopsies were performed in the study, so the level of HER2 expression required for ^{89}Zr-trastuzumab tumour uptake on PET imaging is unknown. In the absence of biopsies, it is unclear whether the relatively low rate of HER2 tumour detection (50% for cohort 2 and 3 combined) was due to variable HER2 tumour expression or limitations of ^{89}Zr-trastuzumab PET imaging (Dijkers, Oude Munnink et al. 2010).

Recently, a study treated metastatic breast cancer patients (HER2-positive or oestrogen receptor-positive) with weekly intravenous NVP-AUY922. For HER2-positive patients (n=5), the percentage change in SUV_{max} of lesions assessed by ^{89}Zr-trastuzumab PET scans at baseline and after 3 weeks of treatment, positively correlated with the percentage change in size of lesions on CT scans at baseline and after 8 weeks of treatment. Thus, early changes on ^{89}Zr-trastuzumab PET could potentially predict treatment response (Gaykema, Schroder et al. 2014).

Copper-64 (^{64}Cu, half-life 12.8 h) conjugated with 1,4,7,10-tetraazacyclododecane-1,4,7,10-tetraacetic acid (DOTA) to trastuzumab for PET imaging was used to assess eight patients with HER2-positive metastatic disease, the patients had not received anti-HER2 therapy for ≥ 4 months. An initial ^{18}F-FDG-PET/CT scan was

performed to localise tumour sites, defining the axial coverage for ^{64}Cu-DOTA trastuzumab PET scanning, to overcome the constraints of the short half-life of ^{64}Cu. Two patients received 5 mg ^{64}Cu-DOTA trastuzumab but following the publication by Dijkers *et al*. all subsequent patients received 45 mg non-radiolabelled trastuzumab immediately before ^{64}Cu-DOTA trastuzumab to reduce non-specific liver uptake (Dijkers, Oude Munnink et al. 2010; Mortimer, Bading et al. 2013).

^{64}Cu-DOTA trastuzumab had a sensitivity of 89% for all CT detected tumour lesions at 2 days post-administration, compared to 93% for ^{18}F-FDG-PET. Inter-patient and intra-patient heterogeneity of ^{64}Cu-DOTA trastuzumab tumour uptake was observed, if this reflected genuine differences in HER2 tumour expression then it could have a role in selecting patients for anti-HER2 therapy. Non-radiolabelled trastuzumab reduced liver uptake by 75-80% and increased blood pooling, enabling visualisation of all liver lesions at 2 days post-administration. In the absence of patients with HER2-negative disease, the specificity of ^{64}Cu-DOTA trastuzumab imaging is unknown and based on this study alone it has no advantage over ^{18}F-FDG-PET (Mortimer, Bading et al. 2013). Furthermore, the long half-life of trastuzumab limits the ability of ^{64}Cu-DOTA trastuzumab to identify lesions in areas with high blood activity such as the mediastinum (Mortimer, Bading et al. 2013; Tamura, Kurihara et al. 2013).

1.3.4 Antibody fragments

Radiolabelled fragment antigen binding (Fab) regions of trastuzumab have been developed for HER2 imaging, since their lower molecular weight is associated with a shorter circulatory half-life, which results in the faster clearance of background radiation. Potentially, this enables both scanning at earlier time points when tumour uptake levels are highest and shorter intervals between scans (Figure 1.2).

Single photon emission computed tomography with antibody fragments

Among six patients with HER2-positive in situ or invasive ductal carcinoma who received ^{111}In-DTPA-trastuzumab Fab (50 kDa) prior to breast-conserving surgery, SPECT scans failed to identify any of the breast tumours. The excised tumours had low counts of radiation. Although the resection margins had higher radiation counts, this did not correlate with the presence of tumour at the margins. Thus, ^{111}In-DTPA-trastuzumab Fab was not reliable in the detection of HER2-positive in situ or invasive ductal carcinoma at the resection margin (Holloway, Scollard et al. 2013).

To improve the biodistribution and tumour uptake of Fab, Dennis *et al.* assessed a bifunctional molecule, AB.Fab4D5 which can simultaneously bind to HER2 and albumin. Histological assessment revealed tumour AB.Fab4D deposition in HER2-positive tumour bearing mice from 2 to 24 h. By contrast, the trastuzumab derived Fab, Fab4D5 had only transient tumour uptake at 2 h, while trastuzumab only achieved significant tumour uptake at 24 h. On SPECT/CT scans of HER2-positive tumour bearing mouse xenografts, ^{111}In-AB.Fab4D5 achieved higher tumour uptake at most time points over 48 h than either ^{111}In-Fab4D5 or ^{111}In-trastuzumab. As expected, the association between AB.Fab4D5 and albumin reduced its renal secretion compared to Fab4D5. Despite this encouraging pre-clinical study there have been no recent updates (Dennis, Jin et al. 2007).

Positron emission tomography with antibody fragments

A F(ab')$_2$ fragment of trastuzumab (~110 kDa) conjugated with DOTA has been radiolabelled with gallium-68 (^{68}Ga; half-life 1.14 h) for PET imaging. In pre-clinical studies, microPET imaging with ^{68}Ga-DOTA-F(ab')$_2$-trastuzumab identified decreases in HER2 tumour expression 24 h after administration of an Hsp90 inhibitor (Smith-Jones, Solit et al. 2004). Furthermore, in mice bearing HER2-positive human breast tumours (BT474), ^{68}Ga-DOTA-F(ab')$_2$-trastuzumab PET imaging identified HER2 down-regulation associated with Hsp90 inhibition prior to changes in glycolysis seen on ^{18}F-FDG-PET scanning (Smith-Jones, Solit et al. 2004; Smith-Jones, Solit et al. 2006).

Beylergil *et al*. performed ^{68}Ga-DOTA-F(ab')$_2$-trastuzumab PET scans on 15 patients with metastatic HER2-positive (n=8) and HER2-negative (n=7) breast cancer who had avid disease on ^{18}F-FDG-PET scanning. The study population included trastuzumab-naïve patients (n=8), patients receiving concomitant trastuzumab (n=3) and patients who had previously received trastuzumab (n=4) (Table 1.3). There were no significant adverse events related to ^{68}Ga-DOTA-F(ab')$_2$-trastuzumab. Although the half-life of the radioligand was short, 3.6 ± 0.9 h, there was high background radiation uptake in the liver, blood and kidneys (Beylergil, Morris et al. 2013). Among the eight HER2-positive patients, four patients had no visible lesions on ^{68}Ga-DOTA-F(ab')$_2$-trastuzumab PET scans and ^{68}Ga-DOTA-F(ab')$_2$-trastuzumab PET imaging failed to identify all lesions among the other four patients. The radioligand failed to identify any tumours in four of the five patients who were HER2-positive and either trastuzumab-naïve or had not received trastuzumab for ≥ 2 months. There was no tumour uptake among the assessed HER2-negative patients. It is likely that the short half-life of ^{68}Ga (1.14 h) is not compatible with DOTA-F(ab')$_2$-trastuzumab (half-life ~4h) and a radioisotope which enables imaging at later time points is required. Based on these results this approach lacks sensitivity for routine clinical use, even among patients who are not receiving concomitant trastuzumab. (Beylergil, Morris et al. 2013).

1.3.5 Anti-HER2 Diabody

Diabodies are non-covalent single chain fragment variable (scFv) dimers, which can be formed by producing scFv molecules with amino acid chain linkers between their variable light (V_L) and variable heavy (V_H) chains (Figure 1.2). The V_H from one molecule associates with the V_L from another molecule and vice versa, this creates a functional scFv capable of binding to two antigens simultaneously (Perisic, Webb et al. 1994).

C6.5 diabody for single photon emission computed tomography and positron emission tomography

The C6.5 diabody (C6.5db) is derived from the human anti-HER2 scFV, C6.5 (Adams, Schier et al. 1998). C6.5db specifically targets HER2 and its linkers between V_L and V_H chains are five amino acids in length. It has a low molecular

weight (52 kDa), resulting in first pass renal clearance and short half-life of 6.4 h in circulation (Robinson, Shaller et al. 2008). C6.5db can be produced in *Pichia pastoris* (*P. pastoris*) or *Escherichia coli* (*E. coli*), P-C6.5db and E-C6.5db, respectively (Miller, Doss et al. 2012).

E-C6.5db radiolabelled with iodine-124 (^{124}I, half-life 4.2 days) identified HER2-positive SKOV3 tumours in mouse xenografts on PET scanning from 4 h post-administration. At 24 and 48 h the tumour-to-blood ratios for ^{124}I-E-C6.5db were 6.7 and 13.4, respectively. By contrast, for mice bearing HER2-negative MDA-MB-468 tumours, the tumour and blood levels of ^{124}I-E-C6.5db were equivalent (Robinson, Doss et al. 2005). ^{125}I-E-C6.5db tumour uptake has been shown to vary with HER2 expression levels, in xenografts with SKOV3 (1 X 10^6 HER2/cell, IHC 3+) and MDA-MB-231 (2.3 X 10^4 HER2/cell, IHC 0) tumours, the uptake was 1.91% ID/g and 0.31% ID/g at 24 h post-infusion, respectively (Reddy, Shaller et al. 2011).

Both direct iodination of the tyrosine residues (non-residualising) and water soluble Bolton-Hunter reagent sulfosuccinimidyl-3-(4-hydroxyphenyl)propionate (SHPP, partially residualising) methods were used for ^{124}I radiolabelling. ^{124}I-E-C6.5 and ^{124}I-E-SHPP-C6.5 degraded after binding and internalisation of HER2, leading to low tumour retention of radioiodine and accumulation in normal tissues that expressed the sodium-iodide symporter e.g. thyroid, salivary glands and stomach, which could obscure tumour uptake (Robinson, Doss et al. 2005).

Expression of recombinant proteins in *P. pastoris* can result in glycosylation with branched mannose sugar structures. ^{125}I-P-C6.5db is glycosylated and this resulted in faster systemic clearance and lower tumour uptake compared to ^{125}I-E-C6.5db which is not glycosylated. In SKOV3 tumour bearing xenografts, ^{125}I-P-C6.5db and ^{125}I-E-C6.5db had similar tumour-to-blood ratios at 48 h post-infusion, 36.7 and 29.5 respectively, as ^{125}I-P-C6.5db serum levels were significantly lower than ^{125}I-E-C6.5db. PET imaging of mice bearing HER2-positive tumours with ^{124}I-P-C6.5db and ^{124}I-E-C6.5db, demonstrated high background liver, bladder, thyroid and stomach uptake. ^{124}I-P-C6.5bd had greater liver uptake between 24 and 120 h than ^{124}I-E-C6.5db due to its glycosylation status (Miller, Doss et al. 2012).

In vitro, pertuzumab and C6.5db compete with each other for HER2 binding, while trastuzumab and C6.5db appear to be able to bind to the HER2 receptor simultaneously. Yet, in SKOV3 and BT474 xenografts mice pre-treated with trastuzumab prior to ^{125}I-E-C6.5db injection, there was decreased HER2-positive tumour uptake compared to rituximab (anti-CD20 IgG) pre-treated controls at 24 h post injection (42% decrease for SKOV3 and 60% decrease for BT474 tumour xenografts vs. rituximab pre-treatment). This decrease in ^{125}I-E-C6.5db tumour uptake did not correlate with a change in gross tumour size or loss of HER2 expression on IHC post-trastuzumab (Reddy, Shaller et al. 2011). Since the C6.5db is unable to bind to HER2 in the presence of trastuzumab and pertuzumab, it has not been developed for clinical application.

Anti-HER2 diabody derived from trastuzumab for positron emission tomography

An anti-HER2 diabody derived from trastuzumab was radiolabelled with fluorine-18 (^{18}F, half-life 109.7 min) by reaction with its lysine residues, using N-succinimidyl-4-[^{18}F]fluorobenzoate ([^{18}F]SFB). In mouse xenografts, the mean uptake for HER2-positive breast tumours (MCF-7) was only 2.87% ID/g and 1.0% ID/g for HER2-negative rat glioma tumours (C6) at 6 h post administration. There was high background uptake in the kidneys and bladder. At 6 h post administration, the tumour-to-blood ratios was only 1.7 and tumour-to-liver ratio was 5.5. On microPET scanning, there was uptake in HER2-positive and HER2-negative tumours at 4 h but higher uptake in the HER2-positive tumour. The low HER2-positive tumour uptake and or retention are likely to limit ^{18}[F]SFB-anti-HER2 diabody clinical development (Olafsen, Sirk et al. 2012).

1.3.6 Nanobodies

Nanobodies arise from *Camelidae* antibodies and are the smallest naturally derived antigen binding fragments. They contain a functional heavy chain without an associated light chain and their molecular weight is approximately 15 kDa (Figure 1.2). The anti-HER2 nanobody, 2Rs15d specifically binds to HER2 recombinant protein and HER2 expressing cells with low nanomolar affinities. Furthermore,

2Rs15d does not compete with trastuzumab and pertuzumab for HER2 binding (Vaneycken, Devoogdt et al. 2011) .

Nanobodies for single photon emission computed tomography imaging

SPECT imaging of mice xenografts with HER2 expressing tumours (SKOV3) by ^{99m}Tc-2Rs15d-His_6, which incorporates a hexahistidine tag (His_6) for radiolabelling, demonstrated rapid renal clearance resulting in low blood levels (0.26±0.03% ID/g at 1.5 h post infusion). The pharmacokinetics was in keeping with other low molecular weight hydrophilic proteins. There was low accumulation in non-target organs except the kidneys (154.7±17.7% ID/g at 1.5 h post infusion). The normal liver uptake was reasonably low at 1.5 h post infusion, 0.72±0.14% ID/g. The tumour uptake was 4.19±0.47% ID/g at 1.5 h post injection resulting in a tumour-to-blood ratio of 16.4±3.6 (Vaneycken, Devoogdt et al. 2011; Xavier, Vaneycken et al. 2013).

Nanobodies for positron emission tomography imaging

The HER2 nanonbodies, 2Rs15d and 2Rs15d-His_6 were conjugated via 1,4,7-triazacyclononane-1,4,7-triacetic acid (NOTA) for ^{68}Ga radiolabelling. At 1 h post administration to rat tumour xenografts, both ^{68}Ga-NOTA-2Rs15d-His_6 and ^{68}Ga-NOTA-2Rs15d had moderate HER2-positive tumour uptake (SKOV3) 3.13±0.06% ID/g and 4.34±0.90% ID/g, respectively, yet had low uptake in HER2-negative tumours (MDA-MB-435D). In SKOV3 tumour bearing rats, ^{68}Ga-NOTA-2Rs15d had considerably lower kidney uptake than ^{68}Ga-NOTA-2Rs15d-His_6; 45.00±11.42% ID/g vs. 116.67±1.83% ID/g but similar uptake in the liver and other assessed organs. In urine, only intact ^{68}Ga-NOTA-nanobody was detected confirming good stability. Absence of the C-terminal His_6 tag lowers renal retention, possibly due to the charge effects exerted by imidazole groups within the histidine residues. On PET/CT scanning of rat xenografts with ^{68}Ga-NOTA-2Rs15d, there was high uptake in SKOV3 tumours but no uptake in MDA-MB-435D tumours at 1 h post administration. Besides, high uptake in the kidneys and bladder, uptake in other normal organs was low. ^{68}Ga-NOTA-2Rs15d is currently being developed for clinical imaging (Xavier, Vaneycken et al. 2013).

Nanobodies for radio-immunotherapy

2Rs15d-His_6 radiolabelled with the lutetium-177 (^{177}Lu) using bifunctional chelators is being developed for HER2-positive breast cancer radio-immunotherapy. Pre-clinical studies demonstrated high uptake in HER2 expressing tumours with low background activity except for high kidney uptake. 2Rs15d-His_6 radiolabelled with ^{177}Lu via a DTPA based chelator was able to achieve high tumour-to-blood ratios in SKOV3 mouse xenografts, which peaked at 1264±53 24 h post-infusion, while tumour uptake in HER2-negative mouse xenografts was negligible (D'Huyvetter, Aerts et al. 2012). This approach can only be developed for clinical application if renal uptake can be minimised.

1.3.7 Affibody molecules targeting HER2

Affibody molecules are small (6-7 kDa) non-immunoglobulin binding proteins which provide an alternative to antibody-based constructs. They are based on a 58 amino acid Z-domain scaffold, that are derived from the B domain of staphylococcal surface protein A (Nilsson, Moks et al. 1987; Orlova, Magnusson et al. 2006). They form a three-helix bundle protein which lack cysteines (Figure 1.3). Large combinatorial libraries of affibody molecules have been generated by randomising 13 amino acids within the ligand binding domain and phage display is used to select affibody molecules which bind to desired target proteins (Nord, Gunneriusson et al. 1997). The affibody molecule $Z_{HER2:342}$, specifically binds to HER2 with picomolar affinity (K_D = 22 pmol/L) and was developed for HER2 imaging (Orlova, Magnusson et al. 2006). $Z_{HER2:342}$ can be site specifically radiolabelled for imaging without affecting *in vivo* HER2 tumour binding and HER2 binding is not compromised by the presence of trastuzumab (Orlova, Tolmachev et al. 2007).

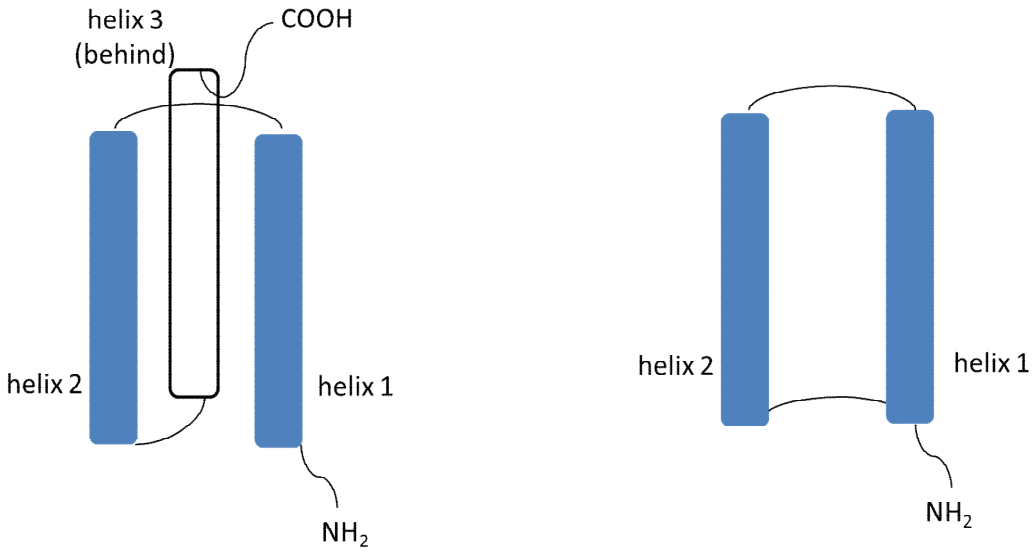

Figure 1.3 Three-helix affibody molecule and two-helix protein scaffold (blue helices are involved in HER2 receptor binding).

1.3.7.1 Pre-clinical development of affibody molecule based positron emission tomography

To compare the potential of $Z_{HER2:342}$ and trastuzumab for HER2 PET imaging, they were radiolabelled with ^{124}I using *p*-iodobenzoate (PIB) as a linker. In some experiments ^{125}I-PIB was used as an analogue for ^{124}I-PIB. Both ^{125}I-PIB-trastuzumab and ^{125}I-PIB-$Z_{HER2:342}$ specifically bound to HER2 expressing cells *in vitro* and specifically identified HER2 expressing tumours *in vivo*. ^{125}I-PIB-trastuzumab was rapidly taken up by HER2 expressing cells, while ^{125}I-PIB-$Z_{HER2:342}$ remained on the cell surface for longer and consequently was degraded at a slower rate. In mouse xenografts with HER2-positive tumours, ^{125}I-PIB-trastuzumab had higher tumour uptake than ^{124}I-PIB-$Z_{HER2:342}$ over 72 h but ^{124}I-PIB-$Z_{HER2:342}$ achieved higher tumour-to-normal tissue ratios at most time points in the blood, liver and lungs due to faster blood clearance. Pre-administration of non-radiolabelled trastuzumab did not alter ^{124}I-PIB-$Z_{HER2:342}$ HER2-positive tumour uptake *in vivo*, while pre-administration of non-radiolabelled $Z_{HER2:342}$ reduced ^{124}I-PIB-$Z_{HER2:342}$ tumour uptake; confirming receptor-specific tumour uptake. On PET scanning, ^{124}I-PIB-$Z_{HER2:342}$ achieved superior tumour-to-normal tissue contrast at 6 h than ^{124}I-PIB-trastuzumab could achieve at 72 h post administration (Orlova, Wallberg et al. 2009). This study demonstrated that for molecular imaging, small high affinity proteins have advantages over whole antibodies.

^{68}Ga-DOTA-$Z_{HER2:342}$ PET and ^{111}In-DOTA-$Z_{HER2:342}$ SPECT imaging have been compared pre-clinically. DOTA-$Z_{HER2:342}$ was efficiently radiolabelled with ^{68}Ga (>95%) and maintained specific HER2 binding *in vitro* and *in vivo*. In mice bearing HER2-positive tumours (SKOV3), ^{68}Ga-DOTA-$Z_{HER2:342}$ and ^{111}In-DOTA-$Z_{HER2:342}$ achieved similar tumour uptake at 2 h, 12.4±3.8% ID/g and 15.2±4.8% ID/g, respectively. However, ^{68}Ga-DOTA-$Z_{HER2:342}$ achieved a higher tumour-to-blood ratio at 2 h than ^{111}In-DOTA-$Z_{HER2:342}$ (31±13 vs. 17±6) due to faster clearance (Tolmachev, Velikyan et al. 2010). In SKOV3 xenografts, ^{68}Ga-DOTA-$Z_{HER2:342}$ PET scans at 2 h and ^{111}In-DOTA-$Z_{HER2:342}$ SPECT scans after 24 h demonstrated specific tumour targeting. Thus, ^{68}Ga-DOTA-$Z_{HER2:342}$ could potentially enable convenient same day HER2 PET scanning (Tolmachev, Velikyan et al. 2010).

Cheng *et al.* assessed a commercially available HER2 targeting affibody, $Z_{HER2:477}$, in both its monomeric ($Z_{HER2:477}$) and dimeric form $(Z_{HER2:477})_2$. The affibody molecules were site specifically radiolabelled with the positron emitter, ^{64}Cu at a C-terminal cysteine via maleimido-mono-amide DOTA. In HER2-positive tumour (SKOV3) bearing mice, ^{64}Cu-DOTA-$Z_{HER2:477}$ achieved much higher tumour uptake and higher tumour-to-blood ratios than its dimeric counterpart. Consequently, ^{64}Cu-DOTA-$Z_{HER2:477}$ achieved superior images of SKOV3 tumour bearing mice on PET imaging due to lower background radiation. In mice bearing both the melanoma tumour, MDA-MB-435 and HER2-positive ovarian tumour, SKOV3, only the SKOV3 tumours were visible with the radiolabelled monomeric and dimeric HER2 affibody molecules. However, pre-treatment of SKOV3 tumour bearing mice with trastuzumab, prevented visualisation of tumours on ^{64}Cu-DOTA-$Z_{HER2:477}$ PET scanning over 24 h, which could limit future clinical application (Cheng, De Jesus et al. 2010).

Following confirmation that the smaller monomeric affibody molecule is superior to its dimeric counterpart, Ren *et al.* developed a smaller 2-helix affibody, MUT-DS by truncating one of the three α-helices which is not involved in receptor recognition (Figure 1.3) (Ren, Zhang et al. 2009). ^{64}Cu-DOTA-MUT-DS identified HER2 expressing SKOV3 tumours in mouse xenografts and achieved reasonable tumour-to-blood and tumour-to-muscle ratios, 3.05 and 3.48 at 1 h post infusion, respectively. The smaller MUT-DS affibody needs to be compared with the intact

three helical affibody to determine whether the smaller size translates into improved clearance and tumour uptake (Ren, Zhang et al. 2009; Ren, Webster et al. 2012).

$Z_{HER2:342}$ has been radiolabelled with ^{18}F, by conjugation with N-2-(4-[^{18}F]fluorobenzamido)ethyl]maleimide ([^{18}F]FBEM) at a C-terminal cysteine for PET imaging (Kiesewetter, Kramer-Marek et al. 2008). [^{18}F]FBEM-$Z_{HER2:342}$ PET imaging of mice bearing HER2-positive tumours (SKOV3), demonstrated tumour uptake at 20 min (SUV = 2.4) which was maintained for at least 2 h (SUV = 3.43) post infusion. Liver and kidney uptake was high for the first hour and gradually fell, so the optimal time for imaging was 1 h post injection. These imaging results were confirmed by biodistribution studies (Kramer-Marek, Kiesewetter et al. 2008).

In mouse xenografts, [^{18}F]FBEM-$Z_{HER2:342}$ has been used to assess HER2 expression and changes in expression following Hsp90 inhibitor administration. PET scans with [^{18}F]FBEM-$Z_{HER2:342}$ were performed on five different mouse xenograft models with varying levels of HER2 tumour expression. [^{18}F]FBEM-$Z_{HER2:342}$ rapidly accumulated in HER2-positive tumours and achieved high tumour-to-blood and tumour-to-muscle ratios within 20 min of administration. The tumour tracer uptake on PET scanning correlated with Western blotting, ELISA and IHC (HercepTest). Following Hsp90 inhibition of two HER2-positive mice xenograft models (MCF7/clone18 and BT474) tracer uptake on PET scanning decreased by 33% and 71% compared to pre-treatment levels, respectively. Although *ex vivo* analysis of treated tumours with ELISA and Western blotting confirmed significant HER2 down regulation, the BT474 tumours maintained a score of 3+ after Hsp90 inhibitor treatment on the HercepTest. The ^{18}F radiolabelled affibody may have a potential future role in monitoring changes in HER2 expression following treatment (Kramer-Marek, Kiesewetter et al. 2009).

1.3.7.2 Pre-clinical development of affibody molecule based single photon emission computed tomography

Technetium-99m (^{99m}Tc; half-life 6.02 h) is suitable for SPECT imaging due to its favourable photon energy (140 keV), low cost, low dose burden and wide availability. ^{99m}Tc radiolabelling of the affibody molecule can be performed at an N-terminal His_6 tag (^{99m}Tc-His_6-$Z_{HER2:342}$-C) or at an inserted C-terminal cysteine residue (^{99m}Tc-$Z_{HER2:342}$-C). Both methods achieved radiolabelling yields >90%. In

HER2-positive tumour bearing xenografts, ^{99m}Tc-His$_6$-Z$_{HER2:342}$-C demonstrated rapid and specific tumour visualisation on SPECT scanning. Furthermore, ^{99m}Tc-Z$_{HER2:342}$-C has lower background liver uptake which has clear advantage over ^{99m}Tc-His$_6$-Z$_{HER2:342}$-C for HER2 SPECT imaging (Ahlgren, Wallberg et al. 2009).

1.3.7.3 Clinical assessment of the first generation HER2 binding affibody molecule

Baum *et al.* conducted the first clinical study of Z$_{HER2:342-pep2}$ (ABY-002, peptide synthesis in a single chemical process) (Table 1.3). Three patients with metastatic HER2-positive breast cancer who had been recently staged with a CT or ^{18}F-fluorodeoyglucose (^{18}F)-FDG PET/CT scan, received ^{111}In-DOTA-Z$_{HER2:342-pep2}$ for SPECT imaging and/or ^{68}Ga-DOTA-Z$_{HER2:342-pep2}$ for PET imaging. The five administrations (3 patients received ^{68}Ga-DOTA-Z$_{HER2:342-pep2}$ and 2 patients received ^{111}In-DOTA-Z$_{HER2:342}$) were well tolerated. Radiolabelled Z$_{HER2:342-pep2}$ demonstrated rapid blood clearance; the first half-life of ^{111}In-DOTA-Z$_{HER2:342-pep2}$ was 4-11 min and 10-14 min for ^{68}Ga-DOTA-Z$_{HER2:342-pep2}$. This enabled high contrast SPECT and PET scans 2-3 h post injection (Baum, Prasad et al. 2010).

For one patient, ^{111}In-DOTA-Z$_{HER2:342-pep2}$ SPECT imaging detected four out of five metastatic sites identified by ^{18}F-FDG PET/CT, including a latissimus dorsi metastasis, that was subsequently excised confirming an IHC score of 3+ (HercepTest). A patient receiving concomitant trastuzumab had a ^{111}In-DOTA-Z$_{HER2:342-pep2}$ SPECT scan and ^{68}Ga-DOTA-Z$_{HER2:342-pep2}$ PET scan within 24 h of each other, both scans identified all five hyper-metabolic areas seen on a ^{18}F-FDG PET/CT scan, including a sartorius muscle lesion. The sartorius muscle lesion was reported as inflammatory or metastatic on ^{18}F-FDG PET/CT scanning, a muscle biopsy confirmed metastatic breast cancer with heterogeneous HER2 expression on the HercepTest (mean IHC score 2+). For the same patient, the ^{68}Ga-DOTA-Z$_{HER2:342-pep2}$ PET scan identified a lesion in the right anterolateral chest wall which was not seen by any other imaging modality, however it was not biopsied (Baum, Prasad et al. 2010).

There was high background kidney and liver uptake of the radiolabelled DOTA-Z$_{HER2:342-pep2}$, consequently a liver metastasis and a lesion adjacent to the kidney (possible lymph node or adrenal metastasis) identified by ^{18}F-FDG PET/CT could

not be visualised with the affibody scan. In addition, a mediastinal lymph node seen on ^{18}F-FDG PET/CT was not visualised with the radiolabelled affibody (Baum, Prasad et al. 2010).

1.3.7.4 Effect of tags on the biodistribution of the HER2 binding affibody molecule

Attempts have been made to reduce affibody molecule normal liver uptake, to enable visualisation of HER2-positive liver metastases. It is known that chelators at the N-terminal domain which are positively charged and lipophilic, increase hepato-biliary excretion (Tran, Engfeldt et al. 2007). Conventionally, $Z_{HER2:342}$ has an N-terminal His_6 tag (His_6-$Z_{HER2:342}$), which facilitates purification by immobilised metal ion affinity chromatography (IMAC) and labelling with $[^{99m}Tc(CO)_3]^+$ but is associated with increased hepatic radioactivity uptake (Hofstrom, Orlova et al. 2011; Hofstrom, Altai et al. 2013).

$Z_{HER2:342}$ was produced with an N-terminal negatively charged and hydrophilic histidine-glutamate $(HE)_3$ tag, to improve biodistribution and maintain purification by IMAC. $(HE)_3$-$Z_{HER2:342}$ retained specific binding to HER2 expressing cells. Biodistribution studies were performed in non-tumour bearing mice with $(HE)_3$-$Z_{HER2:342}$, His_6-$Z_{HER2:342}$ and $Z_{HER2:342}$-His_6 site specifically radiolabelled with ^{111}In, ^{125}I or ^{99m}Tc at a C-terminal cysteine. The three constructs had similar normal tissue biodistribution profiles, except $(HE)_3$-$Z_{HER2:342}$ had lower liver uptake for ^{111}In and ^{99m}Tc radiolabelling. ^{111}In-$(HE)_3$-$Z_{HER2:342}$ had 5.7-fold lower liver uptake than ^{111}In-His_6-$Z_{HER2:342}$ and ^{99m}Tc-$(HE)_3$-$Z_{HER2:342}$ had 19-fold lower liver uptake than ^{99m}Tc -$Z_{HER2:342}$-His_6. The three ^{125}I-radiolabelled constructs had similar liver uptake, as the liver is involved in metabolism and excretion of iodine radionuclides (Hofstrom, Orlova et al. 2011).

Ten variants of $Z_{HER2:342}$ with different histidine-based tags, $(HX)_3$, positioned at the N- and C-terminus that altered charge and lipophilic properties of the affibody molecules were labelled with $[^{99m}Tc(CO)_3]^+$ and assessed in non-tumour bearing mice. For $Z_{HER2:342}$ radiolabelled with $[^{99m}Tc(CO)_3]^+$, liver uptake is enhanced by positive charge and lipophilic properties. The N-terminal positioning of the $(HX)_3$-tags appeared to have a greater effect on liver uptake than C-terminal positioning. The $Z_{HER2:342}$ with a $(HE)_3$ tag was the only hydrophilic and negatively charged

construct. $(HE)_3$-$Z_{HER2:342}$ had lowest uptake in the liver and spleen with similar uptake in the other assessed organs as the other constructs (Hofstrom, Altai et al. 2013).

Consequently, a second generation affibody molecule, $Z_{HER2:2891}$-Cys (ABY-025) was produced by substituting 11 amino acids within the non-HER2 binding surface, resulting in increased hydrophilicity as well as improved chemical and thermal stability (Feldwisch, Tolmachev et al. 2010). ^{111}In-DOTA-ABY-025 achieved similar tumour uptake in HER2-positive (SKOV3) tumour bearing mice as the first generation affibody molecule assessed in the clinical trial (^{111}In-DOTA-$Z_{HER2:342-pep2}$), 11±3% ID/g vs. 14±1% ID/g. However, the second generation affibody molecule with increased hydrophilicity ^{111}In-DOTA-ABY-025 had similar liver uptake as the first generation affibody molecule ^{111}In-DOTA-$Z_{HER2:342-pep2}$, 1.7±0.7% ID/g and 1.7±0.3% ID/g, respectively (Ahlgren, Orlova et al. 2010).

1.3.7.5 Clinical assessment of the second generation HER2 binding affibody molecule

In a first in human clinical trial, ^{111}In-DOTA-ABY-025 was safe and well tolerated by seven patients with metastatic breast cancer, including patients who had had HER2-positive (n=5) and HER2-negative (n=2) primary disease. The five patients with HER2-positive primary disease were receiving concomitant trastuzumab at the time of assessment. On SPECT scanning, HER2-positive tumour uptake increased between 4 and 24 h, while HER2-negative tumour uptake was generally lower and decreased between 4 and 24 h. The decay-corrected 24/4h tumour uptake ratio could discriminate between HER2-negative and HER2-positive lesions. Furthermore, the discriminatory capacity of this ratio was confirmed by IHC of biopsied lesions. Interestingly, a patient who had had HER2-positive primary disease had HER2-negative metastatic disease based on the 24/4h tumour uptake ratio, this finding correlated with seven biopsies taken from metastatic sites which were all HER2-negative on IHC (Sorensen, Sandberg et al. 2014).

Despite having high kidney uptake, ^{111}In-DOTA-ABY-025 is able to image HER2-positive adrenal metastases and can also cross the blood brain barrier to identify HER2-positive brain metastases. ^{111}In-DOTA-ABY-025 was capable of imaging liver metastases, by contrast $Z_{HER2:342-pep2}$ (ABY-002) radiolabelled with ^{68}Ga and ^{111}In was

unable to image liver metastases in the previous clinical trial (Baum, Prasad et al. 2010; Sorensen, Sandberg et al. 2014). ^{111}In-DOTA-ABY-025 SPECT scanning appears to be safe and capable of assessing HER2 status in patients with advanced breast cancer but the 24/4h tumour uptake ratio requires scans at 4 and 24 h which is inconvenient for patients (Sorensen, Sandberg et al. 2014).

The therapeutic potential of HER2-binding affibody molecules is being investigated with a variant that contains a C-terminal peptide-based chelator for radiolabelling ($Z_{HER2:V2}$). HER2 binding affibody molecules are rapidly internalised by the kidneys and slowly internalised by HER2-positive cells. Affibody molecules radiolabelled with residualising radio-isotopes have high radioisotope retention in the kidneys, limiting their therapeutic application. However, for affibody molecules radiolabelled with non-residualising radio-isotopes, rapid affibody molecule internalisation in the kidneys leads to rapid clearance of the non-residualising radioisotope in urine. Radiolabelling $Z_{HER2:V2}$ with the non-residualising radio-isotope rhenium-188 (^{188}Re, half-life 17.0 h), has demonstrated high uptake in HER2-positive tumours, without exceeding toxicity limits in the kidneys and bone marrow. Thus, ^{188}Re-$Z_{HER2:V2}$ directed radiotherapy may be suitable for investigation in patients (Altai, Wallberg et al. 2014).

1.3.8 Designed ankyrin repeat proteins

Designed ankyrin repeat proteins (DARPins) are non-immunoglobulin scaffolds, composed of naturally occurring ankyrin repeat proteins which are evolutionary conserved (Bork 1993). DARPins have a range of properties which justify their investigation for molecular imaging in cancer.

Ankyrin repeat proteins have been identified throughout the cellular compartments, bound to the cellular membrane and can also be secreted from cells (Sedgwick and Smerdon 1999). Ankyrin repeat proteins are among the most commonly found binding proteins within the human genome (Lander, Linton et al. 2001). For example, ankyrin repeat proteins form part of the human red cell membrane network and ankyrin-1 gene mutations are the most common cause of the red cell membrane disorder, hereditary spherocytosis in Europe and the United States (Da Costa, Galimand et al. 2013).

1.3.8.1 Structure of designed ankyrin repeat proteins

Each ankyrin repeat usually consists of 33 amino acids, which form a β-turn followed by two anti-parallel α-helices and a loop reaching to bind to the β-turn of the next ankyrin repeat (Sedgwick and Smerdon 1999; Kobe and Kajava 2000). Ankyrin repeat proteins usually consist of four to six repeats (Tamaskovic, Simon et al. 2012). They mediate protein-protein interactions with a vast range of protein targets and consequently have a wide variety of biological functions. Each ankyrin repeat contributes to target binding, which results in high target affinities (Malek, Huxford et al. 1998; Sedgwick and Smerdon 1999). The scaffold structure of ankyrin repeats is highly versatile and repeats can be duplicated, deleted and re-arranged to alter target protein binding (Figure 1.4) (Kobe and Kajava 2000).

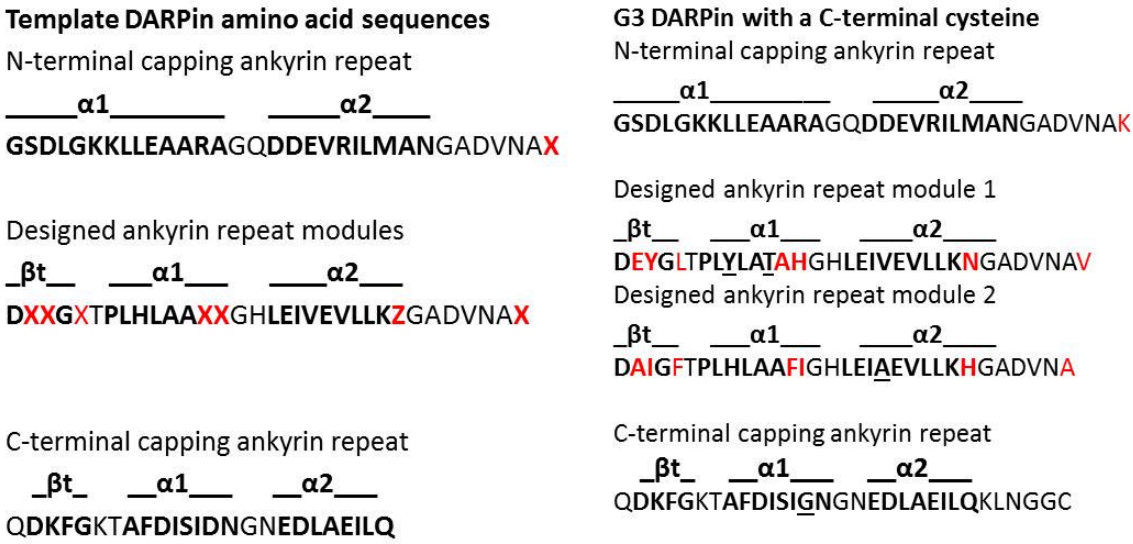

Figure 1.4 Template amino acid sequences of the N-terminal capping ankyrin repeat, designed ankyrin repeat module and C-terminal capping ankyrin repeat, besides the G3 DARPin amino acid sequences.
The secondary structure components are shown above their respective sequences, the amino acid sequences forming the α-helices and β turns are emboldened. The designed ankyrin repeat modules usually consist of 26 defined framework residues, 6 randomised potential interaction residues (X, any of the 20 natural amino acids, except cysteine, glycine or proline) and 1 randomised framework residue (Z, usually asparagine-N, histidine-H or tyrosine-Y). The G3 DARPins amino acid sequence is shown besides the template sequences. The G3 has four mutations at defined framework positions which are underlined. Adapted from (Tamaskovic, Simon et al. 2012).

Consensus design was used to determine the designed ankyrin repeat consensus sequence. Consensus design is based on the principle that functionally important residues, including residues which maintain protein folding are usually conserved, while residues involved in specific target interaction are not conserved (Forrer, Binz et al. 2004). This process involved the alignment of multiple naturally occurring ankyrin repeat proteins to produce a designed ankyrin repeat module consisting of fixed framework residues and randomised potential interaction residues, which were used as the template to produce DARPins (Binz, Amstutz et al. 2004). Each designed ankyrin repeat module consists of 26 defined framework residues, 6 non-conserved randomised target interaction residues and 1 randomised framework residue (usually either asparagine, histidine or tyrosine) (Figure 1.4). Thus, to extend the diversity of the combinatorial library, 7 residues can be randomised to alter the target interaction of the designed ankyrin repeat modules (Binz, Stumpp et al. 2003).

Hydrophilic N-terminal (N) and C-terminal (C) capping ankyrin repeats are used to shield the hydrophobic core of the stacked randomised ankyrin proteins (Figure 1.5). Originally the N-capping and C-capping repeats were based on naturally occurring proteins (Binz, Stumpp et al. 2003; Kohl, Binz et al. 2003). However, a new C-capping repeat based on the consensus sequence has been introduced since it results in greater thermal resistance (Interlandi, Wetzel et al. 2008). The theoretical diversity of ankyrin repeat modules with seven randomised positions is 7.2×10^7 per module (Binz, Stumpp et al. 2003). Thus, the theoretical diversity of the N2C and N3C DARPin libraries are $(7.2 \times 10^7)^2 = 5.2 \times 10^{15}$ and $(7.2 \times 10^7)^3 = 3.8 \times 10^{23}$, respectively (Binz, Stumpp et al. 2003).

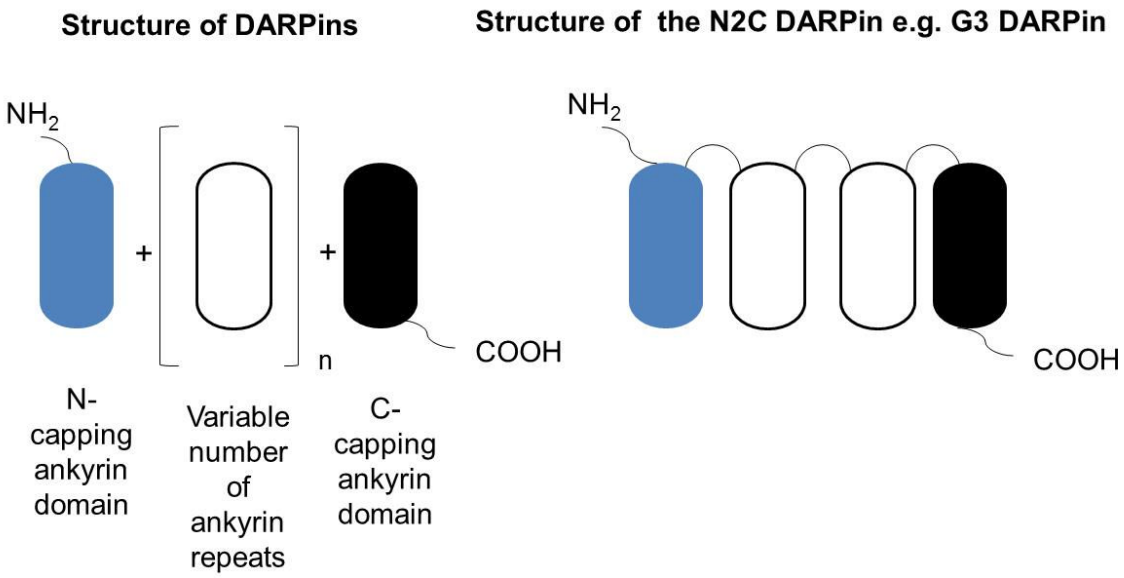

Figure 1.5 Schematic representation of DARPin library generation.
Assembly consists of an N-terminal capping ankyrin repeat (blue), varying the numbers of designed ankyrin repeat modules (white) and a C-terminal capping ankyrin repeat (black), producing combinatorial DARPin libraries with different repeat numbers. The structure of an N2C DARPIN e.g. G3 is shown on right side. Adapted from (Goldstein, Sosabowski et al. 2013).

1.3.8.2 Properties of designed ankyrin repeat proteins

DARPins are cysteine-free and can be expressed in soluble form in the cytoplasm of *E. coli* at very high levels (Binz, Stumpp et al. 2003). They are also soluble and stable under physiological conditions (Binz, Stumpp et al. 2003). They exhibit high thermo-stability which is greater than naturally occurring ankyrin repeats, which may be due to extended H-bond networks (Mosavi, Williams et al. 2002; Kohl, Binz et al. 2003). DARPins have a low molecular weight, 14-15 kDa and 17-18 kDa for N2C and N3C, respectively (Binz, Stumpp et al. 2003). Using ribosome display, DARPins have been selected which bind to targets with high affinity, up to the picomolar range (Binz, Amstutz et al. 2004; Zahnd, Wyler et al. 2007).

1.3.8.3 Designed ankyrin repeat proteins targeting HER2

From DARPin libraries, ribosome display was used to select DARPins which bind to the HER2 ECD. Ribosome display is an *in vitro* method which enables selection of polypeptide binders from large libraries. The ribosome display selected DARPins, then underwent extensive HER2 binding studies (Zahnd, Pecorari et al. 2006). The G3 DARPin which consists of an N-terminal capping repeat with a His_6 tag, two

internal designed ankyrin repeat modules and a C-terminal capping repeat had the highest affinity for HER2 (90 pmol/L) assessed by surface plasmon resonance (SPR) which was maintained when assessed on HER2-positive, BT474 cells (~60-100 pmol/L) (Zahnd, Wyler et al. 2007; Zahnd, Kawe et al. 2010). The G3 DARPin has four mutations at framework positions leading to enhanced affinity compared to the consensus framework variant (Figure 1.4) (Zahnd, Wyler et al. 2007).

The G3 DARPin and trastuzumab bind to adjacent but non-overlapping epitopes of subdomain 4 of the HER2 ECD so do not compete for HER2 binding; this has been determined by both structural modelling of the protein-protein interactions and *in vitro* investigation (Epa, Dolezal et al. 2013). Pertuzumab binds to subdomain 2 of the HER2 ECD, so it can bind in the presence of the G3 DARPin.

1.3.8.4 G3 DARPin assessment of HER2 tumour status

The G3 DARPin with an engineered AviTag for enzymatic biotinylation has been developed for assessment of HER2 protein expression in tissues. Comparison of the FDA-approved Ventana HER2 IHC and DARPin-histochemistry, correlated by FISH has been performed on 793 primary breast cancer tissue microarrays. There was a strong correlation between amplification status measured by FISH with both DARPin-histochemistry and Ventana IHC (p<0.0001, each). The G3 DARPin and Ventana antibody detect HER2 amplification status determined by FISH with similar sensitivities, 98.9% and 96.6%, respectively, however the G3 DARPin has significantly higher specificity (98.6 vs. 96.2%, p=0.0005) (Theurillat, Dreier et al. 2010).

1.3.8.5 Bispecific DARPin incorporating the G3 DARPin for anti-HER2 therapy

Although the G3 DARPin in isolation exerts no biological effects, attaching the G3 DARPin (binds subdomain 4 of HER2 ECD) with a DARPin that binds to subdomain 1 via a short linker, results in a bispecific DARPin that has greater cytotoxicity than trastuzumab against HER2-positive breast cancer cell lines *in vitro*. The bispecific DARPin binds to two membrane-bound HER2 molecules, distorting them so they cannot form dimers, thus preventing intracellular signalling (Jost, Schilling et al. 2013).

1.3.8.6 G3 DARPin single photon emission computed tomography imaging

In non-tumour bearing BALB/c mice, the G3 DARPin had a half-life of less than 3 min and this short half-life was maintained in HER2-positive tumour bearing mice. *In vivo*, there may be an additional slow phase of clearance for 5% of the G3 DARPin which has a half-life of 80-90 min. The G3 DARPin is predominantly eliminated by the kidney and to a lesser extent by the liver. By contrast, attachment of polyethylene glycol (PEG) to the DARPin increased hepatic excretion, prolonging its half-life (Zahnd, Kawe et al. 2010).

In mice bearing HER2 expressing SKOV3 tumours, the G3 DARPin had high levels of tumour uptake, 9.12±1.77% ID/g at 1 h and 6.46±0.96% ID/g at 24 h post-administration. Due to rapid systemic clearance high tumour-to-blood ratios were obtained at 1 h (12.67±3.34), which increased at 48 h (71.78±26.62). The G3 DARPin penetrates the whole tumour mass relatively evenly, with only slightly increased staining at the tumour rim. However, tumour-to-liver ratios are less than 2 over 48 h, which may limit identification of liver metastases. PEG-G3 DARPin had slower tumour accumulation and slower clearance from the bloodstream, resulting in lower tumour-to-blood ratios, 10.77 ± 4.37 at 48 h (Zahnd, Kawe et al. 2010).

A whole body SPECT/CT scan was performed on mice with SKOV3 tumours who received either ^{99m}Tc-G3 DARPin (555 MBq) or ^{99m}Tc-PEG-G3 DARPin (555MBq), directly radiolabeled at the N-terminal His_6 tag. Both DARPins demonstrated high accumulation of radioactivity within the HER2-positive tumours. There was significantly less radioactivity in the kidneys of the mouse injected with ^{99m}Tc-PEG-G3 DARPin, as PEG increased hepatic excretion rates (Zahnd, Kawe et al. 2010). The G3 DARPin has not been investigated in human studies. Although the pre-clinical data is encouraging for the non-PEG format, there are concerns regarding its background liver uptake.

1.4 Aims

The principal aim of the research was to develop pre-clinical G3 DARPin HER2 SPECT and PET imaging, for subsequent assessment within a first-in-human trial, which will recruit patients with advanced metastatic HER2-positive breast cancer.

This work involved testing a series of hypotheses which formed important milestones in the translation from pre-clinical to clinical investigation of the G3 DARPin.

1. Purified G3 DARPins can be produced with and without histidine based N-terminal tags by a *P. pastoris* production platform.

2. N-terminus histidine-based tags affect normal tissue uptake of the G3 DARPin.

3. The G3 DARPin radiolabelled with indium-111 and iodine-123/125 can achieve high tumour-to-blood and high tumour-to-normal tissue ratios for pre-clinical HER2 SPECT imaging.

4. The G3 DARPin can be radiolabelled with gallium-68 for pre-clinical HER2 PET imaging.

5. The unconjugated G3 DARPin is well tolerated by HER2 transgenic and non-transgenic mice.

Chapter 2 Materials and Methods

2.1 Materials

2.1.1 Suppliers

Table 2.1 List of suppliers.

Company name	Company address
American Type Culture Collection	Manassas, Virginia, United States
Amresco	Solon, Ohio, United States
Anachem	Luton, United Kingdom
Baxter	Berkshire, United Kingdom
Beckman Coulter (UK)	High Wycombe, United Kingdom
Becton Dickinson	Oxford, United Kingdom
Bioline Reagents	London, United Kingdom
Biometra	Göttingen, Germany
Bio-Rad Laboratories	Hemel Hempstead, Hertfordshire, United Kingdom
Bioscan	Poway, California, United States
Biosera	Boussens, France
Charles River	Erkrath, Germany
Chematech	Dijon, France
Covidien	Netherlands
Dako	Ely, Cambridgeshire, United Kingdom
DNA Technologies	Leuven, Belgium
Eckert & Ziegler	Berlin, Germany
Elkay Laboratory Products (UK)	Hampshire, United Kingdom
EMP Genetech	Ingolstadt, Germany
Eppendorf UK	Cambridge, United Kingdom
Fisher Scientific	Loughborough, United Kingdom
GE Healthcare	Buckinghamshire, United Kingdom
Generon	Maidenhead, Berkshire, United Kingdom
Genetic Research Instrumentation	Essex, United Kingdom
GenScript	Piscataway, New Jersey, United States
GraphPad Software	La Jolla, California, United States
Greiner bio-one	Frickenhausen, Germany
Harlan Laboratories	Wyton, United Kingdom
IBM	Armonk, New York, United States
Innovative Research of America	Sarasota, Florida, United States
Integrated DNA Technologies	Leuven, Belgium
Leica Biosystems Newcastle	Newcastle Upon Tyne, United Kingdom
Life Technologies	Paisley, United Kingdom
LKB Instruments	Mount Waverley, Victoria, Australia
Lucigen	Wisconsin, United States
Macrocyclics	Dallas, Texas, United States
Marvel	Dublin, United Kingdom
Merck Millipore	Billerica, Massachusetts, United States
Nalgene	Derbyshire, United Kingdom
New England BioLabs	Hitchin, Hertfordshire, United Kingdom

NuSep	Wasserburg, Germany
PAA Laboratories	Yeovil, Somerset, United Kingdom
Pall Life Science	Portsmouth, United Kingdom
PerkinElmer	Llantrisant, United Kingdom
Pharmacia	United Kingdom
Pioneer Research Chemicals	Colchester, Essex, United Kingdom
Proxcys Downstream Biosystems	Nieuw-Amsterdam, Netherlands
Promega	Southampton, United Kingdom
Qiagen	Crawley, West Sussex, United Kingdom
Roche Diagnostics	Burgess Hill, United Kingdom
Sartorius Stedim	Epsom, Surrey, United Kingdom
Scivis	Göttingen, Germany
Sequani	Ledbury, Herefordshire, United Kingdom
Siemens Preclinical Solutions	Knoxville, Tennessee, United States
Sigma-Aldrich	St. Louis, Missouri, United States
Syngene	Cambridge, United Kingdom
Teklab	County Durham, United Kingdom
The Jackson Laboratory	Bar Harbor, Maine, United States
Thermo Scientific	Runcorn, Cheshire, United Kingdom
Tree Star	Ashland, Oregon, United States
UCL Advanced Diagnostics	London, United Kingdom
UCL Cancer Institute	London, United Kingdom
Varian	Palo Alto, California, United States
Ventana Medical Systems	Tucson, Arizona, United States
Waters Corporation	Milford, Massachusetts , United States
Whatman	Maidstone, Kent, United Kingdom

2.1.2 Buffers, media and solutions

A 0.2 µm 500 ml polyethersulfone (PES) filter unit (Nalgene) was used to filter sterilise deionised water (dH_2O), buffers and solutions as required. The composition of buffers, media and solution not described in the main text are outlined below.

Table 2.2 Buffers for protein and nucleic acid manipulation (x; times concentration).

Buffers	Composition
PCR	
dNTP (deoxyribose nucleoside triphosphates, concentration 10 mM)	-10 µl of each dNTP: dATP, dGTP, dCTP & dTTP, concentration 100 mM (Life Technologies) -60 µl dH_2O
Master mix for G3 DARPin DNA PCR	For 8.5 ml final volume: -1 ml 10x PCR Buffer (Life Technologies) -1 ml of dNTPs concentration 10 mM (Life Technologies). -6.5 ml dH_2O

Agarose Gel Electrophoresis	
Tris-acetate-EDTA (TAE) stock (50x)	2 M Tris-acetate, 0.05 M EDTA: -242 g Tris Base -57.1 ml glacial acetic acid -100 ml of 0.5 M EDTA (pH 8.0) solution -Made up to 1L with dH_2O.
TAE (1x)	0.04 M Tris-acetate, 0.001 M EDTA
DNA loading buffer (10x)	For 20 ml volume -6.25 ml of dH_2O -0.025 g of Xylene cyanol -0.025 g of Bromophenol Blue -1.25 ml of 10% SDS -12.5 ml of glycerol
New England BioLabs 1kb DNA Ladder	40 µl dH_2O, 10 µl 6x Blue Loading Dye (provided), 10 µl DNA Ladder
Promega 1kb DNA ladder	40 µl dH_2O , 10 µl 6x Blue Loading Dye (provided), 10 µl DNA Ladder
DNA Molecular Weight Marker IX (Roche)	80 µl dH_2O, 10 µl 10x Blue Loading Dye, 10 µl DNA Ladder
Bioline HyperLadder I (BioLine)	Purchased in ready to use form
Digestion of PCR Product and Plasmid with XbaI and XhoI	
NEBuffer 4 (10x) (New England BioLabs)	50 mM potassium acetate, 20 mM tris-acetate, 10 mM magnesium acetate, 1 mM dithiothreitol, pH 7.9 at 25 °C (purchased in this form)
Purified BSA (bovine serum albumin) (New England BioLabs)	20mM KPO_4, 50 mM NaCl, 0.1 mM EDTA, 5% glycerol, pH 7.0 at 25 °C (purchased in this form)
XbaI (New England BioLabs)	Concentration 100,000 units/ml
XhoI (New England BioLabs)	Concentration 100,000 units/ml
Ligation of PCR Product and Plasmid	
T4 DNA ligase reaction buffer (10x) (New England BioLabs)	50 mM Tris-HCl, 10 mM $MgCl_2$, 1 mM ATP, 10 mM dithiothreitol, pH 7.5 at 25 °C (purchased in this form)
Linearisation of Plasmid/DARPin DNA prior to transformation	
NEBuffer 4 (10x) (New England BioLabs)	50 mM potassium acetate, 20 mM Tris-acetate, 10 mM magnesium acetate, 1 mM dithiothreitol pH 7.9 at 25 °C (purchased in this form)
QIAGEN Plasmid Kit	
Qiagen Buffer P1 (re-suspension)	50 mM Tris·Cl, pH 8.0, 10 mM EDTA,100 µg/ml RNase A (purchased in this form)
Qiagen Buffer P2 (lysis)	200 mM NaOH, 1% SDS (w/v) (purchased in this form)
Qiagen Buffer P3 (neutralisation)	3.0 M potassium acetate, pH 5.5 (purchased in this form)
Qiagen Buffer QBT (equilibration)	750 mM NaCl; 50 mM MOPS, pH 7.0; 15% isopropanol (v/v); 0.15% Triton X-100 (v/v) (purchased in this form)
Qiagen Buffer QC (wash)	1.0 M NaCl, 50 mM MOPS, pH 7.0,15%

	isopropanol (v/v) (purchased in this form)
Qiagen Buffer QF (elution)	1.25 M NaCl, 50 mM Tris-Cl, pH 8.5,15% isopropanol (v/v) (purchased in this form)
SDS PAGE Electrophoresis	
2x SDS-PAGE reducing buffer (final concentration) 4x has approximately one-third higher concentration of components to achieve the same overall concentration with the protein sample	To make 50 ml, add 2 g SDS (4% w/v), 5 ml ß-Mercaptoethanol (10% v/v), 10 ml glycerol (20%), 100 mg bromophenol blue (0.02% w/v), 10 ml 0.5 M Tris pH 6.8 (0.1 M), 25 ml dH_2O
2x SDS-PAGE non-reducing buffer (final concentration) 4x has approximately one-third higher concentration of components to achieve the same overall concentration with the protein sample	To make 50 ml, add 2 g SDS (4% w/v), 10 ml glycerol (20% v/v), 100 mg bromophenol blue (0.02% w/v), 10 ml 0.5 M Tris pH 6.8 (0.1 M), 30 ml dH_2O.
SDS-PAGE running buffer (10x)	10 g SDS, 30.3 g Tris-base, 144 g glycine and add dH_2O to make up to 1L
SDS-PAGE running buffer (1x)	100 ml 10x SDS-PAGE running buffer and 900 ml dH_2O Final concentration 25mM Tris, 192mM glycine, 0.1 % (w/v) SDS
Protein Transfer Buffer (10x)	30.3 g Tris-base and 144 g glycine made up to 1L with dH_2O
Protein Transfer Buffer (1x)	100 ml 10x Protein Transfer Buffer, 200 ml methanol, 700 ml dH_2O (Final concentration 25mM Tris-base, 192mM glycine, 20% (v/v) Methanol)
Western blot analysis	
Solution to visualise protein bands (final concentration)	10 mg 3,3′-Diaminobenzidine tetrahydrochloride (DAB) hydrate ≥ 96% (0.25 mg/ml), 20 µl hydrogen peroxide (0.5 µl/ml) in 40 ml dH_2O
Coomassie staining	
Coomassie stain (final concentration)	1.25 g coomassie brilliant blue (0.25% w/v), 50 ml glacial acetic acid (10% v/v), 150 ml methanol (30% v/v) and 300 ml dH_20.
Destain	200 ml glacial acetic acid (10% v/v), 600 ml methanol (30% v/v) and 1.2 L dH_20
Wizard SV Gel and PCR Clean-Up System (Promega)	
Membrane Binding Solution	4.5 M guanidine isothiocyanate, 0.5M potassium acetate (pH 5.0) (purchased in this form)
Membrane Wash Solution (after 95% ethanol added)	10 mM potassium acetate (pH 5.0), 80% ethanol,16.7 µM EDTA (pH 8.0) (purchased in this form)

Table 2.3 Media and plates for bacterial growth.

Media	Composition
Low Salt LB Medium (with or without Zeocin)	Add dH_2O to 10 g tryptone (1% w/v), 5 g sodium chloride (NaCl) (0.5% w/v) and 5 g Yeast Extract (0.5% w/v) so that volume reaches 1 litre. The pH should be 7. Autoclave. Add 0.25 ml of 100 mg/ml Zeocin (25 µg/ml), once the temperature has cooled to ~55 °C.
Low Salt LB Agar Plates with Zeocin	Add dH_2O to 10 g tryptone (1% w/v), 5 g sodium chloride (NaCl) (0.5% w/v), 5 g Yeast Extract (0.5% w/v) and 15 g agar (1.5% w/v) so that volume reaches 1 litre. Autoclave. Add 0.25 ml of 100 mg/ml Zeocin (25 µg/ml), once the temperature has cooled to ~55 °C. Pour into 10 cm petri plates. Let the plates harden, then invert, and store at 4 °C.

Table 2.4 Media and plates for yeast growth.

Media	Composition
Yeast Extract Peptone Dextrose Medium (YPD) with or without Zeocin	Dissolve 10 g yeast extract (1% w/v) and 20 g peptone (2% w/v) into 900 ml of dH_2O. Autoclave. Once solution has cooled to ~60 °C add 100 ml of 20 % glucose (2 % v/v). Add 1.0 ml of 100 mg/ml Zeocin (100 µg/ml), if required. Store at room temperature if no Zeocin in media but at 4 °C and in dark if contains Zeocin.
YPD with Sorbitol (YPDS) + Zeocin Agar Plates	Dissolve 10 g yeast extract (1% w/v), 182.2 g sorbitol (1 M) and 20 g peptone (2% w/v) in 900 ml of dH_2O. Add 20 g of agar (2% w/v). Autoclave and once cooled to ~60 °C add 100 ml of 20% glucose (2% v/v) and 1.0 ml of 100 mg/ml Zeocin (100 µg/ml). Stored at 4 °C and in the dark.
Buffered Glycerol-complex medium (BMGY) with Zeocin	Dissolve 10 g of yeast extract (1% w/v), 20 g peptone (2% w/v) in 700 ml dH_2O. Autoclave. Once cooled to room temperature add: -100 ml 1 M potassium phosphate buffer, pH 6.0 (100mM), 100 ml 13.4% YNB (1.34% v/v), 2 ml 0.02% Biotin ($4X10^{-5}$ % v/v),100 ml 10% glycerol (1% v/v) and 1.0 ml of 100 mg/ml Zeocin (100 µg/ml). Store at 4 °C and in dark.
Buffered Methanol-complex medium (BMMY) with Zeocin	Dissolve 10 g of yeast extract (1% w/v), 20 g peptone (2% w/v) in 700 ml dH_2O. Autoclave. Once cooled to room temperature add 100 ml 1 M potassium phosphate buffer, pH 6.0 (100mM), 100 ml 13.4% YNB (1.34% v/v), 2 ml 0.02% Biotin ($4X10^{-5}$ % v/v) 100 ml 5% methanol (0.5% v/v). Add 1.0 ml of 100 mg/ml Zeocin (100 µg/ml). Store at 4 °C.

Table 2.5 Media for fermentation of *Pichia pastoris.*

Media	Composition
Yeast extract peptone dextrose medium (YEPD, primary culture medium) with Zeocin	Dissolve 4 g peptone (1.7% w/v), 2 g yeast extract (0.9% w/v), 3 g glucose (1.3% w/v) into 230 ml dH_20, then autoclave. After autoclaved add 230 µl of 100 mg/ml Zeocin (100 µg/ml).
Basic salt medium	For 5.3 L final volume, dissolve 5.4 g $CaSO_4$, 88 g K_2SO_4, 70 g $MgSO_4$: $7H_2O$, 54 g $(NH_4)_2SO_4$ and 300 ml glycerol into 5.0 L dH_20 and then autoclaved in the bioreactor.
Sodium hexametaphosphate	Dissolve 150 g hexametaphosphate in 1 L dH_20, then filter sterilised.
Trace elements (Amresco)	5.99 g $CuSO_4.(H_2O)_5$ 0.08g NaI 3.0 g $MnSO_4.H_2O$, 0.20 g $Na_2MoO_4.(H_2O)_2$ 0.50 g $CoCl_2.(H_2O)_6$ 20.04 g $ZnCl_2.(H_2O)_5$ 65.05 g $FeSO_4.(H_2O)_7$ 0.02 g H_3BO_3 19.2 ml 96.2% H_2SO_4 0.40 g D-biotin Add dH_2O to make final volume 1L (purchased in this form)
Secondary culture medium	300 ml basic salt medium 30 ml sodium hexametaphosphate, 1.2 ml trace elements, then filter sterilised.
Fermentation media	To 5 L of autoclaved basic salt medium, add 970 ml hexametaphosphate, 24 ml trace elements and 1 ml anti-foam.
Limited glycerol feed	300 ml 100 % glycerol, 300 ml water, then autoclaved. Then add 7 ml trace elements.
Limited methanol feed	2 L methanol and 24 ml trace elements.

Table 2.6 Solutions for the radial flow column.

Solution	Composition
0.1 M Copper Sulfate for EAEAHis$_6$-G3 and His$_6$-G3	25 g $CuS0_4$. $5H_2O$ in 1 L dH_2O and then autoclaved.
0.1 M Nickel (II) sulfate for EAEA$(HE)_3$-G3, $(HE)_3$-G3 and cleavable tag-G3	52.56 g $NiS0_4$. $6H_2O$ in 2 L dH_2O and then autoclaved
1 X equilibration/wash solution for EAEAHis$_6$-G3, His$_6$-G3 and cleavable tag-G3	292 g NaCl (0.5 M) and PBS 48 g (0.5x PBS) in 10L dH_2O autoclaved and after cooled to room temperature add 6.8 g imidazole (10mM).

1 X equilibration/wash solution for EAEA$(HE)_3$-G3 and $(HE)_3$-G3	292 g NaCl (0.5 M) and PBS 48 g (0.5x PBS) in 10L dH_2O autoclaved (no imidazole added).
4 X cell application solution for EAEAHis_6-G3, His_6-G3 and cleavable tag-G3	584 g NaCl (2 M) and PBS 96 g (2x PBS) in 5L dH_2O autoclaved and after cooled to room temperature add 13.6 g imidazole (40mM).
4X cell application solution for EAEA$(HE)_3$-G3 and $(HE)_3$-G3	584 g NaCl (2 M) and PBS 96 g (2x PBS) in 5L dH_2O autoclaved (no imidazole).
20 mM imidazole solution for EAEAHis_6-G3, His_6-G3 and cleavable tag His_6-G3	58.4 g NaCl (0.5 M) and PBS 9.6 g (0.5x PBS) in 2L dH_2O autoclaved and after cooled to room temperature add 2.72 g imidazole (20mM).
200 mM imidazole solution to elute all DARPin from IMAC column	58.4 g NaCl (0.5 M) and PBS 9.6 g (0.5x PBS) in 2L dH_2O autoclaved and after cooled to room temperature add 27.2 g imidazole (200mM). Adjusted to pH 7 with 4M HCl.

Table 2.7 Solutions used in G3 DARPin conjugation with maleimido-mono-amide DOTA and purification post-conjugation.

Solution	Constituents
0.1M Phosphate Buffer, pH 7	1.17 g Sodium phosphate monobasic (*Trace*SELECT, ≥ 99.999% metals basis, anhydrous, Sigma-Aldrich) and 2.16g Sodium phosphate dibasic (*Trace*SELECT, ≥ 99.999% metals basis, anhydrous, Sigma-Aldrich) dissolved in 250 ml sterile water (Baxter). The solution was then put through a chelex-100 column (Bio-Rad) and filter sterilised.
0.2 M Ammonium Acetate Buffer, pH 7	3.95 g ammonium acetate (*Trace*SELECT, ≥ 99.9995% metals basis, Sigma-Aldrich) dissolved in 250 ml sterile water (Baxter). The solution was then put through a chelex-100 column (Bio-Rad) and filter sterilised.
0.2 M Ammonium Acetate Dialysis Buffer, pH 6.5 containing chelex-100	15.416 g ammonium acetate for molecular biology (≥ 98%, Sigma-Aldrich) and 10g chelex-100 (Bio-Rad) was dissolved in 1 L sterile water (Baxter). Slowly add 37% hydrochloric acid until pH reaches 6.5 (approx. 150 µl).

Table 2.8 Solutions used for instant thin layer chromatography (iTLC) to assess ^{111}In and $^{123/125}$I radiolabelled G3 DARPins.

Solvent	Constituents	Strips	Separation for indium-111	Separation for iodine-125 and iodine-123
0.1 M ammonium acetate & 25 mM EDTA	7.7 g ammonium acetate and 9.3g EDTA in 1L dH_20 (1.5-2 ml per test strip)	iTLC-SG (Varian)	Origin -^{111}In-DARPin -Insoluble ^{111}In Front -^{111}In-EDTA -^{111}In-DOTA (any free ^{111}In binds to EDTA in the solution)	Origin -^{123}I/^{125}I- DARPin Front -Free ^{123}I/^{125}I
Ammonia-ethanol-water	For 8 ml, use 1 ml of 35% ammonia, 2 ml ethanol, 5 ml dH_20 (1.5-2 ml per test strip)	iTLC-SG (Varian)	Origin -Insoluble ^{111}In Front -^{111}In-DARPin -^{111}In-EDTA -^{111}In-DOTA -Free ^{111}In (if not quenched with EDTA)	Not required

Table 2.9 Solutions used for instant thin layer chromatography (iTLC) to assess ^{68}Ga radiolabelled G3 DARPin.

Solvent	Constituents	Strips	Separation for Gallium-68
0.1 M citrate buffer, pH 5	0.672 g of citric acid anhydrous and 1.911g of trisodium citrate, dehydrate 100 ml dH_2O (1 ml per test strip, control performed without adding protein to detect ^{68}Ga-DARPin)	iTLC-SA (Varian)	Origin -^{68}Ga-DARPin -Insoluble ^{68}Ga Front -^{68}Ga-EDTA -^{68}Ga-Chelator -Free ^{68}Ga

Table 2.10 Solution used for the HotSHOT DNA extraction from mice ear biopsies.

Solution	Composition
Alkaline Lysis Buffer (pH 12) 25 mM NaOH 0.2 mM Na_2EDTA	For 100 ml: 25 ml of 100 mM NaOH, 0.4 ml of 50 mM Na_2EDTA (pH 8), 74.6 ml of dH2O
Neutralizing Solution (pH 5) 40 mM Tris-HCl	For 100 ml: 630 mg of Tris-HCl, 100 ml of dH2O

2.1.3 Electrophoresis and Western Blotting Consumables

Agarose gel electrophoresis was performed with horizontal gels slab run on a Hi-Set mini electrophoresis unit (Anachem). Agarose MP (Roche Diagnostics) was used to produce the gels. The DNA ladders, DNA Molecular Weight Marker IX (Roche Diagnostics), 1 kb DNA Ladder (New England BioLabs), 1 kb DNA Step Ladder (Promega) and Hyperladder I (Bioline Reagents) were selected based on the size of the DNA samples (Figure 2.1). Gel electrophoresis was powered with the Pharmacia LKB-GPS 200/400 power pack (Pharmacia). Images were obtained using the G:BOX gel imaging system (Syngene).

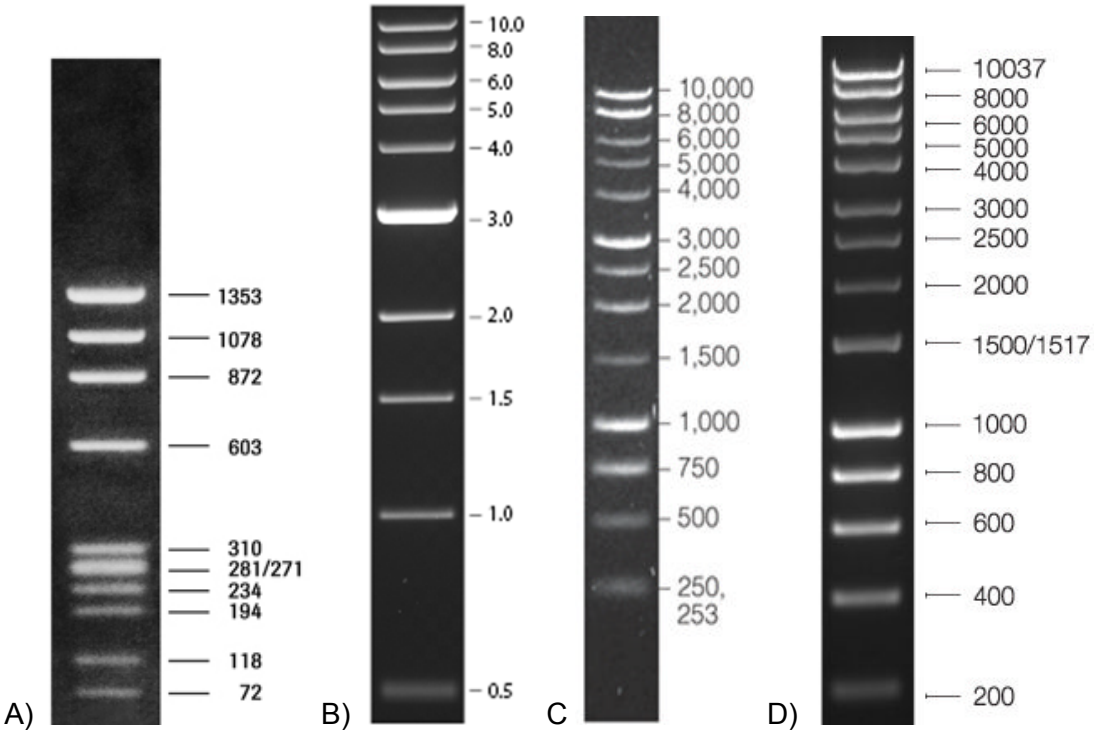

Figure 2.1 DNA Ladders: weight of DNA bands are expressed as base pairs:
A) DNA Molecular Weight Marker IX (Roche Diagnostics) ran on a 1% agarose gel.
B) 1 kb DNA Ladder (New England BioLabs, NEB) ran on a 0.8% TAE agarose gel.
C) 1 kb DNA Step Ladder (Promega) ran on a 0.7% agarose gel.
D) Hyperladder I (Bioline Reagents) ran on a 1 % agarose gel.

For sodium dodecyl sulfate polyacrylamide gel electrophoresis (SDS-PAGE) and western blotting, the SeeBlue Plus2 Pre-Stained Standard (Life Technologies) and Spectra Multicolor Broad Range Protein Ladder (Thermo Scientific) were used (Figure 2.2). Samples were run on either Novex 16% Tris-Glycine Mini Gels 1.0 mm,

10 well pre-cast mini gels (Life Technologies) or 4-20% Tris-Glycine 1.0mm, 10 well pre-cast mini gels (NuSep).

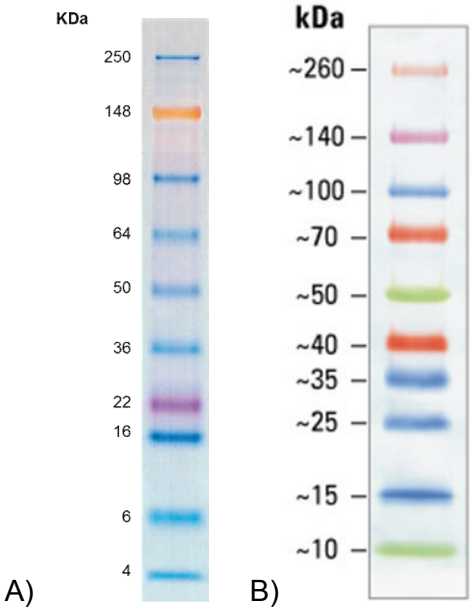

Figure 2.2 Molecular weights of the protein bands.
A) SeeBlue Plus2 Pre-Stained Standard, approximate molecular weights on Tris-Glycine Gel (Life Technologies)
B) Spectra Multicolor Broad Range Protein Ladder, approximate molecular weights on Tris-Glycine Gel (Thermo Scientific)

The PowerEase 500 power supply (Life Technologies) was used for SDS-PAGE and protein transfer. SDS-PAGE was performed in the XCell SureLock Mini-Cell Electrophoresis System (Life Technologies). The immun-blot polyvinylidene difluoride (PVDF) 0.2 µm membranes (Bio-Rad Laboratories) and XCell Blot II Module (Life Technologies) were used in the transfer of protein samples from gels to membranes for western blotting.

2.1.4 Primers for molecular biology techniques, nuclease and proteinase cleavage sites

All primers were purchased from Integrated DNA Technologies, except AOX1 Sense and AOX1 Anti-sense which were purchased from Life Technologies. Primers were purchased in a lyophilised form and dissolved with filtered dH_2O. Primers for G3 DARPin DNA PCR were dissolved to either 1 µg/µL (1x concentration) or 10 µg/µL

(10x concentration) depending on their molecular weights (Table 2.11 and Table 2.12).

Table 2.11 Primers used for the PCR of G3 DARPin DNA.

Primer	Sequence (5' - 3')	Description
EAEAHis$_6$ Sense	5' ATAGAATTC*TC**GAGAAAAGAGAGGCTGAA GCT**CATCACCATCATCACCATGGACCAGGTTC TGATTTGGGAAAGAAATTGTTGGAAGCTGCTA GAGCTG 3'	Sense primer for EAEAHis$_6$-G3 DNA. The sequence which anneals to ANK-1 plasmid is underlined. A His$_6$ tag (red), glycine-proline (blue) and lysine ( ) are introduced. Site cleaved by nuclease XhoI (*). Translated amino acid sequences cleaved by proteinases Kex2 and Ste13 (**bold**).
EAEA(HE)$_3$ Sense	5' ATAGAATTC*TC**GAGAAAAGAGAGGCTGAA GCT**CATGAGCATGAACACGAAGGACCAGGTT CTGATTTGGGAAAGAAATTGTTGGAAGCTGCT AGAGCTG 3'	Sense primer for EAEA(HE)$_3$-G3 DNA. The sequence which anneals to the ANK-1 plasmid is underlined. A (HE)$_3$ tag (red), glycine-proline (blue) and lysine ( ) are introduced. Site cleaved by nuclease XhoI (*). Translated amino acid sequences cleaved by proteinases Kex2 and Ste13 (**bold**).
Cleavable tag Sense	5' C*TC**GAGAAAAGAGAGGCTGAAGCT**CATCA CCATCATCACCATGGAGGTGGCTCTGGATTA GAGGTATTGTTTCAAGGACCAGGTTCTGATTT GGGAAAGAAATTGTTGGAAGCTGCTAGAGCT G 3'	Sense primer for cleavable tag-G3 DNA. The sequence which anneals to the ANK-1 plasmid is underlined. A cleavable His$_6$ tag (red) and lysine ( ) are introduced. The site recognised by HRV 3C protease site including a glycine-proline (blue). Site cleaved by nuclease XhoI (*). Translated amino acid sequences cleaved by proteinases Kex2 and Ste13 (**bold**).
His$_6$ Sense	5' ATAGAATTC*TC**GAGAAAAGA**CATCACCATC ATCACCATGGACCAGGTTCTGATTTGG 3' Please refer to Appendix for plasmid EAEAHis-3/pPICZαB sequence.	Sense primer for His$_6$-G3. The sequence which anneals to the EAEAHis$_6$-G3 plasmid is underlined. The His$_6$ tag (red) and glycine-proline (blue) are maintained. Site cleaved by nuclease XhoI (*). Translated amino acid sequences cleaved by proteinase Kex2 (**bold**).
(HE)$_3$ Sense	5'ATAGAATTC*TC**GAGAAAAGA**CATGAGCATG AACACGAAGGACCAGGTTCTGATTTGG 3'	Sense primer for (HE)$_3$-G3. The sequence which anneals to the EAEA(HE)$_3$-G3 plasmid

	Please refer to Appendix for plasmid EAEAHE-3/pPICZαB sequence.	is underlined. The $(HE)_3$ tag (red) and glycine-proline (blue) are maintained. Site cleaved by nuclease XhoI (*). Translated amino acid sequences cleaved by proteinase Kex2 (**bold**).
Truncated Sense	5 'ATAGAATTC*TC**GAGAAAAGAGAGGCTGAAGC** 3'	Sense primer used for $EAEAHis_6$-G3, $EAEA(HE)_3$-G3, cleavable tag-G3. Site cleaved by nuclease XhoI (*). Translated amino acid sequences cleaved by proteinase Kex2 and Ste13 (**bold**).
AOX1 Sense	5' GACTGGTTCCAATTGACAAGC 3'	Sense control for His_6-G3 and $(HE)_3$-G3 PCR. Binds to pPICZαB sense AOX1 primer site
Anti-sense G3	5' TAATTAT*CTAGATTATTAGCAACCTCCGTTAACTTTTGCAAAATTTCAG 3'	Antisense primer used for $EAEAHis_6$-G3, $EAEA(HE)_3$-G3, cleavable tag-G3, His_6-G3 and $(HE)_3$-G3 DNA, introduces a C-terminal cysteine (red), XbaI nuclease cleavage site (*) and incorporates stop codons (underlined)
AOX1 Anti-sense	5' GCAAATGGCATTCTGACATCC 3'	Anti-sense for His_6-G3 and $(HE)_3$-G3. Anti-sense control for His_6-G3 and $(HE)_3$-G3. Binds to pPICZαB anti-sense AOX1 primer site

Table 2.12 Properties of primers used in the production of G3 DARPin DNA.

Primer	Melting temperature (° C)	Molecular Weight (Da)	Weight (mg)	Conc. (µg/µl)	G3 DARPin DNA PCR
$EAEAHis_6$ Sense	71.7	30,722	3.10	10	$EAEAHis_6$-G3
$EAEA(HE)_3$ Sense	71.2	30,900	3.28	10	$EAEA(HE)_3$-G3
Cleavable tag Sense	71.5	38,584	0.154	1	Cleavable tag-G3
His_6 Sense	67.3	17,528.4	0.48	1	His_6-G3
$(HE)_3$ Sense	67.4	17,706.6	0.46	1	$(HE)_3$-G3
Truncated Sense	59.5	9,650	0.32	1	$EAEAHis_6$-G3, $EAEA(HE)_3$-G3, cleavable tag-G3

AOX1 Sense	54.3	6,430.2	0.21	1	Sense control for His_6-G3 and $(HE)_3$-G3
Anti-sense G3	61.9	15,267	0.61	1	EAEAHis_6-G3, EAEA$(HE)_3$-G3, cleavable tag-G3, His_6-G3 and $(HE)_3$-G3
AOX1 Anti-sense	54.8	6,390.2	0.21	1 or 10	Anti-sense for His_6-G3 and $(HE)_3$-G3. Anti-sense control for His_6-G3 and $(HE)_3$-G3.

Table 2.13 DNA sequences cleaved by restriction endonucleases for G3 DARPin and pPICZαB DNA digestions.

Restriction endonucleases	Source	DNA Cleavage site (*)	DARPin DNA base position	pPICZαB base position
XhoI	*E. coli*	5' C*TCGAG 3'	N-terminus	1184*1185
XbaI	*E. coli*	5' T*CTAGA 3'	C-terminus	1275*1276

Table 2.14 Amino acid sequences cleaved by proteinases.

Proteinase	Source	Protein cleavage site (*)
Kex2 gene product	*P. pastoris*	Glu(E)-Lys(K)-Arg(R) * (amino acid)
Ste13 gene product	*P. pastoris*	Glu (E)-Ala(A) * (amino acid)
Human rhinovirus (HRV) 3C	*Rhinovirus* (recombinant)	Leu(L)-Glu(E)–Val(V)–Leu(L)-Phe(F)-Gln(Q) * Gly(G)-Pro(P)

2.1.5 Plasmids

The plasmid ANK-1 was based on the G3 DARPin *E. coli* DNA sequence (gift from Professor Andreas Plückthun, University of Zurich), which was optimised for *P. pastoris* by GenScript. ANK-1 was used as the DNA template for the PCR amplification of EAEAHis_6-G3, EAEA$(HE)_3$-G3 and cleavable tag-G3 (Figure 2.3). The plasmids produced during the EAEAHis_6-G3 and EAEA$(HE)_3$-G3 development were used as the templates for His_6-G3 and $(HE)_3$-G3, respectively (Appendix).

Figure 2.3: ANK-1 DNA plasmid optimised for *P. pastoris*, encodes for a G3 DARPin which differed from the proposed G3 DARPins in the following respects.

1) C-terminal His_6 tag rather than N-terminal tag
2) No cysteine rather than a solitary C-terminal cysteine
3) Alanine (A) rather than a Lysine (K) at residue 17 (A17K)
4) Add Glycine (G) Proline (P) between N-terminal tag and GDSDL

```
ctcgagaagagagaagctgaagctatggctggttctgatttgggaaaggcttgttggaa
 L  E  K  R  E  A  E  A  M  A  G  S  D  L  G  K  A  L  L  E
gctgctagagctggtcaagatgatgaagttagaattttgatggctaacggtgctgatgtt
 A  A  R  A  G  Q  D  D  E  V  R  I  L  M  A  N  G  A  D  V
aacgctaaggatgaatacggtttgactccattgtacttggctactgctcatggtcatttg
 N  A  K  D  E  Y  G  L  T  P  L  Y  L  A  T  A  H  G  H  L
gaaattgttgaagttttgttgaagaatggagctgatgttaacgctgttgatgctattggt
 E  I  V  E  V  L  L  K  N  G  A  D  V  N  A  V  D  A  I  G
tttactccattgcatttggctgcttttattggtcatttggaaattgctgaagttttgttg
 F  T  P  L  H  L  A  A  F  I  G  H  L  E  I  A  E  V  L  L
aagcatggtgccgacgttaacgctcaggataagtttggaaagactgcttttgatatttct
 K  H  G  A  D  V  N  A  Q  D  K  F  G  K  T  A  F  D  I  S
attggtaacggtaacgaagatttggctgaaattttgcaaaagttgaaccatcatcatcat
 I  G  N  G  N  E  D  L  A  E  I  L  Q  K  L  N  H  H  H  H
catcattaataatctagagcggccgc
 H  H  -  -  S  R  A  A
```

2.2 Methods

2.2.1 Production of ligated pPICZαB plasmid and G3 DARPin DNA

2.2.1.1 Polymerase chain reaction of G3 DARPin DNA

The G3 DARPin PCRs were prepared in a similar way to each other (Table 2.15), except different primers and different primer concentrations were used for each construct (Table 2.16). The DNA templates used for His_6-G3 and $(HE)_3$-G3 were generated during the PCR for EAEAHis_6-G3 and EAEA$(HE)_3$-G3, respectively (Appendix). For His_6-G3 and $(HE)_3$-G3, a control PCR was performed with alcohol oxidase 1 (AOX1) Sense and AOX1 Anti-sense primers which would be expected to produce a larger DNA fragment than G3 DARPin DNA alone, as it would also incorporate pPICZαB DNA.

Table 2.15 G3 DARPin polymerase chain reactions.

Constituent	Volume (µl)	Final reaction concentration
PCR Master Mix	42.5	50.5 nM of each dNTP
Sense primer (concentration 0.1, 1.0 or 10 µg/µl)	1	0.002, 0.02 or 0.2 µg /µl
Anti-sense primer (concentration 1.0 or 10 µg/µl)	1	0.02 or 0.2 µg /µl
Taq polymerase: ampliTaq DNA Polymerase, 5 U/µl (Roche Diagnostics)	1	0.1 U/µl
Template DNA	1	0.16-0.24 µg/µl
Filtered dH_2O	3.5	
Total volume	50	

Table 2.16 Primers and templates used for each G3 DARPin PCR.

DARPin	PCR (no. of cycles)	Template DNA (final conc.)	Sense primer (final conc.)	Anti-sense primer (final conc.)
EAEAHis$_6$-G3	Short PCR (40)	ANK-1 (0.2 µg/µl)	EAEAHis$_6$ Sense (0.002 µg/µl) for cycles 1-10 Truncated Sense (0.02 µg/µl) for cycles 11-40	Anti-sense G3 (0.02 µg/µl) for cycles 1-40
	Long PCR (30)	ANK-1 (0.2 µg/µl)	EAEAHis$_6$ Sense (0.02 µg/µl) for cycles 1-30	Anti-sense G3 (0.02 µg/µl) for cycles 1-30
EAEA(HE)$_3$-G3	Short PCR (40)	ANK-1 (0.2 µg/µl)	EAEA(HE)$_3$ Sense (0.002 µg/µl) for cycles 1-10 Truncated Sense (0.02 µg/µl) for cycles 11-40	Anti-sense G3 (0.02 µg/µl) for cycles 1-40
	Long PCR (30)	ANK-1 (0.2 µg/µl)	EAEA(HE)$_3$ Sense (0.02 µg/µl) for cycles 1-30	Anti-sense G3 (0.02 µg/µl) for cycles 1-30
Cleavable tag-G3	Short PCR (40)	ANK-1 (0.2 µg/µl)	Cleavable tag Sense (0.002 µg /µl) for cycles 1-10 Truncated Sense (0.02 µg/µl) for cycles 11-40	Anti-sense G3 (0.02 µg/µl) for cycles 1-40
	Long PCR (30)	ANK-1 (0.2 µg/µl)	Cleavable tag Sense (0.02 µg/µl) for cycles 1-30	Anti-sense G3 (0.02 µ /µl) for cycles 1-30
His$_6$-G3	His-1 (30)	pPICZαB/EAEAHis3 (0.16 µg/µl)	His$_6$ Sense (0.02 µg /µl) for cycles 1-30	Anti-sense G3 (0.02 µg/µl) for cycles 1-30
	His-2 (30)	pPICZαB/EAEAHis3 (0.16 µg/µl)	His$_6$ Sense (0.02 µg /µl) for cycles 1-30	AOX1 Anti-sense (0.02 µg/µl) for cycles 1-30
	Control (30)	pPICZαB/EAEAHis3 (0.16 µg/µl)	AOX1 Sense (0.2 µg/µl) for cycles 1-30	AOX1 Anti-sense (0.2 µg/µl) for cycles 1-30
(HE)$_3$-G3	HE-1 (30)	pPICZαB/EAEAHE3 (0.24 µg/µl)	(HE)$_3$ Sense (0.02 µg /µl) for cycles 1-30	Anti-sense G3 (0.02 µg/µl) for cycles 1-30
	HE-2 (30)	pPICZαB/EAEAHE3 (0.24 µg/µl)	(HE)$_3$ Sense (0.02 µg /µl) for cycles 1-30	AOX1 Anti-sense (0.02 µg/µl) for cycles 1-30
	Control (30)	pPICZαB/EAEAHE3 (0.24 µg/µl)	AOX1 Sense (0.2 µg/µl) for cycles 1-30	AOX1 Anti-sense (0.2 µg/µl) for cycles 1-30

The same PCR cycle conditions were used for all G3 DARPin PCRs, which were performed with the Personal Cycler (Biometra) (Table 2.17).

Table 2.17 PCR conditions used for EAEAHis$_6$-G3, EAEA(HE)$_3$-G3, cleavable tag-G3, His$_6$-G3 and (HE)$_3$-G3 DARPins.

PCR steps	Conditions
Initialisation	95 °C for 3 min
PCR cycles (n = 30-40)	95 °C for 60 sec (denaturation) 60 °C for 60 sec (annealing) 72 °C for 90 sec (elongation)
Final elongation	72 °C for 10 min
Final hold	4 °C (5 min – 24 h)

2.2.1.2 Agarose gel electrophoresis of G3 DARPin PCR products

Agarose gels were formed by dissolving 0.75 g (1.5% w/v) or 1.0 g (2% w/v) of agarose (Sigma-Aldrich) in 50 ml Tris-acetate-EDTA (TAE) 1x buffer with microwave heating for 2 min. After cooling to 50-55 °C, 5 µl ethidium bromide (concentration 10 mg/ml, Sigma-Aldrich) was added to the gel solution, the gel was then poured into the electrophoresis unit with the appropriate sized well comb and allowed to set. After setting, TAE 1x buffer was poured over the gel.

Conventionally, the DNA ladder (10 µl) was applied to the first well of the agarose gel. DNA 10x loading buffer (5 µl) was added to the PCR samples and the entire PCR sample was applied to an individual well. The electrophoresis was performed at 50 millivolts (mV). Bands were visualised with the UVP transilluminator (Genetic Research Instrumentation) and the desired bands were excised from the gel with a scalpel.

2.2.1.3 Purification of G3 DARPin DNA from agarose gel bands

DNA was purified from excised agarose gel bands using the Wizard SV Gel and PCR Clean-Up System (Promega) by centrifugation, according to the manufacturer's instructions. Each DNA gel band was placed into a 1.5 ml microcentrifuge tube and weighed. Membrane Binding Solution (10 µl/mg of gel) was applied to the gel, which was subsequently vortexed and incubated at 50-65 °C until the gel dissolved. An equal volume of Membrane Binding Solution was added to the dissolved gel.

The dissolved gel was transferred to a SV Minicolumn and incubated at room temperature (RT) for 1 min. The SV Minicolumn was placed into a Collection Tube for centrifugation. The dissolved gel was centrifuged at 16,000 × *g* for 1 min (RT), the flow through was discarded. To wash the DNA, 700 µl Membrane Wash Solution was added to the sample and centrifuged at 16,000 × *g* for 1 min (RT), the flow through was discarded and a second wash was performed with 500 µl Membrane Wash Solution in same way as described. Finally, the Collection Tube was centrifuged for 1 min at 16,000 × *g* (RT) to allow any residual ethanol to evaporate.

The Minicolumn was transferred to a clean 1.5 ml microcentrifuge tube and nuclease-free water (50 µl) was added, it was incubated for 1 min at RT and then centrifuged at 16,000 x *g* for 1 min (RT). The flow through containing DNA was stored at -20 °C.

2.2.1.4 Amplification and extraction of pPICZαB plasmid DNA

Electroporation of electro-competent bacterial cells

Electrocompetent TOP10F´ cells (*E. coli,* Life Technologies) were electroporated with Pme I-linearised pPICZαB plasmid (gift from Dr Kim Vigor, UCL Cancer Institute).

Pme I-linearised pPICZαB plasmid (1 µl) was added to TOP10F´ cells (100 µl) which had been thawed on ice, the mixture was then transferred into a 0.2 cm Gene Pulser/ MicroPulser cuvette (Bio-Rad Laboratories) which had been pre-chilled on ice. The cells were pulsed once using the pre-set 'Eco2' setting on the MicroPulser electroporator (Bio-Rad Laboratories) at 2500 Volts (V) for 5 ms. Ice cold Low Salt Luria Bertani (LB) media (1 ml) was added to the cuvette and incubated at 37 °C for 1 h with no shaking. Electroporated cells were spread onto Low Salt LB plates containing Zeocin (25 µg/ml) in 50 and 100 µl aliquots and incubated at 37 °C for 24 h.

The following day, two colonies were selected and transferred into separate sterile 250 ml conical flasks containing 50 ml of Low Salt LB with Zeocin (25 µg/ml). The flasks were incubated at 37 °C, shaking at 200 revolutions per min (rpm) overnight in the New Brunswick / Innova 4230 Refrigerated Benchtop Incubator Shaker (Eppendorf UK).

pPICZαB plasmid DNA extraction

pPICZαB plasmid was extracted from TOP10F' cells using the QIAGEN Plasmid Midi Extraction Kit (Qiagen), according to the manufacturer's instructions.

To lyse the electroporated TOP10F´cells, 25 ml from the two overnight cultures were centrifuged at 6,000 x *g* for 15 min (4 °C) in separate 50 ml conical polypropylene tubes. The pellets were retained, then the final 25 ml of the overnight cultures was added to the pellets and centrifuged at 6,000 x *g* for 15 min (4 °C). The supernatant was discarded and the two pellets were re-suspended in 4 ml of Qiagen Buffer P1, followed by adding 4 ml Qiagen Buffer P2, inverting 4-6 times and incubating for 5 min at RT. Subsequently, 4 ml of chilled Qiagen Buffer P3 was added, inverted 4-6 times and incubated on ice for 15 min.

The pPICZαB plasmid was removed from the sample by centrifuging at 20,000 x *g* (4 °C) for 30 min and retaining the supernatant. The supernatant was re-centrifuged for 15 min at 20,000 x *g* (4 °C) and supernatant retained.

Two Qiagen-tip 100 columns were equilibrated with 4 ml of Buffer QBT and the supernatant containing the pPICZαB plasmid DNA was applied to the columns. The Qiagen-tip columns were washed twice with 10 ml Qiagen Buffer QC. The DNA was eluted from the columns with 5 ml Qiagen Buffer QF into two clean 15 ml centrifuge tubes.

To precipitate the DNA, 3.5 ml of isopropanol was added to the eluted DNA, the two samples were centrifuged at 15,000 x *g* for 30 min (4 °C) and the supernatant was discarded. To wash the pellet, 2 ml of 70% ethanol was added, then centrifuged at 15,000 x *g* for 10 min (4 °C) and supernatant discarded. After air drying for 5-10 min the pellet of plasmid DNA was re-dissolved in 50 µl of dH_2O. The nucleic acid concentration of the two samples was assed using the NanoDrop 1000 Spectrophotometer (Thermo Scientific); finally it was stored at -20 °C.

2.2.1.5 Digestion of G3 DARPin and pPICZαB Plasmid DNA

Purified G3 DARPin DNA (50 µl) and pPICZαB plasmid DNA (3 µl) were digested separately with 5 µl XbaI (500 Units, concentration 100,000 Units/ml), 5 µl XhoI (500 Units, concentration 100,000 Units/ml), 10 µl NE Buffer 4 (10x concentration), 10 µl

Bovine serum albumin (BSA, 10x concentration) and dH_2O (17 µl) (Figure 2.4 and Table 2.13). The digestions were incubated at 37 °C for 2.5 h.

The digested pPICZαB plasmid was run on an agarose gel electrophoresis (1% agarose gel and Promega 1 kb DNA ladder used). The digested G3 DARPin DNA was not run on an agarose gel electrophoresis.

Figure 2.4 DNA sites cleaved by XbaI and XhoI, nucleic acids retained by DARPin (green) and plasmid (black).

A) XhoI recognition site (v/^) at N-terminus

5'…CvTCGAG…3'

3'…GAGCT^C…5'

B) XbaI recognition site (v/^) at C-terminus

5'… TvCTAGA…3'

3'… AGATC^T…5'

pPICZαB plasmid DNA was purified from the agarose gel using the Wizard SV Gel and PCR Clean-Up System (Promega), as previously described. Digested G3 DARPin DNA was also purified using the Wizard SV Gel and PCR Clean-Up System (Promega) to remove XbaI and XhoI, initially 100 µl of Membrane Binding Solution was added to digested G3 DARPin DNA (100 µl) and purification was completed as outlined previously. The digested pPICZαB plasmid and G3 DARPin DNA were stored at -20 °C.

2.2.1.6 Ligation of PCR Product and pPICZαB plasmid

All ligation buffers and enzymes were purchased from New England BioLabs. Digested DARPin DNA (1 µl) and pPICZαB plasmid DNA (1 µl) were added to 40 µl dH_2O, followed by 5 µl T4 Ligase Reaction Buffer (10x) and 3 µl of ice cold T4 Ligase (1,200 cohesive end units, concentration 400,000 cohesive end units/ml). Control ligations omitted digested G3 DARPin DNA. The ligation mixtures were incubated for 10 min at RT.

2.2.1.7 Phenol-Chloroform extraction of DNA from Ligation Mixture

Ligation and control mixtures (50 µl) were placed in separate 1.5 ml microcentrifuge tubes and 50 µl phenol solution (Sigma-Aldrich) was added to them, the mixtures

were centrifuged for 10 min at 16,000 x *g* (RT). The upper layer was transferred into a new 1.5 ml microcentrifuge tube and an equal volume (~50 µl) of Phenol:Chloroform:Isoamyl Alcohol 25:24:1 saturated with 10 mM Tris, pH 8.0, 1 mM EDTA (Sigma-Aldrich) was added. Once an emulsion formed, it was centrifuged for 10 min at 16,000 x *g* (RT). The upper aqueous phase containing DNA was transferred into a new 1.5 ml microcentrifuge tube and treated with $1/10^{th}$ volume of 3 M sodium acetate (pH 6), 2.5 times volume of absolute ethanol (≥ 99.5%) and 1 µl glycogen. The extraction mixture was incubated either at -20 °C overnight or at -80 °C for 1-2 h, then centrifuged at 16,000 x *g* for 10 min (RT) and the supernatant was discarded. The DNA containing pellet was washed with 195 µl of 70% ethanol and centrifuged at 16,000 x *g* for 10 min (RT). The supernatant was discarded and DNA pellet was air dried. The pellet was solubilised in 10 µl of dH_2O and stored at -20 °C.

2.2.1.8 Bacterial transformations of ligated pPICZαB/DARPin DNA

Electrocompetent TOP10F´ cells (*E. coli*, Life Technologies) or electrocompetent TG1 Cells (*E. coli*, Lucigen Corporation) were used for the bacterial transformations. Ligated pPICZαB/DARPin DNA (2 µl) was added to thawed bacteria (50 µl) and the samples were transferred into 0.2 cm Gene Pulser/ MicroPulser cuvettes (Bio-Rad Laboratories), which had been pre-chilled on ice. The cells were pulsed at 2500 V for 5 ms using the Bio-Rad MicroPulser electroporator (Eco2 setting). Low salt LB without Zeocin (1 ml) was added and the cuvettes were incubated for 1 h at 37 °C. Subsequently, 50-200 µl of the media were plated onto Low Salt LB/ Zeocin (25 µg/ml) plates and incubated overnight at 37 °C.

The following day up to seven colonies were selected from each plate using sterile pipette tips. The pipette tip carrying an individual colony was mixed in 10 µl of dH_2O, to PCR screen colonies for G3 DARPin DNA inserts. Finally, the pipette tip was mixed with 5 ml Low Salt LB media containing Zeocin (25 µg/ml) in a sterile 50 ml conical polypropylene tube. The inoculated media were stored at 4 °C and would later be used to obtain ligations of pPICZαB/DARPin DNA from positive colonies.

2.2.1.9 PCR Colony Screening

The PCR mixture was prepared with 85 µl PCR Master Mix, 5 µl Truncated Sense primer (1 µg/µl), 5 µl Anti-sense G3 primer (1 µg/µl), 10 µl dH_2O and 1 µl ampliTaq

DNA Polymerase (5 U/µl, Roche Diagnostics). Each colony was screened by taking 1 µl of dH_2O exposed to the colony and adding 10 µl PCR reaction mixture.

The PCR cycling was performed using the same equipment and conditions as used for the initial DARPin DNA PCR (Table 2.17) and 30 cycles were performed. Subsequently, 2 µl of 10x DNA loading buffer was added to the reactions and samples were run on a 1.5% agarose gel with a NEB 1 kb DNA ladder (New England BioLabs) or DNA Molecular Weight Marker IX (Roche Diagnostics).

2.2.1.10 Plasmid Extraction of ligated pPICZαB/DARPin DNA

Transformed clones containing G3 DARPin DNA inserts were selected for an overnight culture. Low Salt LB media (100 µl) which had been inoculated with the selected clones was added to sterile 250 ml conical flask containing 50 ml Low Salt LB Media with Zeocin (25 µg/ml). The inoculated media were incubated overnight at 37 °C and shaking at 225 rpm using the New Brunswick / Innova 4230 Refrigerated Benchtop Incubator Shaker (Eppendorf UK).

The ligated pPICZαB/DARPin DNA was extracted from the bacterial cells using the QIAGEN Plasmid Midi Extraction Kit (Qiagen), as described previously. The DNA was sequenced by the DNA Sequencing Service at the UCL Cancer Institute, using the AOX1 Sense and AOX1 Anti-sense primers (Life Technologies).

2.2.2 *Pichia pastoris* expression of G3 DARPin protein

2.2.2.1 Linearisation of pPICZαB plasmid/DARPin DNA ligations

Ligations of pPICZαB/DARPin DNA inserts were linearised with Pme I (enzyme and buffers from New England BioLabs) at the AOX1 promoter region of pPICZαB for transformation into X-33 (*P. pastoris*) yeast genomes (Figure 2.5).

Ligated pPICZαB/DARPin DNA (10 µg of nucleic acid) were digested with 3 µl Pme I (30 units, concentration 10,000 units/ml), 10 µl of 10x NEBuffer 4, 10 µl of 10x Purified BSA and reactions were made up to 100 µl volume with dH_2O. Controls were performed with ligated pPICZαB/DARPin DNA (10 µg of nucleic acid) in dH_2O only or pGAPZαB/DARPin DNA ligations treated in the same way as their pPICZαB counterparts (pGAPZαB is not linearised by Pme I).

Reactions were incubated at 37 °C for 3 h. To assess the linearisation efficiency a 5 µl sample was removed from each reaction and diluted in 20 µl of dH_2O, then run on an agarose gel electrophoresis, 1% or 2% agarose gels with a 1 kb DNA step ladder (Promega) or HyperLadder I (Bioline) were used.

5'… GTTTvAAAC…3'

3'…CAAA^TTTG…5'

Figure 2.5 Pme I Recognition Site (v /^) in the 5' AOX1 promoter region of pPICZαB plasmid (base 413/414).

2.2.2.2 Phenol-Chloroform Extraction of linearised pPICZαB plasmid/DARPin DNA

After linearisation, phenol-chloroform extraction was performed to purify and extract DNA, as previously outlined.

2.2.2.3 Expansion of electrocompetent X-33 cells

Electrocompetent X-33 cells (Life Technologies) were used to inoculate 5 ml of Yeast Extract Peptone Dextrose (YPD) media in a sterile 50 ml conical polypropylene tube, by placing a sterile pipette tip in a vial of frozen X-33 cells (-80 °C) and then mixing the tip with YPD media. The inoculated media was incubated overnight at 30 °C and shaking at 225 rpm within the New Brunswick / Innova 4230 Refrigerated Benchtop Incubator Shaker (Eppendorf UK). The following day, 100 µl of the overnight culture was used to inoculate 250 ml YPD media within a sterile 2 L glass conical flask, the flask was incubated at 30 °C and 225 rpm until the optical density measured at 600 nm (OD_{600}) reached 1.3-1.5 (~16 h post inoculation).

The X-33 culture was centrifuged at 1,500 x *g* for 5 min (4 °C), the supernatant was discarded and subsequent centrifugations were performed in the same way. The pellet was resuspended in 250 ml ice cold sterile dH_2O, re-centrifuged and the supernatant was discarded. The pellet was resuspended in 20 ml ice cold sterile 1 M sorbitol, re-centrifuged and supernatant was discarded. Finally, the X-33 cell pellet was resuspended in 1-2 ml ice cold sterile 1 M sorbitol, stored on ice and used the same day for electroporation.

2.2.2.4 Electroporation of X-33 cells with linearised pPICZαB plasmid/ DARPin DNA

X-33 cells (80 µl) were added to linearised pPICZαB/DARPin DNA (10 µl) and placed on ice for 1 min. Cells were transferred into a pre-chilled 0.2 cm Gene Pulser/ MicroPulser cuvette (Bio-Rad Laboratories) and pulsed with the 'Pic' setting on the MicroPulser electroporator (Bio-Rad Laboratories) at 2000 V for 5 ms. Immediately after electroporation, 1 ml sterile ice cold 1 M sorbitol was added to the cuvette and incubated at 30 °C for 2 h with no shaking. The transformed cells were spread onto YPDS (Yeast Extract Peptone Dextrose Sorbitol) plates containing 100 µg/ml of Zeocin in 50-200 µl aliquots and incubated for 72 h at 30 °C without shaking.

2.2.2.5 Protein expression in X-33 yeast cells

X-33 colonies (4-6) of each construct were selected from the YPDS/Zeocin plates. Each selected colony was used to inoculate separate sterile 50 ml conical polypropylene tubes containing 5 ml of Buffered Glycerol-complex medium (BMGY) with Zeocin 100 µg/ml, then incubated at 30 °C and 225 rpm overnight. At the same time, YPDS containing Zeocin 100 µg/ml plates were streaked with inoculated media and incubated at 30 °C without shaking, these plates would be used to prepare the seed lots, once protein expression was confirmed.

Once the OD_{600} reached 2.5 (~16 h post inoculation), the overnight culture was centrifuged for 5 min at 3,000 x *g* (RT). The supernatant was discarded and pellets were re-suspended in Buffered Methanol-complex medium (BMMY) with Zeocin 100 µg/ml to achieve a final OD_{600} equivalent to 1 (~25 ml). The BMMY containing the electroporated cells were transferred into a sterile 250 ml conical flask, then incubated at 30 °C and 225 rpm for 72 h. At 24, 48 and 72 h incubation, 250 µl of the media was removed and centrifuged at 5,000 rpm for 5 min and the supernatant was mixed with SDS-PAGE reducing buffer and stored at -80 °C. After the samples were taken at 24 and 48 h, 100% Methanol was added to the media, at a volume equivalent to 25 µl/5ml BMMY (~125 µl) to stimulate continued G3 DARPin protein expression through methanol induced AOX1 gene activation.

2.2.2.6 SDS-PAGE

Protein samples were mixed with 4x SDS-PAGE (3 protein: 1 buffer volumes) or 2x SDS-PAGE (1:1) loading buffer. Samples in reducing buffer were denatured by heating for 3 min at 75 °C in a Personal Cycler (Biometra), while samples in non-reducing buffer were not heated.

Up to two gels were fixed in the electrophoresis unit by locking the gel tension wedge, then the unit was filled with 1x SDS-PAGE Running Buffer to cover the gel(s). The samples were loaded using a micropipette; the protein standard was usually loaded into lane 1. Subsequently, samples were loaded. The gels were run at a constant 35 mA (125 V, 5.0 W) for 1 h 30 min. Afterwards the gel(s) were removed from their cassette(s), then the lower (below the dye) and upper (well dividers) aspect of the gels were cut off.

2.2.2.7 Western blot analysis

The electrophoresis gels were transferred to PVDF membranes which had been pre-soaked in methanol for 20 sec, followed by 1x Protein Transfer Buffer. For each transfer 20 pieces of blotting paper (Whatman) and six sponges were pre-soaked in 1x Protein Transfer Buffer. The deep half of the transfer module was loaded in the following order, three sponges, ten pieces of blotting paper, agarose gel, PVDF membrane, ten pieces of blotting paper and three sponges. Two gels could be transferred simultaneously with blotting paper placed between the separate gel-membrane transfers. The chamber was filled with 1x Protein Transfer Buffer and run at 125 mA (25 V, 17 W) for 1 h 30 min.

Following protein transfer, the membrane was placed in 5% (w/v) dried milk powder (Marvel) made up with PBS for 1 h on a shaker. It was washed three times in 0.1% Tween-20/PBS (v/v), followed by three PBS washes. The membrane was placed in 25 ml of 1% milk/PBS (w/v) containing the primary antibody for 1 h shaking (Table 2.18). The Tween-20/PBS and PBS washes were repeated, prior to incubating with the secondary antibody in 25 ml of 1% milk/PBS (w/v) for 1 h shaking (Table 2.18). Afterwards the final Tween/PBS and PBS washes were repeated. The protein bands were visualised by incubating the membrane in 3,3′-Diaminobenzidine tetrahydrochloride (DAB) and hydrogen peroxide solution. Once the bands became

visible the reaction was stopped by rinsing the membrane in dH_2O and then air dried.

Table 2.18 Primary and secondary antibodies used for western blot analysis of G3 DARPin proteins.

Antibody steps	His_6-based G3 and Cleavable tag-G3	$(HE)_3$-based G3
Primary antibody in 1% milk (w/v) with PBS (25 ml)	25 µl (0.1 % v/v) mouse tetra-His antibody, BSA-free (Qiagen)	12.5 µl (0.05% v/v) rabbit anti-DARPin (Gift from Professor Plückthun, University of Zurich)
Secondary antibody in 1% milk (w/v) with PBS (25ml)	25 µl (0.1% v/v) ECL anti-mouse IgG_2 horse radish peroxidase linked $F(ab')_2$ fragment from sheep (GE Healthcare)	25 µl (0.1% v/v) goat anti-rabbit IgG (whole molecule)–peroxidase antibody (Sigma-Aldrich)

2.2.2.8 Coomassie staining

Following SDS-PAGE, the gel was placed in coomassie stain for 1 h. The coomassie stain was poured off and the gel was rinsed in destain until the bands were visible. The gel was then washed in dH_2O for 15 min, followed by soaking in Gel Dry Drying Solution (Life Technologies). The gel was placed in a gel drying rack between two cellophane sheets (Sigma-Aldrich) which had been pre-soaked with Gel Dry Drying Solution 1X. The gel was placed upright and dried overnight.

2.2.2.9 Seed lot preparation

A single X-33 colony confirmed to produce G3 DARPin protein by western blotting analysis and or coomassie staining was selected from the YPDS/Zeocin plates prepared during the protein test expression. The seed lot was prepared in a laminar flow hood. A sterile plastic loop was used to transfer the selected colony from the plate to a sterile 250 ml conical flask containing 50 ml YPD with Zeocin 100 µg/ml. The colony was grown overnight at 30 °C and 250 rpm shaking. Once the OD_{600} reached 15-20, the culture was transferred into a 50 ml conical polypropylene tube and centrifuged at 3,000 rpm for 5 min (RT). The supernatant was discarded and the pellet of G3 DARPin producing X-33 cells were resuspended in YPD/Glucose 15%, to achieve a final OD_{600} equivalent to 1 (~15-20 ml), the suspension was dispensed in 1 ml aliquots into Nunc CryoTubes (Sigma-Aldrich) and stored at -80 °C.

2.2.3 Production of G3 DARPin protein

2.2.3.1 Fermentation of X-33 cells

Fermentation was carried out by Mr Gaurav Bhavsar and Dr Berend Tolner, with assistance from Dr Robert Goldstein (All participants are based at the UCL Cancer Institute).

Fermentation involves generating a large biomass of *P. pastoris* cells during a limited glycerol feed. DARPin protein production is initiated during methanol feeding through the methanol-inducible AOX1 promoter gene within the pPICZαB plasmid. The α-factor signal sequence within the pPICZαB plasmid stimulates secretion of G3 DARPin protein from *P. pastoris* into the media.

The New Brunswick BioFlo 3000 autoclavable 10 L benchtop bioreactor with BioCommand supervisory software (Eppendorf) was used for the fermentations. Each DARPin was broadly produced by the same method but there were some variations to optimise individual yields (Table 2.19). Samples were taken from the bioreactor at different stages of the fermentation process, stored in 4x SDS-PAGE reducing buffer at -80 °C until analysed.

Step 1- Primary Culture:
A 2 L baffle flask containing 230 ml of YEPD was autoclaved, when cooled Zeocin was added. A seed lot vial (1 ml) was thawed in a laminar flow hood, the YPED/Zeocin-100 µg/ml media was inoculated with the entire vial and incubated at 30 °C (200 rpm) until the OD_{600} reached 12 (Table 2.19).

Step 2- Secondary Culture:
The secondary culture media (volume 331.2 ml) within a sterile 2 L baffle flask was inoculated with 1 ml of the primary culture in a laminar flow hood. The secondary culture was incubated at 30 °C (200 rpm) until the OD_{600} reached 5 (Table 2.19).

The 10 L bioreactor was filled with 5.3 L of basic salt media and autoclaved, then 970 ml hexametaphosphate, 24 ml trace elements and 1 ml anti-foam (Sigma-Aldrich) was added. The bioreactor was maintained at 30 °C and pH 5 with 100% ammonium hydroxide and 10% orthophosphoric acid. The bioreactor dissolved oxygen probe was set at 30%. The entire secondary culture (332.2 ml) was transferred to the bioreactor and agitated at 500-1000 rpm.

After approximately 22-24 h, all the glycerol in the media is consumed under aerobic conditions by the yeast. At this point, there is no demand for oxygen, the oxygen levels rapidly rise (oxygen spike) until the bioreactor reduces the dissolved oxygen back to the 30% default setting.

Table 2.19 Variations between the different G3 DARPin production processes.

Production stages	Cleavable tag-G3 DARPin	EAEAHis$_6$-G3 DARPin	His$_6$-G3 DARPin	EAEA(HE)$_3$-G3 DARPin	(HE)$_3$-G3 DARPin
Fermentation					
Primary culture until OD_{600} of 12 reached (h)	12 – 24				
Secondary culture until OD_{600} of 5 reached (h)	14 – 19				
Time from bioreactor inoculation to oxygen spike (h)	22 – 24				
Limited glycerol feed in bioreactor (h)	4	4	4	4	4
Limited methanol feed in bioreactor (h)	0 (10 ml methanol given during glycerol feed)	23	22	1	2
Harvest					
IMAC Column	Nickel (II) sulfate hexahydrate	Copper sulphate pentahydrate	Copper sulphate pentahydrate	Nickel (II) sulfate hexahydrate	Nickel (II) sulfate hexahydrate
Imidazole wash of radial flow column prior to harvesting	Yes	Yes	Yes	No	No
Purification					
Concentration, dialysis and FPLC steps	Yes	Yes	Yes	Yes	Yes
Dialysis fluid	PBS with 10 mM DTT	PBS	PBS with 10 mM DTT	PBS	PBS with 10 mM DTT
FPLC elution fluid	Eluted into PBS	Eluted into PBS	Eluted into PBS	Eluted into PBS	Eluted into PBS

Step 3- Biomass generation (limited glycerol feed)

At the time of the oxygen spike, a limited glycerol feed (volume 607 ml) was commenced and the bioreactor pH was set at 6.5. The limited glycerol feed commenced at 100 ml/h and reduced at pre-determined time points and discontinued at 4 h (Table 2.20). After 1 h of the limited glycerol feed, 10 ml 100% methanol was injected into the bioreactor to induce the AOX gene, facilitating transition from biomass generation into methanol-induced G3 DARPin protein production.

Step 4- Protein generation (limited methanol feed)

The limited methanol feed was commenced immediately after the limited glycerol feed and the methanol flow rate increased incrementally until it reached 45 ml/h, this rate was maintained until harvesting (Table 2.20). The length of the limited methanol feed was altered for each DARPin construct to optimise yields, by balancing DARPin production against DARPin breakdown due to *P. pastoris* proteases. For example, the cleavable tag-G3 DARPin had no limited methanol feed to prevent premature His_6 tag cleavage (Table 2.19).

Table 2.20 Limited glycerol feed for biomass generation and limited methanol feed for protein generation.

Time post oxygen spike (h)	Limited glycerol feed flow rate (ml/h)	Limited methanol feed flow rate (ml/h)
0	100	0
0.5	100	0
1.0	100	0 (10 ml methanol injected)
1.5	100	0
2.0	80	0
2.5	60	0
3.0	40	0
3.5	20	0
4.0	0	10
6.0	0	20
8.0	0	30
10.0 (until harvest)	0	45

2.2.3.2 Harvest

G3 DARPins were captured using a XC15 MD62 Radial Flow IMAC column (Proxcys Downstream Biosystems). Harvesting was tailored for each G3 DARPin.

IMAC purification is based on the principle that proteins with histidine based tags have an affinity for certain metal ions that can be immobilised on chromatographic media ensuring specific capture. Elution from the column is then achieved by increasing the imidazole concentration, as imidazole is a histidine analogue which competes with histidine for column binding (Bornhorst and Falke 2000). Low concentration imidazole buffer washes are commonly used prior to protein elution, to limit non-specific protein binding. However, prior developmental work performed by our Group had demonstrated that low concentration imidazole column washes increased $(HE)_3$-DARPins losses from the IMAC columns (non-published).

Prior to harvesting the radial flow column was prepared by:

1) Neutralising the column with 8 L of dH_2O.
2) Charging the column with metal ions (Table 2.19):
   - EAEAHis_6-G3 and His_6-G3: 1 L autoclaved 0.1M copper sulfate pentahydrate was applied to the column and excess copper removed with 3 L dH_2O.
   - EAEA$(HE)_3$-G3, $(HE)_3$-G3 and cleavable tag-G3: column was charged with 1 L autoclaved 0.1M nickel (II) sulfate hexahydrate and excess nickel was removed with 3 L dH_2O. A nickel charged IMAC column was used, as it had been efficient in purifying the $(HE)_3$-tagged affibody molecule (Tolmachev, Hofstrom et al. 2010).
3) De-gassing the column by applying short pulses of electricity from the feed pump.
4) Equilibrating the column with 1X equilibration/ wash solution:
   - EAEAHis_6-G3, His_6-G3 and cleavable tag-G3 wash solution contained 10 mM imidazole.
   - EAEA$(HE)_3$-G3 and $(HE)_3$-G3 did not contain imidazole.
5) Equilibrated columns stored at 4 °C until used.

At the time of harvesting the bioreactor temperature was reduced from 30 °C to 20 °C. Then 1.5 L of biomass from the bioreactor was added to the 2 L dilution vessel with a stirrer and 0.5 L 4X cell application solution (imidazole free for EAEA$(HE)_3$-G3 and $(HE)_3$-G3) was added to the vessel and the biomass was applied to the IMAC column. This was repeated several times to process the entire biomass. The rate of the limited methanol feed (if in process) was reduced by 2 increments, so that the

amount of methanol feed in proportion to cells in the bioreactor remained fairly constant.

After all of the biomass had been applied to the column, the cell debris was washed from the column with 1X equilibration/ wash solution with or without 10mM imidazole (5L). The matrix of the column was then washed with 20mM imidazole solution but this step was omitted for EAEA$(HE)_3$-G3 and $(HE)_3$-G3.

The DARPins were eluted from the column with 1 L of high concentration imidazole solution (200 mM) and collected in 20 fractions within 50 ml conical polypropylene tubes. Fractions with the highest protein concentrations determined by the optical density measured at 280 nm (OD_{280}) were pooled. The pooled fractions were filtered with a 0.2 µm PES 500 ml filter (Nalgene).

2.2.3.3 Concentration and dialysis

The harvested sample was concentrated using a Labscale TFF system with Pellicon XL 50 cassettes (BioMax 5 kDa filter) (Merck Millipore) which had been washed with dH_2O and then equilibrated with 200 mM imidazole, the stirrer speed was set at 1.5 rpm. When the sample volume reached 20-25 ml, the stirrer was stopped and the OD_{280} was assessed.

For dialysis, the DARPin sample volume was exchanged five to ten times (125-250 ml) against filtered PBS with or without 10 mM dithiothreitol (DTT), using the same system and filters as used for concentration (Table 2.19).

2.2.3.4 Fast protein liquid chromatography

DARPin samples were purified with the AKTA fast protein liquid chromatography (FPLC) system (GE Healthcare) using a Preparative Superdex 75 column (500 ml bed volume, pre-packed with Superdex 75 prep grade) (GE Healthcare). DARPin samples were run through the column at 1.5 ml/min in filtered PBS (pressure ≤ 0.3 MPa) and fractions (1ml) containing the monomer DARPin were collected in microcentrifuge tubes and stored at -80 °C. Samples were stored in filtered PBS with 10 mM DTT and filtered PBS alone.

Purified DARPin samples were analysed by coomassie staining and or FPLC using the Analytical Superdex 75 column (125 ml bed volume, pre-packed with Superdex

75 prep grade) (GE Healthcare) at 1 ml/min (pressure ≤ 0.3 MPa). The protein standards were run on the Analytical Superdex 75 Column to determine the estimated elution volume for the G3 DARPins.

2.2.4 Cleavage of His_6 tag from cleavable tag-G3

The recombinant type 14 3C protease from the human rhinovirus (HRV 3C) (Merck Millipore), is a purified His_6 tag fusion protein which is active at 4 °C (MW 22 kDa). HRV 3C was used to remove the His_6 tag from the cleavable tag-G3. The protease recognises the HRV 3C cleavage site, Leu(L)-Glu(E)–Val(V)–Leu(L)-Phe(F)-Gln(Q) * Gly(G)-Pro(P). This work was performed with assistance from Ms Maria Livanos (UCL Cancer Institute, London).

2.2.4.1 Optimisation cleavage study

The optimisation study assessed a range of conditions, including duration of cleavage, type of cleavage solution and HRV 3C protease concentration. A unit (U) of HRV 3C Protease is defined as the amount of enzyme that will cleave >95% of 100 µg HRV 3C Cleavage Control Protein in Cleavage Buffer at 4 °C over 16 h.

For most assessed cleavage reactions, 2 U of HRV 3C protease was used to treat 26.1 µg of cleavable tag-G3 (~76 U/mg) and the final reaction concentration was maintained at 40 U/ml. The final protease reaction concentration was varied in High Salt Cleavage Buffer to assess the concentration; 0.4, 0.8, 4 and 40 U/ml (Table 2.21).

Three different buffers were assessed, including PBS (155 mM NaCl, pH 7.4), Cleavage Buffer (150mM NaCl, 50mM Tris-HCl, pH 7.5, Merck Millipore) and High Salt Cleavage Buffer (800 mM NaCl, 50mM Tris-HCl, pH 7.5). The cleavable tag-G3 DARPin in PBS with 10 mM DTT was dialysed at 4 °C with 1 L of the appropriate buffer using Slide-A-Lyzer Dialysis Cassettes with 3,500 Da molecular weight cut off (MWCO) membranes and 0.5-3.0 ml capacity (Thermo Scientific). The buffer was changed three times over 24 h.

All test cleavage reactions were performed at 4 °C with 26.1 µg of cleavable tag-G3 DARPin (Table 2.21); samples were taken for analysis and stored in 4x SDS-PAGE reducing buffer. Each reaction was assessed by coomassie staining and western blotting using the antibodies as previously outlined (Table 2.18).

Table 2.21 Cleavage reactions assessed in optimisation cleavage study.

Solution	Volume (µl)
10X HRV Protease 3C Cleavage Buffer	4
Buffer containing cleavable tag-G3 (DARPin mass in each reaction)	45 (26.1µg)
HRV 3C Protease (concentration 2 U/µl)	1 (2 U/reaction)
Total Volume	50

2.2.4.2 Bulk cleavage

The most efficient conditions (HRV 3C Protease concentration, duration and buffer) were used for the bulk cleavage of cleavable tag-G3 (2.25 mg, concentration 0.75 mg/ml) to form untagged-G3.

2.2.4.3 Reverse purification of the untagged-G3 (subtractive IMAC)

Separation of the His_6 tagged HRV 3C Protease and cleaved His_6 tag from the untagged-G3 DARPin was performed by subtractive IMAC. A HisPur Ni-NTA column (4 ml, Thermo Scientific) was packed with HisPur Ni-NTA Resin (Nickel) and washed with three column volumes of dH_20. The column was then equilibrated with four column volumes of the selected buffer containing 10 mM DTT.

The cleavage reaction was applied to the column. The column was washed with two column volumes of the selected buffer containing 10 mM DTT and 1 ml aliquots of flow through were collected (untagged-G3). Two column volumes of elution buffer (250mM Imidazole) were then applied to the column and 1 ml aliquots of flow through were collected (HRV 3C protease and cleaved His_6 tag). The fractions were analysed by western blotting and coomassie staining as performed during the optimization study.

2.2.5 Matrix-assisted laser desorption/ionization (MALDI) Mass Spectrometry

The molecular weights of the G3 DARPins were assessed using the Waters Micromass MALDI micro MX mass spectrometer (Waters Corporation). The matrix was prepared by dissolving 10 mg of sinapic acid powder (Sigma-Aldrich) into 1 ml of 50% (v/v) acetonitrile. For analysis, 1 µl of matrix solution was placed onto the five-spot clusters of the mass spectrometry plate.

Cytochrome C (12,360 Da) was used for calibration prior to DARPin analysis. Stock cytochrome C was prepared by diluting 1 mg cytochrome C (Sigma-Aldrich) into 1 ml of 50% (v/v) acetonitrile (Sigma-Aldrich). Cytochrome C was mixed with an equal volume of 0.1% formic acid for analysis and 1 µl of this solution was placed in the central spot of the 5 spot cluster(s).

For sample analysis, a zip-tip pipette tip (Sigma-Aldrich) was pre-equilibrated by drawing up and expelling 0.1% (v/v) formic acid six times and then 100% (v/v) acetonitrile six times. The G3 DARPin sample was then drawn up and expelled six times. Finally, 3 µl of 0.1% formic acid was drawn up and placed into a microcentrifuge tube, and then 3 µl acetonitrile was drawn up and added to the same tube, using the same zip-tip pipette tip throughout for one sample. Sinapic acid solution (6 µl) was added to the sample tube and vortexed for 30 sec. Samples (1 µl) were analysed in duplicate and calibrated with cytochrome C.

2.2.6 Conjugation of the G3 DARPins

For site specific ^{111}In and ^{68}Ga radiolabelling, G3 DARPins were conjugated with maleimide-DOTA (mal-DOTA) (Macrocyclics), mal-NOTA (Chematech) or mal-CP256 (YM103, gift from King's College London) at the C-terminal cysteine. For conjugation, all solutions were treated with chelex-100 chelating ion exchange resin (Bio-Rad Laboratories) and all size exclusion columns were pre-packed with Sephadex G-25.

Ethylenediaminetetraacetic acid (EDTA) was added to the G3 DARPins (in PBS with 10 mM DTT) to a final concentration of 1 mM and left at RT for 30 min. Any remaining disulphide bonds were reduced with 5 mM Bond-Breaker Tris(2-carboxyethyl)phosphine hydrochloride (TCEP) solution, neutral pH (Thermo Fisher Scientific) for 2 h 30 min at RT. Subsequently, the G3 DARPins were buffer-exchanged using PD-10 size exclusion columns (GE Healthcare) into 0.1 M sodium phosphate buffer, pH 7. The G3 DARPins were then mixed with a 4-fold molar excess of mal-DOTA, mal-NOTA or YM103 at RT under constant gentle agitation for 72 h.

The DARPin conjugates were purified from unconjugated bifunctional chelator using PD-10 size exclusion columns (GE Healthcare), pre-equilibrated and eluted with 0.2 M ammonium acetate buffer, pH 7. The G3 DARPins were further purified by

centrifugation in a 2 ml Vivaspin with a 5,000 MWCO PES membrane (Sartorius Stedim). After each spin the filtered solution was replaced with 0.2 M ammonium acetate buffer, pH 7. Finally, the conjugated DARPins were dialysed at 4 °C against 0.2 M ammonium acetate pH 6.5 containing chelex-100 using a GeBAflex Maxi dialysis tube with a 3,500 Da MWCO membrane (Generon) over 72 h, the dialysis buffer was changed every 24 h. The conjugation efficiency was assessed by MALDI mass spectrometry. For example DOTA conjugation increases the G3 DARPin molecular weight by 526 Da.

2.2.7 G3 DARPin HER2 binding

2.2.7.1 Affinity and binding kinetics assessed by Surface Plasmon Resonance

Conjugated and unconjugated G3 DARPin kinetics and affinities were measured by Surface Plasmon Resonance (SPR) using ProteOn XPR36 (Bio-Rad Laboratories) with recombinant human HER2 extracellular domain (ECD, residues 1-631 of the mature protein) (EMP Genetech). This was performed by Dr Gabriela Nagy-Davidescu (University of Zurich).

Initially, HER2 ECD was biotinylated *in vitro* using EZ-Link Sulfo-NHS-SS-Biotin (six-fold molar excess of the biotinylating reagent relative to the target protein). Excess biotin was removed by a PD-10 size exclusion column (GE Healthcare) and dialysis against PBS.

For affinity determinations samples were assessed in duplicate. Two ligand channels of a Neutravidin Sensor Chip (ProteOn NLC) were coated with 900 resonance units of the biotinylated HER ECD. Five different concentrations of G3 DARPins (0.316 nM; 1 nM; 3.16 nM; 10 nM; 31.6 nM) were injected in parallel at a buffer flow rate of 100 µl/min in PBS containing 0.005% Tween-20, allowing 240 sec for association and 3600 sec for dissociation. Evaluation of the data was performed using the ProteOn Manager software (Bio-Rad Laboratories), to calculate the K_a (on rate or association), K_d (off rate or dissociation) and K_D (binding affinity).

2.2.7.2 Flow cytometry analysis of G3 DARPin binding to HER2-positive and HER2-negative cells

For analysis, DOTA conjugated G3 DARPins were labelled with cold indium chloride (Sigma-Aldrich) in 0.05 M HCl solution and unconjugated G3 DARPins were labelled

with cold sodium iodide (Sigma-Aldrich) in 0.1 M sodium hydroxide, using the same conditions required for ^{111}In and $^{123/125}$I radiolabelling reactions, respectively (see below). NOTA conjugated G3 DARPins were treated with 0.2 M acetate buffer at a range of different pH conditions, to assess NOTA-G3 DARPin compatibility for ^{68}Ga labelling at these conditions (Table 2.22). All assessed G3 DARPins were neutralised to physiological pH with PBS to a final concentration of 10 µg/ml, prior to flow cytometry assessment.

HER2-positive BT474 (American Type Culture Collection), HER2-positive OE-19 (Sigma-Aldrich) cells and HER2-negative MDA-MB-468 (American Type Culture Collection) cells were individually prepared by removal of media and incubation with 5 ml of 0.2% EDTA for 10 min. The cells were then transferred to centrifuge tubes (Elkay Laboratory Products) and centrifuged (4 °C, 4 min, 1000 rpm). The EDTA containing supernatant was removed and 5 ml of fresh media was added. Cells were counted and diluted to 1 million/ml with media, and 1 ml was used for each test condition. After washing the cell pellets with cold PBS (2 ml), 200 µl of DARPin (concentration 10 µg/ml) was added and incubated for 1 h at 4 °C, to minimise HER2 internalisation.

Cells were washed with cold PBS (2 ml) and incubated with 200 µl of mouse anti-DARPin (0.1% v/v in Dulbecco's-PBS) (K. Chester, UCL Cancer Institute, unpublished) for 1 h at 4 °C, then centrifuged as previously outlined and cell pellets retained. Subsequently, the cells were washed with cold PBS (2 ml) and incubated with 200 µl of Alexa Fluor 488 goat anti-mouse IgG (0.1% v/v in Dulbecco's-PBS) (Life Technologies) for 30 min at 4 °C, then centrifuged as outlined and cell pellets retained. After two further washing steps with cold PBS (2 ml), the cells were suspended in 500 µl of cold PBS. Negative control cell samples were not subjected to G3 DARPins but were treated with Dulbecco's-PBS alone or with anti-DARPin antibody followed by Alexa Fluor 488 antibody.

Samples were analysed on a CyAn ADP High-Performance Flow Cytometer (Becton Dickinson); cells were gated according to side scattering, forward scattering and pulse width, to ensure that only single cells were analysed (Figure 2.6). A total of 10,000 cell events were recorded per sample and data was analysed using FlowJo software (version 7; Tree Star).

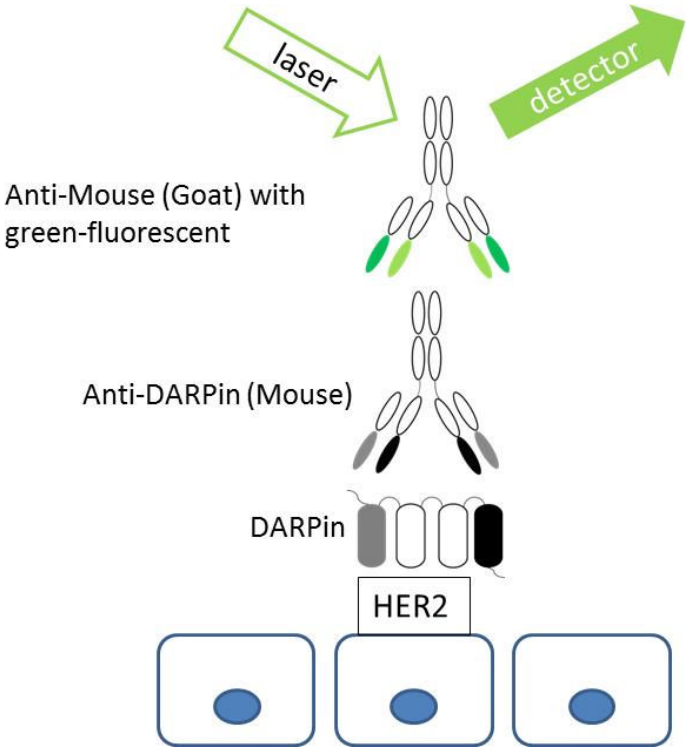

Figure 2.6 Stages required for flow cytometry.

2.2.8 Radiolabelling of the G3 DARPins

For *in vivo* assessment the radiochemical purity of radiolabelled G3 DARPins were >95%. Higher specific activities (SA) were required for the imaging studies (~ 30-60 MBq/nmol) than biodistribution studies (~1-2 MBq/nmol).

2.2.8.1 Radiolabelling with Indium-111

For ^{111}In radiolabelling, DOTA conjugated G3 DARPins in 0.2 M ammonium acetate pH 6.5 (5-60 µg) were mixed with $^{111}InCl_3$ (10-30 MBq, Covidien) and incubated for 2 h at 37 °C. The reactions were stopped by adding EDTA to a final concentration of 5 mM and purified by elution into PBS with a NAP-5 column (GE Healthcare). The radiochemical purity of the ^{111}In-G3 DARPins was determined by instant thin layer chromatography (iTLC) using the solvents 0.1 M ammonium acetate with 25 mM EDTA and 35% ammonia (v/v):ethanol:water (1:2:5) with iTLC- silica gel (SG) strips (Varian) (Table 2.8). If insoluble material was detected on iTLC, the reactions were filtered with 0.2 µm sterile syringe filters with a supor membrane (Pall Life Science).

2.2.8.2 Radiolabelling with Iodine-125

Non-conjugated G3 DARPins in PBS (30-60 µg) were mixed with iodine-125 (^{125}I, PerkinElmer, 10 MBq) in pre-coated Pierce iodination tubes (Thermo Scientific) for 10 min at RT. The reactions were stopped by adding sodium metabisulfite to a final concentration of 1 µM, and then purified by elution into PBS with a NAP-5 column. The radiochemical purity of the ^{125}I-G3 DARPins were determined by iTLC with iTLC-SG (Varian) strips using the solvent 0.1 M ammonium acetate with 25 mM EDTA (Table 2.8).

2.2.8.3 Radiolabelling with Iodine-123

Iodine-123 in 0.05 M NaOH, pH 10 (^{123}I, GE Healthcare) (15-20 MBq) was added to pre-coated Pierce iodination tubes (Thermo Scientific), followed by 100 µl of Tris Iodination Buffer (25 mM Tris-HCl, pH 7.5, 0.4 M NaCl). The non-conjugated DARPin in PBS (5 µg) was added to the tube. The reaction was performed for 10 min at RT and stopped by adding sodium metabisulfite to a final concentration of 1 µM. The radiochemical purity was assessed by the same iTLC method used for ^{125}I-G3 DARPins (Table 2.8) and a purification step was not required. An equivalent molar amount of 'cold' potassium iodide (3.4 X10^{-10} mol) was co-administered with ^{123}I-G3 DARPin, to minimise normal tissue uptake of 'free' ^{123}I (formed by de-iodination *in vivo*).

2.2.8.4 Radiolabelling with Gallium-68

Assessment of optimal pH conditions for Gallium-68 radiolabelling of NOTA-G3 DARPin

NOTA-G3 DARPin was radiolabelled at a range of different pH conditions (pH 3.6 to 7.7) at RT, to determine the optimal pH for ^{68}Ga radiolabelling. The test radiolabelling reactions were performed by adding 200 µl of acetate buffer to 20 µl ^{68}Ga (0.1 MBq/µl) eluted in 0.1 M HCl from an IGG100 ^{68}Ge/^{68}Ga Generator (Eckert & Ziegler) (Table 2.22). Subsequently, NOTA-G3 DARPin in 0.2 M ammonium acetate pH 6.5 (10 µg, concentration 1 mg/ml) was incubated with the buffered ^{68}Ga (pH 3.6 to 7.7). ^{68}Ga radiolabelling efficiency was assessed by iTLC using 0.1 M citrate buffer, pH 5 with iTLC-salicylic acid (SA) strips (Varian).

Table 2.22 Composition of 0.2 M acetate buffers used for ^{68}Ga-NOTA-DARPin radiolabelling.

0.2 M acetate buffer	0.2 sodium acetate (Vol. %)	0.2 M acetic acid (Vol. %)
pH 7.7	100 %	0 %
pH 6.5	95 %	5 %
pH 5.5	80 %	20 %
pH 4.6	49 %	51 %
pH 3.6	8 %	92 %

Gallium-68 radiolabelling of NOTA-G3 and YM103-G3 DARPin

NOTA-G3 DARPin in 0.2 M ammonium acetate pH 6.5 (10-30 µg) was mixed with 0.2 M ammonium acetate buffer pH 5 at a volume equivalent to the intended volume of ^{68}Ga. Subsequently, ^{68}Ga eluted from the IGG100 ^{68}Ge/^{68}Ga Generator (Eckert & Ziegler) in 0.1 M HCl was added to the buffered NOTA-G3 DARPin and incubated at RT for 10 min. The pH of the radiolabelling reaction was pH 4.6.

YM103-G3 DARPin in 0.2 M ammonium acetate pH 6.5 (20-30 µg) was mixed with 0.2 M ammonium acetate buffer pH 5 at a volume equivalent to the intended volume of ^{68}Ga. Subsequently, ^{68}Ga eluted from the IGG100 ^{68}Ge/^{68}Ga Generator (Eckert & Ziegler) in 0.1 M HCl was added to the buffered YM103-G3 DARPin and incubated at RT for 10 min. The pH of the radiolabelling reaction was pH 4.6, as Dr Maggie Cooper (King's College London) had determined this was the optimal pH for ^{68}Ga radiolabelling of YM103-G3 DARPin.

For ^{68}Ga-NOTA-G3 and ^{68}Ga-YM103-G3, iTLC was performed using the solvent 0.1 M citrate buffer, pH 5 with iTLC-SA strips (Varian) (Table 2.9). Insoluble material was detected on iTLC by assessing a control reaction performed with the same conditions but without adding G3 DARPin.

It was not necessary to add EDTA to the reactions for biodistribution studies as a high radiochemical purity was achieved. However, EDTA was added to the reactions prepared for imaging studies, to a final concentration of 5 mM, since their radiochemical purity was not as high.

2.2.9 Biodistribution studies

All animal studies were ethically reviewed and carried out in accordance with the UK Animals (Scientific Procedures) Act 1986 and UK Home Office regulations and local regulations.

2.2.9.1 Biodistribution studies in non-tumour and HER2-positive tumour bearing mice

DARPins were administered in 200 µl aliquots of PBS/0.1% BSA. For ^{111}In-G3 and ^{125}I-G3 DARPin studies mice were sacrificed at 4 h (n=4) and 24 h (n=4). While for ^{68}Ga-G3 DARPin studies mice were sacrificed at 1 h (n=4).

For non-tumour studies, female BALB/c mice aged 6-11 weeks (Charles River, mean weight 19 g), received an intravenous dose of 0.3 MBq of ^{111}In-G3 DARPin (2.2 µg [SA 2.0 MBq/nmol] to 4.3 µg [SA 1 MBq/nmol]) or ^{125}I-labelled G3 DARPin (2.8 µg [SA 1.6 MBq/nmol] to 4.3 µg [SA 1 MBq/nmol]). Based on the results of the studies in BALB/c mice with His_6-, $(HE)_3$- and untagged-G3 DARPins, the construct with the lowest normal tissue uptake (optimal G3 DARPin) was selected for assessment in tumour bearing mice.

For tumour studies, a single 60 day release 0.72 mg 17ß-estradiol pellet (Innovative Research of America) was inserted into the scruff of female SCID-beige mice aged 6-8 weeks (Charles River). The following day, the mice were inoculated by sub-cutaneous injection with BT474 cells (7.5 X 10^6 cells) (American Type Culture Collection) in PBS mixed with equivalent volumes of Basement Membrane Matrix that was growth factor reduced and lactate dehydrogenase-elevating virus free (Becton Dickinson). At 5-7 weeks post inoculation (mean mouse weight 24 g), the tumours reached 25-100 mm^2 and each mouse received 0.3 MBq of ^{111}In-G3 DARPin (2 µg [SA 2.2 MBq/nmol]), 0.3 MBq of ^{125}I-G3 DARPin (3 µg [SA 1.5 MBq/nmol]) or 1 MBq of ^{68}Ga-G3 DARPin (2.5 µg [SA 5.7 MBq/nmol]) intravenously.

In a trastuzumab blocking study, three female SCID-beige mice with BT474 tumours received intravenous trastuzumab (14.2 mg/kg or 350 µg/mouse) (Roche Diagnostics) 24 h prior to intravenous ^{111}In-G3 DARPin. The controls were three BT474 tumour bearing SCID-beige mice who only received intravenous ^{111}In-G3 DARPin. The mice were all sacrificed at 4 h post-administration of 0.3 MBq ^{111}In-G3 DARPin (1.9 µg [SA 2.3 MBq/nmol] per mouse).

Blood, selected organs and tumour (if present) were removed and radioactivity was measured in an LKB Wallac Gamma Counter 1282 Compugamma (LKB Instruments). Uptake was expressed as a mean ± SD of the percentage injected radioactive dose per gram of tissue (% ID/g).

To assess the HER2 tumour status, BT474 tumours were excised from four untreated SCID-beige mice, fixed in 10% formalin, embedded in paraffin and freshly cut (3 µm) for tissue slides. Tissue slides were deparaffinised in xylene and gradually rehydrated in graded alcohols and water. Epitope retrieval and immunohistochemical reactions were performed using the HercepTest (Dako) according to the manufacturer's instructions. The HER2-positive (3+ on IHC) human breast carcinoma cell line SK-BR-3 was used as the positive control. The negative control substituted the primary antibody, rabbit anti-human HER2 with normal rabbit immunoglobulins but used the same secondary antibody (goat anti-rabbit linked with HRP) for assessment of SK-BR-3 tumour cells. The IHC was performed with help from Mr Mohammed Rashid (UCL Cancer Institute).

2.2.9.2 Statistical analysis of normal tissue uptake in non-tumour bearing mice

An independent samples *t*-test was performed with SPSS Statistics 21 (IBM), to compare tissue uptake between the different radiolabelled G3 DARPins, a p value < 0.05 was considered statistically significant.

2.2.10 microSPECT/CT imaging of HER2-positive tumour xenografts

For imaging, the optimal G3 DARPin was radiolabelled directly with ^{123}I and via DOTA for ^{111}In. ^{125}I was substituted with ^{123}I for SPECT imaging, as it has a shorter-half (~13 h vs. ~59 days) and higher gamma energy emission (159 keV vs. 35.5 keV).

Female SCID-beige mice bearing BT474 tumours were injected intravenously with either 10.5 MBq of ^{123}I-G3 (2.1 MBq/µg [SA 30.1 MBq/nmol]) or 8.4 MBq of ^{111}In-G3 (4 MBq/µg [SA 58 MBq/nmol]) in 200 µl PBS/0.1% BSA.

Imaging was performed under isoflurane anaesthesia (2% at 1 L/min) at 4 h post injection using a microSPECT/CT animal scanner (Bioscan) equipped with a heated bed. Helical SPECT images were acquired in 20 projections over 30-40 min using a four-headed camera with 4×9 (1.4 mm) pinhole collimators. The CT images were

acquired in 180 projections with 1000 ms exposure time using a 45 peak kilovoltage (kVP) over 6 min for anatomical reference. Radionuclide images were reconstructed using HiSPECT (Scivis) iterative reconstruction software and fused with CT images using proprietary InVivoScope (Bioscan) software.

2.2.11 PET/CT imaging of mice bearing HER2-positive tumour xenografts

Female SCID-beige mice bearing BT474 tumours were injected intravenously with 4.5 MBq of the optimal ^{68}Ga-G3 DARPin (3.0 µg [SA 14.4 MBq/nmol]) in 200 µl PBS/0.1% BSA, for PET imaging studies.

Mice were scanned under anaesthesia (2% isoflurane in air, 1 L/min) on an animal Inveon PET/CT scanner (Siemens Preclinical Solutions). Mice were placed on the animal bed and then wrapped with SpaceDrape thermal protective material to reduce heat loss. Initially, a PET emission scan was acquired from 30 to 120 min post-administration and was followed by a CT scan (spatial resolution 108 µm, 80 kV, 500 µA) for anatomical reference. Scans were reconstructed using Inveon Acquisition Workplace software (version 1.5; Siemens Preclinical Solutions) with the following parameters: matrix, 128 x 128 x 159; pixel size, 0.776 x 0.776 x 0.796 mm^3; and β-value of 1.5 mm with uniform resolution. Scans were analysed with Inveon Research Workplace software (version 4.0, Siemens Preclinical Solutions), to quantify volume of interest (VOI) in MBq.

2.2.12 Affinity of selected radiolabelled G3 DARPin for HER2-positive cells

A saturation assay with BT474 cells was performed to evaluate the binding affinity of ^{111}In and ^{125}I radiolabelled G3 DARPins assessed in tumour bearing mice. This involves measuring the binding equilibrium by performing a titration of radiolabelled DARPin while keeping the amount of HER2 receptors constant.

BT474 cells were seeded at a density of 1 x 10^6 per well in Cellstar 6-well plates (Greiner bio-one) and grown to confluence over 24 h. The confluent cells were incubated in triplicate with 0.1 to 20 nM radiolabelled DARPin in Dulbecco's Modified Eagle Medium (DMEM) media with high glucose (4.5 g/L) containing 1% Foetal Calf Serum (Biosera) and 0.1% sodium azide (to minimize internalization) for 1 h 30 min at 37 °C. Non-specific binding was determined by a parallel series of radiolabelled G3 DARPins with 1,000 nM non-radiolabelled G3 DARPin assessed in triplicate.

The assays were stopped by removing the media containing radiolabelled G3 DARPin and washing the cells twice with ice cold media and once with ice cold PBS. The cells were lysed with 1 M sodium hydroxide and collected. The wells were washed twice with PBS and the washes were pooled with the cell lysate for analysis. The radioactivity was counted for 1 min in a LKB Wallac Gamma Counter 1282 Compugamma (LKB Instruments). The protein concentration per million cells was assessed from wells containing untreated BT474 cells using the DC (detergent compatible) colorimetric protein assay (Bio-Rad Laboratories) as per the manufacturer's instructions.

The total binding curve was determined from the samples with the increasing concentrations of radiolabelled DARPin in absence of cold DARPin (measures combined specific binding to receptor and non-specific binding). The non-specific binding curve was determined from the increasing concentration of radiolabelled DARPin in presence of cold DARPin (measures non-receptor radioligand binding). Finally, the specific receptor binding is determined from the total binding minus the non-specific binding (Figure 2.7). The affinity and B_{Max} (maximum binding capacity) was calculated by nonlinear regression using Prism software (GraphPad Software).

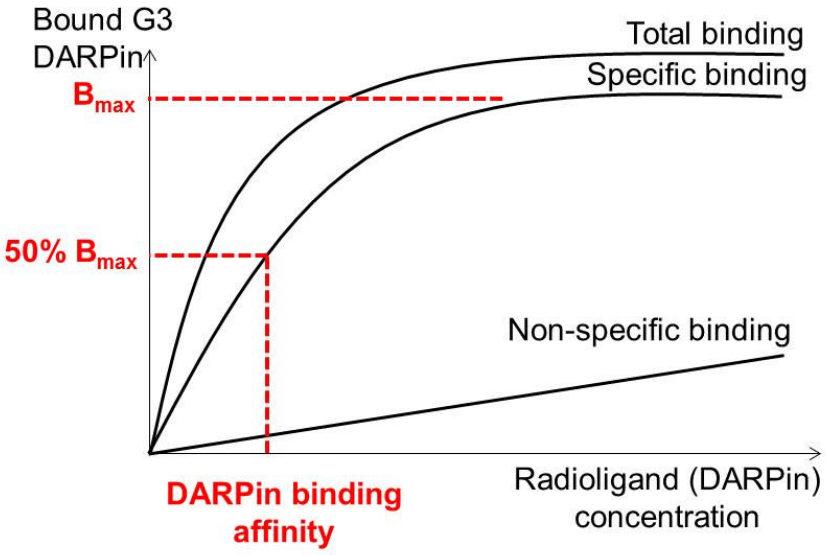

Figure 2.7 Analysis of cell saturation binding assay.

2.2.13 *In vitro* stability of selected radiolabelled DARPin

The stability of the ^{111}In-G3 DARPin administered to HER2-positive tumour bearing mice was assessed in PBS or in human serum:PBS (1:1). The human serum was isolated from whole blood collected in a BD Vacutainer SST gel tubes (Becton Dickinson) by centrifugation at 1,000 x *g* for 10 min. Serum stability was assessed at 37 °C, while stability in PBS was assessed at 4 °, 20 ° and 37 °C for 24 h post radiolabelling by iTLC. After incubation, the stability of the ^{111}In-G3 DARPin was assessed by SDS-PAGE using non-reducing conditions, followed by autoradiography using a Cyclone Storage Phosphor System (PerkinElmer).

2.2.14 Genotyping HER2 transgenic mice

Hemizygous B6.Cg-Tg(Wap-ERBB2)229Wzw/J transgenic mice (The Jackson Laboratory) which express human HER2 in their mammary glands and cerebellum under the control of the mouse whey acidic protein (WAP) promoter were used for pre-clinical toxicity assessment (Piechocki, Ho et al. 2003). A cohort of wild and HER2 transgenic mice were bred and genotyped by The Jackson Laboratory; their HER2 status was verified at UCL.

Ear punch biopsies were taken from The Jackson Laboratory bred mice and a negative control mouse (C57 Black; C57BL/6J). DNA was extracted from the ear biopsies using the HotSHOT genomic DNA isolation protocol. Initially, 75 µl of Alkaline Lysis Buffer was added to the biopsies within 1.5 ml microcentrifuge tube, followed by heating at 95 °C for 40 min. After 1 h of cooling, 75 µl of Neutralisation Buffer was added and the biopsies were centrifuged at 4,000 rpm for 4 min (Table 2.10). PCR was performed on samples of the supernatant.

The lyophilised primers (Integrated DNA Technologies) were dissolved with filtered dH_2O to make a stock solution of 10 µM (Table 2.23). The mouse interleukin-2 (IL-2) gene was used as an internal control, to confirm that there was sufficient DNA in the sampled supernatant for assessment. Negative controls were performed by substituting DNA-containing supernatant with dH_2O.

Table 2.23 Human HER2 transgene and mouse IL-2 gene primers used for mouse genotyping.

Primer name	Sequence (5'-3')	Melting temperature (°C)	Molecular weight (Da)
HER2 transgene Sense	5' GAGCCGCGAGCACCCA 3'	61.8	4,861.2
HER2 transgene Anti-sense	5' GGTGGGCAGGTAGGTGAGTTCC 3'	61.8	6,887.5
Mouse IL-2 Sense	5' CTAGGCCACAGAATTGAAAGATCT 3'	54.7	7,369.9
Mouse IL-2 Anti-sense	5' GTAGGTGGAAATTCTAGCATCATCC 3'	55.2	7,681.0

The IL-2 primers were efficient at 1 µM concentration and HER2 transgene primers were efficient at 0.25 µM concentration (Table 2.24). The conditions for the IL-2 and HER2 PCRs were identical and performed in the GeneAmp PCR System 2700 (Life Technologies) (Table 2.25).

Table 2.24 PCR of the human HER2 transgene and mouse IL-2 gene.

Constituent	Volume (µl)	Final reaction concentration
De-ionised water	14.5 µl (HER2) or 11.5 µl (IL-2)	
Dream Taq Buffer 10x contains 20 mM $MgCl_2$ (Thermo Scientific)	2 µl	1X
dNTPs (10 mM)	0.4 µl	0.2 mM
Sense primer (10 µM)	0.5 µl (HER2) or 2 µl (IL-2)	0.25 µM (HER2) or 1 µM (IL-2)
Anti-sense primer (10 µM)	0.5 µl (HER2) or 2 µl (IL-2)	0.25 µM (HER2) or 1 µM (IL-2)
Dream Taq polymerase (5 U/µl) (Thermo Scientific)	0.1 µl	0.5 U/reaction
Supernatant with extracted DNA	2 µl	
Total volume	20 µl	

Table 2.25 HER2 transgene and IL-2 PCR conditions.

Stage	Temperature (°C)	Time	Cycles
Initialisation	94	3 min	1
Denature	94	30 sec	30
Anneal	66	45 sec	
Elongate	72	45 sec	
Final elongation	72	2 min	1
Hold	5	Until discontinued	

After the PCR, DNA 10x loading buffer (2 µl) was added to the PCR samples and the samples were applied to the wells of 1.5% agarose gels. To confirm the presence of the human HER2 gene and mouse IL-2 gene the DNA from the agarose gel bands of selected mice were extracted and purified with the Wizard SV Gel and PCR Clean-Up System (Promega), as previously outlined. The extracted and purified DNA was sequenced by the DNA Sequencing Service at the UCL Cancer Institute.

2.2.15 Breeding HER2 transgenic mice

The homozygous variant is fatal *in utero*, while the hemizygous variant is viable, so wild and hemizygous mice were bred with each other (Piechocki, Ho et al. 2003). All newborn mice were genotyped when they were weaned and breeding pairs were assigned based on their genotype.

2.2.16 Endotoxin removal from $(HE)_3$-G3 DARPin prior to mouse administration

Endotoxins were removed from the G3 DARPins with the Pierce High-Capacity Endotoxin Removal Resin (Thermo Scientific) according to the manufacturer's instructions. A column with 1 ml resin volume was used; it is capable of removing endotoxins from 2-10 ml samples. All consumables and solutions used were endotoxin-free. This was performed by Miss Maria Livanos and Miss Leah Ensell (UCL Cancer Institute).

Briefly, degassed resin slurry (50% slurry in 20% ethanol) was applied to the column (1 ml volume). The column was washed with five column volumes of 0.2 M sodium hydroxide. Then the column was washed with five column volumes of 2 M sodium chloride, followed by five column volumes of endotoxin-free ultrapure water. The column was equilibrated with five column volumes of Dulbecco's-PBS without calcium and magnesium (PAA Laboratories).

$(HE)_3$-G3 DARPin in PBS was applied to the column and eluted in one column volume of Dulbecco's-PBS without calcium and magnesium (PAA Laboratories), the sample was applied and eluted from the same column five times. After the fifth elution, 10 mM BioUltra DTT (Sigma-Aldrich) was added to the sample to prevent dimerisation and stored at -80 °C.

Prior to mice administration, the $(HE)_3$-G3 DARPin in PBS with DTT was buffer exchanged using a PD-10 column (GE Healthcare) into Dulbecco's-PBS without calcium and magnesium (PAA Laboratories). This was collected as three separate aliquots.

2.2.17 Analysis of $(HE)_3$-G3 DARPin prior to mice administration for toxicity assessment

2.2.17.1 Endotoxin levels

Endotoxin levels were assessed after endotoxin removal, using the Pierce LAL Chromogenic Endotoxin Quantification Kit (Thermo Scientific), according to the manufacturer's instructions.

2.2.17.2 Dimerisation status

$(HE)_3$-G3 DARPin in 4x non-reducing buffer was assessed by SDS-PAGE and coomassie staining, as well as FPLC using the Analytical Superdex 75 column (125 ml bed volume, pre-packed with Superdex 75 prep grade) (GE Healthcare) at 1 ml/min (pressure ≤ 0.3 MPa).

2.2.18 Pre-clinical toxicity study

2.2.18.1 Mouse $(HE)_3$-G3 DARPin dosing

Mice received unconjugated $(HE)_3$-G3 DARPin at 50 or 100 times the human equivalent dose (HED) in Dulbecco's PBS. According to the U.S. Department of Health and Human Services Food and Drug Administration (FDA) Center for Drug Evaluation and Research (CDER) two methods can be used to convert mouse doses into human doses (U.S. Department of Health and Human Services 2005). In this situation, the mouse dose was calculated from the planned human trial dose, 500 µg.

1) Conversion based on body surface area for mice weighing 11-34 g

Mouse dose (mg/kg) = Human dose (mg/kg) multiplied by 12.3.

Human dose is 500 µg, formula assumes human body weight is 60 kg, so human dose is $8.33 X10^{-3}$ mg/kg.

Mouse dose 0.10 mg/kg is the HED ($8.33 X10^{-3}$ mg/kg multiplied by 12.3)

Mouse dose 10 mg/kg is 100 times the HED

2) Conversion based on body surface area for mice weighing more than 34 g

HED (mg/kg) = mouse dose in mg/kg x (animal weight in kg/human weight in kg)$^{0.33}$

e.g. 50 g mouse and formula assumes human weight 60 kg

8.33 X10^{-3} mg/kg = mouse dose x (0.050/60)$^{0.33}$

Mouse dose of 0.087 mg/kg is the HED

Mouse dose of 8.7 mg/kg is 100 times the HED

The assessed HER2 transgenic and wild type mice weighed between 35 and 51 g, while the assessed CD-1 mice weighed between 33 and 36 g. Thus, mice received 9-10 mg/kg intravenously to achieve 100 times the HED or 4.5-5 mg/kg for 50 times the HED.

2.2.18.2 Toxicity study in HER2 transgenic and wild type mice

Four HER2 transgenic and eight wild type B6.Cg-Tg(Wap-ERBB2)229Wzw/J mice received 100 times the HED of $(HE)_3$-G3 DARPin intravenously. Control HER2 transgenic (n=3) and control wild type mice (n=7) received Dulbecco's PBS intravenously. The mice were euthanised at 24 h post-administration and blood sampling was performed under terminal anaesthesia to assess haematology and clinical chemistry. Histological analysis was performed on the liver, heart, kidneys, spleen, brain, adrenals and mammary glands. The six older control mice only had their livers' and blood biochemistry assessed (Table 2.26).

Table 2.26 Trasngenic (T) and wild (W) type mice received 100 X HED of $(HE)_3$-G3 DARPin in Dulbecco's-PBS. Control (C) mice received Dulbecco's-PBS.

Mouse	Sex	Age (months)	Genotype	Dose	Histology	Biochemistry	Haematology
C1	F	3	Wild	PBS	7 organs	Yes	Yes
C2	F	3	Wild	PBS	7 organs	Yes	Yes
C3	M	3	Wild	PBS	7 organs	Yes	Yes
C4	M	3	Wild	PBS	7 organs	Yes	Yes
C5	M	12	HER2	PBS	Liver	Yes	No
C6	M	12	Wild	PBS	Liver	Yes	No
C7	M	11	HER2	PBS	Liver	Yes	No
C8	M	9	Wild	Untreated*	Liver	Yes	No
C9	M	9	Wild	PBS	Liver	Yes	No
C10	M	9	HER2	PBS	Liver	Yes	No
W1	F	6	Wild	100X HED	7 organs	Yes	Yes
W2	F	6	Wild	100X HED	7 organs	Yes	Yes

W3	F	6	Wild	100X HED	7 organs	Yes	Yes
W4	M	6	Wild	100X HED	7 organs	Yes	Yes
W5	M	5	Wild	100X HED	7 organs	Yes	Yes
W6	M	5	Wild	100X HED	7 organs	Yes	Yes
W7	M	5	Wild	100X HED	7 organs	Yes	Yes
W8	F	5	Wild	100X HED	7 organs	Yes	Yes
T1	F	9	HER2	100X HED	7 organs	Yes	Yes
T2	F	9	HER2	100X HED	7 organs	Yes	Yes
T3	M	9	HER2	100X HED	7 organs	Yes	Yes
T4	M	9	HER2	100X HED	7 organs	Yes	Yes

*unable to cannulate tail vein, 7 organs include heart, kidneys, spleen, brain, adrenals, mammary glands and liver.

2.2.18.3 CD-1 mice liver toxicity study

To determine whether $(HE)_3$-G3 DARPin causes liver damage, CD-1 mice were assessed as their normal phenotype is better characterised than the transgenic mice. Male CD-1 mice were treated with 100 times the HED (n=6), 50 times the HED (n=6) or Dulbecco's-PBS (n=6). At 24 h post administration the mice were euthanised and their livers' were removed for histological analysis (Table 2.27).

Table 2.27 Male CD-1 mice treated at 100X HED and 50X HED of $(HE)_3$-G3 DARPin. Control (C) CD-1 mice received Dulbecco's-PBS.

Mouse	Sex	Age (months)	Dose	Histology
C1	M	2	PBS	Liver
C2	M	2	PBS	Liver
C3	M	2	PBS	Liver
C4	M	2	PBS	Liver
C5	M	2	PBS	Liver
C6	M	2	PBS	Liver
50.1	M	2	50X HED	Liver
50.2	M	2	50X HED	Liver
50.3	M	2	50X HED	Liver
50.4	M	2	50X HED	Liver
50.5	M	2	50X HED	Liver
50.6	M	2	50X HED	Liver
100.1	M	2	100X HED	Liver
100.2	M	2	100X HED	Liver
100.3	M	2	100X HED	Liver
100.4	M	2	100X HED	Liver
100.5	M	2	100X HED	Liver
100.6	M	2	100X HED	Liver

2.2.18.4 Blood and histological analysis

Biochemistry samples were collected in BD plasma separation tubes containing lithium heparin (Becton Dickinson). Immediately after collection samples were inverted 10 times, they were centrifuged within 2 h of collection at 1,300 X *g* for 15 min in a fixed angle centrifuge. The plasma was collected and stored at -80 °C until analysis.

Haematology samples were collected in 0.5 ml EDTA containing tubes (Teklab); the samples were inverted 10 times after collection and stored at 4 °C until analysis.

Deceased mice were stored in 10% neutral buffered formalin within 500 ml plastic pots (Pioneer Research Chemicals) until dissection for histological assessment.

All blood and tissue samples were analysed by Sequani. The analysis was performed to Good Laboratory Practice (GLP) standards but was not performed in audited laboratories, so was technically non-GLP compliant.

2.2.18.5 HER2 status of the livers from HER2 transgenic and wild type mice

The HER2 status of livers' from transgenic (n=1) and wild type (n=1) mice were assessed, to determine whether $(HE)_3$-G3 DARPin could bind to HER2 in the liver. This work was performed by UCL Advanced Diagnostics.

HER2 immunohistochemistry

HER2 IHC was performed with the Bond Polymer Refine Detection (Leica Biosystems Newcastle), which utilises a primary rabbit antibody targeting human HER2 and secondary goat anti-rabbit-HRP antibody. DAB was used to visualise the antibody complexes bound to the human HER2 receptors. There is a good concordance between the Bond HER2 IHC and the FDA approved HercepTest which utilises a rabbit anti-human HER2 (O'Grady, Allen et al. 2010).

Human breast cancer tissue microarrays (TMAs) were used as positive and negative controls. In addition, negative controls using only the secondary antibody were performed on each assessed mouse liver.

Chromogenic in situ hybridisation (CISH)

The INFORM HER2 Dual ISH DNA Probe Cocktail (Ventana Medical Systems) which contains a HER2 DNA probe (labelled with the hapten dinitrophenyl or DNP) and a chromosome 17 centromere DNA probe (labelled with the hapten digoxigenin or DIG) was used for CISH analysis. The DNA probes are added first, followed by the primary antibody and secondary antibody conjugated with an enzyme. The black HER2 signal is catalysed by HRP from silver and the red chromosome 17 centromere signal is catalysed by alkaline phosphatase from naphthol, fast red.

For single-probe assessment the HER2 gene is amplified when ≥ 6.0 signals/cell and for dual-probe ISH the HER2 gene is amplified if the HER2/Ch17 ratio is ≥ 2.0. (Wolff, Hammond et al. 2013).

Chapter 3 Production of G3 DARPins with different N-terminus domains

3.1 Introduction

The G3 DARPin has high affinity for the HER-2 receptor assessed by SPR (90 pmol/L) and cell binding analysis (~60-100 pmol/L with BT474 cells) (Zahnd, Wyler et al. 2007; Zahnd, Kawe et al. 2010). The structure of the G3 DARPin includes an N-terminal capping repeat, two internal repeats and a C-terminal capping repeat. Based on structural modelling, the G3 DARPin and trastuzumab bind to adjacent and non-overlapping epitopes of subdomain 4 of the HER2 ECD, by contrast pertuzumab binds to subdomain 2 (Epa, Dolezal et al. 2013). Thus, G3 DARPin should be able to bind in the presence of trastuzumab and pertuzumab.

Development of the G3 DARPin for HER2 molecular imaging depends on minimising normal tissue uptake to achieve high tumour-to-normal tissue ratios. To date, only G3 DARPins with a His_6 tag used for technetium radiolabelling have been assessed *in vivo*. ^{99m}Tc-His_6-G3-DARPin was associated with high HER2-positive tumour uptake (> 8 % ID/g over 24 h) and HER2-positive tumours could be seen on microSPECT/CT scanning. However, ^{99m}Tc-His_6-G3-DARPin had low tumour-to-liver ratios (< 2 for 48 h post-administration), which could prevent the identification of liver metastases on imaging (Zahnd, Kawe et al. 2010).

Exchanging the His_6 tag of an anti-HER2 affibody molecule for a negatively charged $(HE)_3$ tag reduced background liver uptake, while also enabling tag-mediated purification by IMAC (Tolmachev, Hofstrom et al. 2010; Hofstrom, Orlova et al. 2011). The effect of altering or removing the G3 DARPin N-terminus histidine-based tag on normal tissue uptake is unknown (Zahnd, Kawe et al. 2010). The G3 DARPin N-terminus does not participate in HER2 binding, so alteration of the N-terminus tag would not be expected to alter HER2 binding affinity and kinetics (Zahnd, Wyler et al. 2007; Epa, Dolezal et al. 2013). Thus, it is necessary to produce different variants of the G3 DARPin for subsequent *in vivo* comparison.

The *P. pastoris* production platform was selected for G3 DARPin production as it has several advantages compared to mammalian cell lines and the *E. coli* platform. Compared to mammalian cell lines, *P. pastoris* has a shorter fermentation time, faster transition from gene synthesis to protein production, cheaper production costs and use of media without animal derived products thus minimising the potential for

viral contamination. Recombinant protein is secreted from *P. pastoris* cells directly into the media, under the control of the α-factor signal sequence within the pPICZαB plasmid, by contrast recombinant protein is not secreted by *E. coli* cells. *P. pastoris* cells are capable of performing post-translation modifications to proteins, including proteolysis by Ste13 and Kex2 proteases, this does not occur in *E. coli* (Table 3.1). Downstream processing of recombinant proteins produced by *P. pastoris* is easier than processing of recombinant proteins produced by *E. coli,* as only low concentrations of *P. pastoris* host cell proteins are released into the media. The recombinant histidine-based tagged proteins secreted by *P. pastoris* can be isolated via IMAC (Tolner B 2012).

Table 3.1 Amino acid sequences cleaved by *P. pastoris* Kex2 and Ste13 proteinases.

Proteinase	Protein cleavage site(*)
Kex2 gene product	Glu(E)-Lys(K)-Arg(R) * (amino acid)
Ste13 gene product	Glu (E)-Ala(A) * (amino acid)

Aim:

To test the hypothesis that; purified G3 DARPins can be produced with and without histidine based N-terminal tags by a *P. pastoris* production platform.

Objectives:

To produce three variants of the G3 DARPin which only differ from each other at their N-terminus and have a unique C-terminal cysteine for site specific radiolabelling, using the *P. pastoris* expression system (Figure 3.1) (Tolner, Smith et al. 2006).

1) His_6-G3
2) $(HE)_3$-G3
3) Untagged-G3 DARPins

Structure of proposed G3 DARPin variants

The cleavable tag-G3 with a cleavable His_6 was the precursor for the untagged-G3. Initially, the G3 DARPins were designed with LEKREAEA residues preceding their tags, which can potentially be cleaved by the combined action of the *P. pastoris* Kex2 and Ste13 proteinases (Table 3.1), so all G3 DARPin proteins would commence at their histidine based tags (Figure 3.1 and Figure 3.2). This meant that all DARPins could be purified by IMAC and the untagged-G3 could be formed post purification by His_6 tag cleavage (Figure 3.1). The cleavable tag-G3 contained the residues LEVLFQ/GP which forms the site recognised by HRV 3C protease and results in GP being retained, so for consistency purposes all DARPins incorporated a GP sequence at the N-terminus (Figure 3.1).

Pre-cleavage	HHHHHHGGGSGLEVLFQGPGS**D**LGKKLLEAARAGQDDEVRILMANGAD
Untagged G3	GPGS**D**LGKKLLEAARAGQDDEVRILMANGAD
His_6-G3	HHHHHHGPGS**D**LGKKLLEAARAGQDDEVRILMANGAD
$(HE)_3$-G3	HEHEHEGPGS**D**LGKKLLEAARAGQDDEVRILMANGAD

Pre-cleavage	VNAKDEYGLTPLYLATAHGHLEIVEVLLKNGADVNAVDAIGFTPLHLAAF
Untagged G3	VNAKDEYGLTPLYLATAHGHLEIVEVLLKNGADVNAVDAIGFTPLHLAAF
His_6-G3	VNAKDEYGLTPLYLATAHGHLEIVEVLLKNGADVNAVDAIGFTPLHLAAF
$(HE)_3$-G3	VNAKDEYGLTPLYLATAHGHLEIVEVLLKNGADVNAVDAIGFTPLHLAAF

Pre-cleavage	IGHLEIAEVLLKHGADVNAQDKFGKTAFDISIGNGNEDLAEIL**Q**KLNGGC
Untagged G3	IGHLEIAEVLLKHGADVNAQDKFGKTAFDISIGNGNEDLAEIL**Q**KLNGGC
His_6-G3	IGHLEIAEVLLKHGADVNAQDKFGKTAFDISIGNGNEDLAEIL**Q**KLNGGC
$(HE)_3$-G3	IGHLEIAEVLLKHGADVNAQDKFGKTAFDISIGNGNEDLAEIL**Q**KLNGGC

Figure 3.1 Desired amino acid sequences of His_6-G3, $(HE)_3$-G3 and untagged-G3 DARPins.
All constructs have a C-terminal gly-gly-cys tag for maleimide labelling and glycine-proline (GP) residues. The two Tyr that can be labelled with iodine are highlighted (yellow), the first and last residues of the G3 DARPin are emboldened and the common residues are underlined

EAEAHis_6-G3 and EAEA$(HE)_3$-G3 refers to the G3 DARPins which had LEKREAEA residues preceding their histidine based tags prior to the action of Kex2 and Ste13 *P. pastoris* proteinases. While His_6-G3 and $(HE)_3$-G3 refers to G3 DARPins which only had LEKR preceding their histidine based tags prior to the action of Kex2 (Figure 3.2).

A) EAEAHis$_6$-G3

```
          Kex2     Ste13     Ste13
C*TC GAG AAA AGA GAG GCT GAA GCT cat cac cat cat cac cat GGA CCA
  L   E   K   R   E   A   E   A   H   H   H   H   H   H   G   P
ggttctgatttgggaaagaaattgttggaa
 G  S  D  L  G  K  K  L  L  E
gctgctagagctggtcaagatgatgaagttagaattttgatggctaacggtgctgatgtt
 A  A  R  A  G  Q  D  D  E  V  R  I  L  M  A  N  G  A  D  V
aacgctaaggatgaatacggtttgactccattgtacttggctactgctcatggtcatttg
 N  A  K  D  E  Y  G  L  T  P  L  Y  L  A  T  A  H  G  H  L
gaaattgttgaagttttgttgaagaatggagctgatgttaacgctgttgatgctattggt
 E  I  V  E  V  L  L  K  N  G  A  D  V  N  A  V  D  A  I  G
tttactccattgcatttggctgcttttattggtcatttggaaattgctgaagttttgttg
 F  T  P  L  H  L  A  A  F  I  G  H  L  E  I  A  E  V  L  L
aagcatggtgccgacgttaacgctcaggataagtttggaaagactgcttttgatatttct
 K  H  G  A  D  V  N  A  Q  D  K  F  G  K  T  A  F  D  I  S
attggtaacggtaacgaagatttggctgaaattttgcaaaagttgaacGGAGGTTGC
 I  G  N  G  N  E  D  L  A  E  I  L  Q  K  L  N  G  G  C
TAATAAt^ctagataatta
 -  -
```

B) EAEA(HE)$_3$-G3

```
          Kex2     Ste13     Ste13
C*TC GAG AAA AGA GAG GCT GAA GCT cat gag cat gaa cac gaa GGA CCA
 L   E   K   R   E   A   E   A   H   E   H   E   H   E   G   P
ggttct. . . . . . . . . . . . GGAGGTTGCTAATAAt^ctagataatta
 G  S  . . . . . . . . . . . . G  G  C  -  -
```

C) Cleavable tag-G3

```
          Kex2     Ste13     Ste13
C*TC GAG AAA AGA GAG GCT GAA GCT cat cac cat cat cac cat
  L   E   K   R   E   A   E   A   H   H   H   H   H   H
CGG AGG TGG CTC TGG TTA GAG GTA TTG TTT CAA / GGA CCA
 G   G   G   S   G   L   E   V   L   F   Q   /  G   P
ggttct. . . . . . . . . . . . GGAGGTTGCTAATAAt^ctagataatta
 G  S  . . . . . . . . . . . . G  G  C  -  -
```

D) His$_6$-G3

```
          Kex2
C*TC GAG AAA AGA cat cac cat cat cac cat GGA CCA
  L   E   K   R   H   H   H   H   H   H   G   P
ggttct. . . . . . . . . . . . GGAGGTTGCTAATAAt^ctagataatta
 G  S  . . . . . . . . . . . . G  G  C  -  -
```

E) (HE)$_3$-G3

```
          Kex2
C*TC GAG AAA AGA cat gag cat gaa cac gaa gga cca
  L   E   K   R   H   E   H   E   H   E   G   P
ggttct. . . . . . . . . . . . GGAGGTTGCTAATAAt^ctagataatta
 G  S  . . . . . . . . . . . . G  G  C  -  -
```

Figure 3.2 Desired nucleic acid and amino acid sequences of EAEAHis$_6$-G3, EAEA(HE)$_3$-G3, cleavable tag, His$_6$-G3 and (HE)$_3$-G3.
Proteinase site of products from Kex2 and Ste13 genes highlighted, XhoI (*) and (^) XbaI endonuclease sites, site recognised by HRV 3C (underlined and cleavage site denoted by /) and stop codons (-). N-terminus tag and C-terminus shown in red. The complete G3 DARPin sequence is only shown for EAEAHis$_6$-G3 and was identical for all constructs, (.) omission of common amino acid and nucleic acid sequences.

3.2 Results

3.2.1 PCR of G3 DARPin DNA

DNA encoding EAEAHis$_6$-G3, EAEA(HE)$_3$-G3 and cleavable tag-G3 were derived from PCR of the ANK-1 DNA plasmid (please refer to Materials and Methods). A short PCR (utilising the conventional sized Sense primer and Truncated Sense primer) and long PCR (only utilising the conventional sized Sense primer) were performed for each construct. For EAEAHis$_6$-G3, EAEA(HE)$_3$-G3 and cleavable tag-G3 both the short and long PCR methods were successful in amplifying G3 DARPin DNA (Figure 3.3). For consistency purposes, DNA from the short PCR process was used for the subsequent G3 DARPin production.

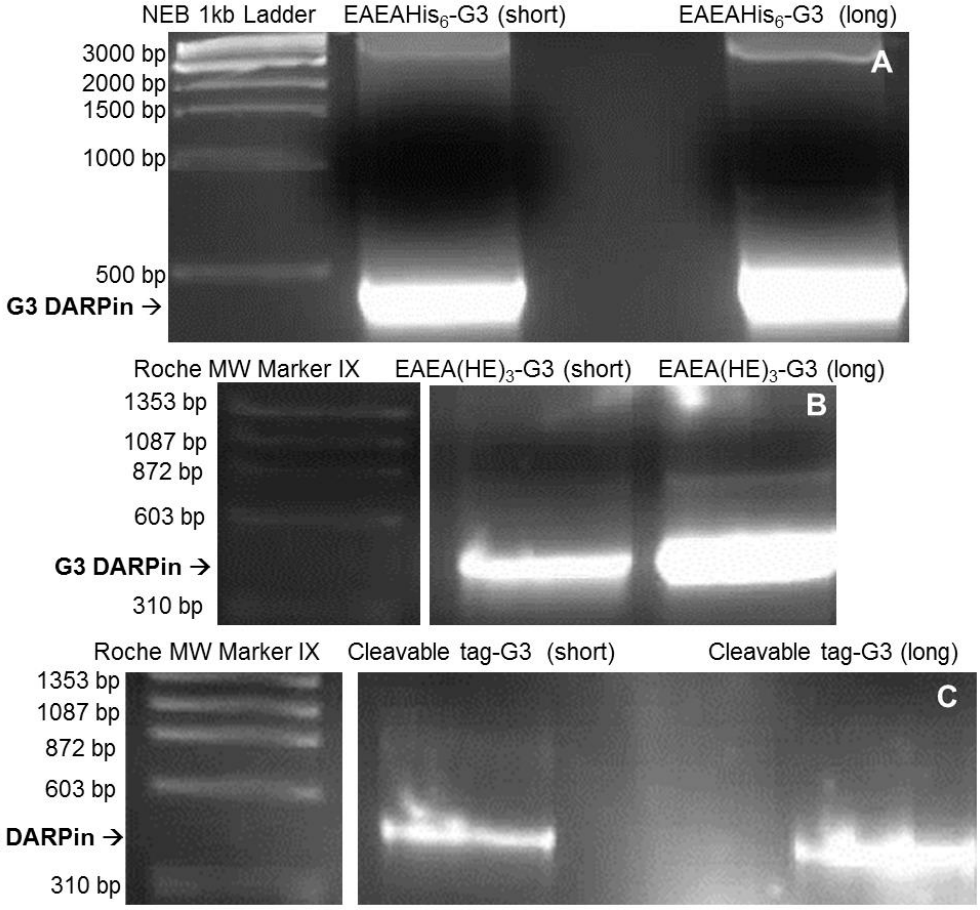

Figure 3.3 Agarose gels (2%) showing G3 DARPin PCR products using ANK-1.
A) EAEAHis$_6$-G3: Short used EAEAHis$_6$ Sense and Truncated Sense with Anti-Sense G3. Long used EAEAHis$_6$ Sense with Anti-Sense G3
B) EAEA(HE)$_3$-G3: Short used EAEA(HE)$_3$ Sense and Truncated Sense with Anti-Sense G3. Long used EAEA(HE)$_3$ Sense with Anti-Sense G3
C) Cleavable tag-G3: Short used Cleavble tag Sense and Truncated Sense with Anti-Sense G3. Long used Cleavable tag Sense with Anti-Sense G3

PCR of the DNA ligations, pPICZαB/EAEAHis3 and pPICZαB/EAEAHE3 were used to produce His_6-G3 and $(HE)_3$-G3 DNA, respectively (Appendix). These PCRs all used the conventional sized Sense primers but assessed different Anti-Sense primers. These included the Anti-sense G3 (His-1 and HE-1 PCRs) and AOX1 Anti-sense (His-2 and HE-2 PCRs). PCR with the AOX1 Anti-sense primer produced larger DNA fragments than PCR with the Anti-sense G3 primer, as the former also amplified sections of the pPICZαB DNA at the 3' end. This was not problematic, as the pPICZαB DNA could be removed by the action of XbaI restriction endonuclease prior to ligation.

The control PCR with AOX1 Sense and AOX1 Anti-sense primers produced the largest DNA construct as it amplifies a long sequence of pPICZαB DNA between the AOX1 priming sites and the incorporated G3 DARPin DNA (Figure 3.4). His-2 and HE-2 DNA were selected for subsequent development, as their DNA bands were clearly defined and presumed less likely to contain contaminants.

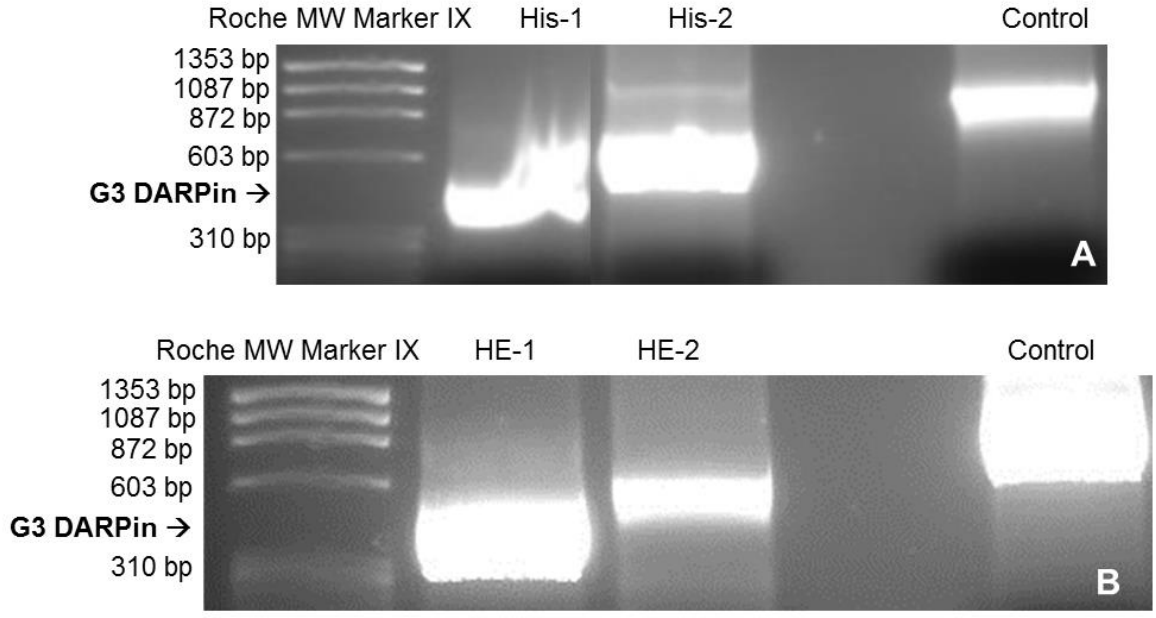

Figure 3.4 Agarose gels (2 %) showing His_6-G3 and $(HE)_3$-G3 DARPin DNA PCR products.
A) His_6-G3 PCR using pPICZαB/His3 template. His-1 used His_6 Sense and Anti-sense G3. His-2 used His_6 Sense and AOX1 Anti-sense
B) $(HE)_3$-G3 PCR using pPICZαB/HE3 template. HE-1 used $(HE)_3$ Sense and Anti-sense G3. HE-2 used $(HE)_3$ Sense and AOX1 Anti-sense
Control PCRs used AOX1 Sense and AOX1 Anti-sense primers

3.2.2 Amplification of pPICZαB plasmid

The overnight cultures of the two colonies of pPICZαB-electroporated TOP10F´ cells yielded 1910.5 ng/µl and 1355.9 ng/µl of pPICZαB plasmid DNA.

3.2.3 XbaI and XhoI digested pPICZαB plasmid

pPICZαB plasmid (3597 bp) was digested by XbaI and XhoI, then purified from the agarose gel (Figure 3.5), for subsequent ligation with XbaI and XhoI digested and purified G3 DARPin DNA.

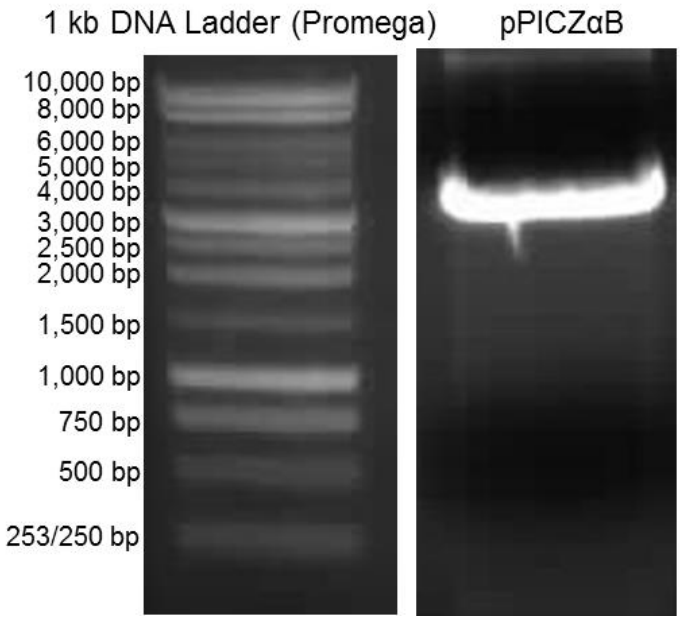

Figure 3.5 Agarose gel (1 %) showing XbaI and XhoI digested pPICZαB plasmid, 1 kb DNA Ladder (Promega) used.

3.2.4 Overnight culture of electroporated TOP10F´ and TG1 cells

For bacteria electroporated with ligated pPICZαB/DARPin DNA, EAEAHis$_6$-G3 (TOP10F' cells), EAEA(HE)$_3$-G3 (TOP10F' cells), cleavable tag-G3 (TG1 cells), His$_6$-G3 (TG1 cells) and (HE)$_3$-G3 (TG1 cells) had 50-200 colonies per Low Salt LB plate. The pPICZαB DNA contains the Zeocin resistance (*Sh ble*) gene, enabling the bacterial cells electroporated with pPICZαB/DARPin DNA to grow on Low Salt LB/ Zeocin (25 µg/ml) plates.

3.2.5 PCR screening of electroporated TOP10F' and TG1 colonies

G3 DARPin DNA contains approximately 450 base pairs (bp). Among the five screened colonies of TOP10F' which were electroporated with ligated PICZαB/EAEAHis$_6$-G3 DNA, four colonies contained G3 DARPin DNA. Colony EAEAHis-3 was selected for DNA sequencing (Figure 3.6). For EAEA(HE)$_3$-G3, two TOP10F' colonies electroporated with PICZαB/EAEA(HE)$_3$-G3 DNA contained G3 DARPin DNA and both colonies (EAEAHE-1 and -3) were selected for DNA sequencing (Figure 3.7). For bacterial electroporated with PICZαB/cleavable tag-G3 DNA, nine of the twenty screened TG1 colonies contained DNA encoding the G3 DARPin. The colony no tag 9 was selected for DNA sequencing (Figure 3.8). Among colonies of TG1 electroporated with PICZαB/His$_6$-G3 DNA, colonies His-5 and -9 contained G3 DARPin DNA and were selected for DNA sequencing (Figure 3.9). Among the nine TG1 colonies electroporated with PICZαB/(HE)$_3$-G3 DNA, three colonies contained G3 DARPin DNA. Colonies HE-3 and -4 were selected for DNA sequencing (Figure 3.10)

Figure 3.6 Agarose gel (1.5 %) showing the PCR colony screening to determine which colonies of electroporated TOP10F' cells contained EAEAHis$_6$-G3 DNA.

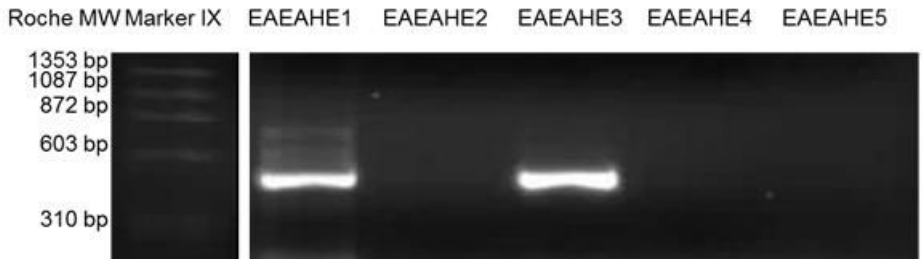

Figure 3.7 Agarose gel (1.5 %) of the PCR colony screening to determine which colonies of electroporated TOP10F' cells contained EAEA(HE)$_3$-G3 DNA.

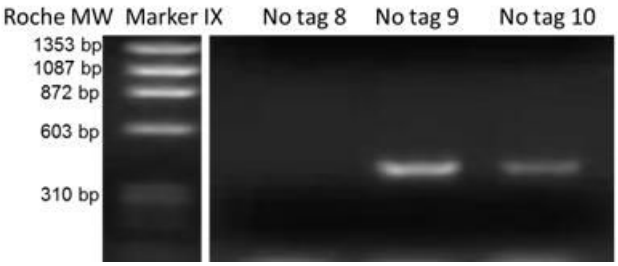

Figure 3.8 Agarose gel (1.5 %) of the PCR colony screening to determine which colonies of electroporated TG1 cells contained cleavable tag-G3 DNA (only colonies 8-10 shown).

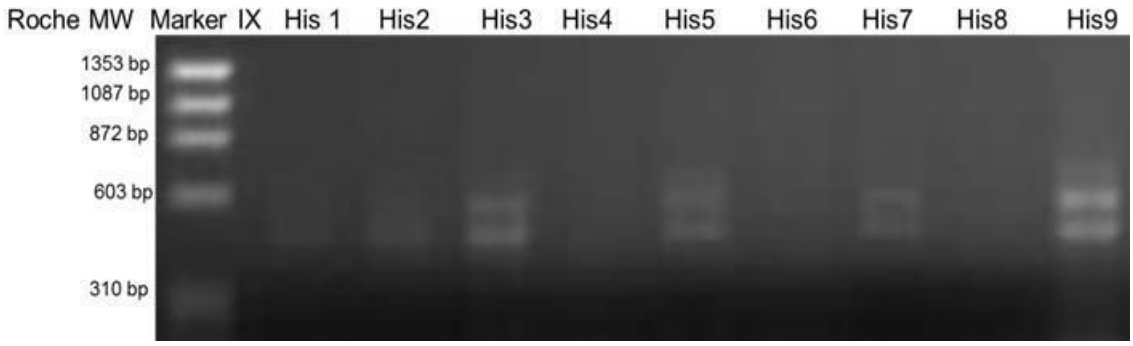

Figure 3.9 Agarose gel (1.5 %) showing the PCR colony screening to determine whether colonies of electroporated TG1 cells encoded His_6-G3 DNA.

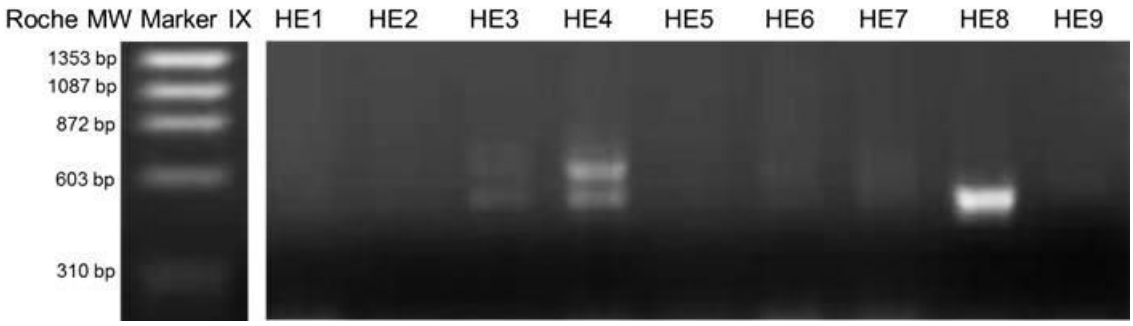

Figure 3.10 Agarose gel (1.5 %) showing the PCR colony screening to determine whether colonies of electroporated TG1 cells had DNA encoding $(HE)_3$-G3.

3.2.6 Sequencing of ligated pPICZαB/ G3 DARPin DNA

For each G3 DARPin construct, at least one pPICZαB/DARPin ligation expressed by transformed bacteria contained the appropriate G3 DARPin DNA sequence (Table 3.2).

Table 3.2 DNA sequencing of results pPICZαB/G3 DARPin DNA ligations.

DNA Construct	Nucleic acid concentration (ng/µl)	DNA Sequencing Results
pPICZαB/EAEAHis-3	784.2	EAEAHis_6-G3 DNA
pPICZαB/EAEAHE-1	1369.9	EAEA$(HE)_3$-G3 DNA
pPICZαB/EAEAHE-3	1204.5	EAEA$(HE)_3$-G3 DNA
pPICZαB/No tag-9	1889.4	Cleavable tag-G3 DNA
pPICZαB/His-5	2323.9	His_6-G3 DNA
pPICZαB/His-9	758.0	His_6-G3 DNA
pPICZαB/HE-3	2458.5	$(HE)_3$-G3 DNA
pPICZαB/HE-4	1764.3	$(HE)_3$-G3 DNA

3.2.7 Linearisation of pPICZαB plasmids containing G3 DARPin DNA

Ligations of pPICZαB/DARPin DNA were linearised with the Pme I enzyme at the 5' AOX1 promoter region of pPICZαB for transformation into X-33 (*P. pastoris*) (Figure 2.5). Linear DNA fragments travel slower on agarose gels than their non-linear (coiled) counterparts. Agarose gel electrophoresis confirmed Pme I linearisation of the pPICZαB/DARPin DNA ligations of each construct. The controls were Pme I untreated or pGAPZαB counterparts treated with Pme I (Pme I cannot linearise pGAPZαB). There was possible cross-contamination of pPICZαB/cleavable tag, pPICZαB/His and pPICZαB/HE controls by Pme I treated counterparts (Figure 3.11).

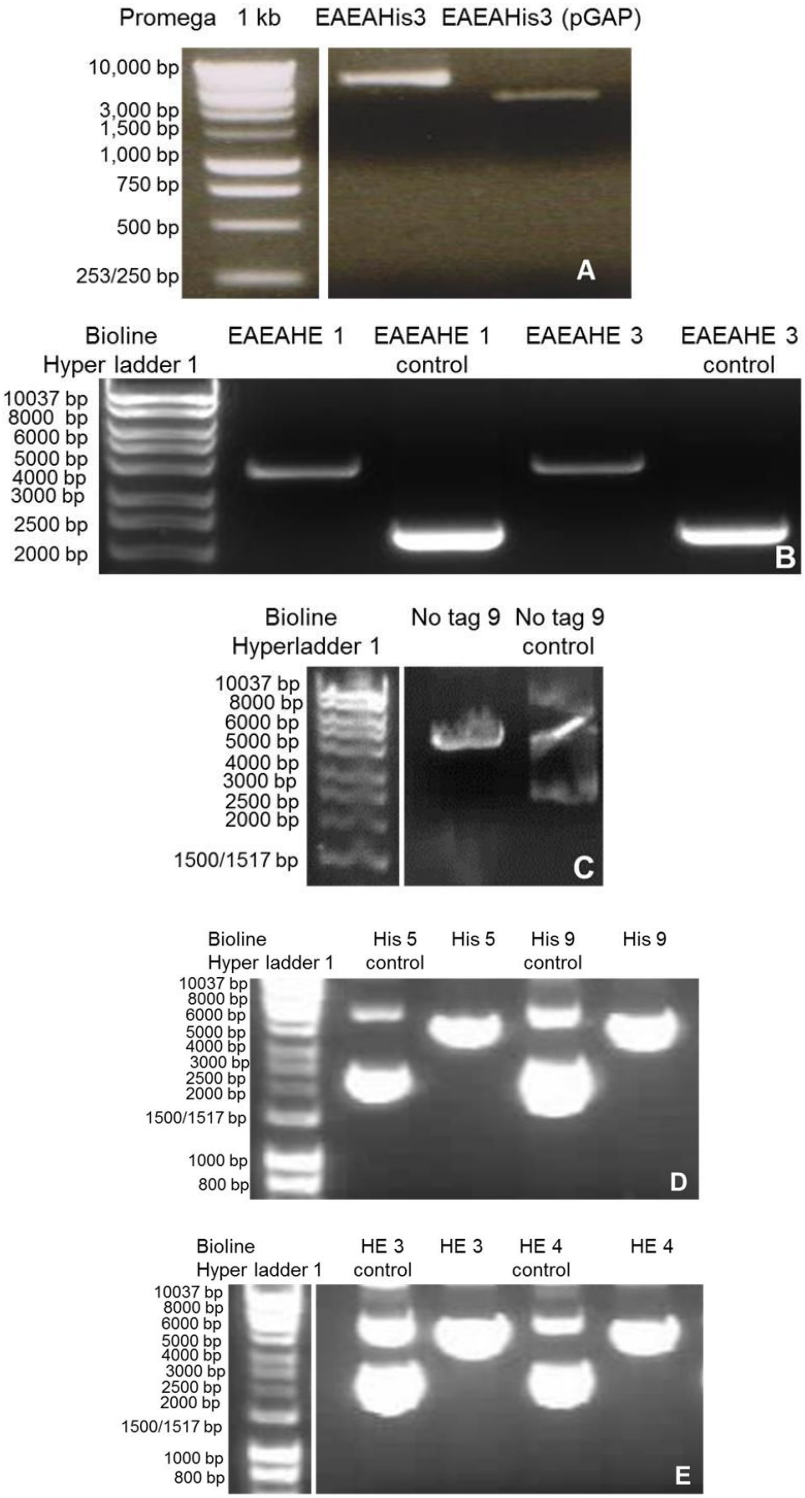

Figure 3.11 Agarose gels (2%) of Pme I linearised pPICZαB/DARPin DNA ligations. A) pPICZαB/EAEAHis, B) pPICZαB/EAEAHE, C) pPICZαB/No tag, D) pPICZαB/His and E) pPICZαB/HE. Controls non-Pme I treated pPICZαB/DARPin (B,C,D,E) or Pme I treated pGAPZαB/DARPin counterparts (A).

3.2.8 Protein expression by X-33 cells

After 72 h incubation, there were approximately fifty colonies of X-33 cells transformed with pPICZαB/EAEAHis-3 DNA. Among the four selected colonies, two colonies expressed 14-15 kDa proteins with a His_6 tag (data not shown). The X-33 cells transformed with pPICZαB/EAEAHE-1 DNA did not have any colonies. However, X-33 cells transformed with pPICZαB/EAEAHE-3 DNA had approximately fifty colonies and all five selected colonies expressed DARPins with the appropriate molecular weight (14-15 kDa), as determined by western blotting using anti-DARPin antibodies. The tetra-His antibody (Qiagen) was able to detect the dimer form of $EAEA(HE)_3$-G3 but was unable to detect the monomer form (Figure 3.12).

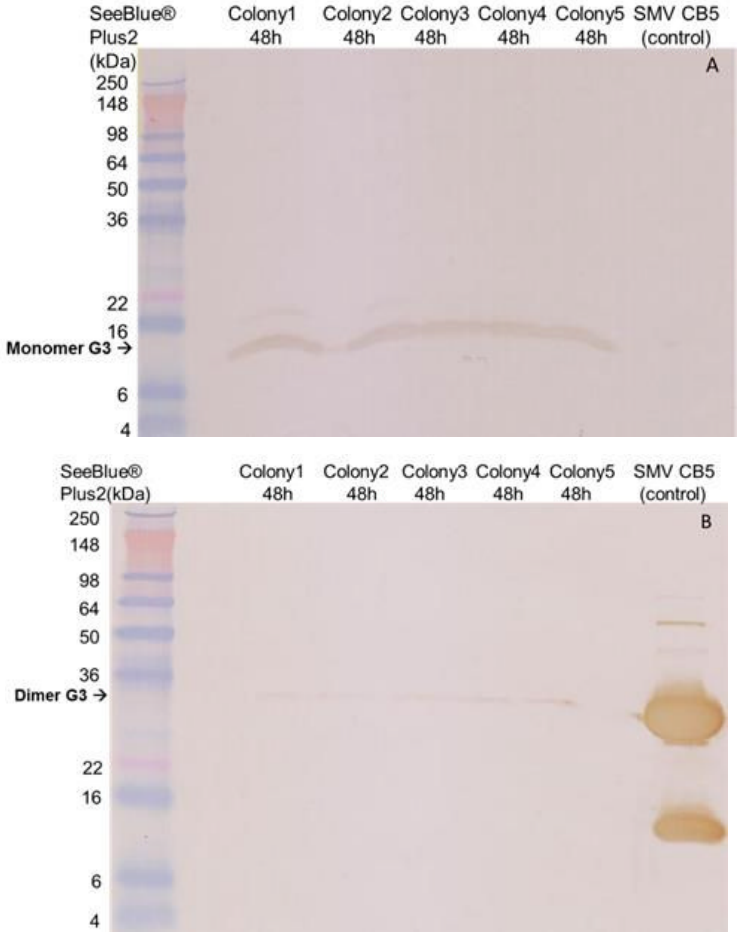

Figure 3.12 Western blots demonstrating $EAEA(HE)_3$-G3 DARPin protein expression by X-33 colonies transformed with pPICZαB/EAEAHE-3 DNA at 48 h incubation.
4x SDS-PAGE reducing buffer and 16% Tris-Glycine gel used. Control SMV CB5 is an anti-CEA diabody, its component parts have a His_6 tag.
A) Rabbit anti-DARPin primary and goat anti-rabbit secondary.
B) Mouse tetra-His antibody primary and sheep anti-mouse secondary.

X-33 cells transformed with pPICZαB/cleavable tag-9 DNA produced 15 colonies. Among the three selected colonies, only one colony expressed protein of the appropriate molecular weight (14-15 kDa). There was possibly premature cleavage of the His_6 tag at 48 h of incubation, as a second smaller protein was identified at this time point which was not been detected at 24 h (Figure 3.13).

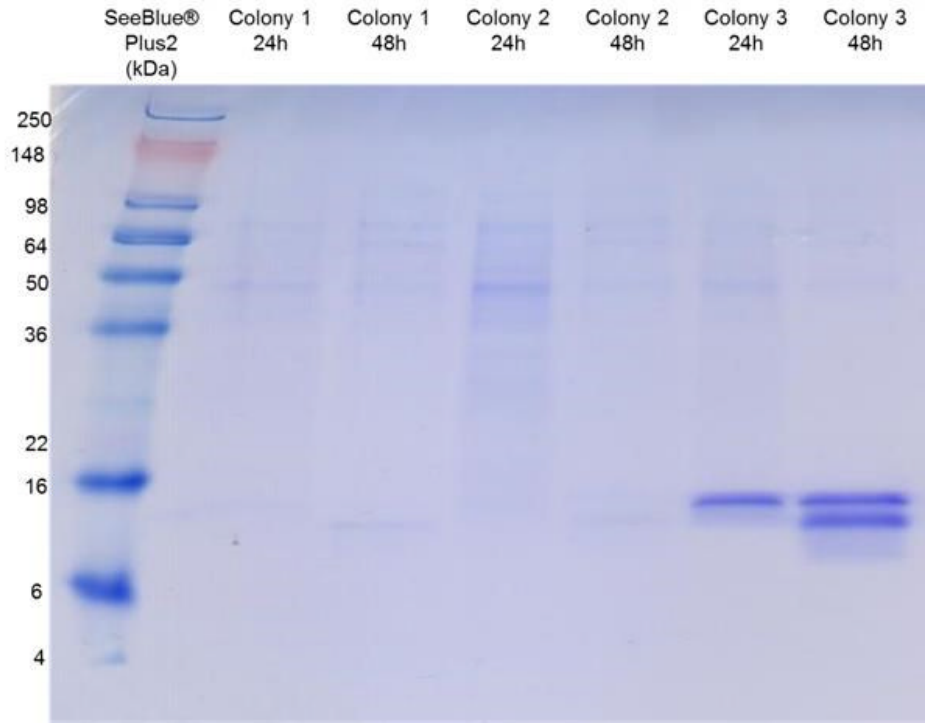

Figure 3.13 SDS-PAGE on 16% Tris-Glycine gel stained with coomassie blue analysing protein expressed by X-33 colonies transformed with pPICZαB/cleavable tag 9 DNA.
Samples were processed with 4x SDS-PAGE reducing buffer.

After 72 h of incubation, there were no colonies of X-33 cells transformed with pPICZαB/His-9 DNA. However, there were approximately thirty colonies of X-33 cells transformed with pPICZαB/His-5 DNA and among the six selected colonies, two colonies expressed protein with a His_6 tag with the appropriate molecular weight (14-15 KDa) at 48 h incubation (data not shown).

X-33 cells transformed with pPICZαB/HE-3 DNA and pPICZαB/HE-4 DNA produced colonies and their selected colonies expressed DARPins with the appropriate molecular weight (14-15 KDa) at 48 h incubation (data not shown).

3.2.9 Yields of purified G3 DARPin protein from fermentations

Yields of purified G3 DARPin ranged from 18 to 85 mg per fermentation and subsequent purification (Table 3.3).

Table 3.3 Yields of purified G3 DARPin protein from a single fermentation.

	Cleavable tag-G3 DARPin	EAEAHis$_6$-G3 DARPin	His$_6$-G3 DARPin	EAEA(HE)$_3$-G3 DARPin	(HE)$_3$-G3 DARPin
Yield (mg)	18	46	32	36	85

The G3 DARPin produced by the fermentations was assessed by SDS-PAGE, FPLC and mass spectrometry. Initially, protein standards were assessed on the Analytical Superdex 75 FPLC Column to determine the appropriate elution volume for the G3 DARPin (14-15 kDa) (Figure 3.14).

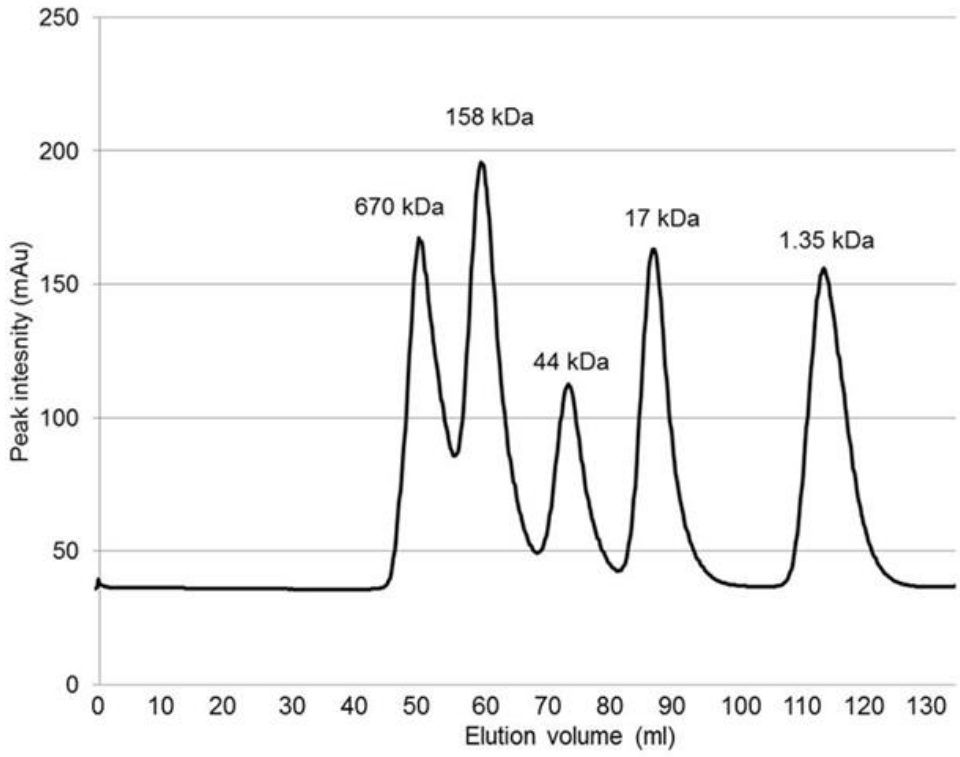

Figure 3.14 Protein standards (Bio-Rad Laboratories) run on the Analytical Superdex 75 FPLC Column (125 ml bed volume, pre-packed with Superdex 75 prep grade).

3.2.10 Analysis of EAEAHis$_6$-G3 fermentation, harvest and purification

During concentration and dialysis negligible amounts of EAEAHis$_6$-G3 DARPin were lost in the flow through and breakdown products > 5kDa were retained owing to the MWCO (5 kDa) of the tangential flow filter (TFF) (Figure 3.15).

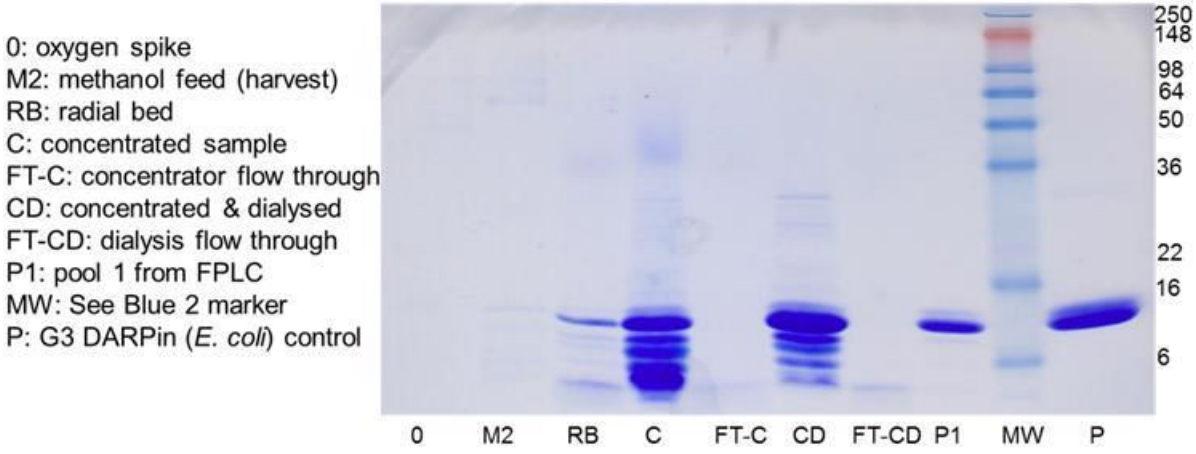

Figure 3.15 Stages of fermentation, harvest and purification of EAEAHis$_6$-G3, assessed by SDS-PAGE on 16% Tris-Glycine gel stained with coomassie blue, samples were processed with 2x SDS-PAGE reducing buffer.

EAEAHis$_6$-G3DARPin was eluted from the FPLC in several different forms including monomer and dimer. Pool 1 (aliquots 29-39) related to the monomer confirmed by coomassie staining (Figure 3.16 and Figure 3.17). Pool 1 was eluted at 90-100 ml on the Analytical Superdex 75 column, relating to the approximate molecular weight (14-15 kDa) (Figure 3.14 and Figure 3.16).

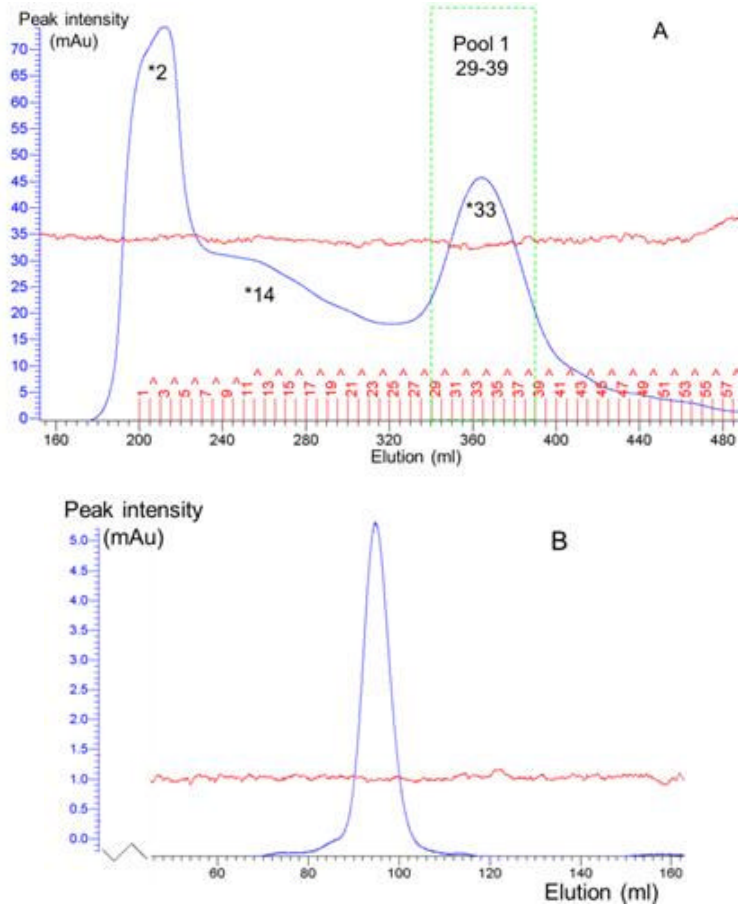

Figure 3.16 FPLC trace of EAEAHis$_6$-G3 DARPin. Red line relates to conductivity and blue line relates to UV.
A) Preparative Superdex 75 column. Aliquots 29-39 (inclusive) related to the monomer (Pool 1). Aliquots collected denoted by ^.
B) Pool 1 on Analytical Superdex 75 column.

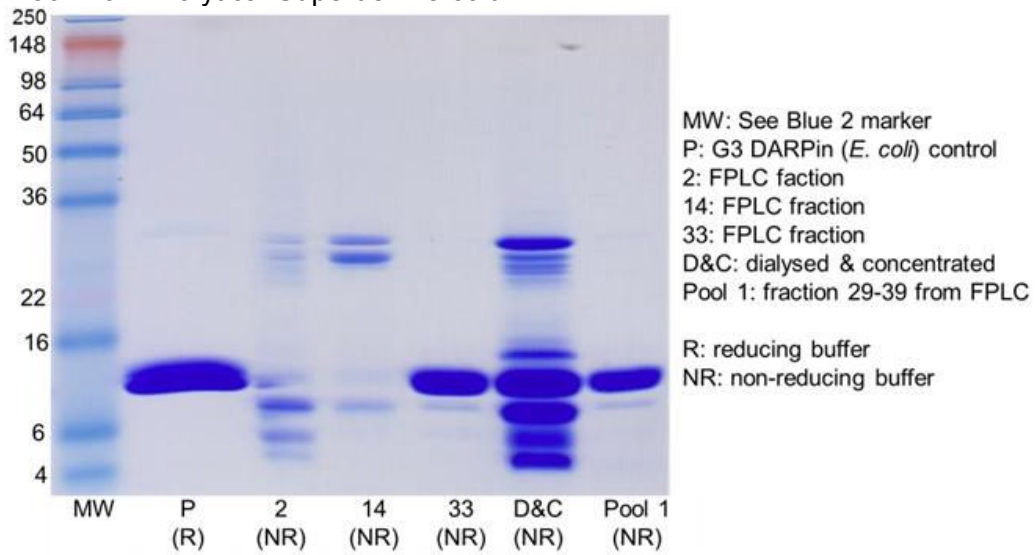

Figure 3.17 SDS-PAGE on 16% Tris-Glycine gel stained with coomassie blue, samples processed with 2x SDS-PAGE non-reducing (NR) buffer. EAEAHis$_6$-G3 DARPin samples *2, *14 and *33 from the Preparative Superdex 75 FPLC column.

The molecular weight of His_6-G3 DARPin is 14,536.3 Da. However, MALDI mass spectrometry confirmed that the glutamic acid (E) and alanine (A) residues preceding the His_6 tag were not efficiently cleaved by Ste13 resulting in $EAEAHis_6$ (14,936.7 Da) and $EAHis_6$ (14,736.5 Da) and the measured mass was between these values, 14,869 Da (Figure 3.18). Thus, it was necessary to produce a His_6-G3 which did not contain EAEA preceding the His_6 tag, to ensure that the G3 DARPin commenced at the His_6 tag.

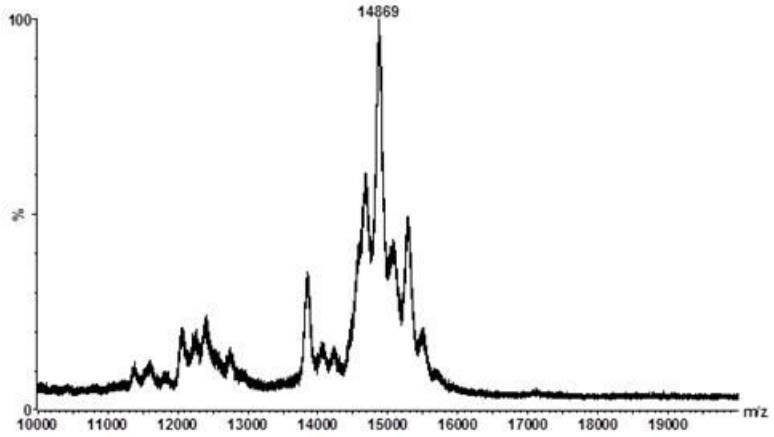

Figure 3.18 MALDI Mass spectrometry of $EAEAHis_6$-G3 DARPin, confirming that there was inefficient cleavage of the N-terminus glutamic acid (E) and alanine (A) residues.

3.2.11 Analysis of $EAEA(HE)_3$-G3 fermentation, harvest and purification

There were only small losses of $EAEA(HE)_3$-G3 DARPin from the IMAC radial flow bed during biomass application (10 L) and column washing with non-imidazole solution. Therefore, most of the DARPin was eluted with 200 mM imidazole, as intended (Figure 3.19). Breakdown products > 5 kDa were retained during concentration and dialysis, owing to the TFF filter size (MWCO 5 kDa) (Figure 3.19).

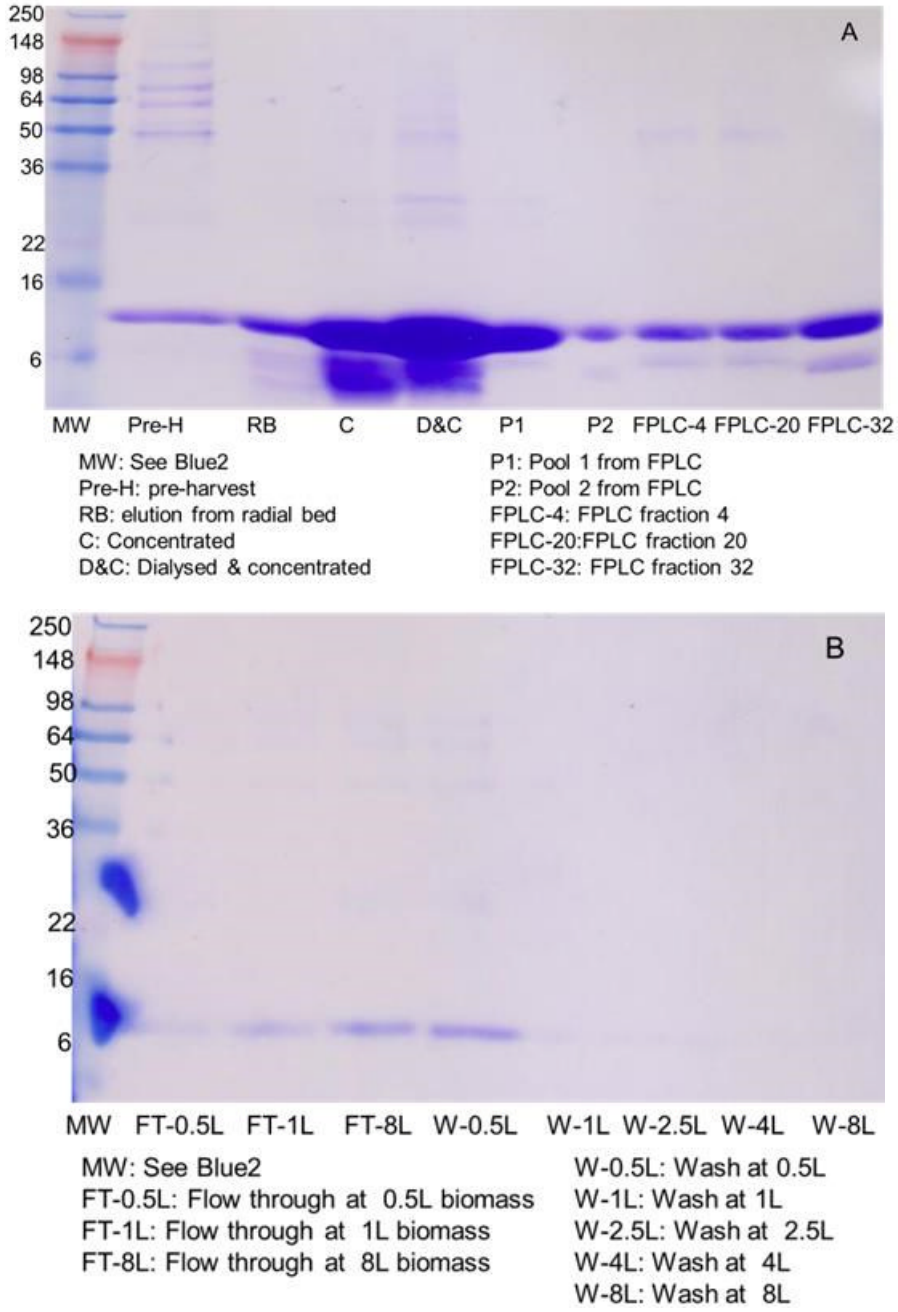

Figure 3.19 SDS-PAGE on 16% Tris-Glycine gel stained with coomassie blue of EAEA$(HE)_3$-G3, samples were processed with 4x SDS-PAGE reducing buffer.
A) Stages of fermentation, harvest and purification of EAEA$(HE)_3$-G3.
B) Minimal loss of EAEA$(HE)_3$-G3 from the radial flow IMAC column during biomass application (10L) and column wash, prior to elution with 200 mM imidazole solution.

EAEA$(HE)_3$-G3 was eluted at three different points from the Preparative Superdex 75 FPLC column (Figure 3.20). Pool 1 (aliquots 18-21) related to the dimer and Pool

2 (aliquot 30-33) related to the monomer. Samples from three different points of FPLC elution were ~14-15 kDa when processed with SDS-reducing buffer for coomassie staining (Figure 3.19). On the Analytical Superdex 75 FPLC column, pool 2 was eluted at 85-95 ml confirming it was close to the anticipated molecular weight of the monomer G3 DARPin (14-15 kDa) (Figure 3.20 and Figure 3.14).

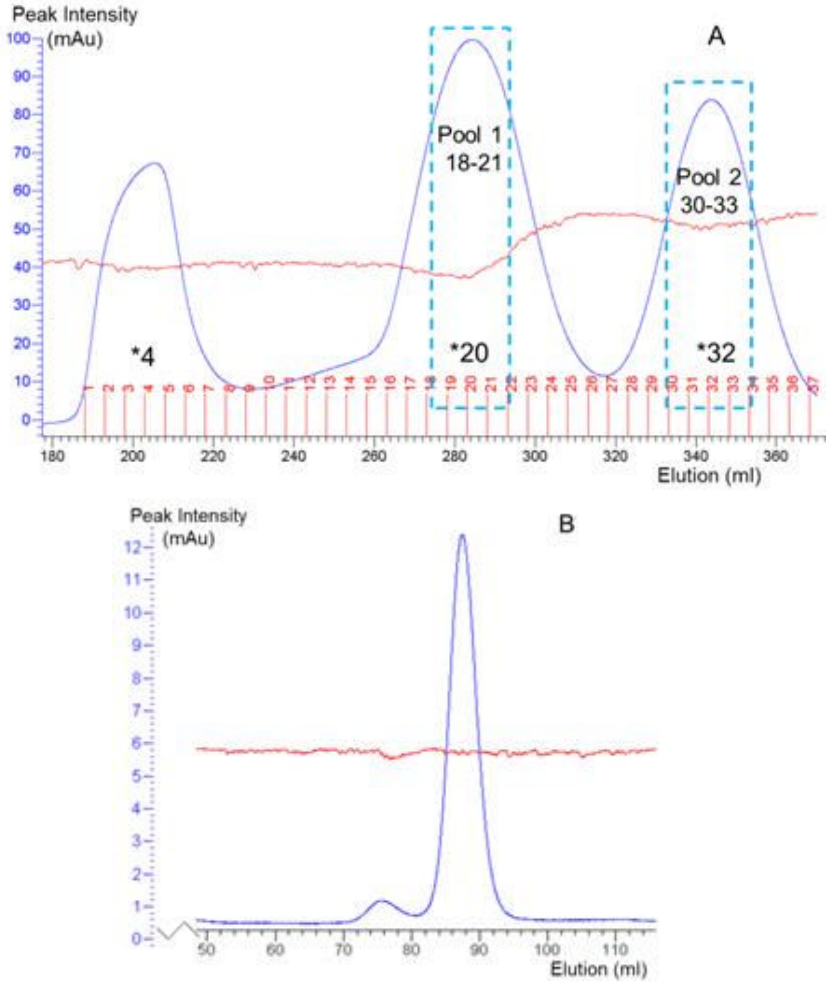

Figure 3.20 FPLC traces of EAEA$(HE)_3$-G3 DARPin. Red line relates to conductivity and blue line relates to UV.
A) Preparative Superdex 75 column. Aliquots 18-21 (inclusive) related to the dimer and aliquots 30-33 (inclusive) related to the monomer.
B) Analytical Superdex 75 column of Pool 2.

The molecular weight of $(HE)_3$-G3 DARPin which starts at the $(HE)_3$ tag is 14,512.2 Da. However, on mass spectrometry the molecular weight was 14,846.4 Da, consistent with inefficient Ste13 cleavage resulting in EAEA$(HE)_3$-G3 (14,912.6 Da) and EA$(HE)_3$-G3 (14,712.4 Da) production (Figure 3.21). Thus, it was necessary to

omit the EAEA residues preceding the $(HE)_3$ tag, to produce the $(HE)_3$-G3 DARPin commencing at the $(HE)_3$ tag.

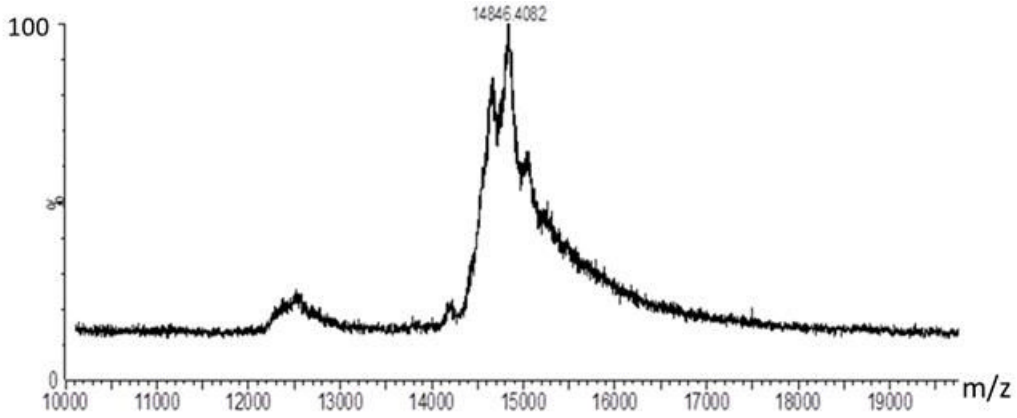

Figure 3.21 MALDI Mass spectrometry of EAEA$(HE)_3$-G3 DARPin, confirming there was inefficient cleavage of N-terminus glutamic acid (E) and alanine (A) residues.

3.2.12 Analysis of His_6-G3 fermentation, harvest and purification

There was increased His_6-G3 protein production throughout the limited glycerol feed (oxygen spike to 4 h post oxygen spike) and limited methanol feed (22 h duration) (Figure 3.22). The His_6-G3 was captured with the radial flow column, retained during dialysis and concentration, for subsequent FPLC purification.

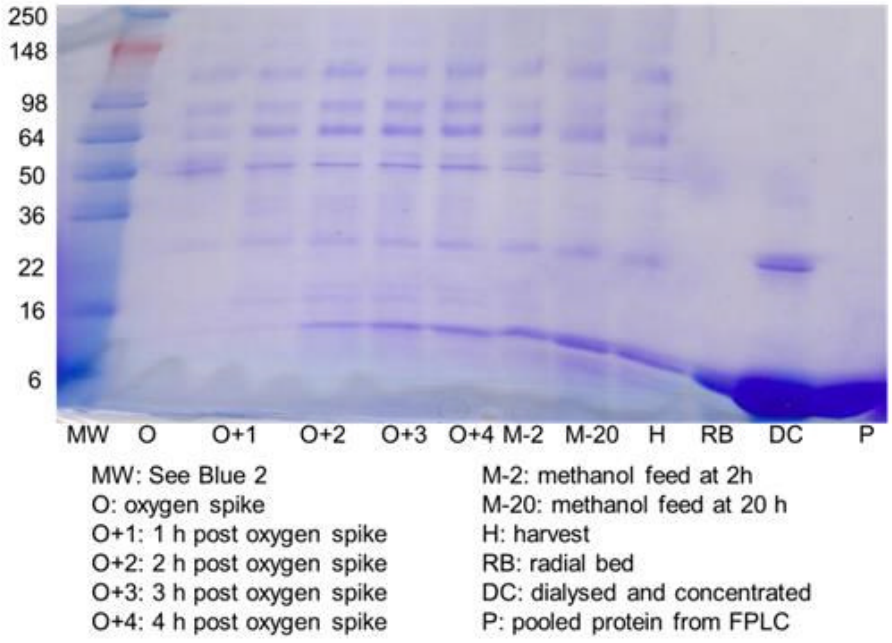

Figure 3.22 Fermentation, harvest and purification of His_6-G3 DARPin assessed by SDS-PAGE on 16% Tris-Glycine gel stained with coomassie blue, samples were processed with 4x SDS-PAGE reducing buffer.

The His_6-G3 DARPin was dialysed into PBS containing 10 mM DTT and then applied to the Preparative Superdex 75 FPLC column. Comparison of the FPLC traces of His_6-G3 and EAEAHis_6-G3 (dialysed into PBS alone), demonstrates that DTT increases the relative proportion of monomer G3 DARPin (Figure 3.16 and Figure 3.23). Fractions 16-20 related to the monomer and were retained (Figure 3.23). Evaluation on the Analytical Superdex 75 FPLC column revealed that the monomer pool was eluted at 95-100 ml which related to the anticipated molecular weight 14-15 kDa (Figure 3.23 and Figure 3.14).

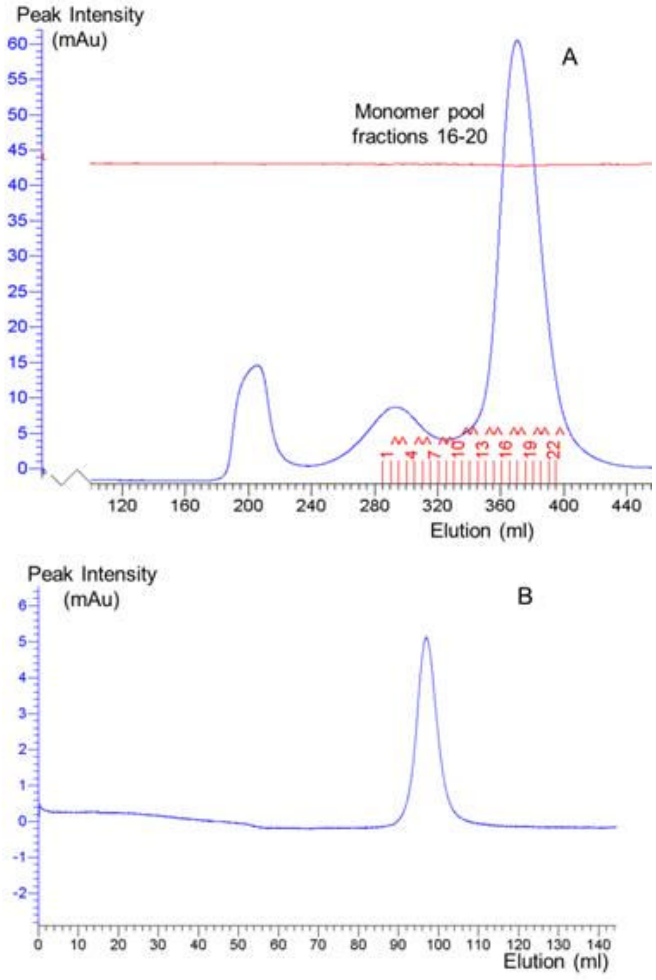

Figure 3.23 FPLC traces of His_6-G3 DARPin. Red line relates to conductivity and blue line relates to UV.
A) His_6-G3 DARPin in PBS with 10 mM DTT applied to the Preparative Superdex 75 column. Aliquots 16-20 (inclusive) related to the monomer. Aliquots collected denoted by ^. The presence of DTT increases the proportion of monomer.
B) Monomer pool applied to the Analytical Superdex 75 column.

The His_6-G3 DARPin had no EAEA at the N-terminus so did not rely on Ste13 cleavage. The molecular weight on MALDI mass spectrometry was 14,447 Da which was closer to the anticipated weight (14,536.3 Da) than EAEAHis_6-G3 (14,869 Da) (Figure 3.24).

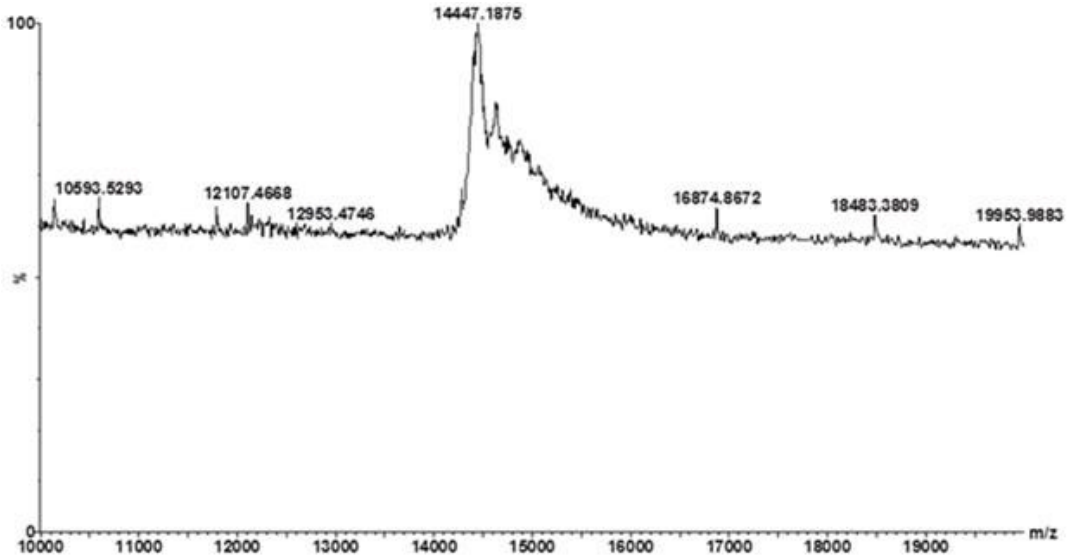

Figure 3.24 MALDI mass spectrometry of His_6-G3, the molecular weight was close to the anticipated molecular weight (14,536.3 Da).

3.2.13 Analysis of $(HE)_3$-G3 fermentation, harvest and purification

There was increased $(HE)_3$-G3 protein production from the oxygen spike to the harvest (at 2h of limited methanol feed or 6 h post-oxygen spike) (Figure 3.25). Breakdown products were retained during the concentration and dialysis, as observed previously. At the time of harvesting, there were some losses in the flow through from the IMAC column but minimal losses from the column during the imidazole-free wash (data not shown).

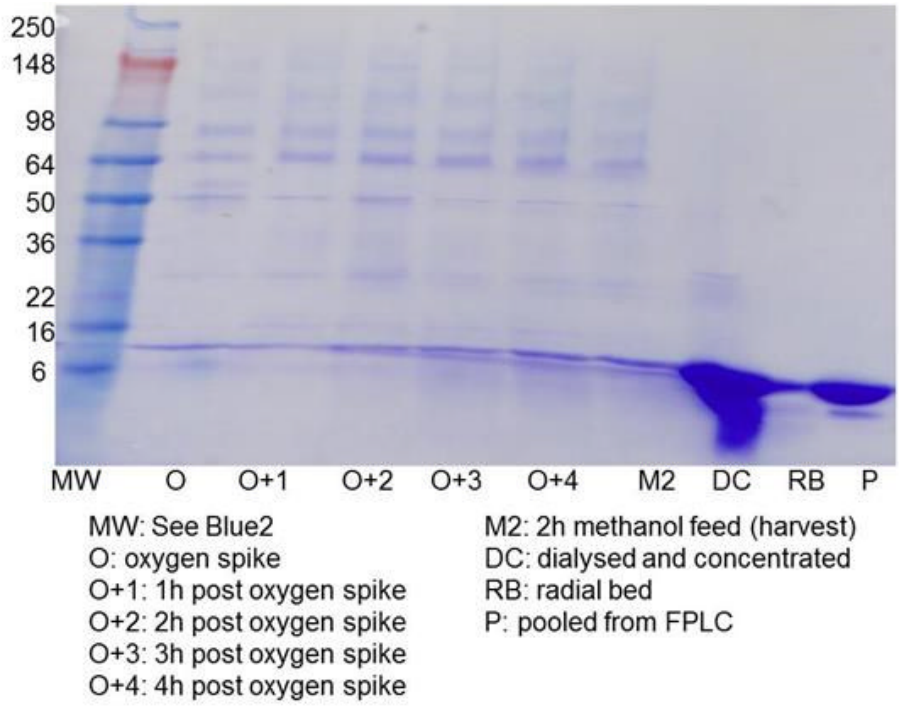

Figure 3.25 Fermentation, harvest and purification of $(HE)_3$-G3 DARPin assessed by SDS-PAGE on 16% Tris-Glycine gel stained with coomassie blue, samples were processed with 4x SDS-PAGE reducing buffer.

$(HE)_3$-G3 DARPin in PBS with 10 mM DTT was eluted on the Preparative Superdex 75 FPLC column, the presence of DTT ensured that the majority of $(HE)_3$-G3 DARPin was eluted in monomer form (fractions 31-37) (Figure 3.26). On the Analytical Superdex 75 column the monomer pool was eluted at 85-95 ml which relates to the anticipated molecular weight, 14-15 kDa. A small protein fragment (at 140-150 ml equates to ~1 KDa molecular weight) was detected on the Analytical Column, which is likely to be a breakdown product. This product may have been retained during dialysis/concentration or formed spontaneously post-dialysis/concentration as the TFF MWCO was 5 kDa (Figure 3.26 and Figure 3.14).

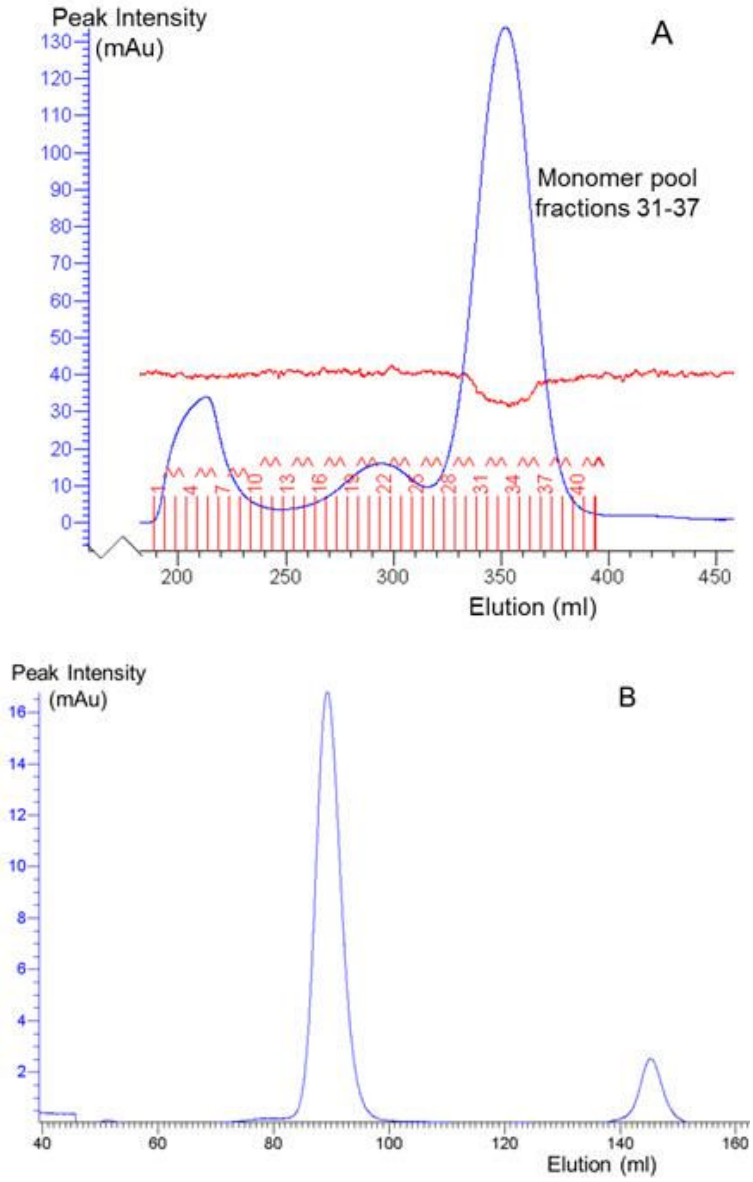

Figure 3.26 FPLC traces of $(HE)_3$-G3 DARPin. Red line relates to conductivity and blue line relates to UV.
A) Preparative Superdex 75 column. Aliquots 31-37 (inclusive) related to the monomer and were stored at -80 °C. Aliquots collected denoted by ^.
B) Analytical Superdex 75 column of $(HE)_3$-G3 DARPin monomer pool.

The anticipated molecular weight of $(HE)_3$-G3 DARPin which starts at the $(HE)_3$ tag is 14,512.2 Da. The molecular weight of $(HE)_3$-G3 DARPin on MALDI mass spectrometry was 14511.7 Da, as production did not rely on Ste13 cleavage of EAEA residues (Figure 3.27).

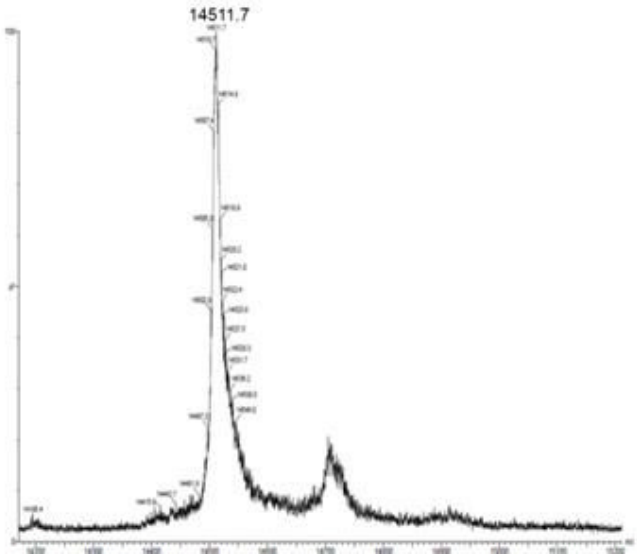

Figure 3.27 MALDI mass spectrometry of $(HE)_3$-G3 DARPin. The molecular weight was close to the anticipated molecular weight (14,512.2 Da).

3.2.14 Analysis of cleavable tag-G3 Fermentation, Harvest and Purification

The cleavable tag-G3 was harvested at 4 h post oxygen spike. During the harvest, there were substantial DARPin losses in the column flow through but only small losses when the column was washed with low concentration imidazole solution. Western blotting confirmed that the cleavable tag-G3 DARPin lost in the flow through and eluted from the FPLC retained its His_6 tag (Figure 3.28).

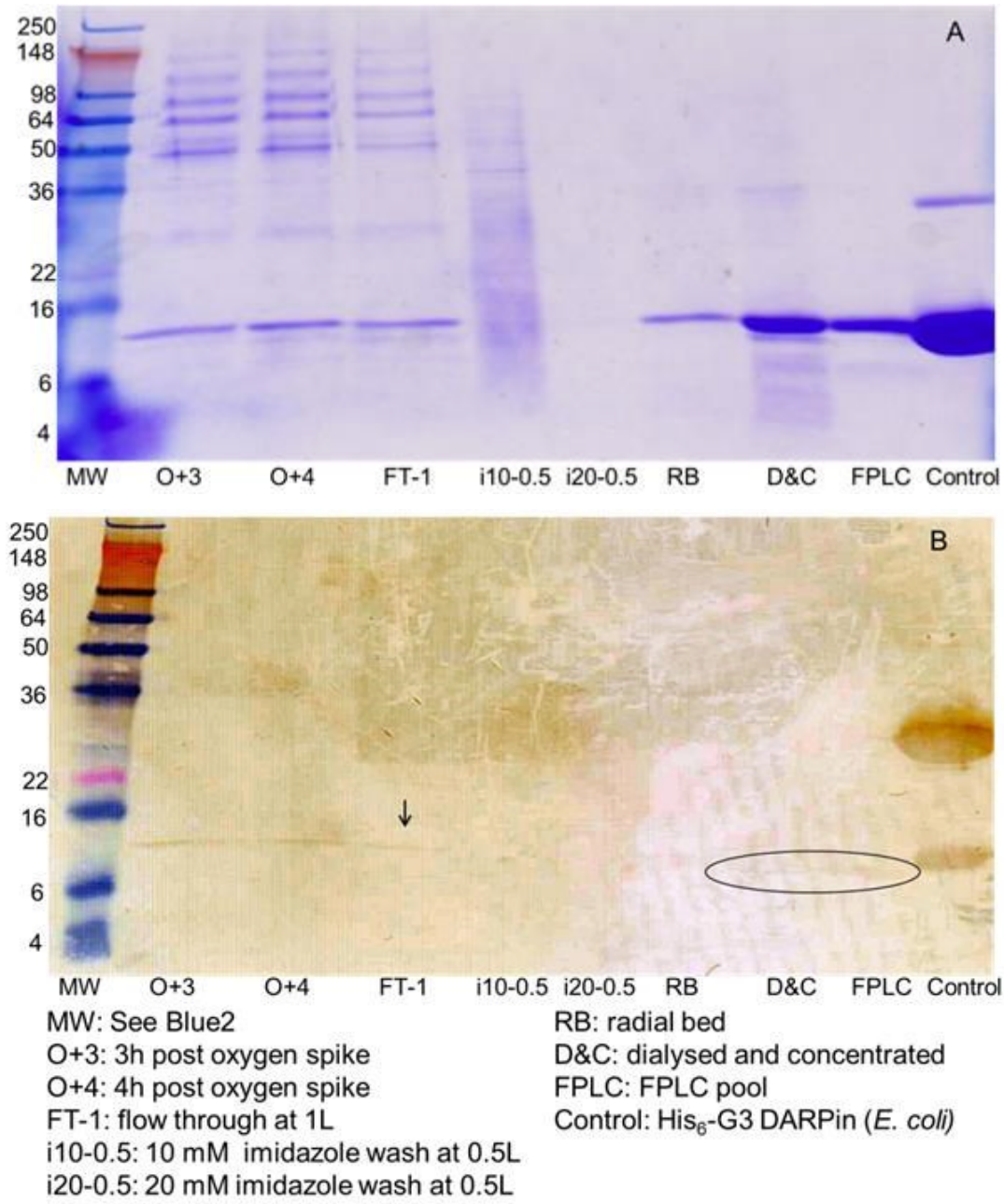

Figure 3.28 Analysis of the fermentation, harvest and purification of cleavable tag-G3 DARPin. Samples run on 16% Tris-Glycine gel and processed with 4x SDS-PAGE reducing buffer.
A) Coomassie blue stained gel.
B) Western blot demonstrating that the cleavable tag-G3 DARPin lost in the flow through had a His_6 tag (arrowed). The dialysed-concentrated and FPLC eluted DARPin had a His_6 tag (circled). Primary mouse anti-His, secondary sheep anti-mouse.

The cleavable tag-G3 DARPin was predominantly eluted in monomer form, as it had been dialysed in PBS containing 10 mM DTT prior to FPLC purification (Figure 3.29).

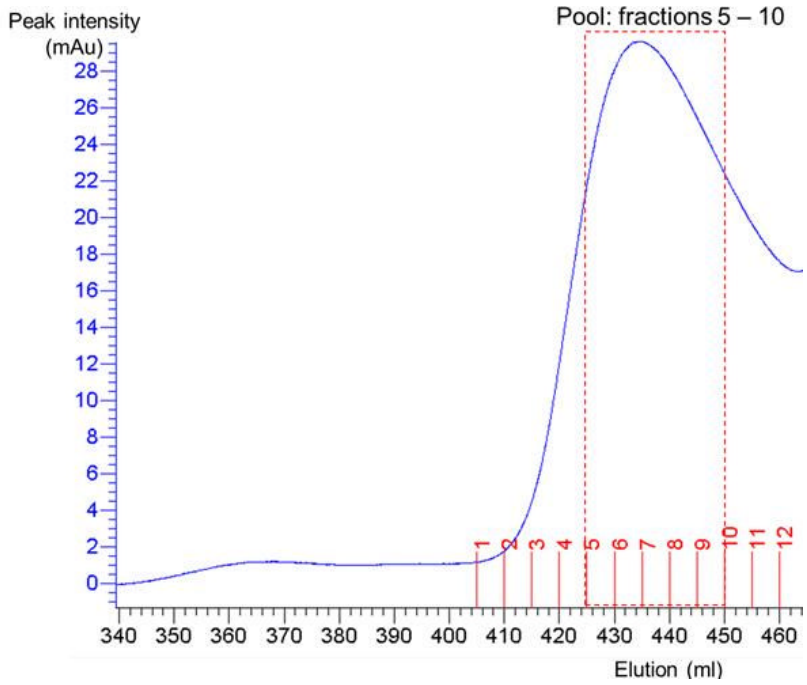

Figure 3.29 FPLC trace of cleavable tag-G3 DARPin run on a Preparative Superdex 75 column. Aliquots 5-10 (inclusive) formed the pool of monomer DARPin.

The molecular weight of the cleavable tag-G3 DARPin commencing at the His_6 tag (prior to cleavage) is 15,581.5 Da. However, due to inefficient Ste13 activity, the cleavable tag-G3 had a molecular weight of 15,934 Da (Figure 3.30). The molecular weights of the variants with an EAEA-cleavableHis_6 tag G3 and EA-cleavableHis_6 tag G3 at the N-terminus are 15,981.8 and 15,781.7 Da, respectively. However, cleavage by human rhinovirus 3C protease would ensure that the untagged-G3 DARPin would commence at the appropriate amino acid residue, glycine (G). Thus, it was not necessary to produce a cleavable tag-G3 without EAEA residues at the N-terminus.

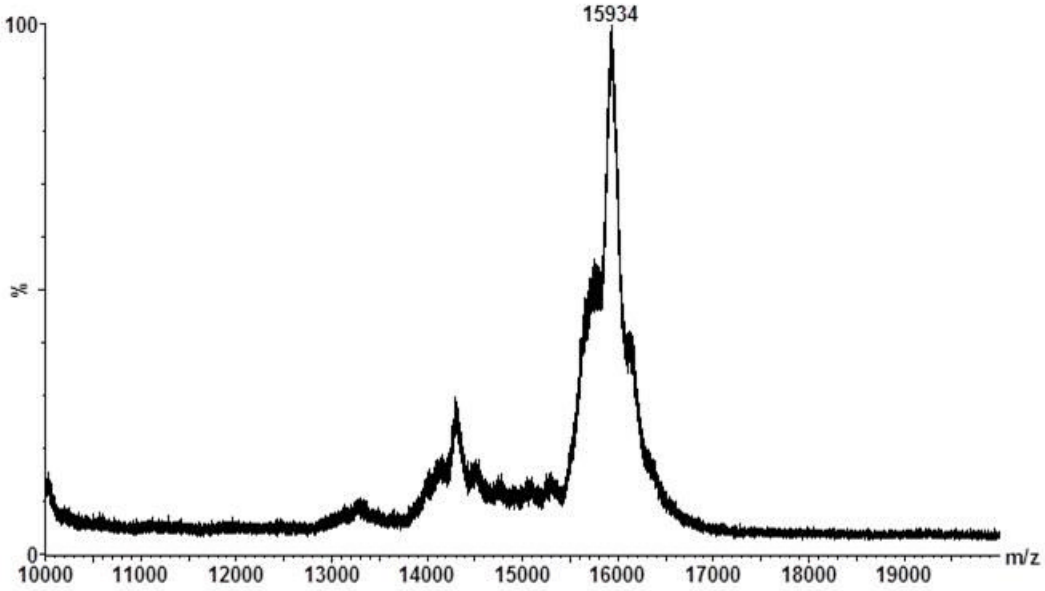

Figure 3.30 MALDI mass spectrometry of cleavable tag-G3

3.2.15 Cleavage of the cleavable tag-G3 DARPin

3.2.15.1 Optimisation of cleavage conditions

Removal of the His_6 tag from the cleavable tag-G3 was assessed in PBS, Cleavage Buffer and High Salt Cleavage Buffer by HRV 3C protease at 4 °C (concentration 40 U/ml or ~76 U/mg of cleavable tag-G3 DARPin). Cleavage in High Salt Cleavage Buffer was efficient over 18 h, as there was no detectable His_6 tagged protein. By comparison, there was incomplete cleavage of the cleavable tag-G3 in the PBS and Cleavage Buffer at 18 h, as there was detectable His_6-tagged protein on western blotting. Thus, cleavage in High Salt Cleavage Buffer was selected for further assessment (Figure 3.31).

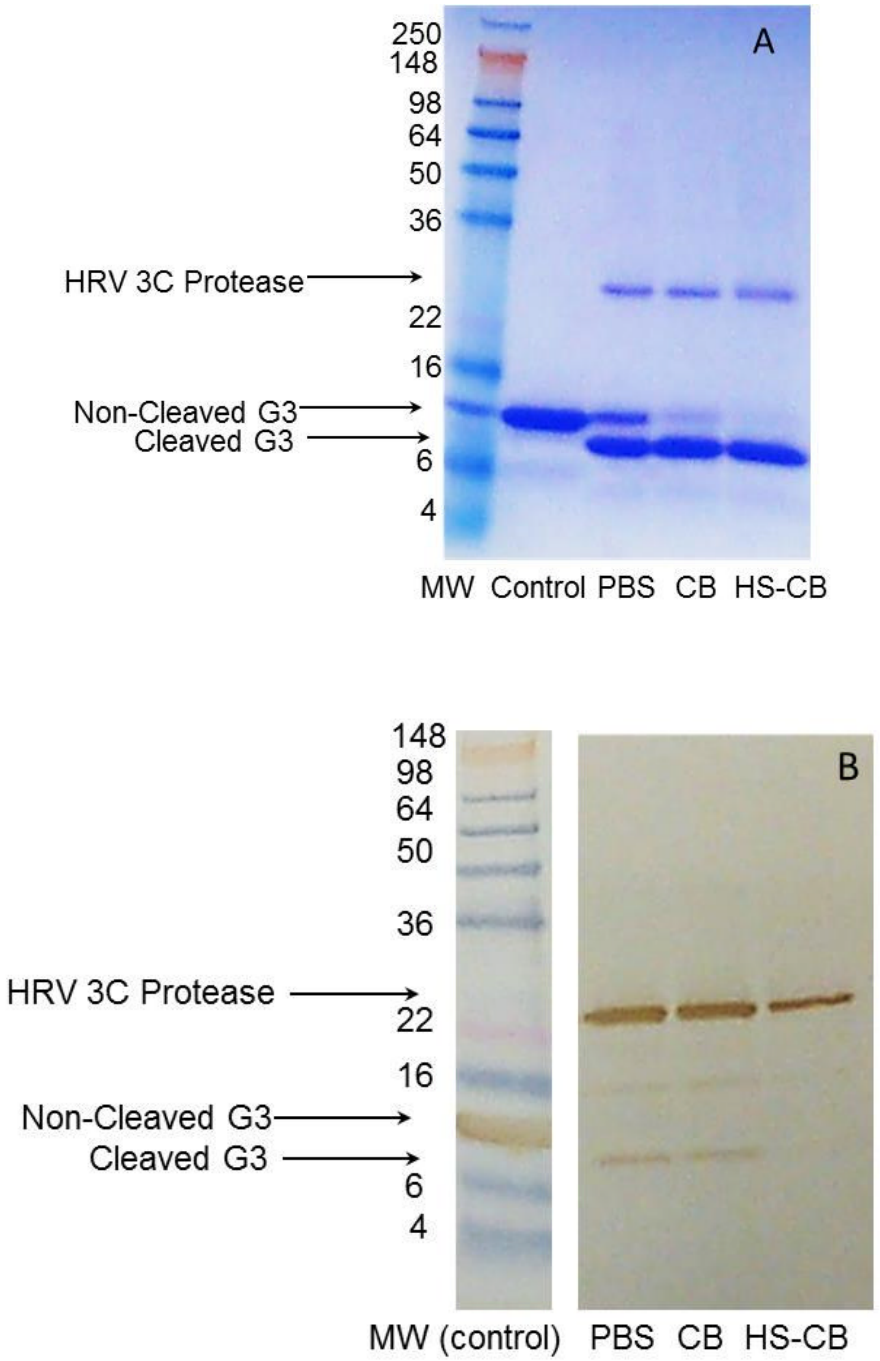

Figure 3.31 Analysis of His_6 tag cleavage of the cleavable tag-G3 DARPin in PBS, Cleavage Buffer (CB) and High Salt Cleavage Buffer (HS-CB) for 18 h with 40 U/ml HRV 3C Protease (22 kDa).
All samples were processed with 4x SDS-PAGE reducing buffer and run on a 16% Tris-Glycine gel. Control was an untreated cleavable tag-G3 DARPin.
A) SDS-PAGE gel stained with coomassie blue.
B) Western blot demonstrating His_6 tag loss form cleavable tag-G3 DARPin in HS-CB (primary antibody mouse anti-His, secondary antibody sheep anti-mouse).

In High Salt Cleavage Buffer at 4 °C, cleavage of the His_6 tag from the cleavable tag-G3 with HRV 3C Protease was less efficient at ≤ 4 U/ml than at 40 U/ml concentration. At 40 U/ml (equivalent to 76 U/mg of cleavable tag-G3DARPin) cleavage could be completed within 2 h (Figure 3.32).

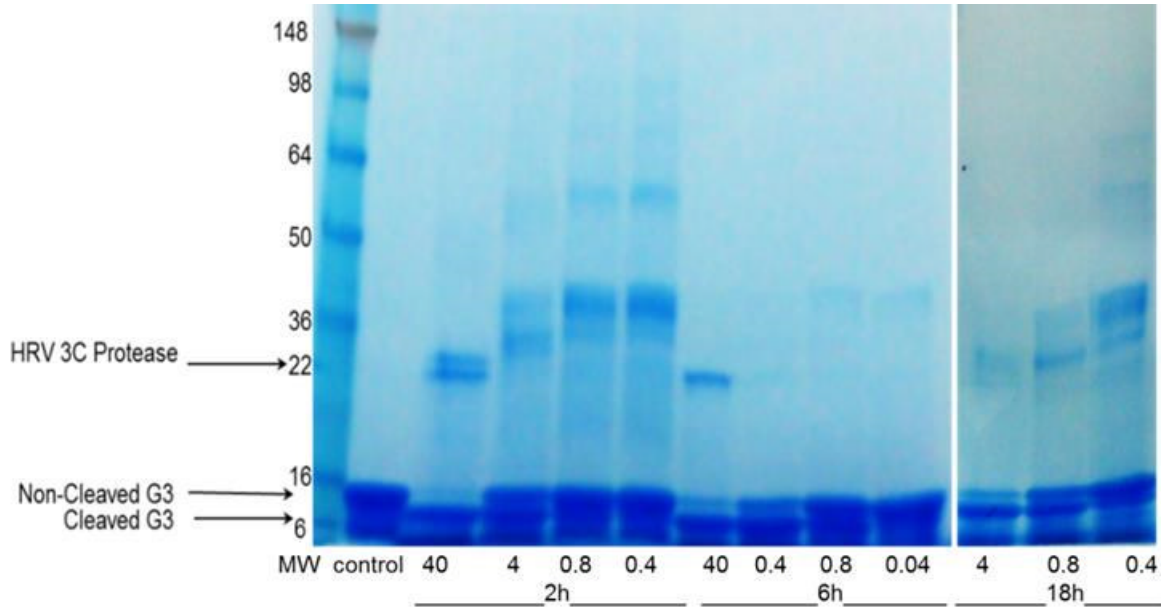

Figure 3.32 Effect of different HRV 3C Protease concentrations (0.4-40 U/ml) on cleavage in High Salt Cleavage Buffer, tested at 2, 6 and 18 hours (4 °C).
SDS-PAGE on 16% Tris-Glycine gel stained with coomassie blue, samples were processed with 4x SDS-PAGE reducing buffer. Control untreated cleavable tag-G3 DARPin.

3.2.15.2 Bulk cleavage

Based on the optimisation study, the cleavable tag-G3 was dialysed into High Salt Cleavage Buffer containing 10 mM DTT and the bulk cleavage was performed over 2 h with HRV 3C protease at concentration 76 U/mg of DARPin (4 °C). A reverse purification step of the untagged-G3 (subtractive IMAC) separated the untagged-G3 (eluted in High Salt Cleavage Buffer with 10 mM DTT wash) from the HRV 3C protease (eluted in 250 mM Imidazole in the final step), as the HRV 3C protease has a His_6 tag. The untagged-G3 in the flow through was retained and stored (Figure 3.33).

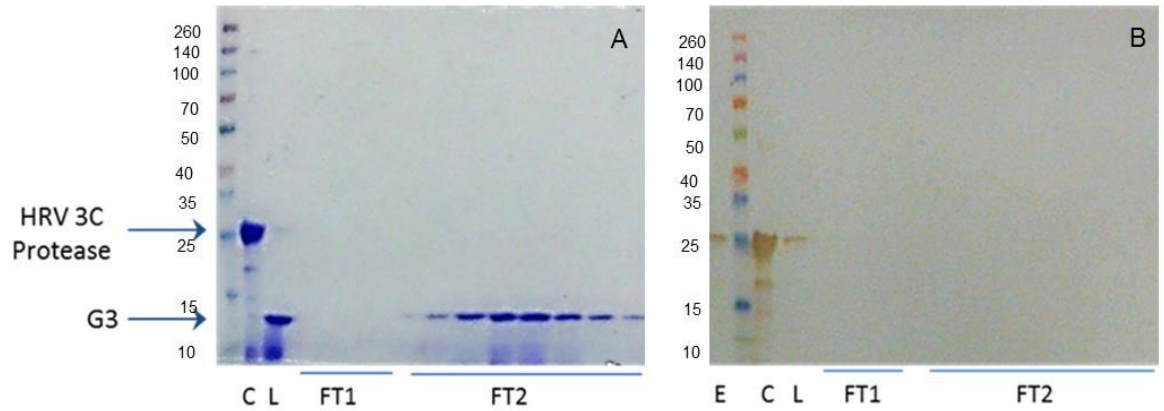

Figure 3.33 Bulk conjugation demonstrating untagged-G3 in the flow through (FT2) of High Salt Cleavage Buffer (HS-CB) with 10 mM DTT which was retained and HRV 3C protease in the final elution (E) in 250 mM imidazole.
Samples were processed with 4x SDS-PAGE reducing buffer on 16% Tris-Glycine gel. A) Staining with coomassie blue. B) Western blot (primary antibody mouse anti-His, secondary antibody sheep anti-mouse).

3.3 Discussion

The aim of the work presented in this Chapter was to produce purified G3 DARPins with and without histidine based N-terminal tags using a *P. pastoris* production platform. His_6-G3, $(HE)_3$-G3 and untagged-G3 DARPins which only differed at the N-terminus by the presence or absence of their tags were successfully produced.

It was not possible to produce His_6-G3 and $(HE)_3$-G3 DARPins from the template which incorporated LEKREAEA preceding the histidine based tags, since the Ste13 gene product was inefficient in EA cleavage. The Kex2 gene product efficiently removed LEKR residues, so the DARPins commenced with the residues EAEAH.. or EAH.. (Sasagawa, Matsui et al. 2011).

The EA and EAEA extensions form part of the pro-sequence of the *Saccharomyces cerevisiae* α-factor secretion signal which precedes the recombinant protein DNA. The α-factor secretion signal allows efficient secretion of proteins from *P. pastoris*, it consists of a pre-sequence (19 amino acids) and pro-sequence (66 amino acids). The EA repeats are located at the C-terminus of the pro-sequence (Kurjan and Herskowitz 1982). The pre-sequence is the signal peptide that facilitates protein secretion across the cytoplasmic membrane into the media and is removed by a signal peptidase system (Raemaekers, de Muro et al. 1999). The pro-sequence acts as an intra-molecular chaperone and guides protein folding, the pro-sequence can be cleaved from the mature protein through auto-proteolysis performed by Kex2 and Ste13 (He, Huang et al. 2012).

Interestingly, the recombinant small protein 1 (Sm1) expressed in *P. pastoris* has a larger molecular mass than native Sm1 produced by the fungus *Trichoderma virens*. This difference arises, as the N-terminus of *P. pastoris* produced Sm1 is extended by the presence of EAEAYV residues, due to inefficient Ste13 protease activity downstream of the Kex2 cleavage site (Buensanteai, Mukherjee et al. 2010).

It was necessary to produce pPICZαB/G3 DARPin DNA which did not encode EAEA but relied solely on the removal of the α-factor secretion signal pro-sequence by Kex2 cleavage of LEKR residues. This change to the pro-sequence of the α-factor secretion signal did not affect Kex2 functioning and DARPin secretion from the cytoplasm into the media (reflected by the fermentation yields). Removal of EAEA

ensured that the G3 DARPin sequences commenced at the histidine based tags (Table 3.3).

Although the cleavable tag-G3 DARPin also had EAEA residues at the N-terminus, it was not necessary to produce an alternative construct, as the action of HRV 3C protease ensured all residues preceding the GP were removed. Subsequently, subtractive IMAC was able to isolate the untagged-G3 from the His_6 tagged HRV 3C protease.

In conclusion, three variants of the G3 DARPin were successfully produced using the *P. pastoris* expression system which could be used to assess the influence of N-terminal histidine based tag on normal tissue biodistribution. The Ste13 gene product is inefficient in cleavage of Glutamate (E)-Alanine (A) repeats from the C-terminus of the α-factor secretion signal and in their absence the G3 DARPin can still be efficiently secreted from *P. pastoris*.

Chapter 4 Indium-111 and iodine-125 radiolabelled G3 DARPins in non-tumour bearing mice

4.1 Introduction

In Chapter 3, $(HE)_3$-G3, His_6-G3 and untagged-G3 DARPins which only differed from each other by the presence or composition of their N-terminal histidine tags were successfully produced using the *P. pastoris* production platform. They were designed to be site-specifically radiolabelled via a bifunctional chelator at their unique C-terminal cysteine or directly with radioiodine at one or both of their two tyrosine residues.

Comparative assessment of the $(HE)_3$-G3, His_6-G3 and untagged-G3 DARPins in mice, could determine the influence of the N-terminus histidine-based tags on normal tissue biodistribution. Differences in the biodistribution profiles would be easier to assess with radio-isotopes that have a long half-life, thus ^{111}In (half-life ~2.8 days) and ^{125}I (half-life ~60 days) were selected. Both residualising (^{111}In) and non-residualising (^{125}I) radio-isotopes were assessed as they have different cellular fates, which can also affect tumour-to-normal tissue ratios.

Previously, only G3 DARPins with a His_6 tag for $[^{99m}Tc(CO)_3]^+$-radiolabelling had been assessed *in vivo*. It was necessary to investigate the influence of the histidine-based tag on normal liver uptake, as $[^{99m}Tc(CO)_3]^+$-His_6-G3 had relatively high liver uptake (7.27 ± 1.04% ID/g at 4 h) and low tumour-to-liver ratios (< 2:1 over 48 h), despite achieving reasonably high HER2-positive tumour uptake (8.02 ± 2.85% ID/g at 4 h) in SKOV3-tumour bearing mice (Zahnd, Kawe et al. 2010). Thus, G3 DARPin normal liver uptake could compromise the ability to identify HER2-positive liver metastases on imaging (Zahnd, Kawe et al. 2010).

For the HER2 binding affibody molecule, $Z_{HER2:342}$, the histidine-based tag amino acid configuration and position (N or C-terminus) effected normal tissue biodistribution. $[^{99m}Tc(CO)_3]^+$-$(HE)_3$-$Z_{HER2:342}$ (N-terminus tag) had lower liver uptake than counterparts with different histidine-based tags (Hofstrom, Altai et al. 2013).

The influence of the N-terminus histidine based tag on G3 DARPin normal tissue uptake is unknown (Zahnd, Kawe et al. 2010). A G3 DARPin with low normal tissue uptake could facilitate high tumour-to-normal tissue ratios, a prerequisite for successful HER2 molecular imaging.

Aim:

To test the hypothesis the N-terminus histidine-based tags affect normal tissue uptake of the G3 DARPin.

Objectives:

1) Assess $(HE)_3$-G3, His_6-G3 and untagged-G3 DARPin kinetics and affinities for HER2.
2) Assess cold labelled $(HE)_3$-G3, His_6-G3 and untagged-G3 DARPin HER2 specificity *in vitro*.
3) Assess normal tissue biodistribution of $(HE)_3$-G3, His_6-G3 and untagged-G3 DARPins radiolabelled with ^{111}In and ^{125}I.

The G3 DARPin construct with the lowest normal tissue uptake was validated further *in vitro* and assessed in HER2-positive tumour bearing mice in Chapter 5.

4.2 Results

Prior to assessing the $(HE)_3$-G3, His_6-G3 and untagged-G3 DARPins in normal mice, it was important to confirm that they had equivalent HER2 binding affinities unaffected by DOTA-conjugation and equivalent HER2 specificities unaffected by labelling with indium or iodine. This is because loss of HER2 affinity and or HER2 specificity would adversely affect clinical utility and discourage further pre-clinical development.

4.2.1 G3 DARPin affinity and binding kinetics with HER2 extracellular domain

The unconjugated His_6-G3 DARPin produced in *P. pastoris* and *E. coli* had sub-nanomolar affinities for the HER2 ECD, 0.204 and 0.111 nmol/L, respectively (Table 4.1). All of the assessed unconjugated and conjugated G3 DARPins had picomolar binding affinities for the HER2 ECD. DOTA conjugation of the G3 DARPins was not expected to affect G3 DARPin kinetics and affinities, since the G3 DARPin C-terminus (where DOTA binds) does not form part of the HER2 ECD binding site (Epa, Dolezal et al. 2013). Instead, the two central ankyrin repeats within the four ankyrin repeat G3 DARPin structure contribute to HER2 binding. These SPR results suggest that DOTA conjugation did not markedly alter G3 DARPin binding kinetics and affinities with the HER2 ECD (Table 4.1).

Table 4.1 G3 DARPin affinities and kinetics with the HER2 ECD assessed by Surface Plasmon Resonance (data presented as mean of duplicate assessments).

G3 DARPin	Production	K_a or K_{on} (M^{-1} s^{-1})	K_d or K_{off} (s^{-1})	K_D (nmol/L)
Untagged-G3	*P. pastoris*	$4.2x10^5$	$2.6x10^{-4}$	0.649
DOTA-Untagged-G3	*P. pastoris*	$6.7x10^5$	$2.6x10^{-4}$	0.397
His_6-G3	*P. pastoris*	$9.7x10^5$	$2.0x10^{-4}$	0.204
DOTA-His_6-G3	*P. pastoris*	$6.1x10^5$	$2.2x10^{-4}$	0.361
$(HE)_3$-G3	*P. pastoris*	$1.0x10^6$	$1.9x10^{-4}$	0.184
DOTA-$(HE)_3$-G3	*P. pastoris*	$1.0x10^6$	$2.4x10^{-4}$	0.228
His_6-G3*	*E. coli*	$2.7x10^6$	$2.9x10^{-4}$	0.111

*Control His_6-G3: His_6-G3 produced in *E. coli* without a C-terminal cysteine which has a reported binding affinity of 0.091 nM (Zahnd, Kawe et al. 2010).

4.2.2 G3 DARPin specificity for HER2 *in vitro*

Flow cytometry demonstrated that cold indium and cold iodine labelled G3 DARPins bind to HER2-positive human breast adenocarcinoma cells (BT474) and HER2-positive human gastro-oesophageal junction adenocarcinoma cells (OE-19).

However, the cold labelled G3 DARPins did not bind to HER2-negative human breast adenocarcinoma cells (MDA-MB-468). The unlabelled G3 DARPin with a C-terminus His_6 (G3-His_6) was the first version of G3 DARPin produced at UCL in *P. pastoris* and was used as a control. These results confirmed HER2 specificity of the cold labelled His_6-G3, $(HE)_3$-G3 and untagged-G3 DARPins *in vitro* (Figure 4.1).

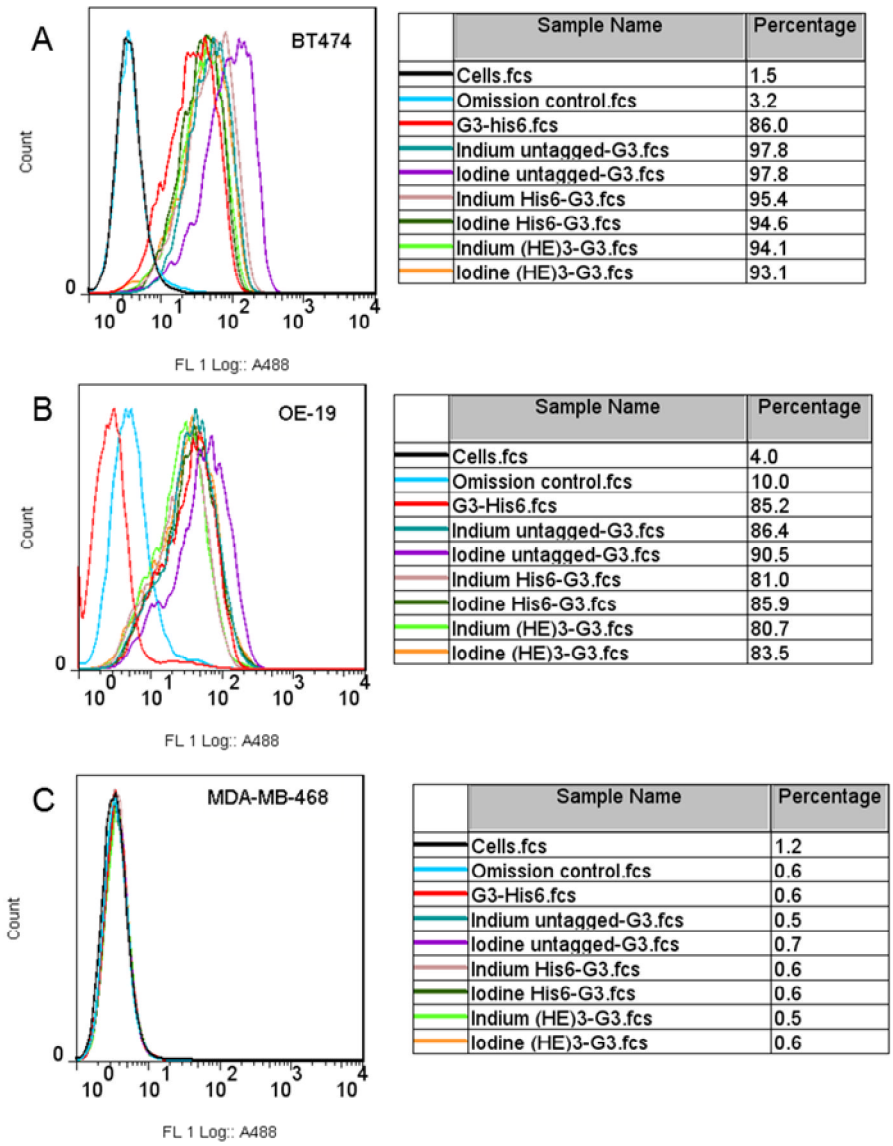

Sample Name	Percentage
Cells.fcs	1.5
Omission control.fcs	3.2
G3-his6.fcs	86.0
Indium untagged-G3.fcs	97.8
Iodine untagged-G3.fcs	97.8
Indium His6-G3.fcs	95.4
Iodine His6-G3.fcs	94.6
Indium (HE)3-G3.fcs	94.1
Iodine (HE)3-G3.fcs	93.1

Sample Name	Percentage
Cells.fcs	4.0
Omission control.fcs	10.0
G3-His6.fcs	85.2
Indium untagged-G3.fcs	86.4
Iodine untagged-G3.fcs	90.5
Indium His6-G3.fcs	81.0
Iodine His6-G3.fcs	85.9
Indium (HE)3-G3.fcs	80.7
Iodine (HE)3-G3.fcs	83.5

Sample Name	Percentage
Cells.fcs	1.2
Omission control.fcs	0.6
G3-His6.fcs	0.6
Indium untagged-G3.fcs	0.5
Iodine untagged-G3.fcs	0.7
Indium His6-G3.fcs	0.6
Iodine His6-G3.fcs	0.6
Indium (HE)3-G3.fcs	0.5
Iodine (HE)3-G3.fcs	0.6

Figure 4.1 Flow cytometry of cold indium and cold iodine labelled G3 DARPins assessed with HER2-positive and HER2-negative human cell lines.
A) Human HER2-positive breast adenocarcinoma cells (BT474), B) Human HER2-positive gastro-oesophageal junction adenocarcinoma cells (OE-19) and C) Human HER2-negative breast adenocarcinoma cells (MDA-MB-468). G3-His_6 was unlabelled. Omission control cells were treated with antibodies in the absence of G3 DARPin.

4.2.3 Biodistribution of ^{111}In-G3 DARPins in non-tumour bearing mice

Untagged-G3, His_6-G3 and $(HE)_3$-G3 DARPins were radiolabelled with ^{111}In via a C-terminal DOTA for administration to female BALB/c mice. For each construct, eight mice were assessed and four mice were euthanised at each time point, 4 h and 24 h post-administration.

^{111}In-$(HE)_3$-G3 DARPin had lower uptake in the pancreas, spleen, stomach, liver, heart, lung, blood, muscle and bone marrow at 4 h compared to ^{111}In-His_6-G3 and ^{111}In-untagged-G3. At 24 h, ^{111}In-$(HE)_3$-G3 had lowest uptake in the intestine, pancreas, spleen, stomach, liver, muscle and bone marrow compared to its ^{111}In radiolabelled counterparts (Figure 4.2). The kidneys are the main route of G3 DARPin excretion and kidney uptake was greater than 200% ID/g for all ^{111}In-G3 DARPins at 4 h. Kidney uptake was higher at 4 h than 24 h post-administration, due to radioactive decay and or excretion from the kidneys (Figure 4.2 and Table 4.2). Bone uptake was largely attributed to the marrow, as marrow uptake was similar to intact bone uptake.

At 4 h post-administration, ^{111}In-$(HE)_3$-G3 had significantly lower liver uptake (1.569 ± 0.042% ID/g) than both^{111}In-untagged-G3 (4.312 ± 0.401% ID/g, p=0.001) and ^{111}In-His_6-G3 (3.724 ± 0.386% ID/g, p=0.001). In addition, at 24 h ^{111}In-$(HE)_3$-G3 had significantly lower liver uptake than both ^{111}In-untagged-G3 (p=0.002) and ^{111}In-His_6-G3 (p=0.001) (Figure 4.2 and Table 4.2). Interestingly, there was no significant difference in liver uptake between the ^{111}In-untagged-G3 and ^{111}In-His_6-G3 at 4 h and 24 h post-administration. This suggests a specific favourable influence of the $(HE)_3$-tag, rather than the liver preferentially binding to the His_6-tag.

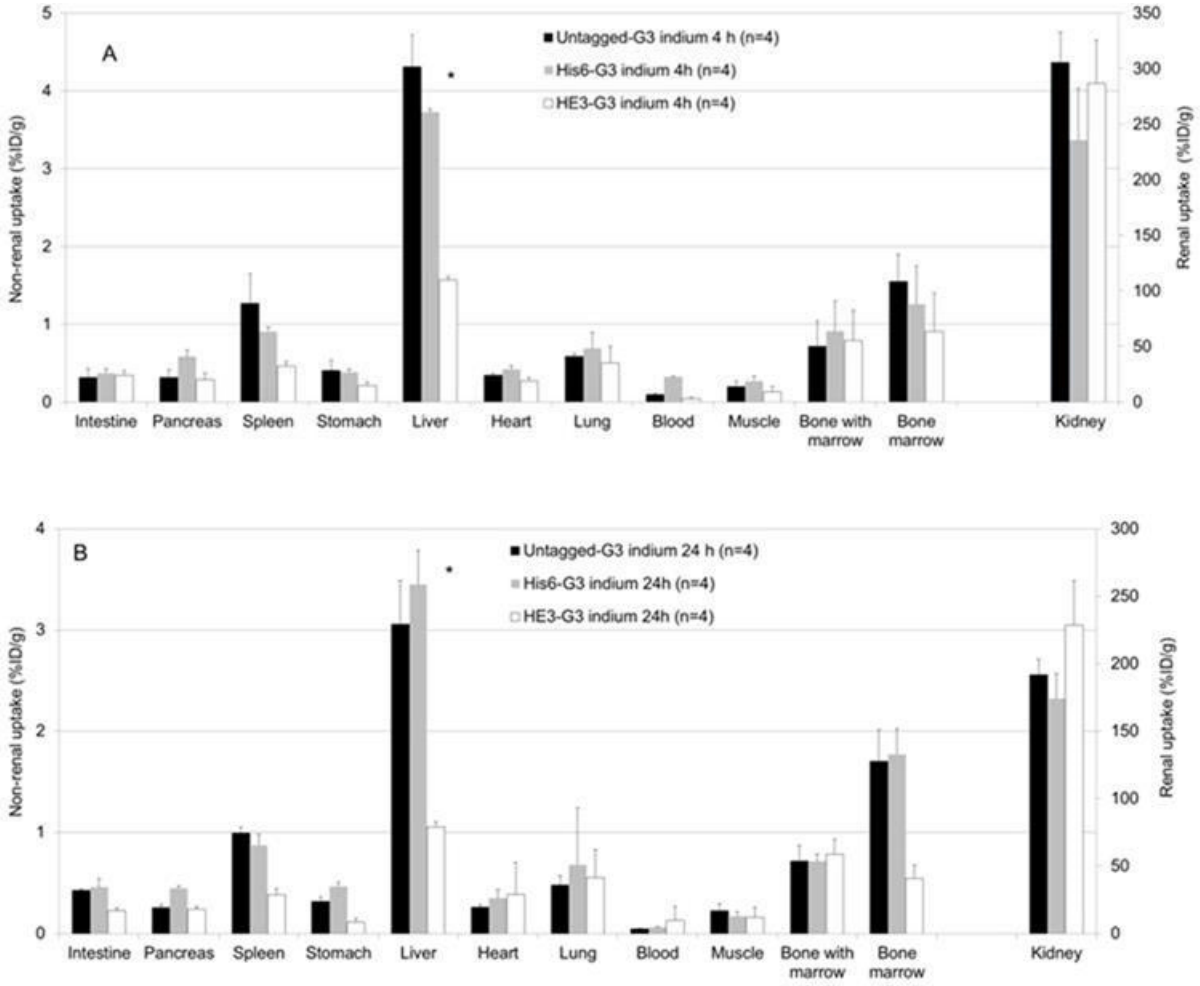

Figure 4.2 Biodistribution of ^{111}In-G3 DARPins in female BALB/c mice.
A) 4 h and B) 24 h post-administration. Data expressed as the mean % ID/g ± SD.
* Statistically significant difference between $(HE)_3$-G3 and the other ^{111}In-G3 DARPins.

Table 4.2 Biodistribution of ^{111}In-G3 DARPins in female BALB/c mice.
G3 DARPin with lowest uptake for each normal tissue is emboldened.

A) 4 hour post-administration of ^{111}In-G3 DARPins

Tissue	Untagged-G3 ^{111}In % ID/g ± SD at 4 h (n=4)	His_6-G3 ^{111}In % ID/g ± SD at 4 h (n=4)	$(HE)_3$-G3 ^{111}In % ID/g ± SD at 4 h (n=4)
Intestine	**0.314 ± 0.113**	0.369 ± 0.070	0.345 ± 0.059
Pancreas	0.317 ± 0.099	0.582 ± 0.095	**0.288 ± 0.085**
Spleen	1.269 ± 0.374	0.906 ± 0.075	**0.461 ± 0.056**
Stomach	0.407 ± 0.135	0.377 ± 0.273	**0.210 ± 0.047**
Kidney	305.715 ± 27.245	**235.727 ± 46.615**	286.665 ± 38.607
Liver	4.312 ± 0.401	3.724 ± 0.386	**1.569 ± 0.042**
Heart	0.343 ± 0.025	0.420 ± 0.071	**0.269 ± 0.048**
Lung	0.588 ± 0.040	0.688 ± 0.446	**0.503 ± 0.210**
Blood	0.097 ± 0.017	0.326 ± 0.236	**0.047 ± 0.008**
Muscle	0.199 ± 0.065	0.269 ± 0.087	**0.131 ± 0.066**
Bone with marrow	**0.713 ± 0.330**	0.908 ± 0.142	0.788 ± 0.387
Bone marrow	1.549 ± 0.350	1.257± 0.154	**0.908 ± 0.488**

B) 24 hour post-administration of ^{111}In-G3 DARPins

Tissue	Untagged-G3 ^{111}In % ID/g ± SD at 4 h (n=4)	His_6 -G3 ^{111}In % ID/g ± SD at 4 h (n=4)	$(HE)_3$-G3 ^{111}In % ID/g ± SD at 4 h (n=4)
Intestine	0.427 ± 0.012	0.459 ± 0.081	**0.225 ± 0.026**
Pancreas	0.256 ± 0.032	0.449 ± 0.024	**0.240 ± 0.025**
Spleen	0.991 ± 0.060	0.874 ± 0.108	**0.383 ± 0.064**
Stomach	0.317 ± 0.044	0.465 ± 0.041	**0.110 ± 0.040**
Kidney	191.954 ± 11.245	**174.190 ± 18.759**	228.576 ± 32.920
Liver	3.057 ± 0.432	3.449 ± 0.337	**1.054 ± 0.054**
Heart	**0.260 ± 0.028**	0.353 ± 0.083	0.390 ± 0.315
Lung	**0.480 ± 0.091**	0.679 ± 0.564	0.554 ± 0.274
Blood	**0.046 ± 0.005**	0.061 ± 0.005	0.130 ± 0.136
Muscle	0.224 ± 0.071	0.169 ± 0.048	**0.158 ± 0.104**
Bone with marrow	0.718 ± 0.153	**0.714 ± 0.074**	0.788 ± 0.143
Bone marrow	1.701 ± 1.169	1.773 ± 1.557	**0.547 ± 0.103**

4.2.4 Biodistribution of ^{125}I-G3 DARPins in non-tumour bearing mice

At 4 h post-administration, ^{125}I-$(HE)_3$-G3 and ^{125}I-untagged-G3 had the lowest uptake in all assessed normal tissues (Figure 4.3). ^{125}I-$(HE)_3$-G3 had significantly lower liver uptake than ^{125}I-His_6-G3 (p=0.015) at 4 h but there was no significant difference in liver uptake between ^{125}I-$(HE)_3$-G3 and ^{125}I-untagged-G3 (p=0.494) at 4 h. At 24 h, ^{125}I-$(HE)_3$-G3 had significantly lower liver uptake than ^{125}I-untagged-G3

(p=0.004) and His_6-G3 (p=0.003). There was no significant difference in normal liver uptake between ^{125}I-His_6-G3 and ^{125}I-untagged-G3 at 4h and 24h.

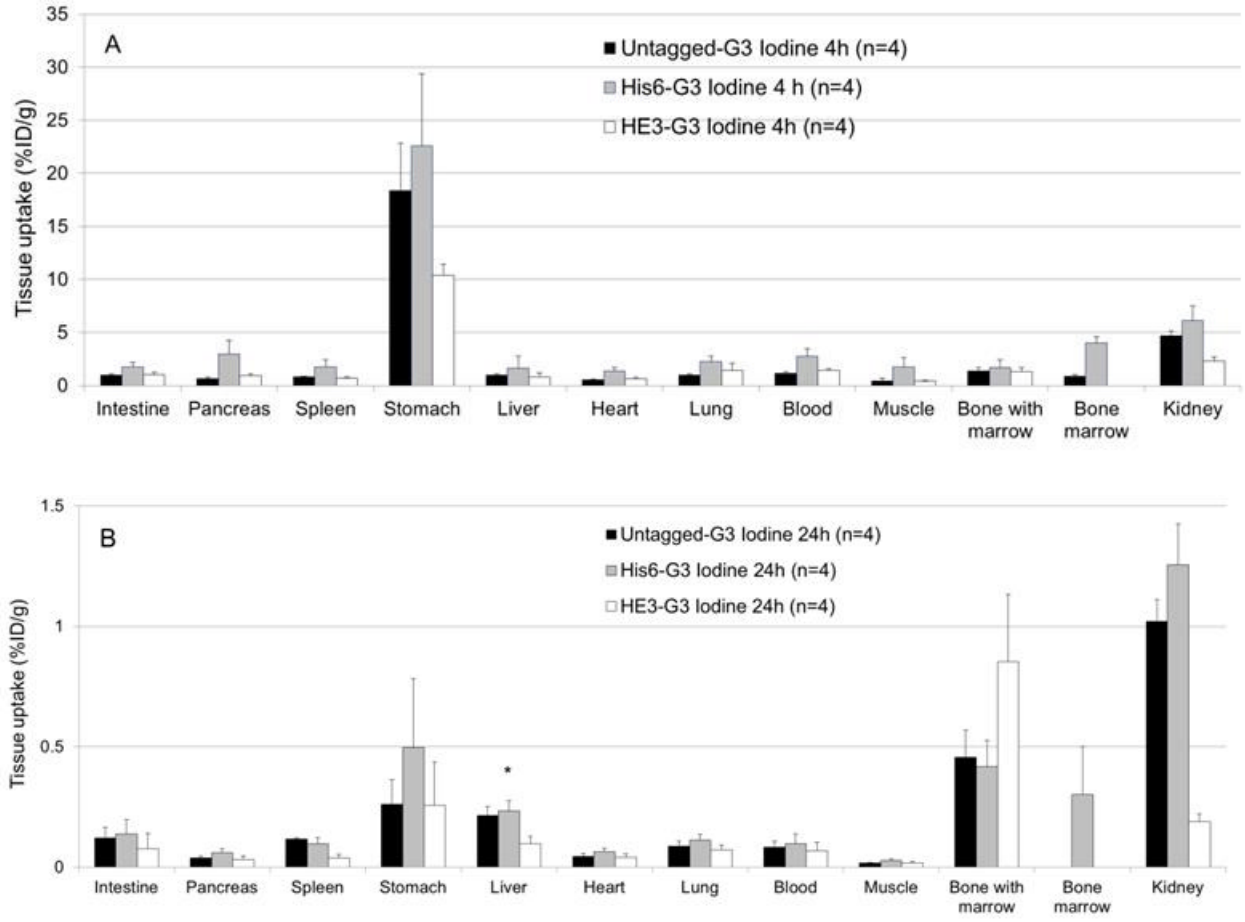

Figure 4.3 Biodistribution of ^{125}I-G3 DARPins in female BALB/c mice.
A) 4 h and B) 24 h post-administration. Data expressed as mean % ID/g ± SD.
* Statistically significant difference between $(HE)_3$-G3 and the other ^{125}I-G3 DARPins.

For ^{125}I radiolabelled G3 DARPins, normal tissue uptake was considerably higher at 4 h than at 24 h post-administration, the normal tissue uptake was <1.3% ID/g for all ^{125}I-G3 DARPins at 24 h. By contrast, ^{111}In-G3 DARPin normal tissue uptake was better maintained between 4 and 24 h (Figure 4.2 and Figure 4.3). ^{125}I is a non-residualising radio-isotope so it is not as well retained within tissues compared with ^{111}In which is a residualising isotope. Kidney uptake was lower for ^{125}I-G3 DARPins than their ^{111}In counterparts, while gastric uptake was higher for the ^{125}I-G3 DARPins where 'free' ^{125}I (formed by de-iodination *in vivo*) is known to accumulate.

$(HE)_3$-G3 was selected for assessment in HER2-positive tumour bearing mice, on the basis of its lower normal tissue uptake which could facilitate imaging of HER2-positive tumours by achieving greater contrast between tumours and normal tissues.

Table 4.3 Biodistribution of ^{125}I-G3 DARPins in female BALB/c mice.
The G3 DARPin with lowest uptake for each normal tissue is emboldened.

A) 4 h post-administration of ^{125}I-G3 DARPins

Tissue	Untagged-G3 ^{125}I mean % ID/g ± SD at 4 h (n=4)	His_6-G3 ^{125}I mean % ID/g ± SD at 4 h (n=4)	$(HE)_3$-G3 ^{125}I mean % ID/g ± SD at 4 h (n=4)
Intestine	**0.971 ± 0.124**	1.763 ± 0.460	1.054 ± 0.202
Pancreas	**0.652 ± 0.142**	2.994 ± 1.246	0.914 ± 0.170
Spleen	0.809 ± 0.088	1.772 ± 0.622	**0.700 ± 0.105**
Stomach	18.379 ± 4.471	22.553 ± 6.813	**10.401 ± 1.052**
Kidney	4.717 ± 0.400	6.119 ± 1.120	**2.336 ± 0.348**
Liver	0.980 ± 0.113	1.655 ± 0.337	**0.841 ± 0.346**
Heart	**0.526 ± 0.050**	1.372 ± 0.480	0.676 ± 0.077
Lung	**0.960 ± 0.151**	2.255 ± 0.698	1.450 ± 0.660
Blood	**1.158 ± 0.151**	2.771 ± 0.892	1.416 ± 0.159
Muscle	0.439 ± 0.270	1.749 ± 0.723	**0.433 ± 0.077**
Bone with marrow	1.369 ± 0.308	1.694 ± 0.545	**1.291 ± 0.395**
Bone marrow	**0.861 ± 0.167**	4.026 ± 1.947	Not isolated

B) 24 h post-administration of ^{125}I-G3 DARPins

Tissue	Untagged-G3 ^{125}I mean % ID/g ± SD at 24 h (n=4)	His_6-G3 ^{125}I mean % ID/g ± SD at 24 h (n=4)	$(HE)_3$–G3 ^{125}I mean % ID/g ± SD at 24 h (n=4)
Intestine	0.122 ± 0.043	0.138 ± 0.060	**0.076 ± 0.063**
Pancreas	0.038 ± 0.009	0.059 ± 0.018	**0.033 ± 0.015**
Spleen	0.116 ± 0.006	0.098 ± 0.024	**0.039 ± 0.013**
Stomach	0.260 ± 0.102	0.497 ± 0.287	**0.256 ± 0.181**
Kidney	1.020 ± 0.091	1.255 ± 0.171	**0.188 ± 0.033**
Liver	0.214 ± 0.039	0.233 ± 0.043	**0.098 ± 0.029**
Heart	0.044 ± 0.015	0.064 ± 0.015	**0.041 ± 0.013**
Lung	0.088 ± 0.021	0.112 ± 0.024	**0.072 ± 0.019**
Blood	0.083 ± 0.025	0.098 ± 0.041	**0.068 ± 0.036**
Muscle	**0.017 ± 0.003**	0.028 ± 0.006	0.018 ± 0.006
Bone with marrow	0.456 ± 0.113	**0.418 ± 0.108**	0.852 ± 0.280
Bone marrow	Weight too low for analysis	**0.300 ± 0.200**	Not isolated

4.2.5 Binding affinity

On the basis of the biodistribution results in non-tumour bearing mice, the $(HE)_3$-G3 DARPin was selected for further assessment. The binding affinity of radiolabelled $(HE)_3$-G3 to HER2-positive human breast adenocarcinoma cells (BT474) was assessed by a saturation assay.

B_{Max} calculates the maximum amount of radiolabelled $(HE)_3$-G3 which can bind to HER2 receptors in the BT474 cell preparation. For ^{111}In-$(HE)_3$-G3 and ^{125}I-$(HE)_3$-G3, the B_{Max} was not reached at the highest assessed DARPin concentration (20 nM), so the B_{Max} had to be extrapolated by extending the curve beyond the measured values. ^{125}I-$(HE)_3$-G3 had a higher B_{Max} than ^{111}In-$(HE)_3$-G3, so higher amounts of ^{125}I-$(HE)_3$-G3 DARPin were required to saturate the HER2 receptors of the BT474 preparation than for ^{111}In-$(HE)_3$-G3. The observed differences in B_{Max} between ^{111}In-$(HE)_3$-G3 and ^{125}I-$(HE)_3$-G3, could be due to different HER2 affinities and kinetics of these radioligands. It could also reflect differences in HER2 expression levels between the BT474 cell preparations. Furthermore, if 0.1% sodium azide failed to prevent HER2 receptor internalisation, then the differences in B_{Max} could reflect different internalisation and externalisation rates of ^{125}I-$(HE)_3$-G3 and ^{111}In-$(HE)_3$-G3.

The K_D (binding affinity) is calculated at half of the B_{Max} (Figure 2.7). Affinity for the HER2 receptor of the BT474 cells, was 12.82 nmol/L for ^{111}In-$(HE)_3$-G3, compared with 15.74 nmol/L for ^{125}I-$(HE)_3$-G3 (Table 4.4 and Figure 4.4). The direct radiolabelling of the $(HE)_3$-G3 DARPin with ^{125}I to tyrosine residue(s) does not appear to impact greatly upon the affinity for HER2 of BT474 cells compared to ^{111}In-$(HE)_3$-G3 which is site specifically radiolabelled via DOTA.

The G3 DARPin affinity measured by SPR was in the picomolar range (Table 4.1). During SPR assessment the non-radiolabelled G3 DARPin flows directly over the HER2 ECD. However, the membrane bound HER2 receptor is less accessible, which could explain the lower affinities (nanomolar) for the radiolabelled $(HE)_3$-G3 DARPin assessed by the saturation assay. Although DOTA conjugation does not appear to affect HER2 binding affinity based on SPR assessment (Table 4.1), it is possible that the ^{111}In and ^{125}I radiolabelling reactions could affect HER2 binding affinity.

Table 4.4 Binding affinity of ^{111}In-DOTA-$(HE)_3$-G3 and ^{125}I-$(HE)_3$-G3 to HER2-positive human breast cells (BT474).

	B_{Max} (fmol/mg)	K_D assessed on BT474 cells (nmol/L)*	K_D assessed by SPR (nmol/L)#
^{111}In-DOTA-$(HE)_3$-G3	3747	12.82	0.228
^{125}I-$(HE)_3$-G3	5219	15.74	0.184

*Single assessment and # duplicate assessment.

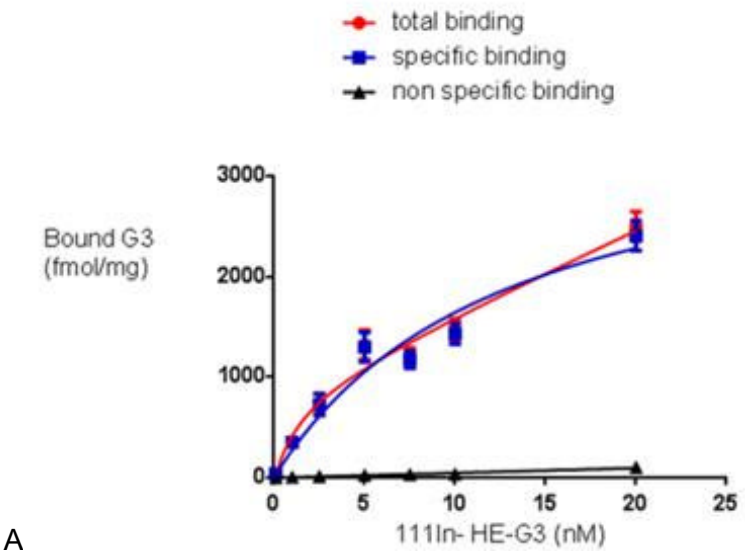

A

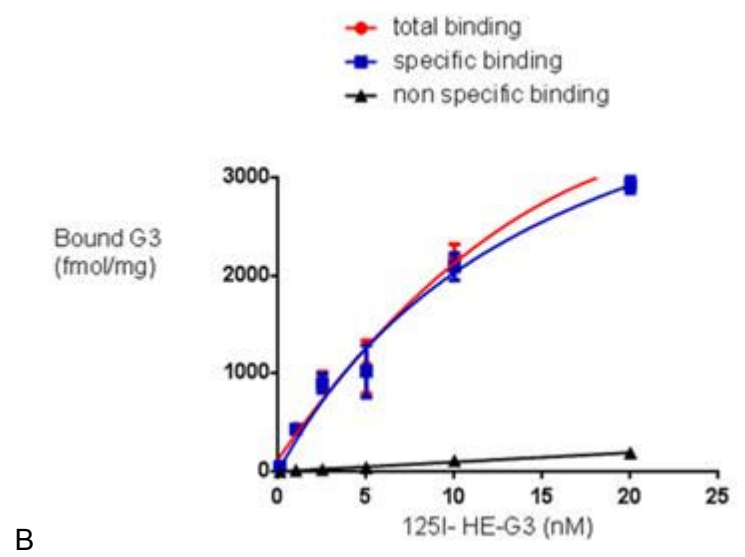

B

Figure 4.4 Saturation binding assay with HER2-positive (BT474) cells. A) ^{111}In-$(HE)_3$-G3 DARPin and B) ^{125}I-$(HE)_3$-G3 DARPin

4.3 Discussion

The work in this Chapter was focused on investigating the research hypothesis, N-terminus histidine-based tags affect normal tissue uptake of the G3 DARPin. It is important to assess this, as the identification of metastases on imaging relies upon minimising normal tissue radioligand uptake.

Initial, *in vitro* studies demonstrated that cold indium and iodine labelled untagged-G3, His_6-G3 and $(HE)_3$-G3 DARPins specifically bind to HER2-positive cells. Conjugation with DOTA did not alter the kinetics and binding affinities of the G3 DARPins with the HER2 ECD assessed by SPR, HER2 binding affinity is in the picomolar range both pre- and post-conjugation. This is because the HER2 binding site is not at the C-terminus where DOTA binds. However, ^{111}In-$(HE)_3$-G3 and ^{125}I-$(HE)_3$-G3 have similar nanomolar binding affinities to the membrane-bound HER2 receptor of BT474 cells. The differences in HER2 binding affinities could reflect the greater accessibility of the HER2 ECD on SPR than with the cell-based assay.

Histidine based tags enable IMAC purification and can be used for the chelation of $[^{99m}Tc(CO)_3]^+$. The G3 DARPins assessed only differed at their N-terminal tags. The presented ^{111}In and ^{125}I biodistribution studies, demonstrated that the presence of the $(HE)_3$ tag rather than the absence of the His_6 tag is responsible for reducing normal liver G3 DARPin uptake. Thus, confirming the research hypothesis.

For the affibody molecule, $Z_{HER2:342}$ radiolabelled with $[^{99m}Tc(CO)_3]^+$, $(HE)_3$-$Z_{HER2:342}$ was associated with lower liver uptake than counterparts with different histidine tag configurations (Tolmachev, Hofstrom et al. 2010; Hofstrom, Orlova et al. 2011; Hofstrom, Altai et al. 2013). Yet, some of the comparative $Z_{HER2:342}$ biodistribution studies are limited, as there were other differences in the amino acid sequences besides the composition of the histidine-based tags (Hofstrom, Orlova et al. 2011).

For affibody molecules radiolabelled with ^{111}In via DOTA, ^{111}In-His_6-$Z_{HER2:342}$-C had higher liver uptake than ^{111}In-untagged-$Z_{HER2:342}$-C and ^{111}In-$(HE)_3$-$Z_{HER2:342}$-C, however the uptake in non-hepatic organs was similar for the different constructs (Ahlgren, Orlova et al. 2008; Hofstrom, Orlova et al. 2011). The presented work demonstrated that ^{111}In-$(HE)_3$-G3 had significantly lower liver uptake than ^{111}In-

untagged-G3 and ^{111}In-His_6-G3. In addition, there was no significant difference in liver uptake between the ^{111}In-untagged-G3 and ^{111}In-His_6-G3.

^{125}I-HPEM-$(HE)_3$-$Z_{HER2:342}$-C and ^{125}I-HPEM-His_6-$Z_{HER2:342}$-C (1-[2-(4-hydroxyphenyl)ethyl]pyrrole-2,5-dione) have similar biodistribution profiles, including low liver uptake, high stomach uptake and low kidney uptake in non-tumour bearing mice (Hofstrom, Orlova et al. 2011). In addition, liver uptake for ^{125}I-HPEM-$(HE)_3$-$Z_{HER2:342}$-C and ^{125}I-HPEM-His_6-$Z_{HER2:342}$-C at 4 h post-administration were similar (Hofstrom, Orlova et al. 2011).

Direct iodination of the G3 DARPins results in higher stomach uptake where free iodine (formed by de-iodination *in vivo*) is known to accumulate and lower kidney uptake compared to their ^{111}In radiolabelled counterparts. ^{111}In is a residualising radio-isotope so remains inside the cells post-internalisation, reflected by similar uptake in the assessed normal tissues at 4 and 24 h. By contrast, ^{125}I is a non-residualising radioisotope, resulting in lower radio-iodine uptake in normal tissues at 24 h compared to 4 h. At 24 h post-administration, there was a significantly lower liver uptake for ^{125}I-$(HE)_3$-G3 compared to both ^{125}I-His_6-G3 and ^{125}I-untagged-G3.

The mechanism of $(HE)_3$ tag mediated reduction in G3 DARPin liver uptake has not been established. For affibody molecules, it has been proposed that positively charged and hydrophobic tags enhance liver uptake (Hofstrom, Altai et al. 2013). However, the untagged and His_6-tagged affibody molecules have basic isoelectric points (pI), which is brought to a more acidic region by switching to an $(HE)_3$ tag, such that the overall pI of the different affibody constructs tested differed greatly. By contrast, the $(HE)_3$, His_6 and untagged-G3 DARPins have similar pIs of 4.79, 5.41 and 4.71, respectively (Hofstrom, Altai et al. 2013). Furthermore, the $(HE)_3$, His_6 and untagged-G3 DARPins have similar grand average of hydropathy (GRAVY) scores -0.12, -0.12 and +0.02, respectively, indicating other factors are involved, while the corresponding affibody molecules have slightly more divergent scores of -1.03, -0.97 and -0.85.

In non-tumour bearing mice, $(HE)_3$-G3 DARPin had lower or equivalent normal tissue uptake compared with both His_6-G3 and untagged-G3, so was selected for assessment in HER2-positive tumour bearing mice. In particular, ^{111}In-$(HE)_3$-G3 had

significantly lower liver uptake than ^{111}In-His$_6$-G3 and ^{111}In-untagged-G3 at 4 and 24 h post-administration, while ^{125}I-(HE)$_3$-G3 had significantly lower liver uptake than both of its ^{125}I radiolabelled counterparts at 24 h. Comparing the 4 h normal liver uptake of [^{99m}Tc(CO)$_3$]$^+$-His$_6$-G3 (7.27 ± 1.04% ID/g) with ^{111}In-(HE)$_3$-G3 (1.569 ± 0.042% ID/g) and ^{125}I-(HE)$_3$-G3 (0.841 ± 0.346% ID/g), demonstrates that the (HE)$_3$-G3 DARPin represents a promising development that warrants further investigation (Zahnd, Kawe et al. 2010).

Chapter 5 SPECT imaging with indium-111 and iodine-123/125 radiolabelled G3 DARPin

5.1 Introduction

The work in this Chapter was primarily focused on evaluating HER2 SPECT imaging with the ^{111}In- and $^{123/125}$I-radiolabelled $(HE)_3$-G3 DARPin. A preliminary study, performed by Dr Kim Vigor (UCL Cancer Institute), had established HER2 tumour specificity *in vivo* with a G3 DARPin radiolabelled with $[^{99m}Tc(CO)_3]^+$ via a C-terminal His_6-tag ($[^{99m}Tc(CO)_3]^+$-G3-His_6) (Waibel, Alberto et al. 1999). $[^{99m}Tc(CO)_3]^+$-G3-His_6 had significantly higher uptake in HER2-positive (BT474) tumours than in HER2-negative (MDA-MB-468) tumours, 3.5 ± 1.1 vs. 1.0 ± 0.2% ID/g at 24 h post-administration (p=0.004). Uptake in normal tissues was similar in the HER2-positive and HER2-negative tumour bearing mice (Table 5.1). The differences in tumour uptake were also apparent on microSPECT/CT scans (Figure 5.1). However, $[^{99m}Tc(CO)_3]^+$-G3-His_6 did not appear optimal for HER2 imaging, since in the HER2-positive xenograft, the tumour-to-liver ratios were low (1.2:1 at 24 h), in the presence of good tumour-to-blood ratios (26:1 at 24 h). As previously discussed, a similar G3 DARPin construct radiolabelled with $[^{99m}Tc(CO)_3]^+$ assessed in a SKOV3 tumour model, demonstrated a low tumour-to-liver ratio (1.7:1 at 24 h) in the presence of a high HER2-positive tumour uptake (8.06 ± 2.38 at 24 h) (Zahnd, Kawe et al. 2010).

Table 5.1 Biodistribution of $[^{99m}Tc(CO)_3]^+$-G3-His_6 in HER2-positive and HER2-negative tumour bearing SCID-beige mice (unpublished).

Organ	HER2-positive (BT474) tumours at 24 h, mean % ID/g ± SD (n=4)	HER2-negative (MDA-MB-468) tumours at 24 h, mean % ID/g ± SD (n=4)
Tumour	3.5 ± 1.1	1.0 ± 0.2
Spleen	0.9 ± 0.2	1.0 ± 0.3
Kidney	108.0 ± 7.7	108.6 ± 10.6
Liver	3.0 ± 0.2	2.7 ± 0.7
Lung	0.5 ± 0.1	0.5 ± 0.2
Blood	0.1 ± 0.0	0.1 ± 0.0
Muscle	0.3 ± 0.1	0.2 ± 0.1

In view of the data presented in Chapter 4, all further investigations focused entirely on the $(HE)_3$-G3 DARPin. This included results from non-tumour bearing mice studies, demonstrating that ^{111}In-$(HE)_3$-G3 and ^{125}I-$(HE)_3$-G3 had significantly lower liver uptake than their radiolabelled His_6-G3 and untagged-G3 counterparts. At 24 h, the liver uptake of ^{111}In-$(HE)_3$-G3 (1.1 ± 0.1 % ID/g) and ^{125}I-$(HE)_3$-G3 (0.1 ± 0.0 % ID/g) in non-tumour bearing mice were low, this compared favourably with the liver

uptake for [^{99m}Tc(CO)$_3$]$^+$-His$_6$ in HER2-positive tumour bearing mice (3.0 ± 0.2% ID/g) (Table 5.1). Furthermore, the cold indium and cold iodine labelled (HE)$_3$-G3 DARPin had specificity for HER2-positive cell lines *in vitro*. The (HE)$_3$-G3 DARPin had picomolar affinity for the HER2 ECD assessed by SPR, while ^{111}In-(HE)$_3$-G3 and ^{125}I-(HE)$_3$-G3 both had nanomolar affinities for HER2 expressed by BT474 human breast cancer cells.

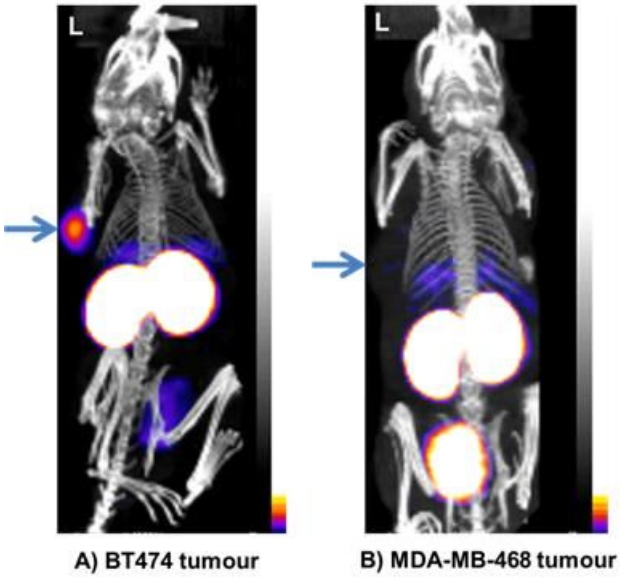

Figure 5.1 MicroSPECT/CT scans at 1 h post-administration of [^{99m}Tc(CO)$_3$]$^+$-G3-His$_6$ to SCID-beige mice bearing tumours (unpublished).
A) HER2-positive human breast tumour (BT474) and B) HER2-negative human breast tumour (MDA-MB-468). Tumours in left (L) side of mouse identified by an arrow (A and B assessed at same level of sensitivity).

It would be advantageous if the G3 DARPin binds to HER2 in the presence of anti-HER2 therapies, so that patients can be scanned without compromising treatment schedules and efficacy. Structural modelling has determined that the G3 DARPin and trastuzumab bind to adjacent but non-overlapping epitopes of subdomain 4 of the HER2 ECD (Epa, Dolezal et al. 2013). However, a lack of competition has not been confirmed *in vivo*. Pertuzumab binds to subdomain 2 of the HER2 ECD, so the G3 DARPin should be able to bind in the presence of pertuzumab.

In summary, G3 DARPins have high affinity for HER2, specificity for HER2-positive breast tumours and could potentially bind to HER2 in the presence of pertuzumab and trastuzumab. The $(HE)_3$-G3 is the most promising variant as it has the lowest normal liver uptake, justifying its investigation in HER2-positive tumour bearing mice.

Aim:

To test the hypothesis, that the G3 DARPin radiolabelled with indium-111 and iodine-123/125 can achieve high tumour-to-blood and high tumour-to-normal tissue ratios for pre-clinical HER2 SPECT imaging.

Objectives:

To determine the suitability of radiolabelled $(HE)_3$-G3 for HER2 imaging by assessing:

1. Tumour uptake and tumour-to-normal tissue ratios in HER2-positive tumour bearing mice.
2. Ability to image HER2-positive tumours in mice by microSPECT/CT scanning.
3. Effect of trastuzumab on tumour uptake in HER2-positive tumour bearing mice.
4. Stability in serum and PBS.

5.2 Results

5.2.1 HER2 status of BT474 tumours excised from untreated mice

Prior to assessing $(HE)_3$-G3 DARPin in HER2-positive tumour bearing mice, it was important to confirm that the BT474 tumours inoculated into the mice were HER2-positive, so tumours from four untreated mice were assessed. The 2013 update of the ASCO/CAP guidelines for HER2 testing in breast cancer, defines IHC 3+, as circumferential membrane staining that is complete, intense, and within >10% of tumour cells (Wolff, Hammond et al. 2013).

The HercepTest (Dako) consists of a primary rabbit anti-human HER2 antibody and a secondary goat anti-rabbit antibody with HRP for IHC assessment. The positive control, HER2-positive human breast tumour tissue (SK-BR-3) scored 3+ with the HercepTest primary and secondary antibodies. The negative control, SK-BR-3 tumour tissue tested with normal rabbit immunoglobulin and secondary goat anti-rabbit antibody with HRP, scored 0 on IHC. Thus, confirming that there is no cross reactivity between the secondary antibody and human breast cancer cells. The four human breast tumours (BT474) excised from untreated SCID-beige mice all scored 3+ on IHC (Figure 5.2).

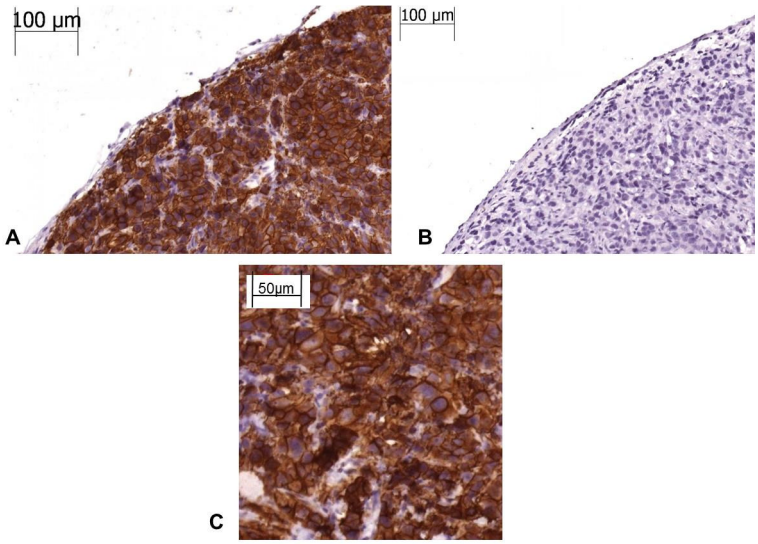

Figure 5.2 Immunohistochemistry of human breast tumours with HercepTest. Primary, rabbit anti-human HER2 antibody and secondary, goat anti-rabbit antibody with HRP, control SK-BR-3 (HER2-positive breast tumour), 20x magnification:
A) Positive control, SK-BR-3 tumour with primary and secondary Ig (3+).
B) Negative control, SK-BR-3 tumour with normal rabbit Ig and secondary Ig (0).
C) BT474 tumour from untreated SCID-beige mice tested with primary and secondary Ig (3+).

5.2.2 Normal tissue biodistribution of ^{111}In-$(HE)_3$-G3 and ^{125}I-$(HE)_3$-G3 DARPins in HER2-positive tumour bearing mice and non-tumour bearing mice

The decision to exclusively investigate $(HE)_3$-G3 DARPin in tumour bearing mice was based on its normal tissue biodistribution in BALB/c mice, including lower normal liver uptake for $(HE)_3$-G3 compared to untagged-G3 and His_6-G3 DARPins when radiolabelled with ^{125}I and ^{111}In. Thus, it was important to confirm that ^{111}In-$(HE)_3$-G3 and ^{125}I-$(HE)_3$-G3 normal tissue uptake in BALB/c mice and tumour bearing SCID-beige mice were comparable.

For ^{111}In-$(HE)_3$-G3, there was relatively similar normal tissue uptake in tumour bearing SCID-beige mice and non-tumour bearing BALB/c mice at 4 and 24 h post-administration. The major exceptions were the liver, heart, lung and bone, where there was higher tissue uptake for BALB/c mice than SCID-beige mice. ^{111}In-$(HE)_3$-G3 normal liver uptake was two-fold higher for BALB/c mice than tumour bearing SCID-beige mice at 4 h, 1.6 ± 0.0 vs. 0.7 ± 0.1% ID/g, however the differences in normal liver uptake were smaller at 24 h (Figure 5.3).

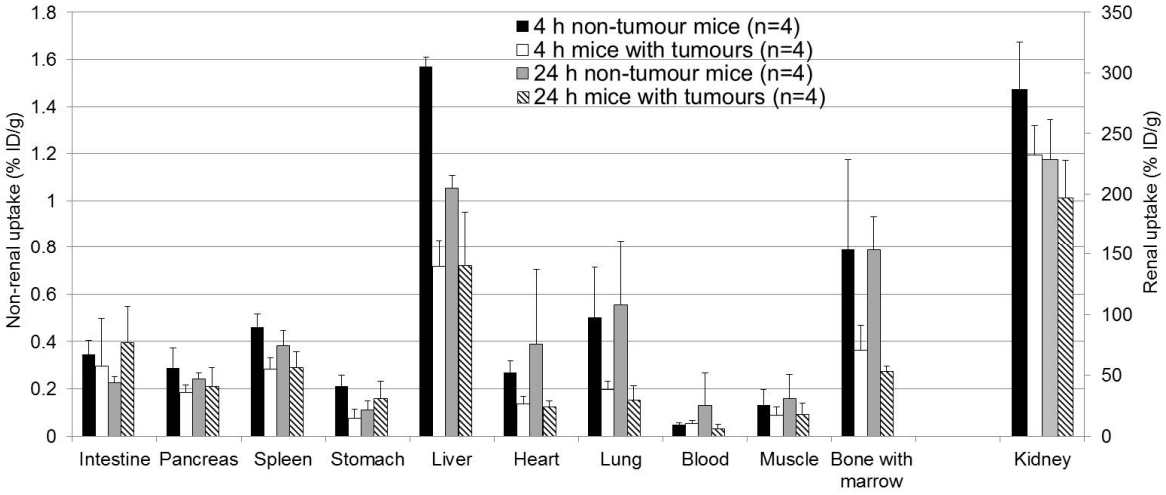

Figure 5.3 Biodistribution of ^{111}In-$(HE)_3$-G3 DARPin in female BALB/c mice and female SCID-beige mice bearing HER2-positive human breast tumours (BT474) (tumour uptake omitted). Data expressed as mean % ID/g ± SD.

The normal tissue uptake for tumour bearing SCID-beige mice and non-tumour bearing BALB/c mice treated with ^{125}I-(HE)$_3$-G3 were similar at 24 h but normal tissue uptake was higher for most assessed normal tissues in tumour bearing SCID-beige mice at 4 h. For example, 4 h blood uptake was 1.4 ± 0.2% ID/g for BALB/c mice and 3.6 ± 2.2% ID/g for SCID-beige mice, yet blood levels were similar at 24 h for both mice (Figure 5.4).

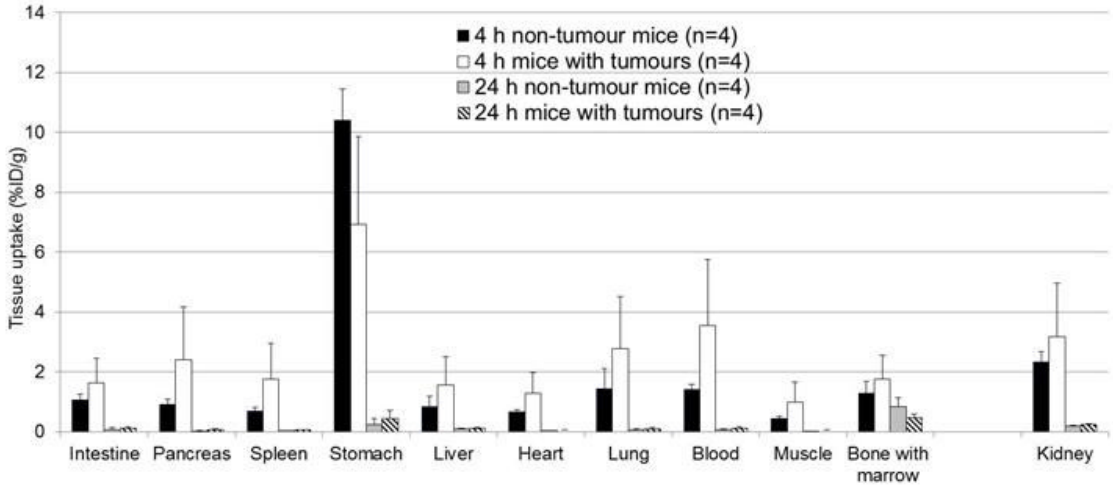

Figure 5.4 Biodistribution of ^{125}I-(HE)$_3$-G3 DARPin in female BALB/c mice and female SCID-beige mice bearing HER2-positive human breast tumours (BT474 (tumour uptake omitted). Data expressed as mean % ID/g ± SD.

5.2.3 Biodistribution of ^{111}In-(HE)$_3$-G3 and ^{125}I-(HE)$_3$-G3 DARPins in HER2-positive tumour bearing mice

At 4 h post-administration, ^{125}I-(HE)$_3$-G3 and ^{111}In-(HE)$_3$-G3 had similar uptake in HER2-positive tumours, 11.3 ± 3.2 and 8.8 ± 1.3% ID/g, respectively. ^{111}In is a residualising radio-isotope and remains inside the tumour cells after internalisation, by contrast ^{125}I is a non-residualising radio-isotope and is not retained by cells. Consequently, at 24 h post-administration HER2-positive tumour uptake was over 3 -fold higher for ^{111}In-(HE)$_3$-G3 than ^{125}I-(HE)$_3$-G3, 8.1 ± 0.9 vs. 2.4 ± 0.6% ID/g (Figure 5.5 and Figure 5.6).

Table 5.2 Tumour-to-normal tissue ratios of ^{111}In-$(HE)_3$-G3 and ^{125}I-$(HE)_3$-G3 in female SCID-beige mice bearing HER2-positive human breast tumours (BT474).

Mean tumour-to-tissue ratios	^{111}In-$(HE)_3$-G3		^{125}I-$(HE)_3$-G3	
	4h tumour-to-tissue ratio (n=4)	24h tumour-to-tissue ratio (n=4)	4h tumour-to-tissue ratio (n=4)	24h tumour-to-tissue ratio (n=4)
Intestine	39.4 ± 21.1	21.8 ± 5.1	8.0 ± 3.6	20.8 ± 10.9
Pancreas	50.1 ± 15.3	41.5 ± 12.7	6.6 ± 4.2	36.2 ± 11.6
Spleen	32.3 ± 9.6	28.6 ± 5.0	8.5 ± 5.1	34.2 ± 11.2
Stomach	148.8 ± 91.1	67.5 ± 46.6	1.3 ± 0.8	6.4 ± 2.501
Liver	12.4 ± 1.8	12.0 ± 3.6	9.3 ± 5.7	21.0 ± 8.1
Heart	69.3 ± 25.2	66.5 ± 8.1	10.4 ± 5.1	37.8 ± 11.5
Lung	46.4 ± 12.6	60.8 ± 24.9	5.4 ± 3.6	23.2 ± 9.1
Blood	174.7 ± 26.1	343.7 ± 161.3	4.4 ± 3.4	22.0 ± 11.3
Muscle	114.3 ± 55.5	105.8 ± 51.7	18.6 ± 17.0	58.0 ± 26.6
Bone with marrow	25.9 ± 8.3	28.1 ± 2.7	6.9 ± 2.0	5.2 ± 0.4
Kidney	0.04 ± 0.008	0.04 ± 0.005	4.3 ± 2.2	9.8 ± 2.5

Normal tissue uptake in HER2-positive tumour bearing mice was lower for ^{111}In-$(HE)_3$-G3 than ^{125}I-$(HE)_3$-G3 at 4 h, except in the kidneys where uptake was higher for ^{111}In-$(HE)_3$-G3. Consequently, tumour-to-normal tissue ratios at 4 h were higher for ^{111}In-$(HE)_3$-G3 than ^{125}I-$(HE)_3$-G3 for all tissues, except the kidneys (Table 5.2). High tumour-to-normal tissue ratios are favourable for tumour imaging. At 24 h, the differences in tumour-to-normal tissue ratios were less marked between ^{111}In-$(HE)_3$-G3 and ^{125}I-$(HE)_3$-G3 (Table 5.2).

^{111}In-$(HE)_3$-G3 kidney uptake was higher than any other tissue tested; it was 232.0 ± 24.1% ID/g at 4 h and decreased to 196.5 ± 31.0% ID/g at 24 h (Figure 5.5 and Figure 5.6). Rapid serum clearance and or uptake of ^{111}In-$(HE)_3$-G3 via the kidneys resulted in higher tumour-to-blood ratios of 174.7 ± 26.1 at 4 h for ^{111}In-$(HE)_3$-G3 compared to 4.4 ± 3.4 at 4 h for ^{125}I-$(HE)_3$-G3 (Table 5.2).

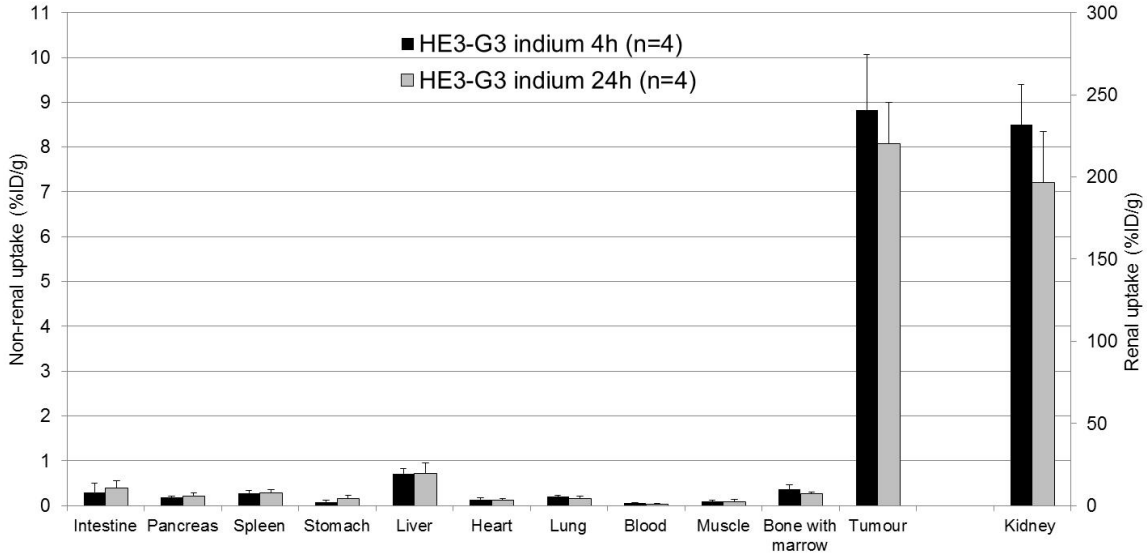

Figure 5.5 Biodistribution of ^{111}In-(HE)$_3$-G3 DARPin in female SCID-beige mice bearing HER2-positive human breast tumours (BT474). Data expressed as mean % ID/g ± SD.

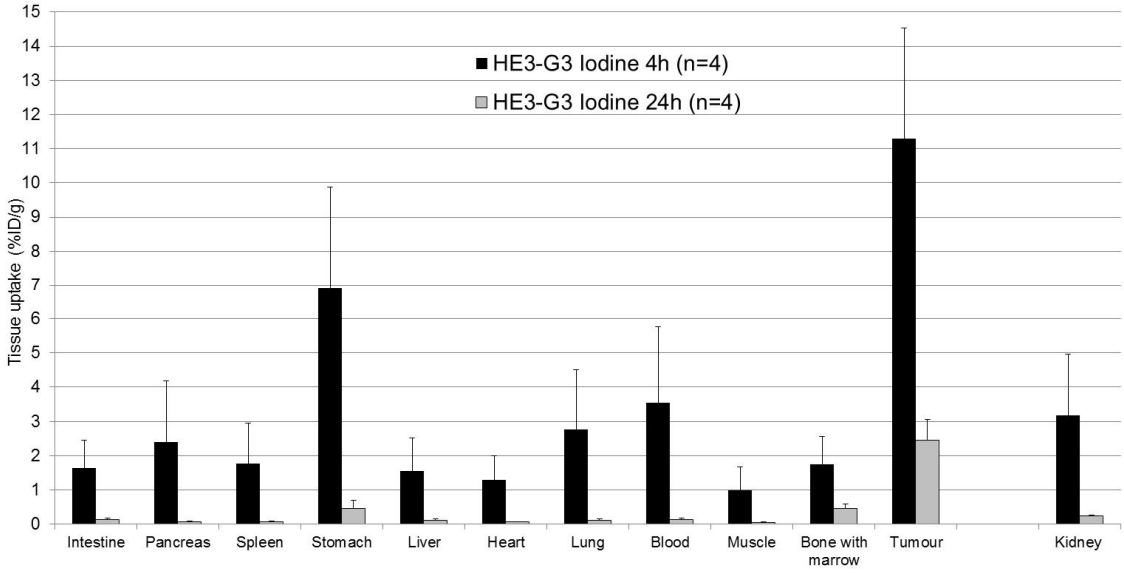

Figure 5.6 Biodistribution of ^{125}I-(HE)$_3$-G3 DARPin in female SCID-beige mice bearing HER2-positive human breast tumours (BT474). Data expressed as mean % ID/g ± SD.

5.2.4 SPECT/CT scans with ^{123}I-(HE)$_3$-G3 and ^{111}In-(HE)$_3$-G3 DARPins

^{123}I-(HE)$_3$-G3 DARPin was used for SPECT scanning, as ^{123}I has higher gamma energy emission than ^{125}I (159 vs. 35.5 KeV). HER2-positive tumour uptake could be detected on the ^{123}I-(HE)$_3$-G3 microSPECT/CT scan at 4 h but there was non-

specific uptake in the stomach, kidneys, bladder and thyroid. On the ^{111}In-$(HE)_3$-G3 microSPECT/CT scan at 4 h, HER2-positive tumour uptake was detected and there was minimal uptake in all organs, besides the kidneys (Figure 5.7). Thus, the acquired SPECT/CT scan images reflect the biodistribution profiles of ^{125}I-$(HE)_3$-G3 and ^{111}In-$(HE)_3$-G3 DARPins in tumour and non-tumour bearing mice. ^{111}In-$(HE)_3$-G3 was selected for further development, in view of its higher tumour-to-blood ratios, higher tumour-to-normal tissue uptake (except for the kidneys) and better maintained HER2-positive tumour uptake over 24 h than $^{123/125}$I-$(HE)_3$-G3.

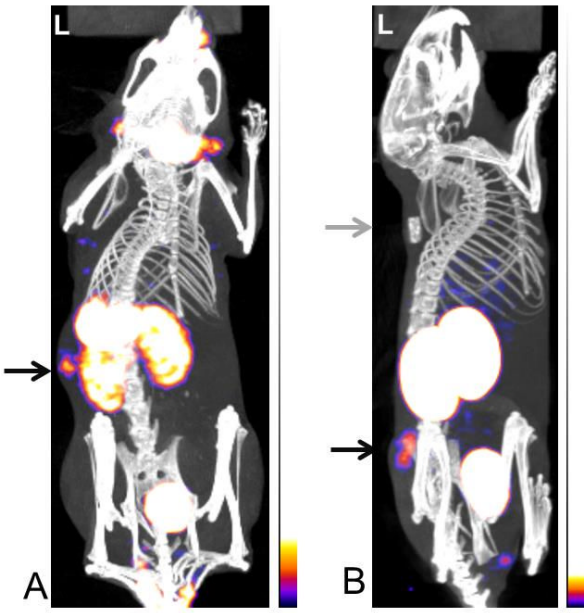

Figure 5.7 MicroSPECT/CT scans of SCID-beige mice bearing HER2-positive (BT474) tumours beside their left (L) hip (black arrow).
A) ^{123}I-$(HE)_3$-G3 DARPin at 4 h, demonstrating HER2-positive tumour uptake associated with high uptake in the kidneys, bladder, stomach and thyroid.
B) ^{111}In-$(HE)_3$-G3 DARPin at 4 h, demonstrating HER2-positive tumour uptake associated with high uptake in the kidneys and bladder (oestrogen pellet visible, grey arrow).

5.2.5 Effect of trastuzumab on ^{111}In-$(HE)_3$-G3 DARPin HER2-positive tumour uptake

Pre-administration of an 18-fold molar excess of intravenous non-radiolabelled trastuzumab (350 µg trastuzumab/mouse) 24 h prior to intravenous ^{111}In-$(HE)_3$-G3 (1.9 µg ^{111}In-$(HE)_3$-G3 DARPin/mouse) did not significantly effect 4 h HER2-positive tumour uptake compared to mice which only received ^{111}In-$(HE)_3$-G3, 7.2 ± 1.3 vs.

7.1 ± 1.9% ID/g, respectively (p=0.95) (Figure 5.8). Confirming that the G3 DARPin can bind in the presence of trastuzumab, as they bind to non-overlapping epitopes within subdomain 4 of the HER2 ECD (Jost, Schilling et al. 2013).

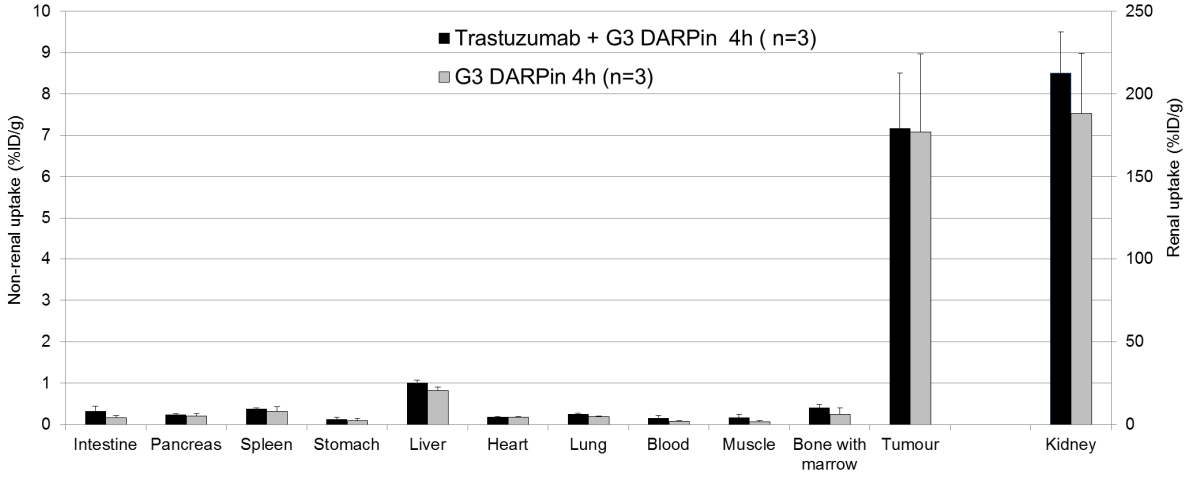

Figure 5.8 Biodistribution of ^{111}In-$(HE)_3$-G3 DARPin at 4 h in the presence and absence of trastuzumab.
Female SCID-beige mice bearing HER2-positive human breast tumours (BT474) pre-treated with an 18-fold molar excess of trastuzumab, 24 h prior to G3 DARPin administration compared with mice which only received G3 DARPin. Data expressed as the mean % ID/g ± SD.

5.2.6 *In vitro* stability of selected radiolabelled DARPin

^{111}In-$(HE)_3$-G3 DARPin was stable in PBS at 4 °, 20 ° and 37 °C and serum:PBS (1:1) at 37 °C, since > 95% of radiation activity was bound to $(HE)_3$-G3 for 24 h post-radiolabelling (Table 5.3).

Autoradiography of the SDS-PAGE gel of ^{111}In-$(HE)_3$-G3 DARPin stored in human serum:PBS (1:1) and PBS alone determined that there was only a single radiolabelled protein at 24 h post-radiolabelling, coomassie staining confirmed that the radiolabelled proteins were the appropriate molecular weight (14-15 kDa). In addition, there were no detectable radiolabelled or non-radiolabelled breakdown products (Figure 5.9).

Table 5.3 Stability of ^{111}In-$(HE)_3$-G3 DARPin assessed in PBS at 4 °, 20 ° and 37 °C and in serum:PBS (1:1) at 37 °C for 24 h post-radiolabelling assessed by instant thin layer chromatography.

Time post radiolabelling	DARPin radiolabelling (%)	Colloid (%)	Other products (%)
Serum stability: 37 °C - 1 h	100	0	0
2 h	100	0	0
4 h	100	0	0
24 h	100	0	0
PBS stability: 37 °C- 1 h	100	0	0
2 h	100	0	0
4 h	100	0	0
24 h	96.4	0	3.6
PBS stability: 20 °C- 1 h	100	0	0
2 h	100	0	0
4 h	100	0	0
24 h	97.4	0	2.6
PBS stability: 4 °C- 1 h	100	0	0
2 h	100	0	0
4 h	100	0	0
24 h	95.9	0	4.1

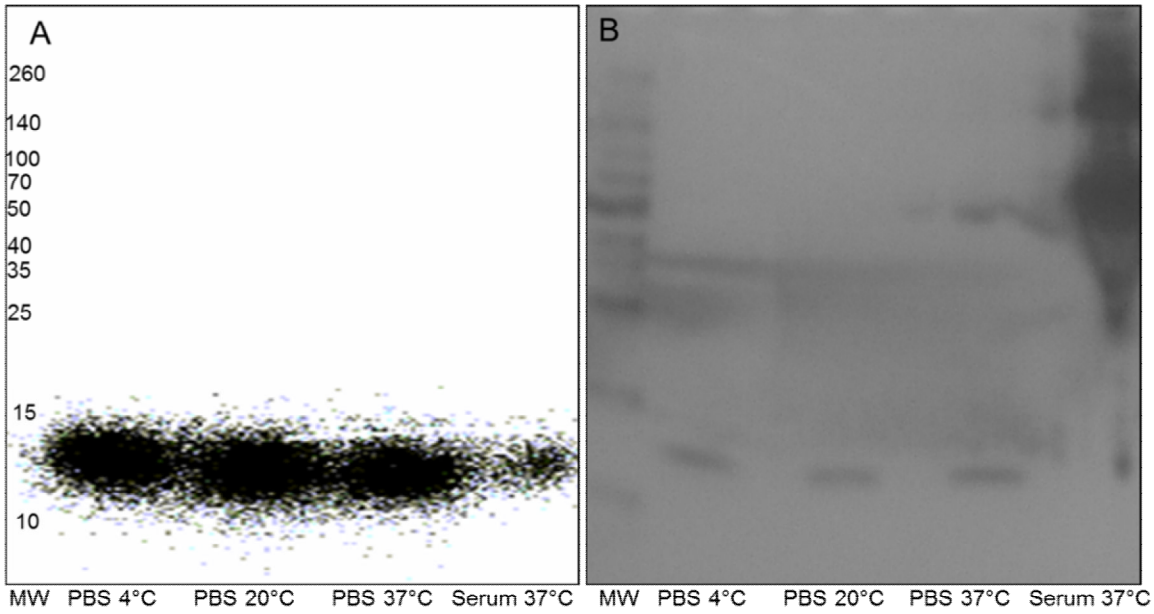

Figure 5.9 SDS-PAGE gel of ^{111}In-$(HE)_3$-G3 DARPin stored in PBS and human serum:PBS (1:1) at 24 h post-radiolabelling at a range of different temperatures. Spectra Multicolor Broad Range Protein Ladder (Thermo Scientific), molecular weights in kDa. Analysed by:
A) Autoradiography: demonstrated a single radiolabelled protein.
B) Coomassie staining: confirmed appropriate size of ^{111}In-$(HE)_3$-G3 DARPin.

5.3 Discussion

The work in this Chapter demonstrated that ^{111}In-(HE)$_3$-G3 is a promising radioligand for HER2 SPECT imaging, which maintains high HER2-positive tumour uptake over 24 h, as ^{111}In is a residualising radioisotope so remains inside the tumour cells post-internalisation. For ^{111}In-(HE)$_3$-G3 the combination of high and well-maintained HER2-positive tumour uptake over 24 h with low normal tissue uptake (except for the kidneys), results in high tumour-to-blood and high tumour-to-normal tissue ratios. This includes tumour-to-liver ratios ≥ 12 over 24 h.

^{111}In-(HE)$_3$-G3 DARPin achieves higher tumour-to-blood ratios within 24 h of administration to mice bearing HER2-positive tumours than any other reported HER2 radioligand, including whole antibodies, Fab regions of trastuzumab and small high affinity proteins (Smith-Jones, Solit et al. 2004; Dijkers, Kosterink et al. 2009; Reddy, Shaller et al. 2011; Perols, Honarvar et al. 2012).

By contrast, ^{125}I-(HE)$_3$-G3 has high tumour uptake at 4 h but falls by approximately 4-fold at 24 h, since ^{125}I is non-residualising and is not retained within the tumour cells after internalisation. ^{125}I-(HE)$_3$-G3 achieves lower tumour-to-blood ratios than ^{111}In-(HE)$_3$-G3, as it is compromised at 4 h by relatively high serum levels and at 24 h by falling HER2-positive tumour levels.

The microSPECT/CT scans at 4 h post-administration reflect the biodistribution results at this time point, confirming that ^{111}In-(HE)$_3$-G3 is superior to ^{123}I-(HE)$_3$-G3 for HER2 whole body imaging, since it is associated with less uptake in normal tissues. Furthermore, ^{111}In-(HE)$_3$-G3 exhibits stability in serum and PBS over 24 h, demonstrated by the lack of G3 DARPin protein breakdown and well-maintained radio-chemical purity.

Pertuzumab binds to subdomain 2 of the HER2 ECD, while trastuzumab and G3 bind to non-overlapping epitopes of subdomain 4 (Zahnd, Pecorari et al. 2006; Zahnd, Wyler et al. 2007; Epa, Dolezal et al. 2013). It has been confirmed that ^{111}In-(HE)$_3$-G3 DARPin can bind to HER2-positive tumours in the presence of trastuzumab *in vivo*, as an 18-fold molar excess of trastuzumab did not alter ^{111}In-(HE)$_3$-G3 HER2-positive tumour uptake. Thus, ^{111}In-(HE)$_3$-G3 DARPin could potentially image treatment naïve patients and patients receiving concomitant anti-HER2 therapy without effecting treatment schedules.

The results for ^{111}In-$(HE)_3$-G3 confirmed the research hypothesis that 'The G3 DARPin radiolabelled with indium-111 and iodine-123/125 can achieve high tumour-to-blood and high tumour-to-normal tissue ratios for pre-clinical HER2 SPECT imaging'. However, ^{123}I/^{125}I-$(HE)_3$-G3 is a less promising radioligand for HER2 SPECT imaging with less impressive ratios.

In conclusion, ^{111}In-$(HE)_3$-G3 has key characteristics needed for a HER2 SPECT imaging agent and represents a significant improvement compared to the His_6 tagged G3 DARPins previously assessed (Zahnd, Kawe et al. 2010).

Chapter 6 PET imaging with gallium-68 radiolabelled G3 DARPin

6.1 Introduction

The work in Chapter 5 outlined the development of G3 DARPin HER2 SPECT imaging. However, PET imaging has a higher sensitivity than SPECT imaging by approximately two to three orders of magnitude, as PET is able to detect a higher proportion of emitted events, justifying investigation of G3 DARPin HER2 PET imaging.

SPECT imaging rejects photons which do not approach the lead collimator at the correct angle to pass through its holes; as a result SPECT detects approximately 0.01% of emitted events. Physical collimators are not required for PET imaging, as each positron interaction with an electron, generates two photons which travel in opposite directions reaching the oppositely paired PET cameras simultaneously (coincidence detection). Consequently, PET detects approximately 1% of emitted events (Rahmim and Zaidi 2008).

The enhanced sensitivity of PET compared with SPECT has a series of important implications for imaging, including:

1. Improved image quality, as superior signal-to-noise ratios are achieved.
2. Shorter scan time to acquire images with equivalent signal-to-noise ratios.
3. Improved temporal resolution, enabling the capture of multiple images of an object in the field of view, to facilitate the study of dynamic biological processes (Rahmim and Zaidi 2008).

^{68}Ga was selected for investigation of G3 DARPin PET scanning for several reasons. Firstly, it has a high positron yield, including an 88% positron branching (88% of decay by positron emission and 12% of decay by electron capture) and high maximum energy of 1.9 megaelectronvolts (MeV). ^{68}Ga is convenient, as it is formed by the decay of its parent isotope, germanium-68 (^{68}Ge) which has a long half-life (280 days), so it is available from in-house ^{68}Ge/^{68}Ga generators. ^{68}Ga has a short half-life (68 min), which is compatible with G3 DARPins half-life (several minutes) (Zahnd, Kawe et al. 2010). Finally, ^{68}Ga forms stable complexes with peptides via bifunctional chelators, thus it is suitable for *in vivo* investigation (Morgat, Hindie et al. 2013).

In aqueous solutions, ^{68}Ga is only stable as a trivalent cation Ga^{3+} under acidic solutions (Morgat, Hindie et al. 2013). At higher pH conditions, $Ga(OH)_3$ is formed (Prata 2012). Therefore, ^{68}Ga is eluted from the $^{68}Ge/^{68}Ga$ generator in 0.1 M HCl and radiolabelling is performed in acidic conditions. However, the stability of the G3 DARPin under acidic conditions is unknown.

Conventionally, ^{68}Ga radiolabelling of DOTA is performed at 100 °C in acidic conditions (pH 4.4) for 30 min, while ^{68}Ga radiolabelling of NOTA is performed at pH 3.6 for 10 min at RT (Figure 6.1 and Figure 6.2) (Berry, Ma et al. 2011). Berry *et al.* have developed a novel tripodal tris(hydroxypyridinone) bifunctional chelator, YM103 (maleimide form of CP256), for ^{68}Ga radiolabelling of proteins. CP256 is based on the structure of a powerful Fe^{3+} chelator, since Ga^{3+} and Fe^{3+} have similar co-ordination chemistry (Figure 6.3). CP256 can be radiolabelled with ^{68}Ga to a high specific activity when performed at pH 6.5 and RT over 5 min. *In vitro*, ^{68}Ga-CP256 is stable in serum and is stable when challenged with over a 100–fold excess of apotransferrin (which could potentially compete for ^{68}Ga binding). Furthermore, ^{68}Ga-CP256 is stable *in vivo* for at least 90 min (Berry, Ma et al. 2011).

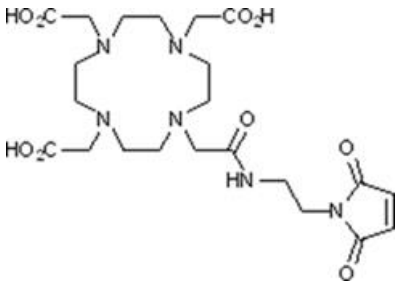

Figure 6.1 Structure of mal-DOTA (Chemical formula: $C_{22}H_{34}N_6O_9$, MW: 526.54 Da, 1Ga:1DOTA).

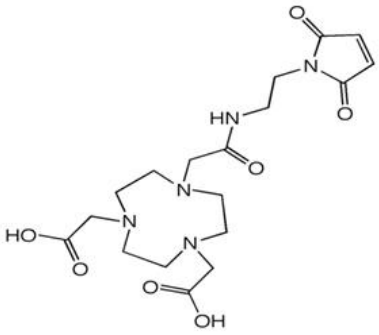

Figure 6.2 Structure of mal-NOTA (Chemical formula: $C_{18}H_{27}N_5O_7$, MW: 425.44 Da, 1Ga:1NOTA).

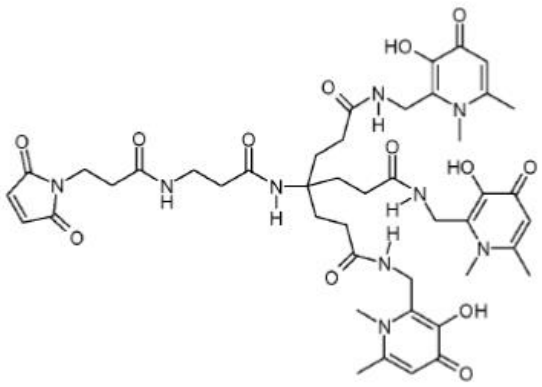

Figure 6.3 Structure of YM103 (Chemical formula: $C_{44}H_{58}N_9O_{13}$, MW: 920.42 Da, 1Ga:1YM103).

In Chapter 3, the untagged-G3 was formed by HRV 3C cleavage of the Leu(L)-Glu(E)-Val(V)-Leu(L)-Phe(F)-Gln(Q) * Gly(G)-Pro(P) site, converting the cleavable tag-G3 into the untagged-G3 DARPin. Consequently, the $(HE)_3$-G3 and His_6-G3 DARPins assessed in Chapter 4 and 5 incorporated a Gly(G)-Pro(P) site, to maintain consistency with the untagged-G3 DARPin.

In Chapter 6 and 7, the assessed $(HE)_3$-G3 DARPin did not contain an N-terminal Gly(G)-Pro(P) site but was produced by the *P. pastoris* production platform as outlined in the Material and Methods (Figure 6.4). The N-terminus of the G3 DARPin does not participate in binding to the HER2 ECD. Interestingly, the presence or absence of a Gly(G)-Pro(P) site does not affect the pI (4.79) of the G3 DARPin, so this change in amino acid sequence was not expected to effect biodistribution and HER2 binding.

A) HEHEHEGP-[G3 DARPin]-**C**

B) HEHEHE-[G3 DARPin]-**C**

Figure 6.4 $(HE)_3$-G3 DARPin amino acid sequences.
A) $(HE)_3$-G3 with a glycine-proline site assessed in Chapter 4 and 5.
B) $(HE)_3$-G3 without a glycine-proline site used in the ^{68}Ga PET studies (Chapter 6) and pre-clinical toxicity studies (Chapter 7)
(**C**- C-terminal cysteine, N-terminal tags underlined and GP glycine-proline).

Aim:

To test the hypothesis that the, G3 DARPin can be radiolabelled with gallium-68 for pre-clinical HER2 PET imaging.

Objectives:

1. Assess the HER2 specificity and normal tissue biodistribution of $(HE)_3$-G3 without a glycine-proline site.
2. Select an appropriate bifunctional chelator for ^{68}Ga radiolabelling of $(HE)_3$-G3, whose radiolabelling conditions will not affect DARPin HER2 binding function.
3. Assess ^{68}Ga-$(HE)_3$-G3 tumour uptake and tumour-to-normal tissue ratios in mice bearing HER2-positive tumour xenografts.
4. Assess the ability of ^{68}Ga-$(HE)_3$-G3 to image mice with HER2-positive tumour xenografts by PET/CT scanning.

6.2 Results

6.2.1 *In vitro* HER2 specificity of $(HE)_3$-G3 DARPin-DOTA without a GP site

Flow cytometry demonstrated that the unlabelled and cold indium labelled DOTA-$(HE)_3$-G3 without a GP-site bound to HER2-positive BT474 and OE-19 cells but did not bind to HER2-negative MDA-MB-468 cells (Figure 6.5). In Chapter 4, the cold indium labelled $(HE)_3$-G3 DARPin-DOTA with a GP-site achieved similar results with BT474, OE-19 and MDA-MB-468 cells, 94.1%, 80.7% and 0.5%, respectively. Thus, confirming that removal of the GP-site did not affect HER2 specificity *in vitro*.

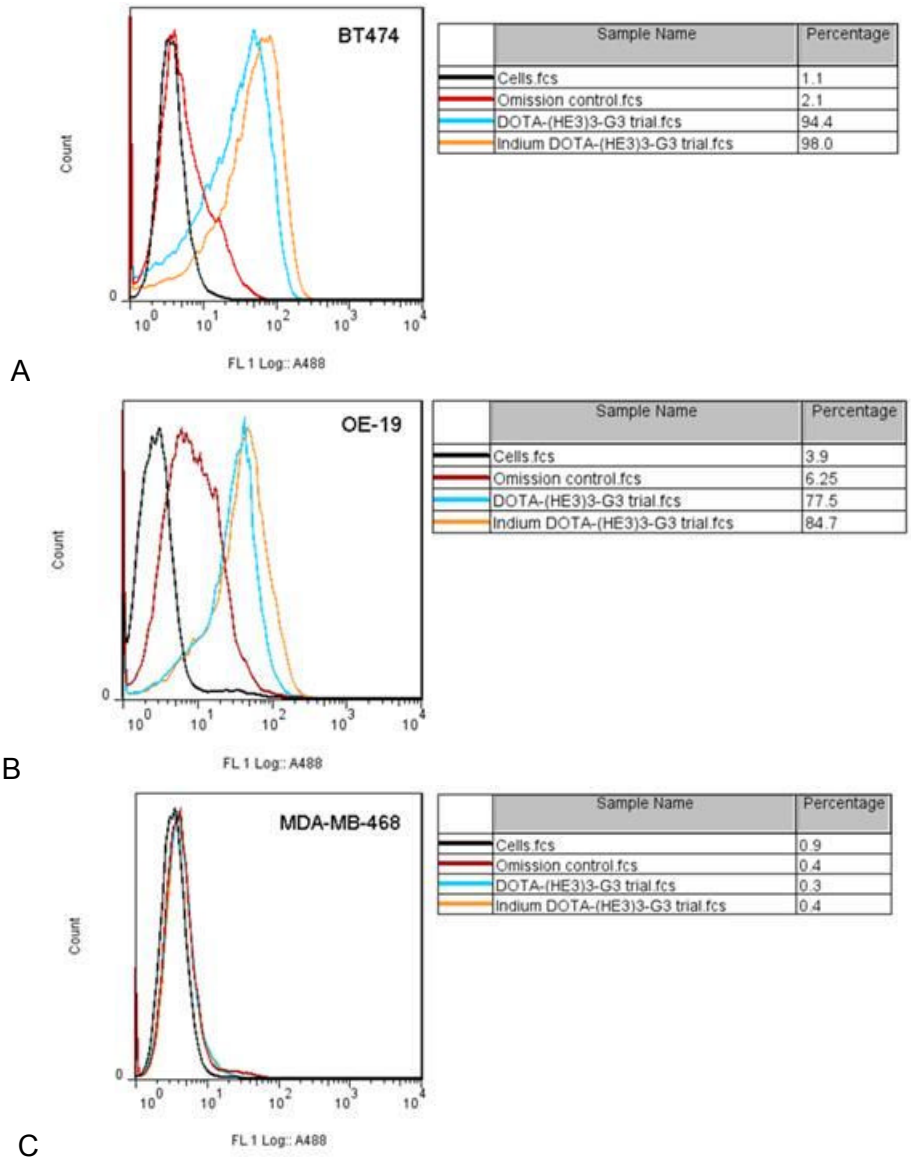

Figure 6.5 Flow cytometry of cold indium labelled and unlabelled $(HE)_3$-G3 DARPin-DOTA without an N-terminus glycine-proline.
A) HER2-positive breast (BT474), B) HER2-positive gastro-oesophageal junction (OE-19) and C) HER2-negative breast adenocarcinoma cells (MDA-MB-468). Omission control cells treated with antibodies in absence of G3 DARPin.

6.2.2 Biodistribution of ^{111}In-DOTA-$(HE)_3$-G3 DARPins with and without an N-terminus glycine-proline in non-tumour bearing mice

Assessment of the ^{111}In-DOTA-$(HE)_3$-G3 DARPins with and without a GP-site in female BALB/c mice demonstrated that both formats had similar normal tissue uptake (Figure 6.6). Urine was also collected from the mice which received ^{111}In-DOTA-$(HE)_3$-G3 without a GP-site, this demonstrated that radioactivity was excreted in urine. The quantity of ^{111}In-DOTA-$(HE)_3$-G3 DARPin and or free ^{111}In in mouse urine was below the detection limit for auto-radiography and SDS-PAGE analysis by coomassie staining at 4 and 24 h post-administration, so the urinary excreted radiolabelled product was not further characterised. All subsequent studies in this thesis assessed the $(HE)_3$-G3 DARPin without a GP-site.

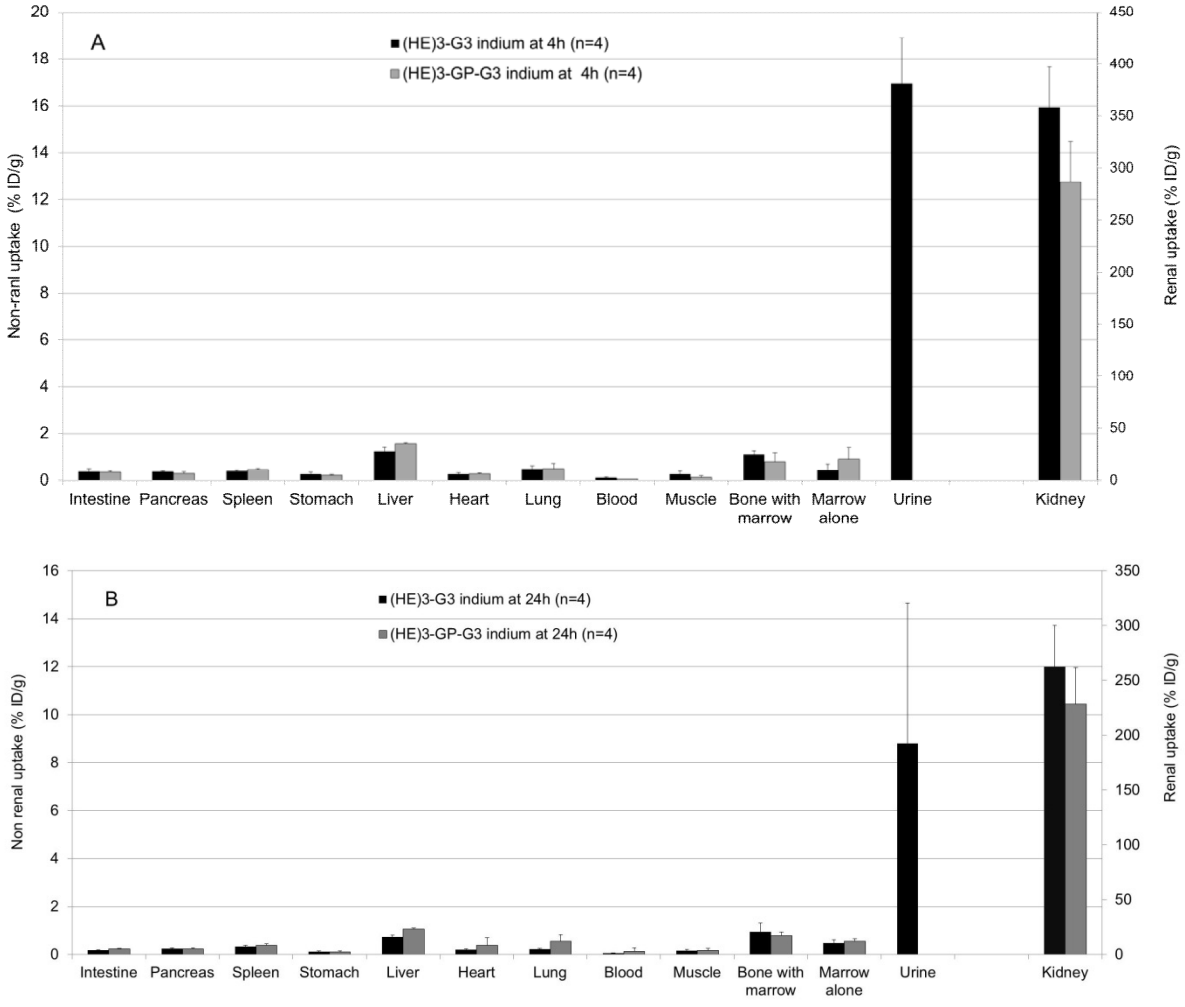

Figure 6.6 Biodistribution of ^{111}In-$(HE)_3$-G3 DARPins with and without an N-terminus glycine-proline (GP) in female BALB/c mice.
A) 4 h and B) 24 h post-administration. Data expressed as the mean % ID/g ± SD.

6.2.3 Temperature stability of DOTA-$(HE)_3$-G3 DARPin

In Chapter 4 and 5, DOTA-$(HE)_3$-G3 was efficiently radiolabelled with ^{111}In at 37 °C (pH 6.0) over 2 h. Importantly, these radiolabelling conditions did not affect the kinetics and affinity of the DOTA-$(HE)_3$-G3 for the HER2 ECD assessed by SPR (Table 6.1).

Table 6.1 Affinities and kinetics of DOTA-$(HE)_3$-G3 with HER2 ECD assessed by Surface Plasmon Resonance after heating to 37 °C for 2 h at pH 6.0.

G3 DARPin conditions	Production platform	K_a or K_{on} $(M^{-1}\ s^{-1})^{\#}$	K_d or K_{off} $(s^{-1})^{\#}$	K_D $(nmol/L)^{\#}$
DOTA-$(HE)_3$-G3 control (pH 6.0)*	*P. pastoris*	9.26 x10^5	2.95 x10^{-4}	0.322
DOTA-$(HE)_3$-G3 heated to 37°C for 2 h (pH 6.0)	*P. pastoris*	6.04 x10^5	3.01 x10^{-4}	0.502

*Control was not heated, #mean of duplicate assessments

Labelling of DOTA with ^{68}Ga requires heating to 100 °C in acidic conditions (pH 4.4) for 30 min (Berry, Ma et al. 2011). Radiolabelling for 30 min is not ideal, as ^{68}Ga has a short half-life (68 min). Heating DOTA-$(HE)_3$-G3 at 80 °C for 15 min resulted in a slower association rate (K_a) with a maintained dissociation rate (K_d). In addition, heating DOTA-$(HE)_3$-G3 to 80 °C decreased its binding affinity for the HER2 ECD (Table 4.1). Consequently, DOTA-$(HE)_3$-G3 DARPin is appropriate for ^{111}In radiolabelling but not for ^{68}Ga radiolabelling.

Table 6.2 Affinities and kinetics of DOTA-$(HE)_3$-G3 with HER2 ECD assessed by Surface Plasmon Resonance after heating to 80 °C for 15 min.

G3 DARPin conditions	Production platform	K_a or K_{on} $(M^{-1}\ s^{-1})^{\#}$	K_d or K_{off} $(s^{-1})^{\#}$	K_D $(nmol/L)^{\#}$
DOTA-$(HE)_3$-G3 control (pH 6.5)*	*P. pastoris*	8.8 x10^5	2.43 x10^{-4}	0.277
DOTA-$(HE)_3$-G3 heated to 80 °C for 15 min (pH 6.5)	*P. pastoris*	1.4 x10^5	2.43 x10^{-4}	2.02

*Control was not heated and #mean of duplicate assessments

6.2.4 NOTA-$(HE)_3$-G3 stability in acidic conditions

6.2.4.1 Surface Plasmon Resonance of acid-treated NOTA-$(HE)_3$-G3

$(HE)_3$-G3 DARPin has a pI of 4.79, so at pH 4.79 it does not have a net electrical charge and is at risk of precipitating out of solution. Radiolabelling of NOTA with ^{68}Ga is optimal at low pH conditions, conventionally pH 3.6 for 10 min at RT. Based on SPR analysis, NOTA-$(HE)_3$-G3 subjected to pH 3.6, 4.6 and 6.5 have similar kinetics and affinities for the HER2 ECD. However, $(HE)_3$-G3 maintained at pH 7 appeared to have superior HER2 binding affinity and faster dissociation than acid-treated NOTA-$(HE)_3$-G3 (Table 6.3).

Table 6.3 Affinities and kinetics of NOTA-$(HE)_3$-G3 with HER2 ECD assessed by Surface Plasmon Resonance after treatment at pH ≤ 7 and maintained at room temperature.

G3 DARPin (treatment conditions)*	Production platform	K_a or K_{on} $(M^{-1}\ s^{-1})^{\#}$	K_d or K_{off} $(s^{-1})^{\#}$	K_D (nmol/L)$^{\#}$
$(HE)_3$-G3 (pH 7.0 for 1 day)	*P. pastoris*	5.6×10^5	2.0×10^{-4}	0.362
NOTA-$(HE)_3$-G3 (pH 6.5 for 1 day)	*P. pastoris*	6.3×10^5	2.9×10^{-4}	0.462
NOTA-$(HE)_3$-G3 (pH 4.6 for 20 min)	*P. pastoris*	7.2×10^5	2.9×10^{-4}	0.398
NOTA-$(HE)_3$-G3 (pH 4.6 for 90 min)	*P. pastoris*	5.5×10^5	3.0×10^{-4}	0.540
NOTA-$(HE)_3$-G3 (pH 3.6 for 20 min)	*P. pastoris*	5.7×10^5	3.0×10^{-4}	0.527
NOTA-$(HE)_3$-G3 (pH 3.6 for 90 min)	*P. pastoris*	5.2×10^5	3.0×10^{-4}	0.579

*NOTA-$(HE)_3$-G3 was neutralised to physiological pH with PBS after being subjected to acidic pH conditions for the stated periods of time, prior to assessment.
$^{\#}$Mean of duplicate assessments.

6.2.4.2 Flow cytometry analysis of acidic treated NOTA-$(HE)_3$-G3

NOTA-$(HE)_3$-G3 subjected to pH 3.6, 4.6 and 6.5 bound to HER2-positive BT474 cells. On flow cytometry, $(HE)_3$-G3 maintained at pH 7 appeared to bind better to BT474 cells than acid treated NOTA-$(HE)_3$-G3 (Figure 6.7). This is consistent with the finding that $(HE)_3$-G3 maintained at pH 7 had superior HER2 ECD binding affinity than the acid treated NOTA-$(HE)_3$-G3 assessed by SPR (Table 6.3).

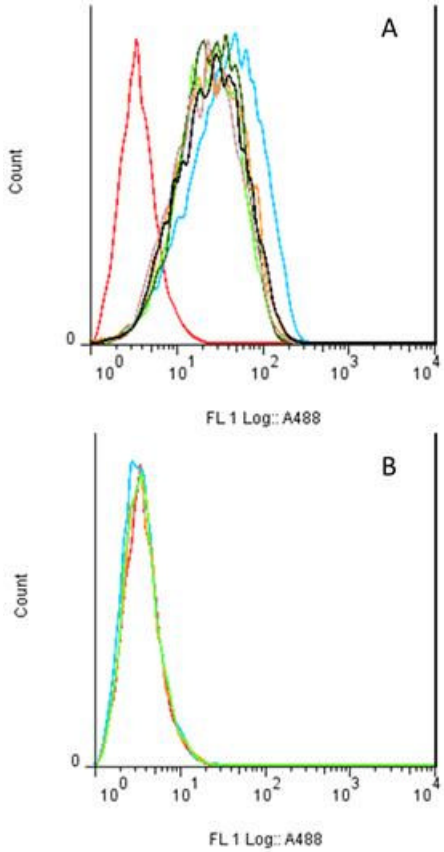

BT474 cells (length of time at pH)	Positive cells (%)
Cells	0.926
$(HE)_3$-G3 DARPin pH 7 (1 day)	83.7
NOTA-$(HE)_3$-G3 DARPin pH 6.5 (1 day)	74.7
NOTA-$(HE)_3$-G3 DARPin pH4.6 (20 min)	75.8
NOTA-$(HE)_3$-G3 DARPin pH4.6 (90 min)	77.8
NOTA-$(HE)_3$-G3 DARPin pH3.6 (20 min)	71.8
NOTA-$(HE)_3$-G3 DARPin pH3.6 (90 min)	75.5

BT474 negative controls	Positive cells (%)
Cells	0.926
Cell + Anti-DARPin	1.05
Cells + Anti-mouse	1.23
Cells + Anti-DARPin+ Anti-mouse	1.12

Figure 6.7 Flow cytometry profiles for BT474 cells treated with unconjugated and NOTA-conjugated $(HE)_3$-G3 DARPins subjected to different pH conditions.
A) Treatment samples and B) Controls.
All $(HE)_3$-G3 DARPins were neutralised to physiological pH with Dulbecco's-PBS prior to cell application, negative controls were not treated with G3 DARPin.

$(HE)_3$-G3 maintained at pH 7 bound poorly to HER2-negative, MDA-MB-468 cells. NOTA-$(HE)_3$-G3 subjected to pH 3.6 bound better to MBA-MB-468 cells than NOTA-$(HE)_3$-G3 subjected to pH 4.6 and pH 6.5 conditions (Figure 6.8). The effect of pH 3.6 treatment upon NOTA-$(HE)_3$-G3 binding, could reflect either loss of specificity or increased sensitivity but is more likely to be due to loss of specificity. This is because BT474 cells have 2.75×10^6 HER2 receptors per cell and the lower pH (pH 3.6) did not improve BT474 binding assessed by flow cytometry but it did improve binding for MDA-MB-468 cells which have only $1X10^3$ HER2 receptors per cell (Figure 6.7 and Figure 6.8) (DeFazio-Eli, Strommen et al. 2011; Hathaway, Butler et al. 2011).

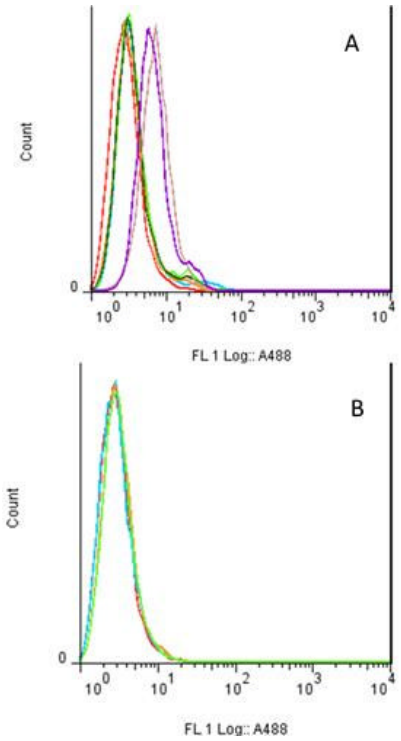

MDA-MB-468 cells (length of time at pH)	Positive cells (%)
Cells	1.37
$(HE)_3$-G3 DARPin pH 7 (1 day)	5.48
NOTA-$(HE)_3$-G3 DARPin pH 6.5 (1 day)	3.81
NOTA-$(HE)_3$-G3 DARPin pH 4.6 (20 min)	6.71
NOTA-$(HE)_3$-G3 DARPin pH 4.6 (90 min)	5.39
NOTA-$(HE)_3$-G3 DARPin pH 3.6 (20 min)	15.7
NOTA-$(HE)_3$-G3 DARPin pH 3.6 (90 min)	13.5

MDA-MB-468 negative controls	Positive cells (%)
Cells	1.37
Cell + Anti-DARPin	1.15
Cells + Anti-mouse	1.60
Cells + Anti-DARPin+ Anti-mouse	1.11

Figure 6.8 Flow cytometry profiles for MDA-MB-468 cells treated with unconjugated and NOTA-conjugated $(HE)_3$-G3 DARPins subjected to different pH conditions.
A) Treatment samples and B) Controls.
All $(HE)_3$-G3 DARPins were neutralised to physiological pH with PBS prior to cell application, negative controls were not treated with G3 DARPins.

6.2.5 Gallium-68 radiolabelling of $(HE)_3$-G3 DARPin at different pH conditions

The flow cytometry results suggested that performing ^{68}Ga radiolabelling of NOTA-$(HE)_3$-G3 at pH ≥ 4.6 would preserve HER2 specificity. Fortunately, ^{68}Ga radiolabelling of NOTA-$(HE)_3$-G3 was most efficient at pH 4.6 (Table 6.4). NOTA-$(HE)_3$-G3 maintained at pH 4.6, selectively bound to HER2-positive breast cancer cells (BT474) and had picomolar affinity for the HER2 ECD (Table 6.3, Figure 6.7 and Figure 6.8). Thus, it appears to be feasible to radiolabel NOTA-$(HE)_3$-G3 with ^{68}Ga at pH 4.6.

Table 6.4 Radiochemical purity of ^{68}Ga-NOTA-$(HE)_3$-G3 radiolabelled at different pH conditions.

^{68}Ga-NOTA-$(HE)_3$-G3 radiolabelling pH*	Radiochemical purity (%)
pH 7.7	9.2
pH 6.2	10.7
pH 5.5	24.4
pH 4.6	83.8
pH 3.6	5.6

*Each reaction was performed with 10 µg of NOTA-$(HE)_3$-G3 and 2 MBq of ^{68}Ga.

By contrast, YM103 (maleimide form of CP256) can be radiolabelled with ^{68}Ga to a high specific activity when performed at pH 4.6 to 6.5 and RT over 5 min (Berry, Ma et al. 2011). However, in view of the SPR and flow cytometry results for NOTA-$(HE)_3$-G3, it is unlikely that these ^{68}Ga radiolabelling conditions (pH 4.6-6.5) would affect YM103-$(HE)_3$-G3 HER2 binding function but this was not formally assessed.

6.2.6 ^{68}Ga-NOTA-$(HE)_3$-G3 and ^{68}Ga-YM103-$(HE)_3$-G3 biodistribution in HER2-positive tumour bearing mice

The normal tissue biodistribution profiles of ^{68}Ga-NOTA-$(HE)_3$-G3 and ^{68}Ga-YM103-$(HE)_3$-G3 differed greatly from each other. In particular, ^{68}Ga-YM103-$(HE)_3$-G3 had higher liver, lung and spleen uptake, while ^{68}Ga-NOTA-$(HE)_3$-G3 had higher kidney and blood uptake. At 1 h post administration, ^{68}Ga-NOTA-$(HE)_3$-G3 and ^{68}Ga-YM103-$(HE)_3$-G3 HER2-positive tumour uptake were 11.8 ± 6.9% ID/g and 6.8 ± 0.9% ID/g, respectively (Figure 6.9).

For all of the assessed tissues, ^{68}Ga-NOTA-$(HE)_3$-G3 achieved higher or equivalent tumour-to-tissue ratios compared with ^{68}Ga-YM103-$(HE)_3$-G3, with the exception of blood uptake. The tumour-to-blood ratio achieved with ^{68}Ga-YM103-$(HE)_3$-G3 was 12.6 ± 5.1, compared to 5.9 ± 3.1 for ^{68}Ga-NOTA-$(HE)_3$-G3, as ^{68}Ga-YM103-$(HE)_3$-G3 had lower blood levels (Table 6.5). Owing to the inferior tumour-to-normal tissue ratios, ^{68}Ga-YM103-$(HE)_3$-G3 was not investigated any further.

Table 6.5 ^{68}Ga-NOTA-$(HE)_3$-G3 and ^{68}Ga-YM103-$(HE)_3$-G3 DARPin tumour-to-normal tissue ratios of in female SCID-beige mice bearing HER2-positive human breast tumours (BT474).

Mean tumour-to-tissue ratios	^{68}Ga-NOTA-$(HE)_3$-G3 at 1 h (n=4)	^{68}Ga-YM103-$(HE)_3$-G3 at 1 h (n=4)
Intestine	21.2 ± 11.7	8.3 ± 3.1
Pancreas	10.5 ± 4.2	6.6 ± 1.8
Spleen	3.3 ± 1.1	0.7 ± 0.2
Stomach	29.0 ± 29.0	6.9 ± 0.4
Liver	1.5 ± 0.6	0.1 ± 0.0
Heart	7.8 ± 3.8	5.5 ± 7.1
Lung	4.6 ± 1.4	1.4 ± 0.7
Blood	5.9 ± 3.1	12.6 ± 5.1
Muscle	25.6 ± 7.0	10.1 ± 3.7
Bone with marrow	10.1 ± 3.9	2.7 ± 0.7
Kidney	0.1 ± 0.1	0.1 ± 0.0

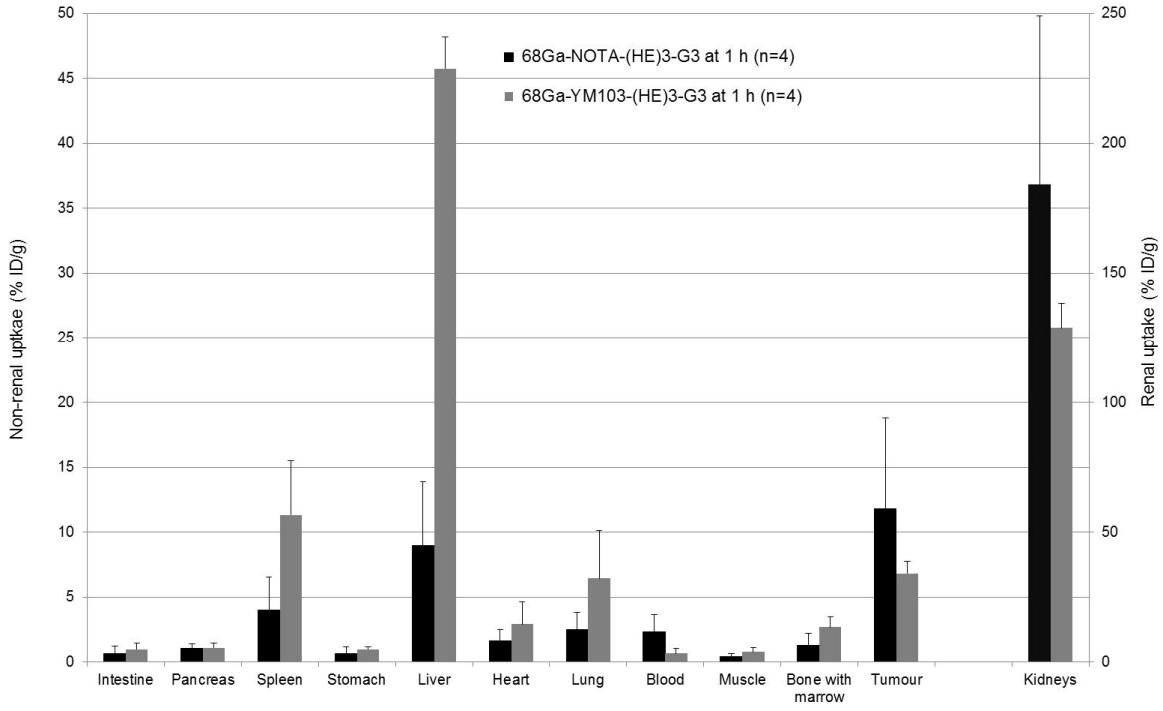

Figure 6.9 Biodistribution of ^{68}Ga-NOTA-(HE)$_3$-G3 and ^{68}Ga-YM103-(HE)$_3$-G3 DARPin in female SCID-beige mice bearing HER2-positive human breast tumours (BT474) at 1 h post-administration. Data expressed as mean % ID/g ± SD.

6.2.7 PET/CT scans with ^{68}Ga-NOTA-(HE)$_3$-G3

HER2-positive tumours can be detected on PET/CT scanning at 30-120 min post ^{68}Ga-NOTA-(HE)$_3$-G3 administration. The kidneys received the highest dose and uptake in other visible normal organs appeared to be low but normal organ uptake was partially obscured by the kidneys (Figure 6.10). The HER2-positive tumour uptake for the scanned mouse was 15.6% ID/g at 2 h, however the liver uptake was 12.6% ID/g at 2 h post-administration (Table 6.6).

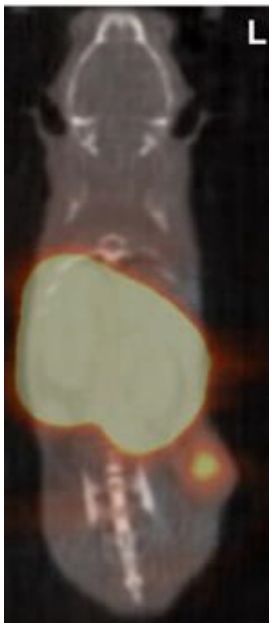

Figure 6.10 PET/CT scan of SCID-beige mouse bearing a HER2-positive (BT474) tumour beside its left (L) hip, acquired 30-120 min post-administration of ^{68}Ga-NOTA-$(HE)_3$-G3.

Table 6.6 Biodistribution of PET/CT scanned female SCID-beige mouse bearing HER2-positive human breast tumours (BT474), at 2 h post-administration of ^{68}Ga-NOTA-$(HE)_3$-G3.

Tissue	Uptake (% ID/g) at 2 h (n=1)
Intestine	0.7
Pancreas	0.7
Spleen	3.4
Stomach	0.7
Kidney	206.0
Liver	12.6
Heart	1.2
Lung	2.0
Blood	1.7
Muscle	0.5
Bone with marrow	1.6
Tumour	15.6

6.3 Discussion

Based on HER2 binding function, the DOTA conjugated $(HE)_3$-G3 DARPin can tolerate heating to 37 °C but does not tolerate heating to 80 °C. Therefore, $(HE)_3$-G3 DARPin conjugated with DOTA is not suitable for ^{68}Ga radiolabelling, as the radiolabelling reaction must be performed at high temperatures (100 °C) for 30 min. Consequently, YM103-$(HE)_3$-G3 and NOTA-$(HE)_3$-G3 were investigated as alternatives, since these chelators can be radiolabelled with ^{68}Ga at room temperature.

The contrasting biodistribution profiles for ^{68}Ga-YM103-$(HE)_3$-G3 and ^{68}Ga-NOTA-$(HE)_3$-G3 could be related to differences in the hydrophilicity of their respective bifunctional chelators. The mal-NOTA bifunctional chelator contains two carboxyl groups, which are polar and contribute to hydrophilicity. While YM103 has a higher molecular weight than mal-NOTA (920.42 vs. 425.44 Da) and is composed of multiple carbon rings and a long unbranched non-polar hydrocarbon chain connecting CP256 to a maleimide group, these components enhance hydrophobicity (Figure 6.2 and Figure 6.3).

The Octanol-Water Partition Coefficient (K_{OW}) can be used to determine a compound's hydrophilicity. K_{OW} represents the ratio of a compound's solubility in octanol (fatty alcohol) compared to its solubility in water. The logP refers to the logarithm of K_{OW} in the assessed compound's non-ionised (neutral) form. Generally, logP values are inversely related to water solubility and directly proportional to molecular weight. Experimentally-derived logP and calculated logP (ClogP) values correlate well with each other (Kah and Brown 2008). The ClogP for mal-NOTA is -7.82 compared with -1.71 for YM103 (Table 6.7). Thus, confirming that YM103 is less hydrophilic than mal-NOTA. As the G3 DARPin is a low molecular weight protein, it is likely that YM103-$(HE)_3$-G3 is relatively hydrophobic compared to NOTA-$(HE)_3$-G3. Consequently, ^{68}Ga-YM103-$(HE)_3$-G3 was found to have higher liver uptake, lower kidney uptake and lower blood uptake than ^{68}Ga-NOTA-$(HE)_3$-G3.

Table 6.7 Calculated log of the Octanol-Water Partition Coefficient (ClogP) for mal-DOTA, mal-NOTA and YM103.

Bi-functional chelator	Molecular weight (Da)	ClogP (Relative water solubility)
Mal-DOTA	526.54	-10.1 (High water solubility)
Mal-NOTA	425.44	-7.82 (High water solubility)
YM103 (maleimide form of CP256)	920.42	-1.71 (Low water solubility)

It is difficult to compare the biodistribution data for ^{111}In-DOTA-$(HE)_3$-G3 and ^{68}Ga-NOTA-$(HE)_3$-G3, as the ^{111}In treated mice were euthanised at 4 or 24 h, while the ^{68}Ga treated mice were euthanised at 1 h post-administration. Both constructs have high kidney uptake and achieve similar HER2-positive tumour uptake, 8.8 ± 1.3% ID/g for ^{111}In-DOTA-$(HE)_3$-G3 at 4 h and 11.8 ± 7.0% ID/g for ^{68}Ga-NOTA-$(HE)_3$-G3 at 1 h.

A protocol for ^{68}Ga radiolabelling of $(HE)_3$-G3 DARPin via NOTA has been successfully developed. In HER2-positive tumour xenografts, ^{68}Ga-NOTA-$(HE)_3$-G3 achieves a tumour-to-blood ratio of 5.9 ± 3.1 and tumour-to-liver ratio of 1.5 ± 0.6 at 1 h. It is unlikely that this tumour-to-liver ratio will be sufficient to identify HER2-positive liver metastases on PET/CT scanning. ^{68}Ga-NOTA-$(HE)_3$-G3 is capable of imaging HER2-positive tumours in the flank region of mice. Therefore, the hypothesis that the 'G3 DARPin can be radiolabelled with gallium-68 for pre-clinical HER2 PET imaging' is in part confirmed. However, the lead construct ^{68}Ga-NOTA-$(HE)_3$-G3 has significant limitations for imaging visceral HER2-positive metastases due to low tumour-to-normal tissue ratios, which will adversely affect the identification of splenic, hepatic, lung and renal metastases.

Chapter 7 Pre-clinical toxicity assessment of the G3-DARPin

7.1 Introduction

The ^{111}In-DOTA-$(HE)_3$-G3 DARPin was the most promising radioligand investigated for HER2 imaging within this thesis, so it was selected for investigation in a first-in-human HER2 SPECT imaging trial. Thus, the work in this Chapter focused on assessing whether it had any toxic effects. The proposed dose of ^{111}In-$(HE)_3$-G3 DARPin for the clinical trial is 0.5 mg with 300 MBq of radiation activity. This dose has been selected on the basis of safety and efficacy considerations, while using the approaches of other HER2 imaging trials as a benchmark (Table 7.1).

The rationale for using 0.5 mg of $(HE)_3$-G3 DARPin (3.4 $X10^{-8}$ mol, MW ~14.4 kDa) is based on the reported HER2 molecular imaging trials with trastuzumab and the second generation HER2 binding affibody molecule (ABY-025). Perik *et al.* investigated SPECT imaging with 5 mg of ^{111}In-DTPA-trastuzumab, equivalent to approximately 3.4 $X10^{-8}$ mol of trastuzumab (148 kDa) (Perik, Lub-De Hooge et al. 2006). Patients received 0.1 mg of ^{111}In-DOTA-ABY-025 (6.5 kDa) for HER2 SPECT imaging, equivalent to approximately 1.5 $X10^{-8}$ mol (Sorensen, Sandberg et al. 2014). Thus, the proposed molar dose of $(HE)_3$-G3-DARPin is approximately 2.3 times higher than the ^{111}In-DOTA-ABY-025 molar dose and equivalent to the ^{111}In-DTPA-trastuzumab molar dose assessed in clinical trials (Perik, Lub-De Hooge et al. 2006; Baum, Prasad et al. 2010).

For 300 MBq of radioactivity, there are 2.1 $X10^{14}$ metal atoms, composed of indium and its decay product cadmium. Using the Avogadro constant (6.022 $X10^{23}$), 0.5 mg or 3.4 $X10^{-8}$ mol of $(HE)_3$-G3 DARPin equates to 2.1 $X10^{16}$ $(HE)_3$-G3 DARPin molecules. Consequently, for each metal ion there will be approximately 100 $(HE)_3$-G3 DARPin molecules. This DARPin excess will help to minimise the amount of 'free' metals which can be absorbed and damage normal organs. In prior HER2 SPECT/CT imaging trials, 150 MBq of radiation activity was administered for the ^{111}In-DTPA-trastuzumab trial (~90-fold excess of trastuzumab vs. metal atoms), while 140 MBq of radiation activity was administered for the ^{111}In-DOTA-ABY-025 trial (~175-fold excess of affibody vs. metal atoms) (Table 7.1) (Perik, Lub-De Hooge et al. 2006; Sorensen, Sandberg et al. 2014).

It is vital to have high specific activity (high radiation activity per ligand dose) for tumour receptor imaging, as non-radiolabelled ligand can potentially saturate the

receptor and limit the ability to visualise tumour receptor expression. Clinical tumour receptor SPECT imaging has been most successful with nanomolar doses of radioligands (Mankoff, Link et al. 2008). The specific activity of the proposed ^{111}In-$(HE)_3$-G3 DARPin dose is 8.6 MBq/nmol, which is similar to the specific activity of ^{111}In-DOTA-ABY-025 successfully used in a clinical trial (9.1 MBq/nmol) (Sorensen, Sandberg et al. 2014).

Table 7.1 Doses assessed in previous HER2 SPECT imaging trials with ^{111}In and proposed ^{111}In-$(HE)_3$-G3 DARPin dose.

Radioligand	Activity (MBq)	Ligand MW (Da)	Ligand dose (mg)	Ligand dose (mol)	Ligand-to-metal ion ratio	Specific activity (MBq/nmol)
^{111}In-ABY-025 Affibody (Sorensen, Sandberg et al. 2014)	140 MBq	6,500	0.1	$1.5X10^{-8}$	175	9.1
^{111}In-trastuzumab (Perik, Lub-De Hooge et al. 2006)	150 MBq	148,000	5	$3.4\ X10^{-8}$	90	4.5
^{111}In-$(HE)_3$-G3 DARPin proposed dose	300 MBq	14,400	0.5	$3.4\ X10^{-8}$	100	8.6

Hemizygous (one allele within a diploid organism) B6.Cg-Tg(Wap-ERBB2)229Wzw/J transgenic mice, express human HER2 under the control of the mouse whey acidic protein (WAP) promoter. They had been generated by microinjection of the WAP regulated human HER2 transgene into mouse embryos (C57BL/6 x C3H) and backcrossed to C57BL/6 for over 25 generations. This HER2 transgenic mouse model was selected for pre-clinical toxicity testing. The WAP promoter directs expression of human HER2 to the mammary glands and molecular layer of the cerebellum (Piechocki, Ho et al. 2003). Thus, potentially enabling the assessment of DARPin related adverse events due to HER2 mediated toxicity and off-target toxicity.

A preliminary toxicity study with the unconjugated and non-radiolabelled $(HE)_3$-G3 DARPin was proposed prior to a regulatory GLP standard toxicity study.

Aim:

To test the hypothesis that unconjugated G3 DARPin is well tolerated by HER2 transgenic and non-transgenic mice.

Objectives:

1) Genotype and breed HER2 transgenic mice for assessment.
2) Prepare unconjugated $(HE)_3$-G3 DARPin for mouse administration.
3) Assess toxicity related to the unconjugated $(HE)_3$-G3 DARPin at 50-100 times the human equivalent dose (HED) in HER2 transgenic and non-transgenic mice, by blood sampling and histological assessment of major organs.

7.2 Results

7.2.1 Genotyping HER2 transgenic mice

Genotyping of the 13 mice purchased from The Jackson Laboratory, demonstrated that there were four female and four male HER2 transgenic mice, which was consistent with The Jackson Laboratory genotype results (Table 7.2). The mouse IL-2 gene was present in all samples, confirming that DNA had been successfully extracted for human HER2 gene assessment (Figure 7.1). The negative control mouse, a C57 Black mouse, had the mouse IL-2 gene but did not have the human HER2 gene. As expected, the water sample did not have the mouse IL-2 gene and human HER2 gene.

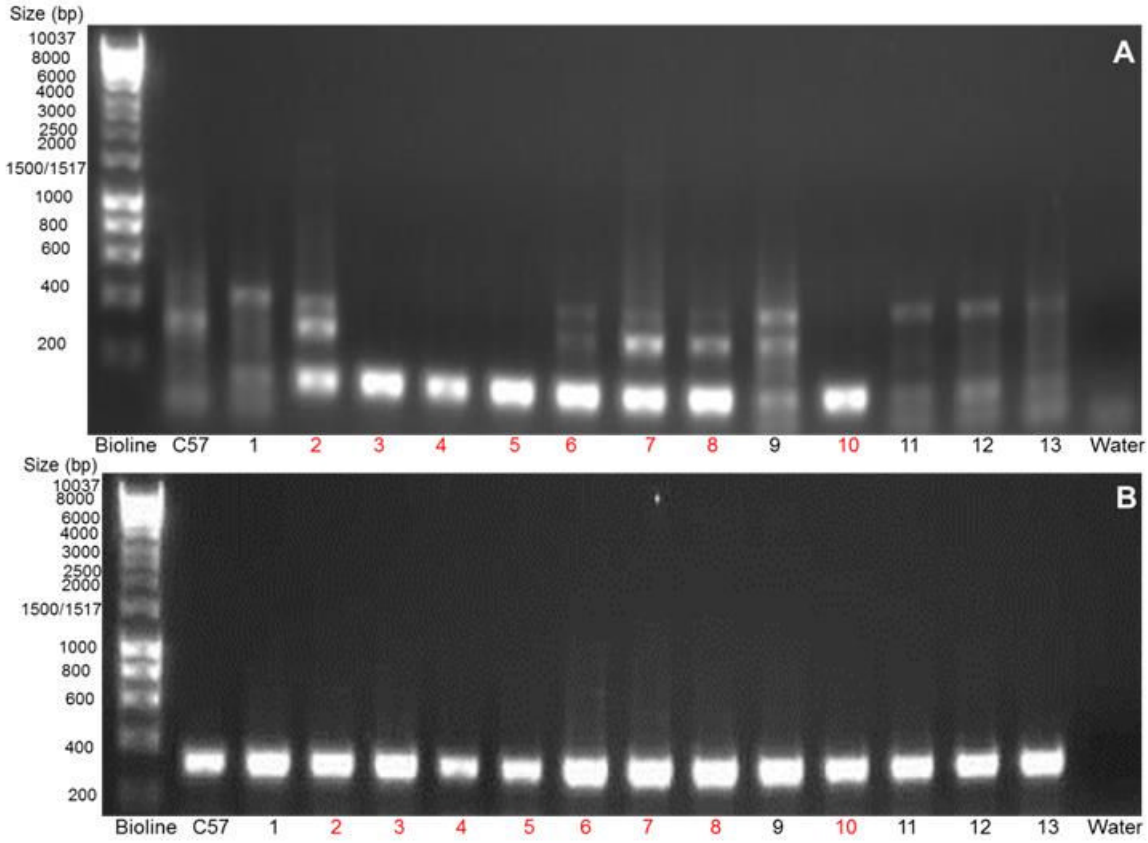

Figure 7.1 Agarose gels (1.5%) of PCRs to assess human HER2 gene status of mice purchased from The Jackson Laboratory.
A) Human HER2 gene (139 bp) and B) Mouse IL-2 gene (internal control, 324 bp).
The identification numbers are in red for HER2 transgenic mice and in black for wild type mice. Controls were a C57 Black mouse and water sample. Bioline hyperladder I used.

DNA of HER2 PCRs extracted from agarose gel bands for mice 2, 6 and 8 contained the human HER2 gene. In addition, extracted DNA from mice 2, 3 and 4 IL-2 PCRs contained the mouse IL-2 gene. Since the homozygous mice die *in utero*, the mice were successfully bred from wild and HER2 transgenic parents.

Table 7.2 Consistent genotyping results performed at UCL and The Jackson Laboratory.

Mouse Identification Number	Gender	Genotype
1	F	Wild
2	F	HER2
3	F	HER2
4	F	HER2
5	F	HER2
6	M	HER2
7	M	HER2
8	M	HER2
9	M	Wild
10	M	HER2
11	M	Wild
12	M	Wild
13	M	Wild

7.2.2 Preparation and assessment of the $(HE)_3$-G3 DARPin without a GP-site for mouse administration

As previously outlined in Chapter 6, the HE_3-G3 DARPin selected for clinical development was produced without the GP residue at the N-terminus.

7.2.2.1 Endotoxin levels

To minimise toxic effects in mice unrelated to the $(HE)_3$-G3 DARPin, endotoxins and the reducing agent (DTT) were removed prior to administration. Endotoxins arise from Gram-negative bacteria outer cell membranes and are not found in *P. pastoris* cells. Yet, prior to endotoxin removal, the $(HE)_3$-G3 DARPin endotoxin concentration was 67.3 Endotoxin Units (EU) per ml, from possible bacterial contaminants. After elution from the first endotoxin column, the endotoxin concentration was 2.16 EU/ml and decreased to 1.19 EU/ml after elution from the fifth endotoxin column (Figure 7.2). Following buffer exchange into DTT-free PBS buffer with a PD-10 column, the $(HE)_3$-G3 DARPin had 0.65-0.74 EU/ml (DARPin concentration 1.5-2.0 mg/ml).

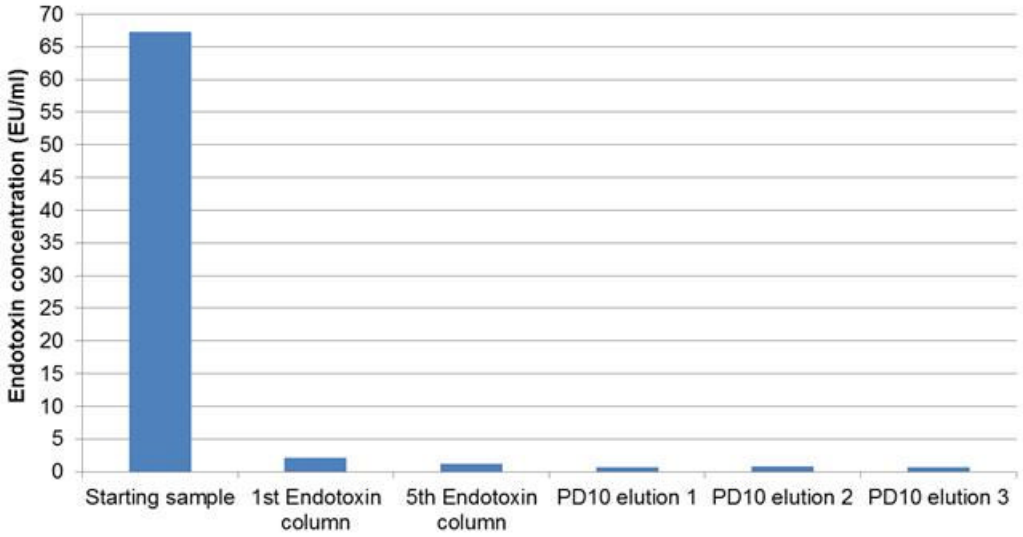

Figure 7.2 Endotoxin removal from $(HE)_3$-G3 DARPin by endotoxin removal columns, followed by elution into DTT-free PBS with a PD-10 column collected as three separate aliquots.

7.2.2.2 Dimerisation status

The $(HE)_3$-G3 DARPin in DTT-free PBS was predominantly in monomer form but contained a higher proportion of dimer than the $(HE)_3$-G3 DARPin in PBS with 10 mmol DTT prior to endotoxin removal (Figure 7.3). In addition, there was a single peak at 90 ml on the Analytical FPLC column which corresponds to the molecular weight of the $(HE)_3$-G3 DARPin (14.4 kDa) (Figure 3.14 and Figure 7.4).

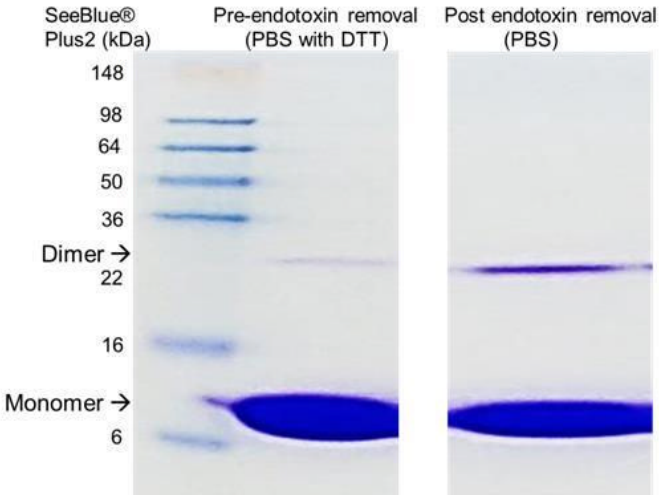

Figure 7.3 SDS-PAGE on a 16% Tris-Glycine gel stained with coomassie blue, to assess $(HE)_3$-G3 DARPin dimerisation status pre- and post-endotoxin removal. Samples were processed with 4x SDS-PAGE non-reducing buffer. Molecular weight marker was SeeBlue Plus2 (Life Technologies).

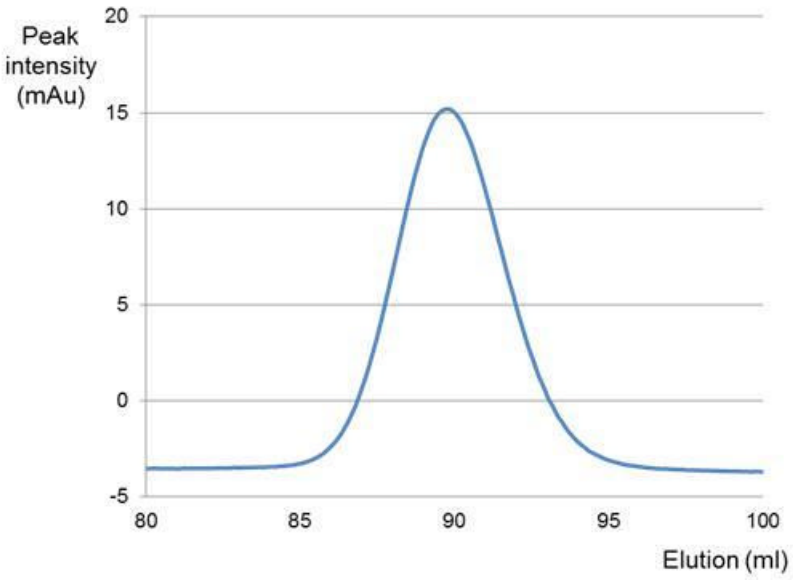

Figure 7.4 FPLC trace of $(HE)_3$-G3 DARPin run on a Analytical Superdex 75 column (125 ml bed volume) (GE Healthcare).
Protein (2 ml, ~3-4 mg) was run through the column at 1 ml/min in filtered PBS at maximum pressure of 0.3 MPa. Blue line relates to UV.

7.2.3 Bloods results

All DARPin-treated mice which underwent blood sampling were treated at 100X HED of $(HE)_3$-G3 DARPin. The control mice were treated with PBS alone. Blood sampling was only performed at 24 h post treatment. It was not possible to obtain pre-DARPin treatment blood samples, as each sample required relatively high blood volumes.

7.2.3.1 Haematology

All HER2 transgenic (4/4) and wild type mice (7/7) treated at 100X HED of $(HE)_3$-G3 DARPin had normal haemoglobin concentrations and normal total white cell counts. However, the mice were euthanized at 24 h post DARPin administration, so it is unlikely that any myelosuppressive effects would have been detected at this early time point.

Thombocytopenia affected transgenic (2/4) and wild type mice (2/5) treated at 100X HED of $(HE)_3$-G3 DARPin, as well as PBS treated control mice (1/2). Assessment of platelet counts was limited by blood clot formation in samples. Among the mice treated at 100X HED of $(HE)_3$-G3 DARPin, 1/7 of the wild type mice and 1/4 of the

transgenic mice had increased eosinophil counts, compared with none of the PBS treated control mice (0/4) (Table 7.3). The eosinophilia could possibly reflect an immune response to the $(HE)_3$-G3 DARPin.

Table 7.3 Haematology results.

Animal	Sex	Gene	Hb (g/dl)	PCV (%)	MCV (fl)	Platelet (10^3/ul)	WBC (10^3/µl)	Neut (%)	Lymph (%)	Mono (%)	Eosin (%)	Baso (%)
Ref. range male (M)			12.3-15.7	39.6-50.3	42.7-57.4	953-2044	2.82-13.39	0-37.1	56.4-97.0	0.5-4.3	0.5-4.4	0-0.7
Ref. range female (F)			12.7-15.8	40.5-50.1	43.3-58.0	832-1777	1.56-11.68	0.9-25.1	65.5-95.3	0-6.7	0.6-5.1	0-0.8
Control (C) mice treated with PBS, age 3 months*												
C1	F	Wild	15.3	48.7	47.8	572	8.93	7.5	84.8	1.9	4.3	0.2
C2	F	Wild	14.6	46.8	47.0	CLOT	9.15	5.3	89.5	1.1	2.2	0.3
C3	M	Wild	10.2	34.5	46.5	1239	8.00	22.0	72.2	0.8	3.9	0.1
C4	M	Wild	14.4	46.2	46.2	CLOT	9.63	13.7	80.2	1.2	3.1	0.3
Wild (W) mice treated with 100X HED $(HE)_3$-G3 DARPin, age 5-6 months												
W1	F	Wild	14.6	46.9	45.7	941	9.11	8.5	86.7	1.2	2.1	0.2
W2	F	Wild	13.9	46.0	46.9	736	7.15	9.0	86.0	2.0	2.0	0.2
W3	F	Wild	13.4	43.3	46.9	905	4.05	10.0	75.5	3.8	6.8	0.2
W4	M	Wild	15.6	48.7	46.6	777	11.48	7.3	86.9	1.4	2.1	0.2
W5	M	Wild	INS	INS	INS	INS	INS	INS	INS	INS	INS	INS
W6	M	Wild	14.2	47.5	48.1	1132	13.34	8.3	85.4	1.5	3.2	0.2
W7	M	Wild	12.8	40.6	45.7	CLOT	4.84	5.4	90.4	1.3	2.0	0.1
W8	F	Wild	15.0	46.7	46.5	CLOT	9.64	5.8	88.2	1.6	2.2	0.3
HER2 transgenic (T) mice treated with 100X HED $(HE)_3$-G3 DARPin, age 9 months												
T1	F	Her2	13.2	43.5	45.6	796	5.47	9.9	82.6	1.3	4.5	0.1
T2	F	Her2	14.2	45.3	47.8	883	8.84	8.2	83.8	1.2	5.4	0.1
T3	M	Her2	12.8	41.8	46.8	1407	4.33	10.9	83.5	1.7	3.1	0.1
T4	M	Her2	14.1	45.0	47.0	599	8.30	7.7	87.4	0.9	2.4	0.1

*Control (C) mice 5-10 did not undergo haematological assessment.
Abnormal results in red, CLOT = clot in sample, INS = insufficient sample.

7.2.3.2 Clinical Chemistry

Hyperglycaemia affected 2/4 HER2 transgenic (aged 9 months) and 2/8 wild type mice (aged 5-6 months) treated with $(HE)_3$-G3 DARPin at 100X HED. The younger control mice (C1-4, aged 3 months) were all normoglycaemic, while 3/6 of the older control mice (C5-10, aged 9-12 months) were hyperglycaemia. In all cases, the blood glucose concentrations were <20% above the upper limit of the reference range. Thus, it is likely that hyperglycaemia is age and or weight related, rather than $(HE)_3$-G3 DARPin related.

The DARPin treated HER2 transgenic mice (0/4) and PBS treated control mice (0/10) did not have any biochemical features of kidney impairment. Among the eight DARPin treated wild type mice, one mouse had a slightly increased creatinine concentration, 0.13 mg/dL (reference range 0.04-0.11) associated with a normal

urea concentration. It is difficult to know whether this case of mild renal impairment is DARPin related (Table 7.4 and Table 7.5).

There was no evidence of liver dysfunction in DARPin treated HER2 transgenic and wild type mice. Among the wild type DARPin treated mice, 2/8 had a raised albumin which is not a feature of liver impairment (Table 7.4 and Table 7.5).

Table 7.4. Blood chemistry results for control and wild mice (AP: alkaline phosphatase, ALT & AST: alanine & aspartate transaminase).

Animal	Sex	Gene	Na^+ (mmol/L)	K^+ (mmol/L)	Urea (mg/dL)	Creatinine (mg/dL)	Ca^+ (mg/dL)	Glucose (mg/dL)	Cholesterol (mg/dL)	AP (U/L)	ALT (U/L)	AST (U/L)	Total protein (g/dL)	Albumin (g/dL)	Bilirubin (mg/dL)
Ref. Range Male (M)			145-154	3.3-5.0	27.9-58.0	0.04-0.11	9.2-10.5	150-318	92-182	22 -152	0-685	0-302	4.6-5.7	2.6-3.5	0.05-0.19
Ref. Range Female (F)			145-153	2.7-4.4	25.0-54.4	0.05-0.12	9.2-10.7	133-301	64-137	37-171	0-118	0-173	4.7-5.6	3.1-3.8	0.06-0.14
Control (C) mice treated with PBS, C1-4 age 3 months and C5-10 age 9-12 months															
C1	F	Wild	148	4.0	39.8	0.09	9.6	189	60	83	25	71	4.7	3.3	0.20
C2	F	Wild	151	3.7	47.4	0.09	9.1	291	80	71	25	128	4.9	3.5	0.09
C3	M	Wild	151	3.6	45.2	0.08	9.1	270	85	37	34	59	4.2	2.5	0.06
C4	M	Wild	151	3.8	45.1	0.07	9.8	247	117	45	34	76	4.8	3.1	0.08
C5	M	Her2	150	4.6	51.9	0.07	9.8	324	137	65	31	63	4.9	3.1	0.01
C6	M	Wild	148	5.2	53.0	0.09	9.4	319	129	62	53	229	4.9	2.9	0.04
C7	M	Her2	152	4.5	57.6	0.07	9.8	234	133	61	31	62	5.2	3.4	0.02
C8	M	Wild	153	3.6	45.2	0.06	9.5	226	142	56	35	61	5.3	3.6	0.05
C9	M	Wild	150	4.7	44.8	0.09	9.6	328	146	43	42	153	4.9	3.2	0.04
C10	M	Her2	149	3.8	49.9	0.09	9.4	268	110	48	27	49	4.9	2.9	0.04
Wild (W) mice treated with 100X $(HE)_3$-G3 DARPin, age 5-6 months															
W1	F	Wild	149	4.1	44.7	0.10	9.8	276	135	85	39	69	5.6	3.9	0.10
W2	F	Wild	150	3.5	45.3	0.10	9.8	278	101	78	20	67	5.1	3.5	0.12
W3	F	Wild	148	4.4	42.6	0.09	9.3	269	80	59	18	49	5.1	3.6	0.13
W4	M	Wild	149	4.2	37.4	0.13	9.6	237	127	88	56	109	5.2	3.5	0.10
W5	M	Wild	151	4.0	46.8	0.07	9.8	246	132	82	89	89	5.5	3.7	0.07
W6	M	Wild	151	3.8	43.0	0.07	10.0	360	127	56	31	47	5.2	3.4	0.08
W7	M	Wild	150	3.4	40.8	0.07	9.9	352	121	74	49	87	5.1	3.5	0.08
W8	F	Wild	152	3.7	44.1	0.09	9.5	218	104	82	27	83	5.1	3.6	0.12

Table 7.5 Blood chemistry results for transgenic mice (AP: alkaline phosphatase, ALT & AST: alanine & aspartate transaminase).

Animal	Sex	Gene	Na^+ (mmol/L)	K^+ (mmol/L)	Urea (mg/dL)	Creatinine (mg/dL)	Ca^+ (mg/dL)	Glucose (mg/dL)	Cholesterol (mg/dL)	AP (U/L)	ALT (U/L)	AST (U/L)	Total protein (g/dL)	Albumin (g/dL)	Bilirubin (mg/dL)
Ref. Range Male (M)			145-154	3.3-5.0	27.9-58.0	0.04-0.11	9.2-10.5	150-318	92-182	22 -152	0-685	0-302	4.6-5.7	2.6-3.5	0.05-0.19
Ref. Range Female (F)			145-153	2.7-4.4	25.0-54.4	0.05-0.12	9.2-10.7	133-301	64-137	37-171	0-118	0-173	4.7-5.6	3.1-3.8	0.06-0.14
HER2 transgenic (T) mice treated with 100X $(HE)_3$-G3 DARPin, age 9 months															
T1	F	Her2	150	4.4	40.9	0.10	9.2	227	85	63	25	83	5.1	3.2	0.10
T2	F	Her2	149	3.4	47.0	0.07	9.6	350	124	74	71	157	5.7	3.7	0.13
T3	M	Her2	151	3.7	41.7	0.05	9.9	296	139	56	33	50	5.3	3.4	0.10
T4	M	Her2	150	4.0	32.8	0.09	10.0	368	154	79	51	66	5.2	3.4	0.09

7.2.4 Histology results

7.2.4.1 HER2 transgenic and wild type mouse study

The heart, kidneys, spleen, brain, adrenal glands and mammary glands of the PBS treated control mice (n=4 wild type mice aged 3 months) and mice treated at 100X HED of $(HE)_3$-G3 DARPin (n=8 wild mice aged 5-6 months and n=4 transgenic mice aged 9 months) were normal on histological examination.

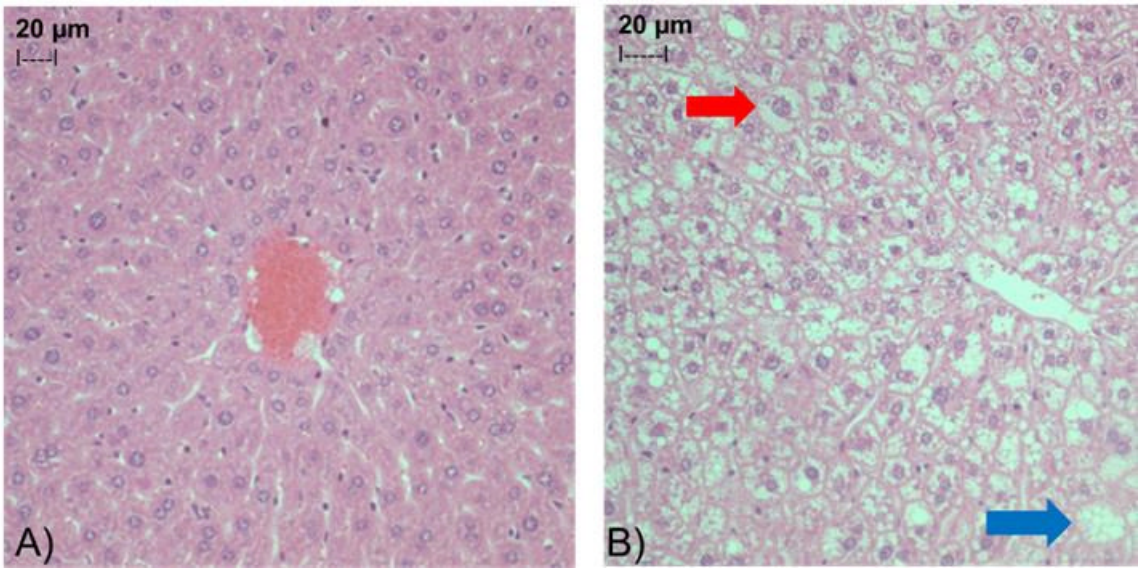

Figure 7.5 Haemotoxylin and Eosin staining of mouse livers, post $(HE)_3$-G3 DARPin administration.
A) Normal mouse liver.
B) Abnormal mouse liver with vacuolated hepatocytes due to fat accumulation (blue arrow) and hepatocytes containing lysosome bound glycogen (red arrow).
Performed by Dr Noel Downes, Pathologist at Sequani.

Fat and glycogen related hepatic vacuolation was seen in PBS and DARPin treated mice on Haemotoxylin and Eosin (H&E) staining (Figure 7.5). Hepatic vacuolation was identified in PBS treated male wild type mice (2/5) and PBS treated male transgenic mice (1/3). However, hepatic vacuolation was not identified in the PBS treated female wild type mice (0/2), who were younger than their male counterparts.

All DARPin treated male wild type mice (4/4) had hepatic vacuolation but age matched DARPin treated female wild type mice (0/4) did not have hepatic vacuolation on histological analysis. All of the DARPin treated male transgenic (2/2) and DARPin treated female transgenic (2/2) mice had evidence of hepatic vacuolation. Since hepatic vacuolation affected both PBS and DARPin treated mice,

it is probably a phenotype of the mice rather than related to DARPin administration (Table 7.6).

Table 7.6 Prevalence and severity of hepatic vacuolation in mice treated at 100 X HED of $(HE)_3$-G3 DARPin and control mice treated with PBS (n/a: not available).

Gender	Males				Females		
Treatment & genotype	PBS Wild	PBS Transgenic	DARPin Wild	DARPin Transgenic	PBS Wild	DARPin Wild	DARPin Transgenic
Mice examined	5	3	4	2	2	4	2
Age range (months)	3-9	9-12	5-6	9	3	5-6	9
Weight range (g)	n/a	n/a	48-51	47-48	n/a	26-43	36-51
Mice with hepatocyte vacuolation	2	1	4	2	0	0	2

7.2.4.2 CD-1 mouse study

To clarify whether the hepatic histological abnormalities observed in the transgenic and wild type mice were a phenotype of this mouse strain or DARPin-related, 2 month old CD-1 mice were also assessed. The CD-1 mice were treated with 100X HED of $(HE)_3$-G3 DARPin, 50X HED of $(HE)_3$-G3 DARPin or PBS, then they were euthanised at 24 h for histological examination.

Examination of the livers from the CD-1 mice aged 2 months (weight 31-36 g), revealed that there were no abnormal histological changes in the PBS treated control mice (n=6), 50X HED DARPin treated mice (n=6) and 100X HED DARPin treated mice (n=6). Thus, suggesting that the vacuolated hepatocytes previously observed in the transgenic and wild type mice, was related to the mouse strain (generated from C57BL/6 and C3H mice) rather than caused by the $(HE)_3$-G3 DARPin.

7.2.4.3 Human HER2 status of transgenic and wild mouse livers

The livers from transgenic and wild type mice were assessed for expression of human HER2, to determine whether there was a mechanism for preferential $(HE)_3$-G3 DARPin hepatic binding in these mice. Initially, a panel of human breast cancer TMAs confirmed that the Bond Polymer Refine Detection assessed human HER2 status appropriately (Figure 7.6).

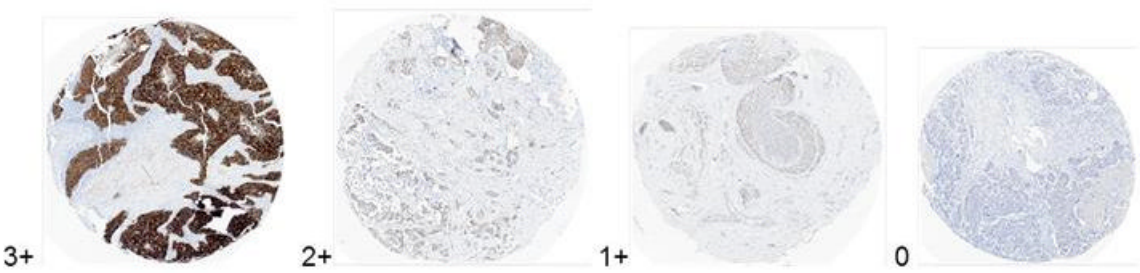

Figure 7.6 Immunohistochemistry with Bond Polymer Refine Detection of human breast cancer tissue microarrays.
(Known HER2 status displayed on left side, x10 magnification, UCL Advanced Diagnostics).

The livers from the transgenic and wild type mice did not express human HER2 protein, so they are unlikely to preferentially bind to $(HE)_3$-G3 DARPin. Thus, consistent with reports that human HER2 receptor expression is limited to the mammary glands and cerebellum of the transgenic mice (Figure 7.7 and Figure 7.8) (Piechocki, Ho et al. 2003).

Figure 7.7 Immunohistochemistry of a transgenic mouse liver with the Bond Polymer Refine Detection.
A) Haemotoxylin and Eosin stain, B) Negative control (primary antibody omitted), C) Assessment with the primary and secondary antibodies (x10 magnification, UCL Advanced Diagnostics).

Figure 7.8 Immunohistochemistry of a wild type mouse liver with the Bond Polymer Refine Detection.
A) Haemotoxylin and Eosin stain, B) Negative control (primary antibody omitted), C) Assessment with the primary and secondary antibodies (x10 magnification, UCL Advanced Diagnostics).

It was not possible to assess HER2/CEP17 ratios, as the chromosome 17 detection signal utilises a goat anti-mouse antibody which results in a non-specific background red signal in the mouse livers. In fact, determination of the HER2/CEP17 ratio was not relevant, as the human HER2 gene is under the control of the WAP promoter in the transgenic mice, while in humans it is located on chromosome 17 (Piechocki, Ho et al. 2003). The nuclei of the assessed wild type mouse hepatocytes did not have any human HER2 genes, while the nuclei of the transgenic mouse hepatocytes had up to four human HER2 genes per nucleus (Figure 7.9). Thus, the transgenic mice had human HER2 genes but did not express membranous HER2 in their livers. The lack of membranous human HER2 expression in the wild and transgenic mouse hepatocytes substantiates the view that the observed hepatic vacuolation was not related to $(HE)_3$-G3 DARPin administration.

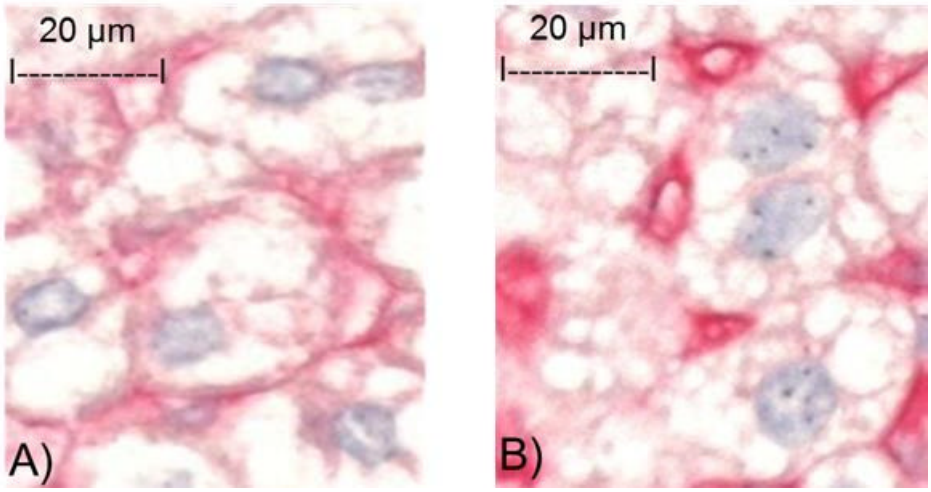

Figure 7.9 Chromogenic in situ hybridisation: Images taken at 40x magnification.
A) Wild type mouse liver: No black in situ hybridisation reaction for HER2 DNA detection in liver nuclei.
B) Transgenic mouse liver: Up to four black in situ hybridisation reactions for HER2 DNA detection in each liver nucleus (UCL Advanced Diagnostics).

7.3 Discussion

In the preliminary pre-clinical toxicity study, the $(HE)_3$-G3 DARPin was well tolerated by the transgenic, wild type and CD-1 mice treated at 50-100 X HED over 24 h post-administration. The main abnormal findings were hyperglycaemia and hepatic vacuolation related to fat and glycogen retention. However, it is unlikely that these abnormalities were DARPin related, as they were also observed in control mice treated with PBS.

The DARPin treated transgenic and wild type mice with hepatocyte vacuolation were generally older and heavier (5-9 months and weight 26-51 g), than the DARPin treated CD-1 mice (2 months old, weight 31-36 g) whose livers were histologically normal. In addition, hepatic vacuolation was observed in PBS treated male transgenic and male wild type mice. The histological abnormalities in the livers were not associated with biochemical evidence of liver impairment. Furthermore, the transgenic and wild type mice livers are unlikely to preferentially bind to $(HE)_3$-G3 DARPin, as they do not express membranous human HER2 protein.

In humans, non-alcoholic fatty liver disease (NAFLD) is characterised by lipid deposition in the hepatocytes in the absence of significant alcohol consumption and is usually related to obesity (Tannapfel, Denk et al. 2011). An inflammatory reaction to hepatocyte fat deposition results in non-alcoholic steatohepatitis (NASH), which may lead to liver cirrhosis. Patients with NASH exhibit fatty degeneration of hepatocytes characterised by vacuolation (Tannapfel, Denk et al. 2011).

The mice received the 2018 Teklad Global 18% Protein Rodent Diet (Harlan Laboratories) which supports gestation, lactation, and growth. In this diet 18% and 58% of the calories are derived from fats and carbohydrates, respectively. Studies have shown that rodents consuming high fat diets for 4 weeks develop hepatocyte vacuolation and necrosis as found in NAFLD, these findings were not seen in rodents who received a standard diet (4% fat) (Dhibi, Brahmi et al. 2011). Thus, the hepatocyte vacuolation of the DARPin treated transgenic and wild type mice is probably caused by prolonged high fat dietary intake. In addition, hyperglycaemia which affected both the PBS and DARPin treated mice probably reflects weight gain and insulin resistance caused by their diet.

This study only assessed acute adverse effects of the $(HE)_3$-G3 DARPin, the medium and long-term adverse effects of $(HE)_3$-G3 DARPin in mice are unknown, including any possible myelosuppressive effects. The HER2 transgenic mice were selected to assess direct toxic effects related to the interaction between the DARPin and human HER2 in the mouse brains and mammary glands. However, human HER2 is only expressed in the mammary glands during pregnancy and lactation, so was probably not expressed in the mammary glands of the assessed transgenic mice. In addition, human HER2 is constitutively expressed in the Bergman glia cells within the molecular layer of the cerebellum, compared to the normal human brain where HER2 is consistently found in oligodendrocytes, astrocytes and microglial cells (Cannella, Pitt et al. 1999; Piechocki, Ho et al. 2003). Thus, even in the absence of histological abnormalities in the brain and mammary glands of the assessed HER2 transgenic mice, direct toxic effects cannot be entirely excluded based on this study. Furthermore, it is unknown whether ligand binding to the human HER2 of transgenic mice has any intracellular effects and it is unknown whether any potential intracellular effects in mice are comparable with the effects in humans.

The regulatory pre-clinical toxicity study will need to be conducted to GLP standards, so will be performed entirely by Sequani. Following a meeting with the Medicines and Healthcare Products Regulatory Agency (MHRA) in which the data herein was presented, the design of the regulatory pre-clinical toxicity study was agreed. The regulatory study will assess both acute and long term toxic effects in CD-1 mice who will receive intravenous $(HE)_3$-G3 DARPin conjugated with DOTA at 50X HED. CD-1 mice have been selected as their phenotype is better characterised than the HER2 transgenic mice, so it will easier to identity DARPin related adverse events (Morgan, Elangbam et al. 2013).

Chapter 8 Discussion and future directions

8.1 Discussion

For breast cancer, the reported rates of HER2 discordance between primary and metastatic sites, range from 0 to 34 % (Turner and Di Leo 2013). The literature is predominantly based on retrospective studies and include cases of both HER2 loss and HER2 gain (Turner and Di Leo 2013). To determine HER2 evolution and heterogeneity, HER2 imaging could provide whole body assessment of HER2 expression at tumour sites over time and during therapy, which is both more feasible and acceptable to patients than serial and multiple biopsies. Furthermore, considerably less is known about gastric cancer HER2 biology and HER2 imaging could help to address this knowledge gap (Boku 2014).

HER2 is an important therapeutic target in cancer and HER2 imaging could be used to select patients for therapy by identifying HER2 gain and the need to introduce anti-HER2 therapy, as well as HER2 loss necessitating discontinuation of anti-HER2 therapy (Arteaga, Sliwkowski et al. 2012). Whole body HER2 scans could potentially improve clinical outcomes and ensure appropriate allocation of expensive anti-HER2 therapies.

Molecular imaging requires high tumour uptake and low normal tissue uptake, to facilitate high tumour-to-normal tissue ratios. The liver is a common site for breast cancer metastases and is involved in drug metabolism and excretion. Therefore, it is important to minimise normal liver uptake to enable identification of liver metastases on imaging. Factors which are known to influence radioligand liver uptake, include the composition of the histidine tag, chelator structure, radioisotope residualising properties, radioisotope-chelator stability and radio-colloid impurities (Hosseinimehr, Tolmachev et al. 2012). To determine the G3 DARPin construct with lowest normal liver uptake, His_6-G3, $(HE)_3$-G3 and untagged-G3 DARPins were produced using a GMP-compatible *P. pastoris* protocol for initial *in vivo* assessment with ^{111}In (residualising) and ^{125}I (non-residualising).

The His_6-G3 and $(HE)_3$-G3 DARPins were designed to commence at their histidine-based tags. However, the initial production of His_6-G3 and $(HE)_3$-G3 DARPins from the template which incorporated LEKREAEA preceding the histidine based tags, resulted in G3 DARPins commencing with EAEAH or EAH residues. This occurred as the Ste13 gene product was inefficient in EA cleavage, while the Kex2 gene

product efficiently removed LEKR residues (Sasagawa, Matsui et al. 2011). Consequently, it was necessary to produce pPICZαB/G3 DARPin DNA which did not encode EAEA residues. The modified pro-sequence of the α-factor secretion signal still enabled DARPin secretion from the cytoplasm into the media for harvesting. It was not necessary to re-produce the cleavable tag-G3 without EAEA residues, as HRV 3C protease cleavage ensured that the untagged-G3 commenced at the appropriate N-terminus site (GP).

For direct radiolabelling with ^{125}I and site-specific radiolabelling with ^{111}In via DOTA of the G3 DARPins, the $(HE)_3$ tag rather than the absence or presence of the His_6 tag was associated with significantly lower liver uptake without compromising uptake in other assessed normal tissues. Direct iodination of the G3 DARPins resulted in a considerably different biodistribution profile compared to site-specific ^{111}In radiolabelling. ^{125}I-$(HE)_3$-G3 had higher stomach uptake (where free iodine is known to accumulate) and lower kidney uptake than ^{111}In-$(HE)_3$-G3.

For the HER2 affibody molecule, $Z_{HER2:342}$ radiolabelled with $[^{99m}Tc(CO)_3]^+$ and ^{111}In, the N-terminal $(HE)_3$ tagged variant is associated with lowest normal liver uptake (Hofstrom, Orlova et al. 2011; Hofstrom, Altai et al. 2013). Yet, some of the $Z_{HER2:342}$ biodistribution studies are limited, as there were other differences in the amino acid sequences besides the composition of the histidine-based tags (Hofstrom, Orlova et al. 2011). The G3 DARPins assessed in this thesis, which confirmed that $(HE)_3$-G3 DARPin had the lowest normal liver uptake, only differed by the presence or composition of their histidine-based tags.

Hofström *et al.* concluded that for $Z_{HER2:342}$ radiolabelled with $[^{99m}Tc(CO)_3]^+$, lipophilic and positively charged N-terminal histidine based tags promote liver uptake (Hofstrom, Altai et al. 2013). The charge of $(HE)_3$-$Z_{HER2:342}$ and His_6-$Z_{HER2:342}$ differ greatly; by contrast $(HE)_3$, His_6 and untagged-G3 have similar isoelectric points (pI) (Hofstrom, Altai et al. 2013). In addition, $(HE)_3$, His_6 and untagged-G3 DARPins have similar grand average of hydropathy (GRAVY) scores -0.12, -0.12 and +0.02, respectively, indicating other factors are involved.

^{111}In-$(HE)_3$-G3 achieves a higher tumour-to-blood ratio than ^{125}I-$(HE)_3$-G3, as it is cleared faster from the blood stream and ^{111}In is residualising, so remains within the HER2-positive tumours over 24 h. HER2-positive tumour uptake of ^{111}In-$(HE)_3$-G3 is

unaffected by the presence of trastuzumab, so DARPin HER2 imaging should not affect treatment scheduling. MicroSPECT/CT imaging demonstrates that HER2-positive tumour uptake is associated with high renal uptake for ^{111}In-$(HE)_3$-G3 and ^{123}I-$(HE)_3$-G3 but considerably greater non-specific uptake with ^{123}I-$(HE)_3$-G3, including higher gastric uptake. Consequently, ^{123}I-$(HE)_3$-G3 SPECT scanning would not be suitable for assessing gastric and gastro-oesophageal junction cancer patients.

Although DOTA-$(HE)_3$-G3 was successfully used for ^{111}In radiolabelling, it was not feasible to use it for ^{68}Ga radiolabelling. This is because ^{68}Ga radiolabelling of DOTA requires heating to 100 °C for 30 min and the G3 DARPin is not stable at this temperature, confirmed by the loss of HER2 ECD binding affinity on SPR. By contrast, NOTA-$(HE)_3$-G3 is potentially suitable for ^{68}Ga radiolabelling, as it does not require heating and the G3 DARPin can tolerate the acidic radiolabelling conditions (pH 4.6). In HER2-positive tumour bearing mice, ^{68}Ga-NOTA-$(HE)_3$-G3 achieved good HER2-positive tumour uptake but had a low tumour-to-liver ratio (< 2) at 1 h post administration, which would limit the identification of liver metastases, so is not suitable for clinical application.

In pre-clinical toxicity studies, CD-1 mice, wild type mice and HER2 transgenic mice tolerated 50 to 100 times the HED of unconjugated and non-radiolabelled $(HE)_3$-G3 DARPin over 24 h. The main abnormal findings were hyperglycaemia and hepatic vacuolation related to fat and glycogen retention within the liver. However, it is unlikely that either of these abnormalities were DARPin-related, as they affected both PBS and DARPin treated transgenic and wild type mice. Furthermore, human HER2 was not expressed in the livers of HER2 transgenic and wild type mice to mediate preferential G3 DARPin binding and there was no evidence of hepatic vacuolation in CD-1 mice treated with similar doses of $(HE)_3$-G3 DARPin. This $(HE)_3$-G3 DARPin toxicity study only assessed acute toxic effects, so the longer term effects will be assessed in a subsequent pre-clinical toxicity study.

The HER2 transgenic mice were selected to assess direct toxic effects related to the interaction between the G3 DARPin and human HER2 in the mouse brains and mammary glands. However, in the transgenic mice, human HER2 is only expressed in the Bergman glia cells within the molecular layer of the cerebellar cortex and in

the mammary glands during pregnancy and lactation (Piechocki, Ho et al. 2003). Consequently, there may have been no mammary gland human HER2 expression and only focal cerebellar human HER2 expression in the assessed HER2 transgenic mice, so direct toxic effects cannot be entirely excluded with this mouse model.

Imaging trials of most HER2 radioligands have had disappointing results, due to limitations related to their pharmacokinetics for imaging, which were predictable based on their pre-clinical performance (Smith-Jones, Solit et al. 2004; Dijkers, Kosterink et al. 2009; Reddy, Shaller et al. 2011; Perols, Honarvar et al. 2012). It should be noted that the majority of clinical HER2 imaging studies have not assessed HER2 tumour status histologically for correlation with HER2 scans, thus limiting the evaluation of these imaging agents.

Trastuzumab radiolabelled with ^{64}Cu, ^{89}Zr or ^{111}In demonstrated the potential for HER2 imaging by identifying known and or previously unknown tumour lesions in patients but lacked sensitivity compared to conventional imaging, owing to its long half-life and high blood pool activity (Perik, Lub-De Hooge et al. 2006; Dijkers, Oude Munnink et al. 2010; Mortimer, Bading et al. 2013). Fab fragments of trastuzumab were developed for HER2 imaging, since their lower molecular weight is associated with a shorter half-life in serum than trastuzumab. However, ^{68}Ga-F(ab')$_2$-trastuzumab PET imaging failed to identify any tumours among four of the eight metastatic HER2-positive breast cancer patients assessed. This poor performance was due to relatively high liver uptake and high blood pool activity, as well as potential competition with therapeutically administered trastuzumab (Beylergil, Morris et al. 2013).

The radiolabelled HER2 binding affibody molecule, $Z_{HER2:342}$ assessed three patients with HER2-positive metastatic breast cancer by PET (^{68}Ga) and or SPECT (^{111}In) imaging. Although for two patients not all known tumour lesions were identified, there was limited tumour biopsy sampling to systematically evaluate the accuracy of the HER2 affibody molecule imaging. Unfortunately, there was high background liver uptake in this initial study which limited its clinical potential (Baum, Prasad et al. 2010). Recently, a phase I trial demonstrated that the second generation affibody ^{111}In-ABY-025 had superior distribution, dosimetry, and accuracy for assessing patients with HER2-positive and HER2-negative metastatic breast cancer than its

first generation counterpart. There was good correlation between HER2 status assessed by ^{111}In-ABY-025 SPECT/CT imaging and immunohistochemistry with the HercepTest. This included confirmation that a patient who had had HER2-positive primary disease developed HER2-negative metastases, furthermore HER2-positive brain metastases were detected (Sorensen, Sandberg et al. 2014).

The pharmacokinetics of ^{111}In-$(HE)_3$-G3 is well suited for HER2 imaging, including short half-life in serum, high tumour-to-blood ratios and low non renal tissue uptake. The kidneys received the highest radiation dose. Based on medical internal radiation dose (MIRD) estimates, the maximum absorbed kidney dose in patients with the proposed clinical dose of ^{111}In-$(HE)_3$-G3 (300 MBq) is 1,000-fold lower than the dose associated with a 5 % rate of radiation nephritis within 5 years of administration ($TD_{5/5}$), 9.75 mGy vs. 10 Gy (Wessels, Konijnenberg et al. 2008). However, MIRD estimates are based on external beam radiation administration, so are limited in determining the potential toxicity related to intravenous radioligands.

Conventionally, His_6 tagged proteins have been produced for human administration and $(HE)_3$ tagged proteins represent a relatively new development, so less is known about their safety in humans. Interestingly, a Blast search (NCBI) for a short input sequence with HEHEHE as the query, yielded a variety of hits within the Homo sapiens database of almost identical sequences, e.g. HEHEH in the human zinc transporter (Gene ID: SLC39A9) and HEHEQE in kinase 3 (Gene ID: TAOK3). The HHHHHH sequence cannot be found using a Blast search within the Homo sapiens database. Instead clusters of histidine are found that co-ordinate with metal ions, e.g. Ca^{2+}, Mg^{2+} and Zn^{2+}.

HER2 molecular imaging for breast cancer and gastric or gastro-oesophageal junction cancer needs a radioligand with minimal normal liver and gastric uptake, as well as the ability to bind to HER2 in the presence of concomitant anti-HER2 therapy. The work in this thesis has demonstrated that ^{111}In-DOTA-$(HE)_3$-G3 DARPin has high affinity for HER2, binds in the presence of trastuzumab, achieves high tumour-to-blood ratios and tumour to non-renal tissue ratios, including a tumour-to-liver ratio ≥ 12 over 24 h. In addition, $(HE)_3$-G3 can be radiolabelled with ^{68}Ga for PET imaging but does not achieve sufficiently high tumour-to-liver ratios which will compromise its utility. To develop $(HE)_3$-G3 PET/CT imaging,

investigation of alternatives radio-isotopes and or bifunctional chelators must be performed. Initially, a first in human study is planned to assess ^{111}In-DOTA- $(HE)_3$-G3 SPECT/CT imaging.

8.2 Milestones achieved towards phase I trial implementation

- Trial sponsorship:

During the course of the PhD I have been involved in a successful application to Cancer Research UK (CRUK). CRUK have agreed to fund the regulatory GMP pre-clinical toxicity study and sponsor the proposed clinical trial.

- Regulatory approval:

I helped to organise a Scientific Advice Meeting with the MHRA to discuss the design of the proposed regulatory GMP pre-clinical toxicity study and proposed phase I trial. This meeting was informative and will hopefully facilitate the application for Clinical Trial Authorisation.

- Clinical trial protocol development

I attended the Methods in Clinical Cancer Research, Waldhaus Flims, Switzerland in June 2011. This was a great opportunity to develop the clinical trial design and write a draft clinical trial protocol with support from leading experts in cancer imaging trials.

Appendix 1 Supplementary data

Chapter 1

Email received on 2nd January 2014 from the Commissioning Editor at Expert Review of Anticancer Therapy (Informa Healthcare), granting permission to reproduce the article:

Goldstein R, Sosabowski J, Vigor K, Chester K, Meyer T. Developments in SPECT and PET based HER2 molecular imaging for breast cancer. *Expert Rev Anticancer Ther.* March 2013.

Dear Rob,

Thank you for your message and apologies for the delay in getting back to you due to being out of the office.

Happy new year to you also!

Regarding your request – happy for you to use the review in your introduction but please ensure that the article is fully cited wherever it is used.

Thank you once again for your contribution to the journal, and I hope to collaborate again in 2014. If you or your colleagues would be interested in submitting / proposing an article at any time please do feel free to contact me directly – I would be delighted to hear from you.

Best wishes,

Sophia

Sophia Maprayil
Commissioning Editor
Expert Reviews
Informa Healthcare
1-2 Bolt Court
London, EC4A 3DQ
Tel.: +44 (0) 207 701 74595
sophia.maprayil@informa.com
www.expert-reviews.com

Chapter 2 and Chapter 3

Plasmids/DARPin templates used to generate His_6-G3 and $(HE)_3$-G3 DARPin

Figure A: Plasmid pPICZαB/EAEAHis3 which had been generated during the EAEAHis_6-G3 DARPin production was used to produce His_6-G3. The EAEAHis3 DNA differed from the proposed His_6-G3 DARPin construct in one respect there would be no glutamic acid (E) and Alanine (A) residues preceding the His_6 tag. The pPICZαB sequence is highlighted (grey) and includes part of the XhoI and XbaI restriction endonucleases sites.

```
ctcgagaaaagaggctgaagctcatcaccatcatcaccatggaccaggttctgatttg
 L  E  K  R  E  A  E  A  H  H  H  H  H  H  G  P  G  S  D  L
ggaaagaaattgttggaagctgctagagctggtcaagatgatgaagttagaattttgatg
 G  K  K  L  L  E  A  A  R  A  G  Q  D  D  E  V  R  I  L  M
gctaacggtgctgatgttaacgctaaggatgaatacggtttgactccattgtacttggct
 A  N  G  A  D  V  N  A  K  D  E  Y  G  L  T  P  L  Y  L  A
actgctcatggtcatttggaaattgttgaagttttgttgaagaatggagctgatgttaac
 T  A  H  G  H  L  E  I  V  E  V  L  L  K  N  G  A  D  V  N
gctgttgatgctattggttttactccattgcatttggctgcttttattggtcatttggaa
 A  V  D  A  I  G  F  T  P  L  H  L  A  A  F  I  G  H  L  E
attgctgaagttttgttgaagcatggtgccgacgttaacgctcaggataagtttggaaag
 I  A  E  V  L  L  K  H  G  A  D  V  N  A  Q  D  K  F  G  K
actgcttttgatatttctattggtaacggtaacgaagatttggctgaaattttgcaaaag
 T  A  F  D  I  S  I  G  N  G  N  E  D  L  A  E  I  L  Q  K
ttgaacggaggttgctaataatctagaacaaaaactcatctcagaagaggatctgaatag
 L  N  G  G  C  -  -  S  R  T  K  T  H  L  R  R  G  S  E  -
cgccgtcgacca
 R  R  R  P
```

Figure B: Plasmid pPICZαB/EAEAHE3 which had been generated during EAEA$(HE)_3$-G3 DARPin production was used to produce $(HE)_3$-G3. The EAEAHE3 DNA differed from the proposed **(**$HE)_3$-G3 DARPin construct in one respect there would be no glutamic acid (E) and Alanine (A) residues preceding the $(HE)_3$ tag. The pPICZαB sequence is highlighted (grey) and includes part of the XhoI and XbaI restriction endonucleases sites.

```
ctcgagaaaagaggctgaagctcatgagcatgaacacgaaggaccaggttctgatttg
 L  E  K  R  E  A  E  A  H  E  H  E  H  E  G  P  G  S  D  L
ggaaagaaattgttggaagctgctagagctggtcaagatgatgaagttagaattttgatg
 G  K  K  L  L  E  A  A  R  A  G  Q  D  D  E  V  R  I  L  M
gctaacggtgctgatgttaacgctaaggatgaatacggtttgactccattgtacttggct
 A  N  G  A  D  V  N  A  K  D  E  Y  G  L  T  P  L  Y  L  A
actgctcatggtcatttggaaattgttgaagttttgttgaagaatggagctgatgttaac
 T  A  H  G  H  L  E  I  V  E  V  L  L  K  N  G  A  D  V  N
gctgttgatgctattggttttactccattgcatttggctgcttttattggtcatttggaa
 A  V  D  A  I  G  F  T  P  L  H  L  A  A  F  I  G  H  L  E
attgctgaagttttgttgaagcatggtgccgacgttaacgctcaggataagtttggaaag
 I  A  E  V  L  L  K  H  G  A  D  V  N  A  Q  D  K  F  G  K
actgcttttgatatttctattggtaacggtaacgaagatttggctgaaattttgcaaaag
 T  A  F  D  I  S  I  G  N  G  N  E  D  L  A  E  I  L  Q  K
Ttgaacggaggttgctaataatctagaacaaaaactcatctcagaagaggatctgaatag
 L  N  G  G  C  -  -  S  R  T  K  T  H  L  R  R  G  S  E  -
cgccgtcgacca
 R  R  R  P
```

Appendix 2 Publications and presentations

Publications

Developments in SPECT and PET based HER2 molecular imaging for breast cancer. Goldstein R, Sosabowski J, Vigor K, Chester K, Meyer T. *Expert Rev Anticancer Ther.* 2013;13(3): 359-73.

Development of the G3 Designed ankyrin repeat protein (DARPin) for HER2 molecular imaging. Goldstein R**,** Sosabowski J, Livanos M**,** Leyton J, Vigor K, Bhavsar G, Nagy-Davidescu G, Rashid M, Miranda E, Yeung J, Tolner B, Plückthun A, Mather S, Meyer T, Chester K. *Eur J Nucl Med Mol Imaging*. 2014 [in Print]

Presentations

HER2 imaging with the G3 Designed ankyrin repeat protein (DARPin). Goldstein R, Tolner B, Leyton J, Livanos M, Bhavsar G, Vigor K, Nagy G, Mather S, Plückthun A, Sosabowski J, Meyer T, Chester K. Poster presented at NCRI Conference, Liverpool, UK, November 2013.

Pre-clinical developments of the G3 Designed ankyrin repeat protein (DARPin) for in vivo assessment of HER2 expression. Goldstein R, Tolner B, Leyton J, Livanos M, Bhavsar G, Vigor K, Nagy G, Mather S, Plückthun A, Sosabowski J, Meyer T, Chester K. Poster presented at AACR Annual Meeting, Washington DC, USA, April, 2013.

Appendix 3 References

Adams, G. P., R. Schier, et al. (1998). "Prolonged in vivo tumour retention of a human diabody targeting the extracellular domain of human HER2/neu." British Journal of Cancer **77**(9): 1405-1412.

Agus, D. B., M. S. Gordon, et al. (2005). "Phase I clinical study of pertuzumab, a novel HER dimerization inhibitor, in patients with advanced cancer." J Clin Oncol **23**(11): 2534-2543.

Ahlgren, S., A. Orlova, et al. (2008). "Evaluation of maleimide derivative of DOTA for site-specific labeling of recombinant affibody molecules." Bioconjug Chem **19**(1): 235-243.

Ahlgren, S., A. Orlova, et al. (2010). "Targeting of HER2-expressing tumors using 111In-ABY-025, a second-generation affibody molecule with a fundamentally reengineered scaffold." J Nucl Med **51**(7): 1131-1138.

Ahlgren, S., H. Wallberg, et al. (2009). "Targeting of HER2-expressing tumors with a site-specifically 99mTc-labeled recombinant affibody molecule, ZHER2:2395, with C-terminally engineered cysteine." J Nucl Med **50**(5): 781-789.

Akiyama, T., C. Sudo, et al. (1986). "The product of the human c-erbB-2 gene: a 185-kilodalton glycoprotein with tyrosine kinase activity." Science **232**(4758): 1644-1646.

Altai, M., H. Wallberg, et al. (2014). "188Re-ZHER2:V2, a Promising Affibody-Based Targeting Agent Against HER2-Expressing Tumors: Preclinical Assessment." J Nucl Med.

Amir, E., M. Clemons, et al. (2012). "Tissue confirmation of disease recurrence in breast cancer patients: Pooled analysis of multi-centre, multi-disciplinary prospective studies." Cancer Treat Rev **38**(6): 708-714.

Arteaga, C. L., M. X. Sliwkowski, et al. (2012). "Treatment of HER2-positive breast cancer: current status and future perspectives." Nat Rev Clin Oncol **9**(1): 16-32.

Baselga, J., J. Cortes, et al. (2012). "Pertuzumab plus trastuzumab plus docetaxel for metastatic breast cancer." N Engl J Med **366**(2): 109-119.

Baum, R. P., V. Prasad, et al. (2010). "Molecular imaging of HER2-expressing malignant tumors in breast cancer patients using synthetic 111In- or 68Ga-labeled affibody molecules." J Nucl Med **51**(6): 892-897.

Berry, D. J., Y. Ma, et al. (2011). "Efficient bifunctional gallium-68 chelators for positron emission tomography: tris(hydroxypyridinone) ligands." Chem Commun (Camb) **47**(25): 7068-7070.

Beylergil, V., P. G. Morris, et al. (2013). "Pilot study of 68Ga-DOTA-F(ab')2-trastuzumab in patients with breast cancer." Nucl Med Commun **34**(12): 1157-1165.

Binz, H. K., P. Amstutz, et al. (2004). "High-affinity binders selected from designed ankyrin repeat protein libraries." Nat Biotechnol **22**(5): 575-582.

Binz, H. K., M. T. Stumpp, et al. (2003). "Designing repeat proteins: well-expressed, soluble and stable proteins from combinatorial libraries of consensus ankyrin repeat proteins." J Mol Biol **332**(2): 489-503.

Boku, N. (2014). "HER2-positive gastric cancer." Gastric Cancer **17**(1): 1-12.

Bork, P. (1993). "Hundreds of ankyrin-like repeats in functionally diverse proteins: mobile modules that cross phyla horizontally?" Proteins **17**(4): 363-374.

Bornhorst, J. A. and J. J. Falke (2000). "Purification of proteins using polyhistidine affinity tags." Methods Enzymol **326**: 245-254.

Buensanteai, N., P. K. Mukherjee, et al. (2010). "Expression and purification of biologically active Trichoderma virens proteinaceous elicitor Sm1 in Pichia pastoris." Protein Expr Purif **72**(1): 131-138.

Cameron, D., M. Casey, et al. (2008). "A phase III randomized comparison of lapatinib plus capecitabine versus capecitabine alone in women with advanced breast cancer that has progressed on trastuzumab: updated efficacy and biomarker analyses." Breast Cancer Res Treat **112**(3): 533-543.

Cannella, B., D. Pitt, et al. (1999). "Neuregulin and erbB receptor expression in normal and diseased human white matter." J Neuroimmunol **100**(1-2): 233-242.

Cheng, Z., O. P. De Jesus, et al. (2010). "64Cu-labeled affibody molecules for imaging of HER2 expressing tumors." Mol Imaging Biol **12**(3): 316-324.

Citri, A. and Y. Yarden (2006). "EGF-ERBB signalling: towards the systems level." Nat Rev Mol Cell Biol **7**(7): 505-516.

D'Huyvetter, M., A. Aerts, et al. (2012). "Development of (177) Lu-nanobodies for radioimmunotherapy of HER2-positive breast cancer: evaluation of different bifunctional chelators." Contrast Media Mol Imaging **7**(2): 254-264.

Da Costa, L., J. Galimand, et al. (2013). "Hereditary spherocytosis, elliptocytosis, and other red cell membrane disorders." Blood Rev **27**(4): 167-178.

DeFazio-Eli, L., K. Strommen, et al. (2011). "Quantitative assays for the measurement of HER1-HER2 heterodimerization and phosphorylation in cell lines and breast tumors: applications for diagnostics and targeted drug mechanism of action." Breast Cancer Res **13**(2): R44.

Dennis, M. S., H. Jin, et al. (2007). "Imaging tumors with an albumin-binding Fab, a novel tumor-targeting agent." Cancer Res **67**(1): 254-261.

Dhibi, M., F. Brahmi, et al. (2011). "The intake of high fat diet with different trans fatty acid levels differentially induces oxidative stress and non alcoholic fatty liver disease (NAFLD) in rats." Nutr Metab (Lond) **8**(1): 65.

Dijkers, E. C., J. G. Kosterink, et al. (2009). "Development and characterization of clinical-grade 89Zr-trastuzumab for HER2/neu immunoPET imaging." J Nucl Med **50**(6): 974-981.

Dijkers, E. C., T. H. Oude Munnink, et al. (2010). "Biodistribution of 89Zr-trastuzumab and PET imaging of HER2-positive lesions in patients with metastatic breast cancer." Clin Pharmacol Ther **87**(5): 586-592.

Epa, V. C., O. Dolezal, et al. (2013). "Structural model for the interaction of a designed Ankyrin Repeat Protein with the human epidermal growth factor receptor 2." PLoS One **8**(3): e59163.

Feldwisch, J., V. Tolmachev, et al. (2010). "Design of an optimized scaffold for affibody molecules." J Mol Biol **398**(2): 232-247.

Forrer, P., H. K. Binz, et al. (2004). "Consensus design of repeat proteins." Chembiochem **5**(2): 183-189.

Fu, W., C. A. Lobocki, et al. (2001). "Molecular markers in Paget disease of the breast." J Surg Oncol **77**(3): 171-178.

Gaykema, S. B., C. P. Schroder, et al. (2014). "89Zr-trastuzumab and 89Zr-bevacizumab PET to Evaluate the Effect of the HSP90 Inhibitor NVP-AUY922 in Metastatic Breast Cancer Patients." Clinical Cancer Research **20**(15): 3945-3954.

Gianni, L., T. Pienkowski, et al. (2012). "Efficacy and safety of neoadjuvant pertuzumab and trastuzumab in women with locally advanced, inflammatory, or early HER2-positive breast cancer (NeoSphere): a randomised multicentre, open-label, phase 2 trial." Lancet Oncol **13**(1): 25-32.

Goldhirsch, A., R. D. Gelber, et al. (2013). "2 years versus 1 year of adjuvant trastuzumab for HER2-positive breast cancer (HERA): an open-label, randomised controlled trial." Lancet **382**(9897): 1021-1028.

Goldstein, R., J. Sosabowski, et al. (2013). "Developments in single photon emission computed tomography and PET-based HER2 molecular imaging for breast cancer." Expert Rev Anticancer Ther **13**(3): 359-373.

Hathaway, H. J., K. S. Butler, et al. (2011). "Detection of breast cancer cells using targeted magnetic nanoparticles and ultra-sensitive magnetic field sensors." Breast Cancer Res **13**(5): R108.

He, Z., Y. Huang, et al. (2012). "Comparison of alpha-factor preprosequence and a classical mammalian signal peptide for secretion of recombinant xylanase xynB from yeast Pichia pastoris." J Microbiol Biotechnol **22**(4): 479-483.

Hofstrom, C., M. Altai, et al. (2013). "HAHAHA, HEHEHE, HIHIHI, or HKHKHK: Influence of position and composition of histidine containing tags on biodistribution of [(99m)Tc(CO)3](+)-labeled affibody molecules." J Med Chem **56**(12): 4966-4974.

Hofstrom, C., A. Orlova, et al. (2011). "Use of a HEHEHE purification tag instead of a hexahistidine tag improves biodistribution of affibody molecules site-specifically labeled with (99m)Tc, (111)In, and (125)I." J Med Chem **54**(11): 3817-3826.

Holloway, C. M., D. A. Scollard, et al. (2013). "Phase I trial of intraoperative detection of tumor margins in patients with HER2-positive carcinoma of the breast following administration of 111In-DTPA-trastuzumab Fab fragments." Nucl Med Biol **40**(5): 630-637.

Hosseinimehr, S. J., V. Tolmachev, et al. (2012). "Liver uptake of radiolabeled targeting proteins and peptides: considerations for targeting peptide conjugate design." Drug Discov Today **17**(21-22): 1224-1232.

Hudis, C. A. (2007). "Trastuzumab--mechanism of action and use in clinical practice." N Engl J Med **357**(1): 39-51.

Interlandi, G., S. K. Wetzel, et al. (2008). "Characterization and further stabilization of designed ankyrin repeat proteins by combining molecular dynamics simulations and experiments." J Mol Biol **375**(3): 837-854.

Jacobs, T. W., A. M. Gown, et al. (1999). "Specificity of HercepTest in determining HER-2/neu status of breast cancers using the United States Food and Drug Administration-approved scoring system." J Clin Oncol **17**(7): 1983-1987.

Joensuu, H., P. L. Kellokumpu-Lehtinen, et al. (2006). "Adjuvant docetaxel or vinorelbine with or without trastuzumab for breast cancer." N Engl J Med **354**(8): 809-820.

Jost, C., J. Schilling, et al. (2013). "Structural basis for eliciting a cytotoxic effect in HER2-overexpressing cancer cells via binding to the extracellular domain of HER2." Structure **21**(11): 1979-1991.

Kah, M. and C. D. Brown (2008). "LogD: lipophilicity for ionisable compounds." Chemosphere **72**(10): 1401-1408.

Kiesewetter, D. O., G. Kramer-Marek, et al. (2008). "Radiolabeling of HER2 specific Affibody(R) molecule with F-18." J Fluor Chem **129**(9): 799-805.

King, C. R., M. H. Kraus, et al. (1985). "Amplification of a novel v-erbB-related gene in a human mammary carcinoma." Science **229**(4717): 974-976.

Kobe, B. and A. V. Kajava (2000). "When protein folding is simplified to protein coiling: the continuum of solenoid protein structures." Trends Biochem Sci **25**(10): 509-515.

Kohl, A., H. K. Binz, et al. (2003). "Designed to be stable: crystal structure of a consensus ankyrin repeat protein." Proc Natl Acad Sci U S A **100**(4): 1700-1705.

Kramer-Marek, G., D. O. Kiesewetter, et al. (2009). "Changes in HER2 expression in breast cancer xenografts after therapy can be quantified using PET and (18)F-labeled affibody molecules." J Nucl Med **50**(7): 1131-1139.

Kramer-Marek, G., D. O. Kiesewetter, et al. (2008). "[18F]FBEM-Z(HER2:342)-Affibody molecule-a new molecular tracer for in vivo monitoring of HER2 expression by positron emission tomography." Eur J Nucl Med Mol Imaging **35**(5): 1008-1018.

Krop, I. E., M. Beeram, et al. (2010). "Phase I study of trastuzumab-DM1, an HER2 antibody-drug conjugate, given every 3 weeks to patients with HER2-positive metastatic breast cancer." J Clin Oncol **28**(16): 2698-2704.

Kurjan, J. and I. Herskowitz (1982). "Structure of a yeast pheromone gene (MF alpha): a putative alpha-factor precursor contains four tandem copies of mature alpha-factor." Cell **30**(3): 933-943.

Lal, P., P. A. Salazar, et al. (2004). "HER-2 testing in breast cancer using immunohistochemical analysis and fluorescence in situ hybridization: a single-institution experience of 2,279 cases and comparison of dual-color and single-color scoring." Am J Clin Pathol **121**(5): 631-636.

Lander, E. S., L. M. Linton, et al. (2001). "Initial sequencing and analysis of the human genome." Nature **409**(6822): 860-921.

Leary, A. F., W. M. Hanna, et al. (2009). "Value and limitations of measuring HER-2 extracellular domain in the serum of breast cancer patients." J Clin Oncol **27**(10): 1694-1705.

Lewis Phillips, G. D., G. Li, et al. (2008). "Targeting HER2-positive breast cancer with trastuzumab-DM1, an antibody-cytotoxic drug conjugate." Cancer Res **68**(22): 9280-9290.

Lin, N. U. and E. P. Winer (2007). "Brain metastases: the HER2 paradigm." Clin Cancer Res **13**(6): 1648-1655.

Lub-de Hooge, M. N., J. G. Kosterink, et al. (2004). "Preclinical characterisation of 111In-DTPA-trastuzumab." Br J Pharmacol **143**(1): 99-106.

Malek, S., T. Huxford, et al. (1998). "Ikappa Balpha functions through direct contacts with the nuclear localization signals and the DNA binding sequences of NF-kappaB." J Biol Chem **273**(39): 25427-25435.

Mankoff, D. A. (2007). "A definition of molecular imaging." J Nucl Med **48**(6): 18N, 21N.

Mankoff, D. A., J. M. Link, et al. (2008). "Tumor receptor imaging." J Nucl Med **49 Suppl 2**: 149S-163S.

Marty, M., F. Cognetti, et al. (2005). "Randomized phase II trial of the efficacy and safety of trastuzumab combined with docetaxel in patients with human epidermal growth factor receptor 2-positive metastatic breast cancer administered as first-line treatment: the M77001 study group." J Clin Oncol **23**(19): 4265-4274.

McLarty, K., B. Cornelissen, et al. (2009). "Micro-SPECT/CT with 111In-DTPA-pertuzumab sensitively detects trastuzumab-mediated HER2 downregulation and tumor response in athymic mice bearing MDA-MB-361 human breast cancer xenografts." J Nucl Med **50**(8): 1340-1348.

McLarty, K., B. Cornelissen, et al. (2009). "Associations between the uptake of 111In-DTPA-trastuzumab, HER2 density and response to trastuzumab (Herceptin) in athymic

mice bearing subcutaneous human tumour xenografts." Eur J Nucl Med Mol Imaging **36**(1): 81-93.
Metzger-Filho, O., E. P. Winer, et al. (2013). "Pertuzumab: optimizing HER2 blockade." Clin Cancer Res **19**(20): 5552-5556.
Miller, J., M. Doss, et al. (2012). "Impact of expression system on the function of the C6.5 diabody PET radiotracer." Tumour Biol.
Moasser, M. M. (2007). "The oncogene HER2: its signaling and transforming functions and its role in human cancer pathogenesis." Oncogene **26**(45): 6469-6487.
Molina, M. A., R. Saez, et al. (2002). "NH(2)-terminal truncated HER-2 protein but not full-length receptor is associated with nodal metastasis in human breast cancer." Clin Cancer Res **8**(2): 347-353.
Moreno, A., B. Lloveras, et al. (1997). "Ductal carcinoma in situ of the breast: correlation between histologic classifications and biologic markers." Mod Pathol **10**(11): 1088-1092.
Morgan, S. J., C. S. Elangbam, et al. (2013). "Use of animal models of human disease for nonclinical safety assessment of novel pharmaceuticals." Toxicol Pathol **41**(3): 508-518.
Morgat, C., E. Hindie, et al. (2013). "Gallium-68: chemistry and radiolabeled peptides exploring different oncogenic pathways." Cancer Biother Radiopharm **28**(2): 85-97.
Mortimer, J. E., J. R. Bading, et al. (2013). "Functional imaging of human epidermal growth factor receptor 2-positive metastatic breast cancer using 64Cu-DOTA-trastuzumab PET." J Nucl Med **55**(1): 23-29.
Mosavi, L. K., S. Williams, et al. (2002). "Equilibrium folding and stability of myotrophin: a model ankyrin repeat protein." J Mol Biol **320**(2): 165-170.
Nahta, R., L. X. Yuan, et al. (2005). "Insulin-like growth factor-I receptor/human epidermal growth factor receptor 2 heterodimerization contributes to trastuzumab resistance of breast cancer cells." Cancer Res **65**(23): 11118-11128.
Nilsson, B., T. Moks, et al. (1987). "A synthetic IgG-binding domain based on staphylococcal protein A." Protein Eng **1**(2): 107-113.
Nord, K., E. Gunneriusson, et al. (1997). "Binding proteins selected from combinatorial libraries of an alpha-helical bacterial receptor domain." Nat Biotechnol **15**(8): 772-777.
O'Grady, A., D. Allen, et al. (2010). "An immunohistochemical and fluorescence in situ hybridization-based comparison between the Oracle HER2 Bond Immunohistochemical System, Dako HercepTest, and Vysis PathVysion HER2 FISH using both commercially validated and modified ASCO/CAP and United Kingdom HER2 IHC scoring guidelines." Appl Immunohistochem Mol Morphol **18**(6): 489-493.
Olafsen, T., S. J. Sirk, et al. (2012). "ImmunoPET using engineered antibody fragments: fluorine-18 labeled diabodies for same-day imaging." Tumour Biol **33**(3): 669-677.
Orlova, A., M. Magnusson, et al. (2006). "Tumor imaging using a picomolar affinity HER2 binding affibody molecule." Cancer Res **66**(8): 4339-4348.
Orlova, A., V. Tolmachev, et al. (2007). "Synthetic affibody molecules: a novel class of affinity ligands for molecular imaging of HER2-expressing malignant tumors." Cancer Res **67**(5): 2178-2186.
Orlova, A., H. Wallberg, et al. (2009). "On the selection of a tracer for PET imaging of HER2-expressing tumors: direct comparison of a 124I-labeled affibody molecule and trastuzumab in a murine xenograft model." J Nucl Med **50**(3): 417-425.

Osborne, J. R., E. Port, et al. (2010). "18F-FDG PET of locally invasive breast cancer and association of estrogen receptor status with standardized uptake value: microarray and immunohistochemical analysis." J Nucl Med **51**(4): 543-550.

Oude Munnink, T. H., M. A. Korte, et al. (2010). "(89)Zr-trastuzumab PET visualises HER2 downregulation by the HSP90 inhibitor NVP-AUY922 in a human tumour xenograft." Eur J Cancer **46**(3): 678-684.

Owens, M. A., B. C. Horten, et al. (2004). "HER2 amplification ratios by fluorescence in situ hybridization and correlation with immunohistochemistry in a cohort of 6556 breast cancer tissues." Clin Breast Cancer **5**(1): 63-69.

Pegram, M. D., G. Pauletti, et al. (1998). "HER-2/neu as a predictive marker of response to breast cancer therapy." Breast Cancer Res Treat **52**(1-3): 65-77.

Perik, P. J., M. N. Lub-De Hooge, et al. (2006). "Indium-111-labeled trastuzumab scintigraphy in patients with human epidermal growth factor receptor 2-positive metastatic breast cancer." J Clin Oncol **24**(15): 2276-2282.

Perisic, O., P. A. Webb, et al. (1994). "Crystal structure of a diabody, a bivalent antibody fragment." Structure **2**(12): 1217-1226.

Perols, A., H. Honarvar, et al. (2012). "Influence of DOTA chelator position on biodistribution and targeting properties of (111)In-labeled synthetic anti-HER2 affibody molecules." Bioconjug Chem **23**(8): 1661-1670.

Piccart-Gebhart, M. J., M. Procter, et al. (2005). "Trastuzumab after adjuvant chemotherapy in HER2-positive breast cancer." N Engl J Med **353**(16): 1659-1672.

Piechocki, M. P., Y. S. Ho, et al. (2003). "Human ErbB-2 (Her-2) transgenic mice: a model system for testing Her-2 based vaccines." J Immunol **171**(11): 5787-5794.

Port, E. R., H. Yeung, et al. (2006). "18F-2-fluoro-2-deoxy-D-glucose positron emission tomography scanning affects surgical management in selected patients with high-risk, operable breast carcinoma." Ann Surg Oncol **13**(5): 677-684.

Powell, W. C., D. G. Hicks, et al. (2007). "A new rabbit monoclonal antibody (4B5) for the immunohistochemical (IHC) determination of the HER2 status in breast cancer: comparison with CB11, fluorescence in situ hybridization (FISH), and interlaboratory reproducibility." Appl Immunohistochem Mol Morphol **15**(1): 94-102.

Prata, M. I. (2012). "Gallium-68: a new trend in PET radiopharmacy." Curr Radiopharm **5**(2): 142-149.

Press, M. F., G. Hung, et al. (1994). "Sensitivity of HER-2/neu antibodies in archival tissue samples: potential source of error in immunohistochemical studies of oncogene expression." Cancer Res **54**(10): 2771-2777.

Quenel, N., J. Wafflart, et al. (1995). "The prognostic value of c-erbB2 in primary breast carcinomas: a study on 942 cases." Breast Cancer Res Treat **35**(3): 283-291.

Raemaekers, R. J., L. de Muro, et al. (1999). "Functional phytohemagglutinin (PHA) and Galanthus nivalis agglutinin (GNA) expressed in Pichia pastoris correct N-terminal processing and secretion of heterologous proteins expressed using the PHA-E signal peptide." Eur J Biochem **265**(1): 394-403.

Rahmim, A. and H. Zaidi (2008). "PET versus SPECT: strengths, limitations and challenges." Nucl Med Commun. **29**(3): 193-207.

Reddy, S., C. C. Shaller, et al. (2011). "Evaluation of the anti-HER2 C6.5 diabody as a PET radiotracer to monitor HER2 status and predict response to trastuzumab treatment." Clin Cancer Res **17**(6): 1509-1520.

Ren, G., J. M. Webster, et al. (2012). "In vivo targeting of HER2-positive tumor using 2-helix affibody molecules." Amino Acids **43**(1): 405-413.

Ren, G., R. Zhang, et al. (2009). "A 2-helix small protein labeled with 68Ga for PET imaging of HER2 expression." J Nucl Med **50**(9): 1492-1499.

Robinson, M. K., M. Doss, et al. (2005). "Quantitative immuno-positron emission tomography imaging of HER2-positive tumor xenografts with an iodine-124 labeled anti-HER2 diabody." Cancer Res **65**(4): 1471-1478.

Robinson, M. K., C. Shaller, et al. (2008). "Effective treatment of established human breast tumor xenografts in immunodeficient mice with a single dose of the alpha-emitting radioisotope astatine-211 conjugated to anti-HER2/neu diabodies." Clin Cancer Res **14**(3): 875-882.

Romond, E. H., E. A. Perez, et al. (2005). "Trastuzumab plus adjuvant chemotherapy for operable HER2-positive breast cancer." N Engl J Med **353**(16): 1673-1684.

Rosenthal, S. I., P. L. Depowski, et al. (2002). "Comparison of HER-2/neu oncogene amplification detected by fluorescence in situ hybridization in lobular and ductal breast cancer." Appl Immunohistochem Mol Morphol **10**(1): 40-46.

Ross, J. S. (2009). "Breast cancer biomarkers and HER2 testing after 10 years of anti-HER2 therapy." Drug News Perspect **22**(2): 93-106.

Ross, J. S., E. A. Slodkowska, et al. (2009). "The HER-2 receptor and breast cancer: ten years of targeted anti-HER-2 therapy and personalized medicine." Oncologist **14**(4): 320-368.

Sasagawa, T., M. Matsui, et al. (2011). "High-throughput recombinant gene expression systems in Pichia pastoris using newly developed plasmid vectors." Plasmid **65**(1): 65-69.

Scaltriti, M., F. Rojo, et al. (2007). "Expression of p95HER2, a truncated form of the HER2 receptor, and response to anti-HER2 therapies in breast cancer." J Natl Cancer Inst **99**(8): 628-638.

Schechter, A. L., D. F. Stern, et al. (1984). "The neu oncogene: an erb-B-related gene encoding a 185,000-Mr tumour antigen." Nature **312**(5994): 513-516.

Sedgwick, S. G. and S. J. Smerdon (1999). "The ankyrin repeat: a diversity of interactions on a common structural framework." Trends Biochem Sci **24**(8): 311-316.

Shah, S. and B. Chen (2011). "Testing for HER2 in Breast Cancer: A Continuing Evolution." Patholog Res Int **2011**: 903202.

Shah, S. S., Y. Wang, et al. (2009). "Effect of high copy number of HER2 associated with polysomy 17 on HER2 protein expression in invasive breast carcinoma." Diagn Mol Pathol **18**(1): 30-33.

Shou, J., S. Massarweh, et al. (2004). "Mechanisms of tamoxifen resistance: increased estrogen receptor-HER2/neu cross-talk in ER/HER2-positive breast cancer." J Natl Cancer Inst **96**(12): 926-935.

Slamon, D., W. Eiermann, et al. (2011). "Adjuvant trastuzumab in HER2-positive breast cancer." N Engl J Med **365**(14): 1273-1283.

Slamon, D. J., G. M. Clark, et al. (1987). "Human breast cancer: correlation of relapse and survival with amplification of the HER-2/neu oncogene." Science **235**(4785): 177-182.

Slamon, D. J., B. Leyland-Jones, et al. (2001). "Use of chemotherapy plus a monoclonal antibody against HER2 for metastatic breast cancer that overexpresses HER2." N Engl J Med **344**(11): 783-792.

Smith-Jones, P. M., D. Solit, et al. (2006). "Early tumor response to Hsp90 therapy using HER2 PET: comparison with 18F-FDG PET." J Nucl Med **47**(5): 793-796.

Smith-Jones, P. M., D. B. Solit, et al. (2004). "Imaging the pharmacodynamics of HER2 degradation in response to Hsp90 inhibitors." Nat Biotechnol **22**(6): 701-706.

Sorensen, J., D. Sandberg, et al. (2014). "First-in-human molecular imaging of HER2 expression in breast cancer metastases using the 111In-ABY-025 affibody molecule." J Nucl Med **55**(5): 730-735.

Tamaskovic, R., M. Simon, et al. (2012). "Designed ankyrin repeat proteins (DARPins) from research to therapy." Methods Enzymol **503**: 101-134.

Tamura, K., H. Kurihara, et al. (2013). "64Cu-DOTA-trastuzumab PET imaging in patients with HER2-positive breast cancer." J Nucl Med **54**(11): 1869-1875.

Tannapfel, A., H. Denk, et al. (2011). "Histopathological diagnosis of non-alcoholic and alcoholic fatty liver disease." Virchows Arch **458**(5): 511-523.

Theurillat, J. P., B. Dreier, et al. (2010). "Designed ankyrin repeat proteins: a novel tool for testing epidermal growth factor receptor 2 expression in breast cancer." Mod Pathol **23**(9): 1289-1297.

Tolmachev, V., C. Hofstrom, et al. (2010). "HEHEHE-tagged affibody molecule may be purified by IMAC, is conveniently labeled with [(m)Tc(CO)](+), and shows improved biodistribution with reduced hepatic radioactivity accumulation." Bioconjug Chem **21**(11): 2013-2022.

Tolmachev, V., I. Velikyan, et al. (2010). "A HER2-binding Affibody molecule labelled with 68Ga for PET imaging: direct in vivo comparison with the 111In-labelled analogue." Eur J Nucl Med Mol Imaging **37**(7): 1356-1367.

Tolner B, B. G., Foster B, Vigor K and Chester KA (2012). Laboratory Protocols in Fungal Biology: Current Methods in Fungal Biology. New York, Springer Science & Business Media

Tolner, B., L. Smith, et al. (2006). "Production of recombinant protein in Pichia pastoris by fermentation." Nature protocols **1**(2): 1006-1021.

Tran, T., T. Engfeldt, et al. (2007). "(99m)Tc-maEEE-Z(HER2:342), an Affibody molecule-based tracer for the detection of HER2 expression in malignant tumors." Bioconjug Chem **18**(6): 1956-1964.

Tse, C. H., H. C. Hwang, et al. (2011). "Determining True HER2 Gene Status in Breast Cancers With Polysomy by Using Alternative Chromosome 17 Reference Genes: Implications for Anti-HER2 Targeted Therapy." J Clin Oncol **29**(31): 4168-4174.

Turner, N. H. and A. Di Leo (2013). "HER2 discordance between primary and metastatic breast cancer: assessing the clinical impact." Cancer Treat Rev **39**(8): 947-957.

U.S. Department of Health and Human Services, F. a. D. A., Center for Drug Evaluation and Research (CDER) (2005). "Guidance for Industry Estimating the Maximum Safe Starting Dose in Initial Clinical Trials for Therapeutics in Adult Healthy Volunteers." Pharmacology and Toxicology.

Vaneycken, I., N. Devoogdt, et al. (2011). "Preclinical screening of anti-HER2 nanobodies for molecular imaging of breast cancer." FASEB J **25**(7): 2433-2446.

Vani, K., S. R. Sompuram, et al. (2008). "National HER2 proficiency test results using standardized quantitative controls: characterization of laboratory failures." Arch Pathol Lab Med **132**(2): 211-216.

Verma, S., D. Miles, et al. (2012). "Trastuzumab emtansine for HER2-positive advanced breast cancer." N Engl J Med **367**(19): 1783-1791.

Wahl, R. L., J. M. Herman, et al. (2011). "The promise and pitfalls of positron emission tomography and single-photon emission computed tomography molecular imaging-guided radiation therapy." Semin Radiat Oncol **21**(2): 88-100.

Waibel, R., R. Alberto, et al. (1999). "Stable one-step technetium-99m labeling of His-tagged recombinant proteins with a novel Tc(I)-carbonyl complex." Nat Biotechnol **17**(9): 897-901.

Wessels, B. W., M. W. Konijnenberg, et al. (2008). "MIRD pamphlet No. 20: the effect of model assumptions on kidney dosimetry and response--implications for radionuclide therapy." J Nucl Med **49**(11): 1884-1899.

Wolff, A. C., M. E. Hammond, et al. (2013). "Recommendations for human epidermal growth factor receptor 2 testing in breast cancer: american society of clinical oncology/college of american pathologists clinical practice guideline update." J Clin Oncol **31**(31): 3997-4013.

Wolff, A. C., M. E. Hammond, et al. (2013). "Recommendations for human epidermal growth factor receptor 2 testing in breast cancer: American society of clinical oncology/college of american pathologists clinical practice guideline update." Arch Pathol Lab Med **138**(2): 241-256.

Wolff, A. C., M. E. Hammond, et al. (2007). "American Society of Clinical Oncology/College of American Pathologists guideline recommendations for human epidermal growth factor receptor 2 testing in breast cancer." Arch Pathol Lab Med **131**(1): 18-43.

Xavier, C., I. Vaneycken, et al. (2013). "Synthesis, preclinical validation, dosimetry, and toxicity of 68Ga-NOTA-anti-HER2 Nanobodies for iPET imaging of HER2 receptor expression in cancer." J Nucl Med **54**(5): 776-784.

Yaziji, H., L. C. Goldstein, et al. (2004). "HER-2 testing in breast cancer using parallel tissue-based methods." JAMA **291**(16): 1972-1977.

Yeh, I. T., M. A. Martin, et al. (2009). "Clinical validation of an array CGH test for HER2 status in breast cancer reveals that polysomy 17 is a rare event." Mod Pathol **22**(9): 1169-1175.

Zahnd, C., M. Kawe, et al. (2010). "Efficient tumor targeting with high-affinity designed ankyrin repeat proteins: effects of affinity and molecular size." Cancer Res **70**(4): 1595-1605.

Zahnd, C., F. Pecorari, et al. (2006). "Selection and characterization of Her2 binding-designed ankyrin repeat proteins." J Biol Chem **281**(46): 35167-35175.

Zahnd, C., E. Wyler, et al. (2007). "A designed ankyrin repeat protein evolved to picomolar affinity to Her2." J Mol Biol **369**(4): 1015-1028.

Zanzonico, P. (2012). "Principles of nuclear medicine imaging: planar, SPECT, PET, multi-modality, and autoradiography systems." Radiat Res. **177**(4): 349-364.